Universiteit Leiden
The Netherlands

Novel regulators of endosome dynamics, MHCII antigen presentation and chemosensitivity

Wijdeven, R.H.M.

Citation
Wijdeven, R. H. M. (2017, November 29). *Novel regulators of endosome dynamics, MHCII antigen presentation and chemosensitivity*. Retrieved from https://hdl.handle.net/1887/59471

Version:	Not Applicable (or Unknown)
License:	Licence agreement concerning inclusion of doctoral thesis in the Institutional Repository of the University of Leiden
Downloaded from:	https://hdl.handle.net/1887/59471

Note: To cite this publication please use the final published version (if applicable).

Cover Page



Universiteit Leiden



The following handle holds various files of this Leiden University dissertation:
http://hdl.handle.net/1887/59471

Author: Wijdeven, R.H.M.
Title: Novel regulators of endosome dynamics, MHCII antigen presentation and chemosensitivity
Issue Date: 2017-11-29

Novel regulators of endosome dynamics, MHCII antigen presentation and chemosensitivity

Ruud Hendricus Martinus Wijdeven

ISBN: 978-94-6233-770-1

Copyright: Ruud HM Wijdeven 2017

Cover: Amsterdam as template for the cell, with different modes of transportation connected in a dynamic equilibrium.

The research described in this thesis was performed at the department of Cell Biology II, Netherlands Cancer Institute, Amsterdam, the Netherlands, as well as at the department of Chemical Immunology, LUMC, Leiden, the Netherlands.

Printed by: Gildeprint, Enschede

Novel regulators of endosome dynamics, MHCII antigen presentation and chemosensitivity

Proefschrift

Ter verkrijging van
de graad van Doctor aan de Universiteit Leiden,
op gezag van Rector Magnificus prof.mr. C.J.J.M. Stolker
volgens besluit van het College voor Promoties
te verdedigen op woensdag 29 november
klokke 13.45 uur

Door

Ruud Hendricus Martinus Wijdeven

Geboren te Mill en St. Hubert

op 14 Februari 1985

Promotor:

Prof. Dr. J.J.C. Neefjes

Co-Promotor:

Prof. Dr. H.S. Overkleeft

Promotiecommissie:

Prof. Dr. J. Borst
Universiteit van Amsterdam

Prof. Dr. P. ten Dijke

Prof. Dr. H. Ovaa

Prof. Dr. H.J. Tanke

Dr. E.A.J. Reits
Universiteit van Amsterdam

Dr. W.T. Zwart
Nederlands Kanker Instituut

Table of Contents

Scope of the thesis		**6**
Chapter 1:	ER contact sites direct late endosome transport. *Bioessays (2015)*	**7**
Chapter 2:	Cholesterol and ORP1L-mediated ER contact sites control autophagosome transport and fusion with the endocytic pathway. *Nature Communications (2016)*	**17**
Chapter 3:	An ER-associated pathway defines endosomal architecture for controlled cargo transport. *Cell (2016)*	**45**
Chapter 4:	Identification of DUBs controlling MHCII and vesicular dynamics.	**75**
Chapter 5:	USP54 is a novel regulator of cytoskeletal dynamics.	**91**
Chapter 6:	Exploring genome-wide datasets of MHC class II antigen presentation. *Molecular Immunology (2013)*	**111**
Chapter 7:	Chemical and genetic control of IFNγ-mediated MHCII expression.	**117**
Chapter 8:	Old drugs, novel ways out: drug resistance towards cytotoxic chemotherapeutics. *Drug Resistance Updates (2016)*	**137**
Chapter 9:	Genome-wide identification and characterization of novel factors conferring resistance to topoisomerase II poisons in cancer. *Cancer Research (2015)*	**169**
Chapter 10:	Summary and discussion.	**191**

Nederlandse Samenvatting

Curriculum Vitae

List of Publications

Acknowledgements

An introduction before the Introduction

During the last years I have worked on defining various factors in control of vesicle transport and MHC class II antigen presentation, as well as resistance to anti-cancer drugs. This yielded various chapters describing the role of cholesterol, the ER and membrane contact sites in the control of endosome and autophagosome transport and the elucidation of the role of a novel protein, RNF26, regulating positioning of the entire endosomal system (Chapter 2 and 3). In Chapter 4 and 5 I have focussed on an enzyme class that removes ubiquitin modifications from proteins and used RNAi screening to identify two controllers of endosomal motility and MHC class II expression. We subsequently performed several experiments to dissect the corresponding cell biology, which is work that is still ongoing.

Chapter 6 is an introduction to Chapter 7 that describes a series of experiments where we tried to integrate chemical and genetic data to define novel target-lead combinations in control of MHC class II expression. Using this approach we identified two novel proteins, Keap1 and p62, and two drugs, dimethylfumarate (DMF) and arsenite, that coordinate interferon-γ induced MHCII expression. This system induces the expression of MHC class II in non-hematopoietic cells and may be critical for MHC class II upregulation in inflamed tissue. Interestingly, DMF is already used in the clinic to treat auto-immune diseases.

Chapter 8 continues on drugs, and more specifically the anthracycline cancer drugs. It reviews the current understanding of these anti-cancer drugs as well as their mechanisms of resistance. This is explored further in Chapter 9, where we describe the use of genome-wide screening systems to determine novel factors in control of resistance to the anthracycline doxorubicin, a drug extensively used in anti-cancer treatment. We also delved into the corresponding cell biology and showed that the most prevailing pathway identified revolves around DNA double stranded break repair.

The thesis is wrapped up with a discussion of the different chapters, which in combination cover the cell biology of endosomal transport and the utilization of drugs in control of MHC class II transcription and anti-cancer responses.

Chapter 1:
ER contact sites direct late endosome transport

Ruud H. Wijdeven[1], Marlieke L. M. Jongsma[2], Jacques Neefjes[1] and Ilana Berlin[1]

[1] Division of Cell Biology, The Netherlands Cancer Institute, Plesmanlaan 121, 1066CX Amsterdam, The Netherlands
[2] Department of Immunopathology, Sanquin Research and Landsteiner Laboratory AMC/UvA, Plesmanlaan 125, 1066 CX Amsterdam, The Netherlands

Bioessays. 2015 Dec;37(12):1298-302

Abstract

Endosomes shuttle select cargoes between cellular compartments and, in doing so, maintain intracellular homeostasis and enable interactions with the extracellular space. Directionality of endosomal transport critically impinges on cargo fate, as retrograde (microtubule minus-end-directed) traffic delivers vesicle contents to the lysosome for proteolysis, while the opposing anterograde (plus-end-directed) movement promotes recycling and secretion. Intriguingly, the endoplasmic reticulum (ER) is emerging as a key player in spatiotemporal control of late endosome and lysosome transport, through the establishment of physical contacts with these organelles. Earlier studies have described how minus-end-directed motor proteins become discharged from vesicles engaged at such contact sites. Now, Raiborg et al. implicate ER-mediated interactions, induced by protrudin, in loading plus-end-directed motor kinesin-1 onto endosomes, thereby stimulating their transport toward the cell's periphery. In this review, we recast the prevailing concepts on bidirectional late endosome transport and discuss the emerging paradigm of inter-compartmental regulation from the ER-endosome interface viewpoint.

Introduction

The endocytic compartment is both a critical mediator of intracellular homeostasis and a front line negotiator between the cell and its environment. Captured by plasma membrane invagination and subsequent pinching off of a nascent endosome, internalized cargo progresses through a variety of vesicle maturation stages, each defined by a unique repertoire of resident markers and small GTPases from the Rab, Arl and Arf families. When in their active GTP-bound state, the latter function as scaffolds for assembly of transport and fusion machineries on target vesicles [1]. The first stop along the maturation journey is the early endosome (EE) sorting platform, from where cargo is either recycled or targeted downstream to the late endosome (LE) stage. LEs in turn fuse with or mature into degradative lysosomes (Ly), characterized by an acidic luminal pH and proteolytic enzymes warranting cargo degradation and redistribution of catabolized materials [2]. In addition to extracellular contents and those derived from the plasma membrane, newly synthesized proteins can gain direct access to the LE compartment through the vesicular arm of the trans-Golgi network [3]. Moreover, cytosolic materials and even whole organelles, once incorporated into autophagic vesicles, can be targeted for proteolysis in the lysosome [4]. Within this dynamic membrane system, consisting of a wide variety of specialized vesicles, LEs encounter traffic from the endocytic, biosynthetic and autophagic components alike, and thus occupy its logistic epicenter. In this review, we discuss recent insights into the transport mechanisms of LEs and Lys (hereafter collectively referred to as LEs, unless stated otherwise), with special emphasis on the influence of the ER in this context.

LE transport is orchestrated by Rab7 and its effector proteins

To accommodate long-range endosome movement, required for communication between distant membranes, microtubule-based motor proteins drive cargo either towards (minus-end) or away from (plus-end) the microtubule-organizing center

(MTOC) [5]. Because the balance between retrograde dynein and anterograde kinesin motor binding determines the net directionality of movement and maturation of affected endosomes [2,5], LE transport is inherently linked to cargo localization and fate [6]. Interestingly, most endosomes inside the cell move bi-directionally in a stop-and-go manner, rather than linearly towards either the periphery or the perinuclear region [5,7]. This implies either that specific motor proteins are likely retained for short periods of time, or that additional regulatory mechanisms are in place to monitor and influence switching between opposing transport machineries. Currently, formidable evidence is building up in support of the latter hypothesis, where different effectors responsible for recruitment of opposing motor functions have been shown to utilize a common and potentially competitive mode of LE recognition.
The LE compartment is decorated by the GTPase Rab7, which recruits effectors facilitating endosome transport along microtubule tracks as well as their fusion with lysosomes and autophagosomes (RILP and PLEKHM1, respectively [8-10]). For LEs to move into the perinuclear area of the cell, Rab7 calls on RILP [11,12], an effector that binds to the dynactin subunit of the dynein motor complex [13]. Concurrent association of RILP with the HOPS complex then induces fusion with the lysosome, thereby coupling transport to maturation processes [8]. Conversely, to move into the cell's periphery, Rab7 turns to its effector FYCO1 [14], which attracts the light chain-2 of kinesin-1 (KLC2), thereby linking the plus-end-directed motor complex to LEs [6]. Alternatively, kinesin-1 can be targeted to LEs by the Arl8 effector, SKIP [15]. It is currently unclear whether the GTPases Rab7 and Arl8 occupy the same LEs or distinguish between their respective subpopulations. However, for most LEs, Rab7 appears to be the key that turns both sides, where RILP leads to dynactin and dynein recruitment, while FYCO1 results in acquisition of kinesin-1. In principle, Rab7 binding to either of the above then dictates which way the endosome will go. Both effectors recognize Rab7 using a similar motif, implying that their binding is mutually exclusive on a given Rab7 molecule [16]. This raises the question of which factors govern effector binding to Rab7 and thus effectively decide the direction of endosome movement along microtubules. It has long been known that in an in vitro setting, the net force generated by dynein and kinesin molecules found on the same vesicle decides the contest [5] (reviewed in [7]). Similarly, following the law of mass action, relative amounts of opposing Rab7 effectors determine overall directionality of transport, as shown by overexpression of FYCO1 or RILP [12,14]. Although straightforward in the abstract, coordinating transport as a function of overall effector expression levels would disallow control of LEs on the individual basis and would be incompatible with fast switching of direction. To supervise and fine-tune endosomal transport in the cell's complex environment, elegant regulatory mechanisms have evolved to coordinate association and activation of Rab7 effector proteins.

ER determines directionality of LE transport

Its presence throughout the cell positions the ER as an ideal candidate to accommodate general scaffolding functions for dynamic processes involving endosomes in every corner of the cytoplasm. This is supported by the observation that LEs make recurring contacts with the ER along their transport routes, with contact propensity and dwelling time found to increase with endosome maturation [17]. In the case of

LE transport, its regulatory focal point rests on Rab7, which mediates recruitment of both dynein and kinesin motors to the LE membrane. Similarly, its association with negative regulators of directional transport helps guard the dynamic character of endosomes. The first negative regulator of LE motility ever reported is the oxysterol-binding protein ORP1L [18]. Preferentially associating to Rab7 in the presence of RILP [13], ORP1L can block RILP-mediated recruitment of the dynein motor complex in response to changes in LE cholesterol content [19-21]. Prior to ending up in the LEs, cholesterol must either be endocytosed from the extracellular environment in the form of LDL or synthesized de novo in the ER and subsequently delivered to endosomes (reviewed in [22]). When the cholesterol-sensing domain of ORP1L recognizes cholesterol molecules, it clamps down on the LE membrane in a closed conformation, compatible with minus-end transport. However, under low endosomal cholesterol conditions the cholesterol-sensing domain of ORP1L becomes exposed and allows the neighboring FFAT motif to bind the integral ER protein VAP-A, yielding extensive contact sites between LE and the ER (Figure 1). As a result, dynactin is displaced from RILP, and transport of endosomes towards the minus-end is inhibited. Now, the LE is stabilized at a membrane contact site (MCS) with the ER [19], poised for a change of direction. Factors influencing LE cholesterol levels thus effectively influence directionality of LE transport.

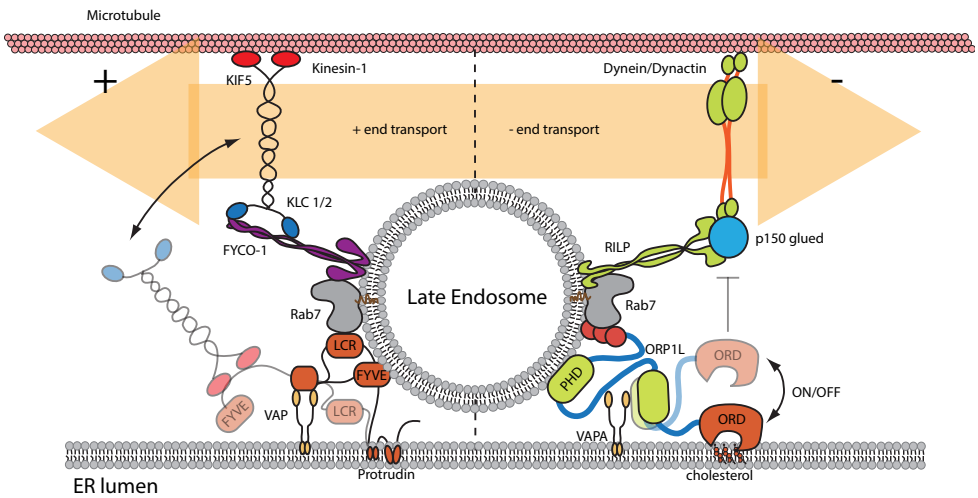


Figure 1: ORP1L and protrudin control motor loading onto Rab7. *Rab7 associates with its effectors, FYCO1 and RILP, which in turn recruit kinesin-1 or dynactin/dynein to respectively mediate plus- or minus-end-directed transport. In the former case, ER-localized protrudin binds VAP-A and kinesin-1 subunit KIF5. Through coincident recognition of PI3P by its FYVE domain and Rab7 with its low complexity region (LCR), protrudin instigates the formation of an ER-LE membrane contact site (MCS), where transfer of kinesin-1 onto FYCO1 provides a plus-end pulse. On the other side, ORP1L inhibits minus-end transport when in complex with VAP-A. At high cholesterol concentrations, the cholesterol-binding domain of ORP1L (ORD) interacts with the LE membrane, allowing minus-end transport to proceed. However, cholesterol depletion exposes the FFAT motif of ORP1L for binding ER-localized VAP-A. VAP-A subsequently binds the dynactin complex, thereby removing dynein from RILP and blocking minus-end transport. Thus, MCSs formed by both ORP1L and protrudin positively contribute to transport of endosomes towards the cell's periphery.*

In a new chapter on LE transport mechanisms, Raiborg et al. demonstrate that plus-end movement of Rab7-positive LEs also falls under ER control, through the actions of an ER-localized protein, protrudin [6]. Previously linked to neurite outgrowth—a process requiring concerted trafficking of vesicle membranes [23]—protrudin is now shown to directly promote LE transport towards and subsequent deposition at the neural protrusion site. Situated in the ER membrane, protrudin is shown to coincidentally engage Rab7 and the LE lipid phosphatidylinositol 3-phosphate (PI3P) [24], leading to ER-LE contact site formation. Biochemical and cell biological analyses by Raiborg et al. demonstrate that, through an interaction with the KIF5 subunit of kinesin-1 [25], protrudin facilitates loading of the plus-end motor complex onto FYCO1 (Figure 1). Observing FYCO1-positive vesicles briefly pause at the ER prior to resuming plus-end-directed motion, the authors suggest that protrudin orchestrates a hand-over of kinesin-1 to FYCO1 at Rab7-mediated contact sites. Taken together with the established functions of the ORP1L/VAP-A system at ER-LE contact sites, these new findings by Raiborg et al. underscore the breadth of ER involvement in the regulation of LE dynamics.

Intriguingly, the above indicates that PI3P is instrumental in targeting LEs for plus-end transport, since localization of both FYCO1 and protrudin to endosomes requires their respective PI3P-binding FYVE domains [6,14]. While EEs are known to contain high concentrations of PI3P, their maturation into LEs is associated with conversion of PI3P into PI(3,5)P. The resulting decrease in PI3P abundance on the LE limiting membranes [24,26] suggests that dephosphorylation of PI(3,5)P [27] may play a role in recruitment of FYCO1 and protrudin to these vesicles. Taken together with the well-established interplay between cholesterol and minus-end-directed LE motility [20,28], the new findings by Raiborg et al. expand the notion that proteins and lipids actively cooperate at the ER-LE interface, integrating cargo selection and motor acquisition, and suggest that cholesterol and PI3P act as opposing lipids in the regulation of minus- versus plus-end-directed LE transport.

Mechanisms and rationale for ER-curated motor engagement with endosomes

It is becoming abundantly clear that cells have evolved complex inter-compartmental controls over motility of endosomes. But what advantage does ER-based regulation in this context serve? One option is that due to their limited processivity, kinesin and dynein motors require continuous external triggers to remain bound. In vitro, kinesin and dynein travel an average distance of 600 nm and 1900 nm along microtubules, respectively [29,30]. Particularly in the former case, these intrinsic parameters are insufficient to afford direct transit between the perinuclear region and the periphery of the cell, and intermittent contacts with protrudin may promote continuity of transport. Moreover, on long journeys, vesicles may encounter crossed microtubule tracks or road blocks in the form of (macro-)molecules and complexes. Reloading motors onto vesicles that have past such barriers could then be critical to maintain a chosen course. Observations of endosome transport in living cells by Raiborg et al. reveal that vesicles captured by protrudin had already been moving in a directional manner en route to the ER, implying active presence of kinesin-1 prior to protru-

din engagement. Authors speculate that protrudin could reload or replace the motor upon contact with the endosome. In addition, the contact site can be envisioned to spatially restrict transport by directing vesicle transport to specific areas of the cell. For instance, during neurite outgrowth, plus-end transport is harnessed specifically in the direction of the growing protrusion, which presumably necessitates limitation of outward vesicle mobility elsewhere in the cell. Selective protrudin activation along microtubules directed into the protrusion site could be implemented to steer endosome transport in accordance with cellular demand. This concept can be further generalized to serve in sequestration of vesicle-associated cargo at specific regions in the cell, enabling localized signaling or polarized secretion [31].
While restricting directionality of cargo traffic may be required in special circumstances, under steady state conditions LE transport rarely follows direct trajectories. Instead, individual vesicles move in a bidirectional manner, switching frequently between plus- and minus-end motility [5,7]. Raiborg et al. note that by way of ORP1L and protrudin systems, both sides of bidirectional transport fall under the control of the ER. This raises the possibility that the two mechanisms may operate simultaneously at the same MCS. If so, the former could promote the release of minus-end-directed dynein and allow the latter to mediate the switch by recruiting plus-end motor machinery. Intriguingly, like ORP1L, protrudin contains an FFAT motif, which binds VAP-A and is required for protrusion formation [32]. Within the ER membrane, VAP-A exists as a dimer [33] and could therefore simultaneously accommodate both ORP1L and protrudin to facilitate motor exchange at the LE-ER contact sites. Alternatively, given its ER location, protrudin could compete away the available VAP-A, thereby inhibiting ORP1L-mediated contact site formation and inducing endosome release. In either scenario, the ER-LE contact sites can be envisioned as comprehensive navigation platforms, coordinating competing directionalities of endosome transport between the MTOC and the cell's periphery.

Roles of ER-LE contact sites in endosome biology beyond transport

The study of mechanisms underlying endosomal transport has produced invaluable understanding of basic molecular principles and yielded numerous tools for manipulation of complex intracellular systems in real time. Remarkably, control of LE transport by the ER highlights the power of cross-compartmental regulation in vesicle biology, and new questions on the topic continue to emerge. MCSs offer a stable platform upon which various complex molecular events may unfold in a spatially and temporally regulated fashion. For instance, recent work has shown that ER-endosome contact sites determine positioning and timing of endosome fission—a process required for compartmentalization within the highly interconnected endosomal system [34,35]. Fission or physical separation of one endosome carrying diverse cargoes results in two new vesicles, each containing cargoes destined for a specific fate [36]. Both position and timing of fission are shaped by the tubular ER, which wraps around the former [34] by an unknown molecular mechanism. Interestingly, fission requires activities of motor proteins to stretch the tubules containing select cargoes away from the scission site [37], and protrudin has been shown to

localize predominantly to tubular ER [38], opening the door to a potential role for this protein in the fission process. Besides those observed in fission, tubule-shaped LEs can also form during autophagic lysosome reformation, as well as upon activation of macrophages and dendritic cells [39-41]. In the latter case, tubulation has been shown to depend on RILP and FYCO1 [42], allowing the possibility that this process may fall under control of the ER. Resolving the molecular composition and function of ER-endosome contact sites and integrating their elements within the larger molecular networks in charge of endosome dynamics presents an exciting new frontier in endosome biology.

In working to shape endosome dynamics, can the ER also extract symbiotic benefits in return? ER-endosome contact sites could serve to fuel the former organelle with nutrients and metabolites. For instance, cholesterol is derived largely from the extracellular environment via endocytosis and must be subsequently transported to the ER [43]. One route for this is the formation of an MCS between lysosomal NPC-1 and ER localized ORP5, which interact with each other and facilitate cholesterol transport, probably directly via its contact site [44]. Additionally, cholesterol transport could potentially be mediated by MCSs formed between VAP-A and MLN64/STARD3 or MENTHO/STARD3NL, both cholesterol-binding proteins found on endosomes [45,46]. Evolution of nutrient exchange between the ER and endosomes argues that vesicle cargo can play an active role in contact site formation. This notion is supported by MCSs instigated between activated EGFR and the ER-localized phosphatase PTP1B, which serves to promote receptor sorting into the intra-luminal vesicles (ILVs) of LEs [47]. On the basis of such examples where cargo is directly involved in MCS formation, integrating various types of cargo may reshape our understanding of regulatory mechanisms underlying minus- and plus-end transport and subsequent maturation events.

Conclusions and outlook

The initial discoveries of MCSs between the ER and endosomes unveiled a new regulatory paradigm, where membrane compartments functionally influence one another in a dynamic manner. For simplicity's sake, it may be tempting to envision the ER as a mere facilitator of predetermined endosomal routes, and by extension cargo fates. However, the emerging understanding of molecular complexity underlying bidirectional transport paints a far more intricate picture. It appears that by providing pit stop opportunities to endosomes along the busy microtubule highways, the ER can actively influence what departure trajectories they should take. Sensitive molecular switches typically consist of positive and negative influences, held in delicate non-linear balance [7], and in the case of LE transport, the ER is a likely candidate to tip the scales. By assembling ORP1L and protrudin complexes in close proximity of one another, the ER could streamline spatiotemporal control of endosome dynamics, resulting in increased sensitivity and efficiency of long-range transport.

While a wide variety of ER-mediated MCSs have been discovered (reviewed in [48,49]), thus far only for late endosomes have they been linked to transport control. This raises the question as to whether the ER could offer the same to other organelles. Most immediately plausible candidates for transport under ER control are autophagosomes and the trans-Golgi network. Both of the above consist of vesicles

subject to long-range transport along microtubules, and the former has already been shown to acquire FYCO1 and Rab7 [14]. Additionally, mitochondria found in the tips of neurons travel vast distances with the help of the dynein motor complex in a manner dependent on the GTPase Miro, found at the ER-mitochondria interaction sites [50,51]. Do ER-assisted transport and membrane dynamics constitute common mechanisms of spatiotemporal organelle control? Thus far, endosomes lead the way to finding the answer.

Acknowledgements

This work was supported by the Institute of Chemical Immunology (ICI), an NWO Gravitation project funded by the Ministry of Education, Culture and Science of the government of the Netherlands and a European Research Council (ERC) advanced grant awarded to J.N.

References

1 Stenmark H. 2009. Rab GTPases as coordinators of vesicle traffic. Nature reviews Molecular cell biology 10: 513-25.

2 Huotari J, Helenius A. 2011. Endosome maturation. The EMBO journal 30: 3481-500.

3 Kienzle C, von Blume J. 2014. Secretory cargo sorting at the trans-Golgi network. Trends in cell biology 24: 584-93.

4 Mizushima N, Levine B, Cuervo AM, Klionsky DJ. 2008. Autophagy fights disease through cellular self-digestion. Nature 451: 1069-75.

5 Soppina V, Rai AK, Ramaiya AJ, Barak P, et al. 2009. Tug-of-war between dissimilar teams of microtubule motors regulates transport and fission of endosomes. Proceedings of the National Academy of Sciences of the United States of America 106: 19381-6.

6 Raiborg C, Wenzel EM, Pedersen NM, Olsvik H, et al. 2015. Repeated ER-endosome contacts promote endosome translocation and neurite outgrowth. Nature 520: 234-8.

7 Hancock WO. 2014. Bidirectional cargo transport: moving beyond tug of war. Nature reviews Molecular cell biology 15: 615-28.

8 van der Kant R, Fish A, Janssen L, Janssen H, et al. 2013. Late endosomal transport and tethering are coupled processes controlled by RILP and the cholesterol sensor ORP1L. Journal of cell science 126: 3462-74.

9 McEwan DG, Popovic D, Gubas A, Terawaki S, et al. 2015. PLEKHM1 regulates autophagosome-lysosome fusion through HOPS complex and LC3/GABARAP proteins. Molecular cell 57: 39-54.

10 Lin X, Yang T, Wang S, Wang Z, et al. 2014. RILP interacts with HOPS complex via VPS41 subunit to regulate endocytic trafficking. Scientific reports 4: 7282.

11 Cantalupo G, Alifano P, Roberti V, Bruni CB, et al. 2001. Rab-interacting lysosomal protein (RILP): the Rab7 effector required for transport to lysosomes. The EMBO journal 20: 683-93.

12 Jordens I, Fernandez-Borja M, Marsman M, Dusseljee S, et al. 2001. The Rab7 effector protein RILP controls lysosomal transport by inducing the recruitment of dynein-dynactin motors. Current biology : CB 11: 1680-5.

13 Johansson M, Rocha N, Zwart W, Jordens I, et al. 2007. Activation of endosomal dynein motors by stepwise assembly of Rab7-RILP-p150Glued, ORP1L, and the receptor betalII spectrin. The Journal of cell biology 176: 459-71.

14 Pankiv S, Alemu EA, Brech A, Bruun JA, et al. 2010. FYCO1 is a Rab7 effector that binds to LC3 and PI3P to mediate microtubule plus end-directed vesicle transport. The Journal of cell biology 188: 253-69.

15 Rosa-Ferreira C, Munro S. 2011. Arl8 and SKIP act together to link lysosomes to kinesin-1. Developmental cell 21: 1171-8.

16 McEwan DG, Richter B, Claudi B, Wigge C, et al. 2015. PLEKHM1 regulates Salmonella-containing vacuole biogenesis and infection. Cell host & microbe 17: 58-71.

17 Friedman JR, Dibenedetto JR, West M, Rowland AA, et al. 2013. Endoplasmic reticulum-endosome contact increases as endosomes traffic and mature. Molecular biology of the cell 24: 1030-40.

18 Johansson M, Lehto M, Tanhuanpaa K, Cover TL, et al. 2005. The oxysterol-binding protein homologue ORP1L interacts with Rab7 and alters functional properties of late endocytic compartments. Molecular biology of the cell 16: 5480-92.
19 Vihervaara T, Uronen RL, Wohlfahrt G, Bjorkhem I, et al. 2011. Sterol binding by OSBP-related protein 1L regulates late endosome motility and function. Cellular and molecular life sciences : CMLS 68: 537-51.
20 Rocha N, Kuijl C, van der Kant R, Janssen L, et al. 2009. Cholesterol sensor ORP1L contacts the ER protein VAP to control Rab7-RILP-p150 Glued and late endosome positioning. The Journal of cell biology 185: 1209-25.
21 Suchanek M, Hynynen R, Wohlfahrt G, Lehto M, et al. 2007. The mammalian oxysterol-binding protein-related proteins (ORPs) bind 25-hydroxycholesterol in an evolutionarily conserved pocket. The Biochemical journal 405: 473-80.
22 Ikonen E. 2008. Cellular cholesterol trafficking and compartmentalization. Nature reviews Molecular cell biology 9: 125-38.
23 Shirane M, Nakayama KI. 2006. Protrudin induces neurite formation by directional membrane trafficking. Science (New York, NY) 314: 818-21.
24 Gruenberg J. 2003. Lipids in endocytic membrane transport and sorting. Current opinion in cell biology 15: 382-8.
25 Matsuzaki F, Shirane M, Matsumoto M, Nakayama KI. 2011. Protrudin serves as an adaptor molecule that connects KIF5 and its cargoes in vesicular transport during process formation. Molecular biology of the cell 22: 4602-20.
26 Gillooly DJ, Morrow IC, Lindsay M, Gould R, et al. 2000. Localization of phosphatidylinositol 3-phosphate in yeast and mammalian cells. The EMBO journal 19: 4577-88.
27 Velichkova M, Juan J, Kadandale P, Jean S, et al. 2010. Drosophila Mtm and class II PI3K coregulate a PI(3)P pool with cortical and endolysosomal functions. The Journal of cell biology 190: 407-25.
28 Lebrand C, Corti M, Goodson H, Cosson P, et al. 2002. Late endosome motility depends on lipids via the small GTPase Rab7. The EMBO journal 21: 1289-300.
29 Vale RD, Funatsu T, Pierce DW, Romberg L, et al. 1996. Direct observation of single kinesin molecules moving along microtubules. Nature 380: 451-3.
30 Reck-Peterson SL, Yildiz A, Carter AP, Gennerich A, et al. 2006. Single-molecule analysis of dynein processivity and stepping behavior. Cell 126: 335-48.
31 Ross JL, Ali MY, Warshaw DM. 2008. Cargo transport: molecular motors navigate a complex cytoskeleton. Current opinion in cell biology 20: 41-7.
32 Saita S, Shirane M, Natume T, Iemura S, et al. 2009. Promotion of neurite extension by protrudin requires its interaction with vesicle-associated membrane protein-associated protein. The Journal of biological chemistry 284: 13766-77.
33 Kaiser SE, Brickner JH, Reilein AR, Fenn TD, et al. 2005. Structural basis of FFAT motif-mediated ER targeting. Structure (London, England : 1993) 13: 1035-45.
34 Rowland AA, Chitwood PJ, Phillips MJ, Voeltz GK. 2014. ER contact sites define the position and timing of endosome fission. Cell 159: 1027-41.
35 Raiborg C, Wenzel EM, Stenmark H. 2015. ER-endosome contact sites: molecular compositions and functions. The EMBO journal 34: 1848-58.
36 Gautreau A, Oguievetskaia K, Ungermann C. 2014. Function and regulation of the endosomal fusion and fission machineries. Cold Spring Harbor perspectives in biology 6.
37 Hunt SD, Townley AK, Danson CM, Cullen PJ, et al. 2013. Microtubule motors mediate endosomal sorting by maintaining functional domain organization. Journal of cell science 126: 2493-501.
38 Hashimoto Y, Shirane M, Matsuzaki F, Saita S, et al. 2014. Protrudin regulates endoplasmic reticulum morphology and function associated with the pathogenesis of hereditary spastic paraplegia. The Journal of biological chemistry 289: 12946-61.
39 Swanson J, Bushnell A, Silverstein SC. 1987. Tubular lysosome morphology and distribution within macrophages depend on the integrity of cytoplasmic microtubules. Proceedings of the National Academy of Sciences of the United States of America 84: 1921-5.
40 Vyas JM, Kim YM, Artavanis-Tsakonas K, Love JC, et al. 2007. Tubulation of class II MHC compartments is microtubule dependent and involves multiple endolysosomal membrane proteins in primary dendritic cells. Journal of immunology (Baltimore, Md : 1950) 178: 7199-210.
41 Yu L, McPhee CK, Zheng L, Mardones GA, et al. 2010. Termination of autophagy and reforma-

tion of lysosomes regulated by mTOR. Nature 465: 942-6.
42 Mrakovic A, Kay JG, Furuya W, Brumell JH, et al. 2012. Rab7 and Arl8 GTPases are necessary for lysosome tubulation in macrophages. Traffic (Copenhagen, Denmark) 13: 1667-79.
43 van der Kant R, Neefjes J. 2014. Small regulators, major consequences - Ca(2)(+) and cholesterol at the endosome-ER interface. Journal of cell science 127: 929-38.
44 Du X, Kumar J, Ferguson C, Schulz TA, et al. 2011. A role for oxysterol-binding protein-related protein 5 in endosomal cholesterol trafficking. The Journal of cell biology 192: 121-35.
45 van der Kant R, Zondervan I, Janssen L, Neefjes J. 2013. Cholesterol-binding molecules MLN64 and ORP1L mark distinct late endosomes with transporters ABCA3 and NPC1. Journal of lipid research 54: 2153-65.
46 Alpy F, Rousseau A, Schwab Y, Legueux F, et al. 2013. STARD3 or STARD3NL and VAP form a novel molecular tether between late endosomes and the ER. Journal of cell science 126: 5500-12.
47 Eden ER, White IJ, Tsapara A, Futter CE. 2010. Membrane contacts between endosomes and ER provide sites for PTP1B-epidermal growth factor receptor interaction. Nature cell biology 12: 267-72.
48 Elbaz Y, Schuldiner M. 2011. Staying in touch: the molecular era of organelle contact sites. Trends in biochemical sciences 36: 616-23.
49 Helle SC, Kanfer G, Kolar K, Lang A, et al. 2013. Organization and function of membrane contact sites. Biochimica et biophysica acta 1833: 2526-41.
50 Russo GJ, Louie K, Wellington A, Macleod GT, et al. 2009. Drosophila Miro is required for both anterograde and retrograde axonal mitochondrial transport. The Journal of neuroscience : the official journal of the Society for Neuroscience 29: 5443-55.
51 Kornmann B, Osman C, Walter P. 2011. The conserved GTPase Gem1 regulates endoplasmic reticulum-mitochondria connections. Proceedings of the National Academy of Sciences of the United States of America 108: 14151-

Chapter 2: Cholesterol and ORP1L-mediated ER contact sites control autophagosome transport and fusion with the endocytic pathway.

Ruud H Wijdeven [1], Hans Janssen [1], Leila Nahidiazar [1], Lennert Janssen [1,2], Kees Jalink [1], Ilana Berlin [1,2] and Jacques Neefjes [1,2]

[1] Division of Cell Biology, The Netherlands Cancer Institute, Plesmanlaan 121, 1066CX Amsterdam, the Netherlands.

[2] Department of Chemical Immunology, Leiden University Medical Center LUMC, 2300 RC Leiden, the Netherlands

Nature Communications. 2016 June 10; 7:11808

Abstract

Autophagy is the main homeostatic pathway guiding cytosolic materials for degradation by the lysosome. Maturation of autophagosomes requires their transport towards the perinuclear region of the cell, with key factors underlying both processes still poorly understood. Here, we show that transport and positioning of late autophagosomes depends on cholesterol, by way of the cholesterol-sensing Rab7 effector ORP1L. ORP1L localizes to late autophagosomes and—under low cholesterol conditions—contacts the ER protein VAP-A, forming ER-autophagosome contact sites, which prevent minus-end transport by the Rab7-RILP-dynein complex. ORP1L-mediated contact sites also inhibit localization of PLEKHM1 to Rab7, PLEKHM1 which, together with RILP, recruits the HOPS complex for fusion of autophagosomes with late endosomes and lysosomes. Thus, ORP1L, via its liganding by lipids and the formation of contacts between autophagic vacuoles and the ER, governs the last steps in autophagy that lead to the lysosomal degradation of cytosolic material.

Introduction

Autophagy is the primary pathway for degradation of cytosolic material, protein aggregates and damaged organelles in lysosomes (Lys), with its de-regulation implicated in neurodegenerative diseases, compromised immunity and cancer [1-3]. Cargo destined for such proteolysis becomes sequestered into double-membraned autophagosomes, lined with the distinguishing modifier LC3. Following membrane closure these structures fuse with lysosomes, giving rise to a hybrid organelle—the autolysosome. Alternatively, autophagosomes progress through an intermediate amphisome stage—the result of fusion with late endosomes (LEs)—and subsequently mature by acquiring lysosomal characteristics or merge with pre-existing lysosomes in a secondary fusion event [4]. While many of the essential molecular players for these processes have been identified, our understanding of the underlying factors controlling transport and fusion of autophagic vacuoles (AVs, that include autophagosomes, amphisomes and autolysosomes) remains incomplete.

Entry of autophagic cargoes into the endocytic system is orchestrated by components from both the autophagosome and the late endosomal/lysosomal (LE/Ly) side. A complex consisting of autophagosome-localized ATG14L, the SNAREs STX17 and SNAP29 as well as endosomal VAMP8 has recently been shown to execute the heterologous autophagosome/LE (or autophagosome/Ly) fusion event [5-8]. Tethering of the participating membranes, which precedes fusion, critically depends on both STX176 and the GTPase Rab7 [9-12], with the latter likely provided by the endosome. STX17 has been shown to recruit the homotypic fusion and vacuole protein-sorting (HOPS) complex, which is thought to bridge the two organelles, thus facilitating their unification by SNARE proteins [13-16]. Additionally, PLEKHM1 as well as RILP—both effectors of Rab7—can bind HOPS [15,17-20], with PLEKHM1 reportedly involved in autophagosome-LE/Ly fusion [17]. The above tethering and fusion proteins are recruited to the autophagosome/LE (or Ly) interface in a stimulus-dependent manner [14,17], suggesting existence of additional factors to influence and fine-tune the fusion process.

Entry of autophagosomes into the late endosomal/lysosomal pathway requires

dynein motor-mediated transport towards the microtubule organizing center (MTOC) [21-26], where most lysosomes reside. However, the nature of motor recruitment control and its effects on transport of autophagosomes is largely unknown. During maturation, autophagosomes acquire Rab7, typically relegated to the LE/Ly [9,10,27], perhaps as a result of fusion with these compartments. On endosomes, Rab7 can associate with several effectors, including RILP, which recruits the dynein-dynactin motor for minus-end transport [28, 29]. Whether autophagosomes utilize this Rab7-associated transport and fusion machinery en route to the lysosome, and if so, what factors control this process, is not known.

Here, we show that transport of autophagosomes is governed by two Rab7 effectors—RILP and the cholesterol-sensor ORP1L. ORP1L localizes to amphisomes and autolysosomes and, under low cholesterol conditions, contacts the ER protein VAP-A to form intimate membrane contact sites (MCSs) with the ER. These ER-autophagosome MCSs prevent dynactin binding to RILP, thus blocking dynein-mediated transport. Furthermore, ORP1L in its low cholesterol state acts as a negative regulator of AV/LE fusion and prevents binding of both PLEKHM1 and HOPS by Rab7-RILP. Thus, our study reveals a molecular mechanism whereby ORP1L, via its liganding by lipids and the formation of contacts between AVs and the ER, controls the degradation of cytosolic components by autophagy.

Results

Cholesterol controls autophagosome positioning

Autophagic vacuoles are dynamic compartments that move bi-directionally along microtubules [20,21,28] and mostly encounter lysosomes in the perinuclear region [30]. Intriguingly, steady-state cellular distribution of AVs varies greatly between different cell types. While in cervical HeLa cells AVs are dispersed throughout the cytoplasm, in melanoma MelJuSo cells most structures containing the autophagy marker LC3 localize at the perinuclear region (Fig. 1a). Since intracellular AV position is determined by the activities of kinesin and dynein motor proteins [21,22,31] common to all cells, these differences might arise from variations in motor activity or recruitment. Strikingly, MelJuSo cells also contain more (endosomal) cholesterol (Fig. 1a), known to promote localization of endosomes and lysosomes at the microtubule minus-end [32,33], close to the nucleus, raising the possibility that AV transport is modulated by endosomal cholesterol levels.

To test this, we reduced cholesterol levels in cells using statin (to inhibit endogenous cholesterol production, supplemented with mevalonate to provide essential nonsteroidal isoprenoids) and lipid-free serum (to inhibit the major source of cholesterol for cells as taken up through the LDL receptor) [34]. In addition, we accumulated cholesterol in the endosomal compartment by exposure of cells to U18666A [32,34], an inhibitor of the endosomal cholesterol exporter NPC1 [35]. Strikingly, in the case of lipid depletion, AVs were found to scatter throughout the cytoplasmic space and accumulate at the tips of the cell, while they concentrated at the perinuclear region under conditions resulting in accumulated endosomal cholesterol. This was observed both in MelJuSo and HeLa cells, as well as for statin and lipid free serum separately, ruling out non-cholesterol mediated effects caused by statin (Fig.

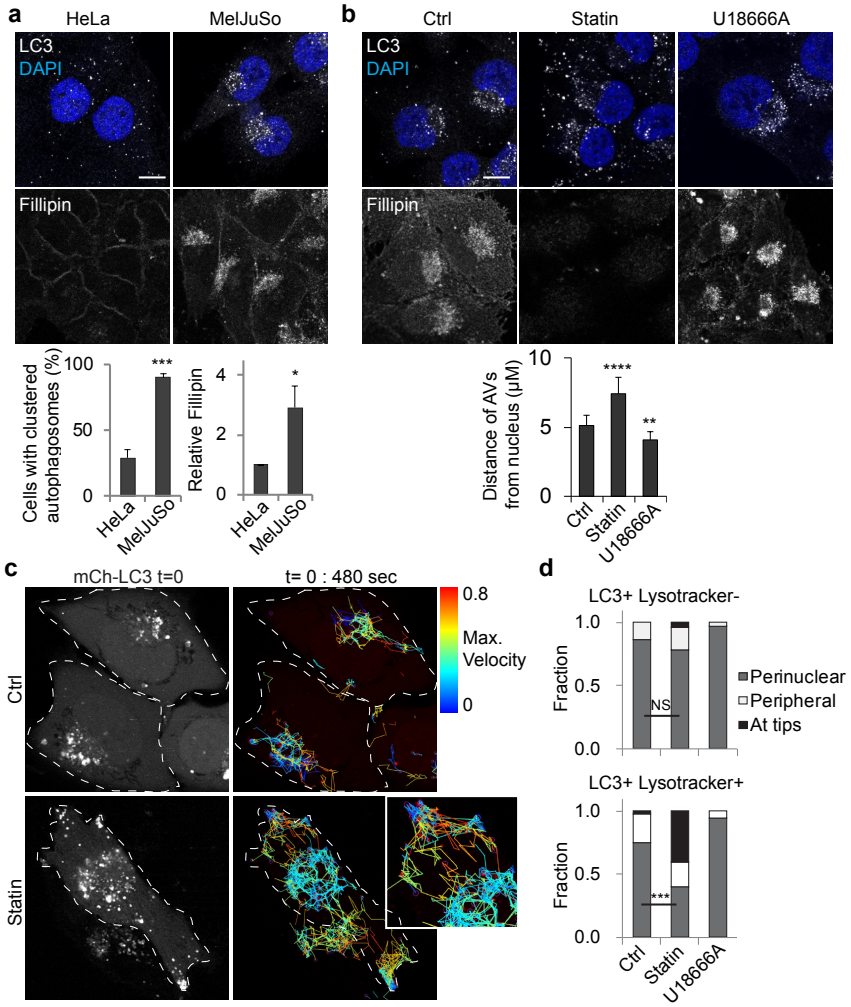


Figure 1. Cholesterol modulates autophagosome positioning. *(a) HeLa or MelJuSo cells were stained for LC3 and DAPI, or with filipin to detect cholesterol. Scale bar, 10μm. Panels below: quantification for the presence of a detectable perinuclear LC3 cluster: >100 cells were analyzed per experiment. For filipin labeling, signal intensity was measured for at least 3 fields per experiment and normalized to signal intensity in HeLa cells, which was set at 1. Bars indicate mean+SD from independent triplicates, significance calculated using Student's t-test. (b) MelJuSo cells cultured for 24h under cholesterol-depleting conditions (see materials and methods) or exposed for 24 hrs to 3μM U18666 were stained for LC3 and DAPI. Scale bar, 10μm. Lower panel: quantification of the average distance (μm) of the AVs from the nucleus (by LasAF software), from >10 cells per experiment. Bars indicate mean+SD from independent triplicates, significance calculated using Student's t-test. (c) Distribution and dynamics of mCherry-LC3 marked vesicles in control versus lipid-depleted MelJuSo cells. Confocal image at start of time-lapse is shown on the left, vesicle trajectories over a 480 sec interval are displayed on the right. Colors of individual vesicle trajectories reflect maximal displacement rate (blue=0, red=0.8 μm/sec) achieved during 480 sec interval. Scale bar, 10 μm. (d) Quantification of the localization of mCherry-LC3 vesicles either or not labeling for Lysotracker in MelJuSo cells treated as indicated. At least five cells per replicate were quantified, bars indicate mean+SD from independent triplicates. Significance calculated using Student's t-test. Corresponding Movies 1-3. NS Not significant, * $p < 0.05$, ** $p < 0.01$, *** $p < 0.001$, **** $p < 0.0001$). AV: Autophagic Vacuole.*

1b and Supplementary Fig. 1a and 1b). To follow the dynamics of these AVs, we performed live-cell imaging using mCherry-LC3 and Lysotracker to label AVs and the late endocytic compartments. This indicated that the AVs localizing to the tips under low cholesterol conditions were relatively static and remained located at their position for prolonged periods of time (Fig. 1c), suggesting a defect in microtubule-based minus-end transport. Furthermore, the majority of these peripheral AVs labelled positive for Lysotracker (Fig. 1d), as well as for Rab7 (Supplementary Fig. 1c), defining them as late or mature autophagosomes (amphisomes and autolysosomes). Thus, manipulating cholesterol affects the transport dynamics of late autophagosomes.

ORP1L senses cholesterol to regulate autophagosome transport

A key distinguishing characteristic between early and late AVs is the presence of Rab7 [36], suggesting that Rab7 effectors could be responsible for cholesterol-dependent late autophagosome re-localization. We, and others, have previously shown that the Rab7 effector ORP1L acts as a cholesterol sensor on late endosomes [33,37]. Upon (membrane) cholesterol binding by its ORD domain, ORP1L maintains a conformation compatible with dynein motor recruitment and minus-end transport, while absence of cholesterol prevents this [33,37]. Silencing ORP1L in MelJuSo cells indeed reduced the fraction of AVs localizing at the cell periphery under basal conditions (Fig. 2a and Supplementary Fig. 2a). Furthermore, ORP1L knockdown strongly inhibited AV scattering caused by cholesterol depletion (Fig. 2a), illustrating a critical role for ORP1L in cholesterol-mediated AV repositioning. To test whether cholesterol controls positioning directly via ORP1L, we expressed GFP-tagged wild-type ORP1L or variants altering its cholesterol sensing properties (Fig. 2b). These were: ΔORD, lacking the cholesterol-interacting ORD domain (thereby mimicking the non-cholesterol bound state of ORP1L and acting as a cholesterol independent inhibitor of dynein recruitment, since this variant cannot be inactivated by cholesterol) and ΔORDPHDPHD, where the ORD domain is replaced by a tandem membrane-targeting PH domain (PHD) to reflect the membrane-bound high cholesterol state (acting as a cholesterol-independent permissive factor for dynein binding, since the tandem PHD domains remain membrane bound and allow dynein recruitment, mimicking the high cholesterol state even under conditions of low cholesterol) [33] (modeled in Supplementary Fig. 2b). These constructs mimic the low or high late endosomal cholesterol states, respectively, independently of the actual cholesterol concentration, since the ORD domain has been removed [33]. Expression of ORP1L and especially ORP1L-ΔORD, but not ORP1L-ΔORDPHDPHD, resulted in profound scattering of AVs (Figs. 2c and 2d), indicating that ORP1L regulates AV positioning as a function of its cholesterol-bound state. Importantly, cholesterol depletion induced scattering of AVs in cells ectopically expressing GFP, but had no effect on cells expressing ORP1L-ΔORDPHDPHD, implying that low cholesterol levels had the effect through the ORP1L protein (Fig. 2d and Supplementary Fig. 2c). In line with this, GFP-ORP1L and even more pronounced the ORP1LΔORD construct resisted AV clustering following cholesterol accumulation by U18666A, unlike GFP or the ORP1LΔORDPHDPHD construct mimicking the high-cholesterol form of ORP1L (Fig. 2d and Supplementary Fig. 2c). While cholesterol manipulation of cells may result in several effects on lipids and proteins, the fact that the low and high-choles-

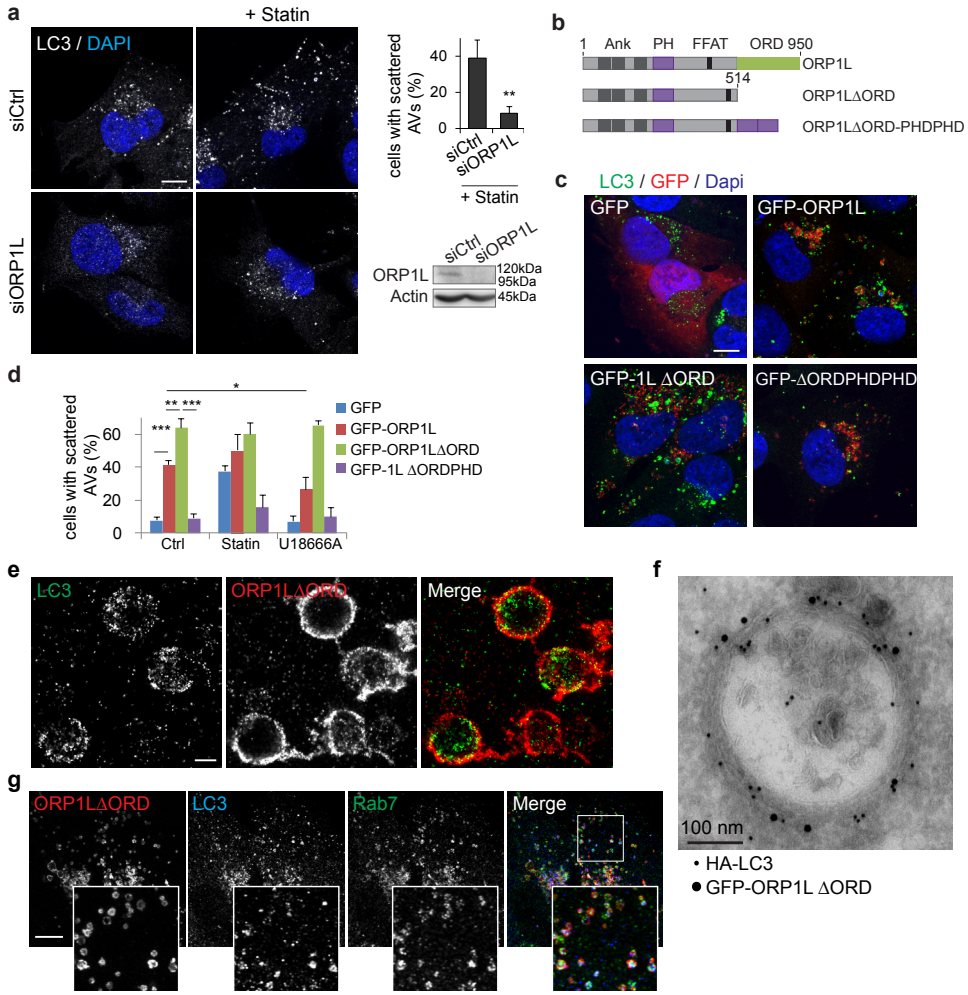


Figure 2. ORP1L senses cholesterol to control autophagosome positioning. *(a) MelJuSo cells transfected with siCtrl or siORP1L were either or not cultured under lipid-depleted conditions and stained for LC3 and DAPI. Scale bar, 10μm. Top right: quantification of scattering of LC3 structures under lipid-depleted conditions, over >100 cells were counted per experiment, bars indicate mean+SD from three experiments. Means were compared using Student's t-test. Lower right: Western blot to validate silencing of ORP1L. (b) Overview of the ORP1L constructs and their domains used in this study. The C-terminal ORD domain binds oxysterols. (c) MelJuSo cells transfected with the indicated GFP-tagged constructs were fixed and stained for LC3 and DAPI. Scale bar, 10μm. (d) Quantification of cells with scattered autophagic vesicles in cells under different cholesterol manipulation conditions and expressing different GFP-tagged constructs, as shown in panel d and Figure S2b. Quantification was performed on >50 transfected cells per experiment, bars indicate mean+SD from independent triplicates. Significance calculated using Student's t-test. (e) Superresolution microscopy on cells expressing HA-ORP1LΔORD, stained for HA and LC3, as indicated. Scale bar, 500nm (f) Cryo-immuno-EM on HeLa cells expressing HA-LC3 and GFP-ORP1LΔORD stained with HA10nm and GFP15nm gold antibodies, respectively. Scale bar, 100nm. (g) MelJuSo cells expressing GFP-ORP1LΔORD were fixed and stained for Rab7 and LC3. Scale bar, 10μm. * p < 0.05, ** p < 0.01, *** p < 0.001. AV: Autophagic Vacuole.*

terol state configurations of ORP1L override these effects suggests that the effects of cholesterol on AV positioning are largely ORP1L mediated.

To investigate which AV substructures are subject to regulation by ORP1L we investigated the types of structures ORP1L localized to. As assessed by superresolution Total Internal Reflection (TIRF) microscopy, ORP1L localized to the limiting mem-

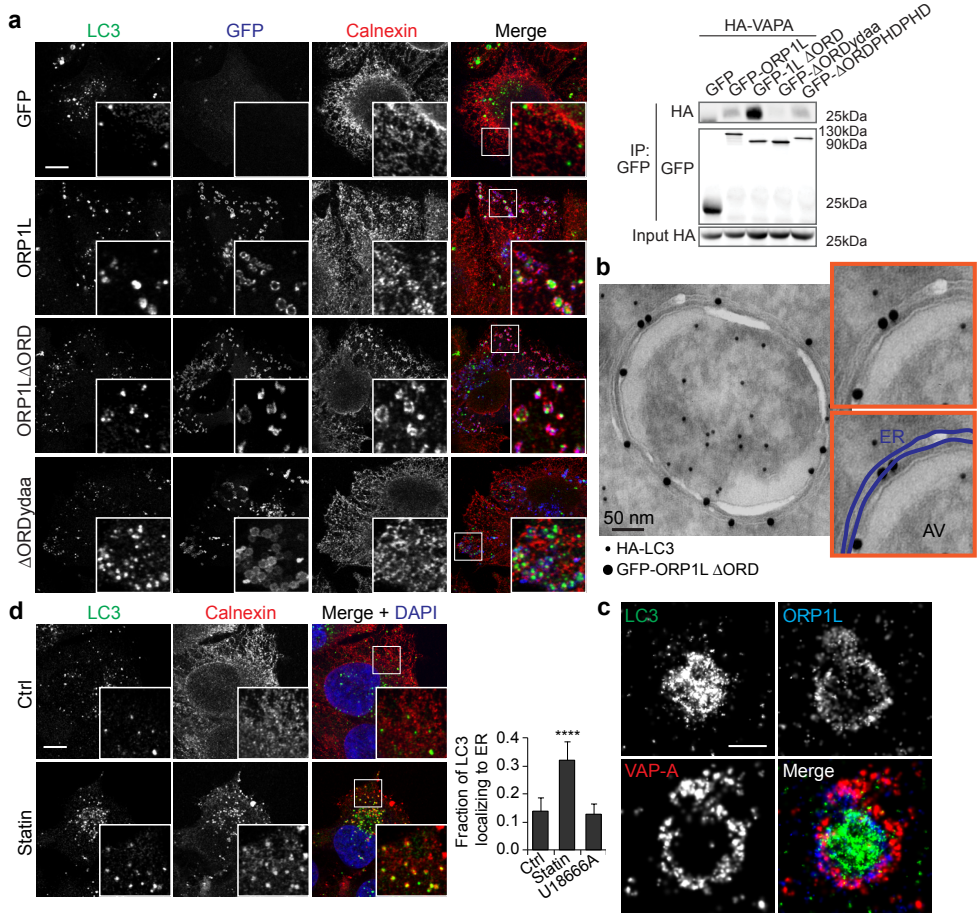


Figure 3. ORP1L and VAP-A form cholesterol dependent ER-AV contact sites *(a) MelJuSo cells expressing GFP or GFP-tagged ORP1L mutants were fixed and stained for LC3 and Calnexin. Y477 and D478 in the FFAT motif were mutated to alanines (A) in the ORP1L ydaa mutant. Scale bar, 10µm. Right: Co-immunoprecipitation for ORP1L (mutants) with VAP-A. GFP-ORP1L mutants or GFP were isolated from lysates of HEK293T cells co-overexpressing HA-VAPA using GFP-Trap beads. Western blot filters were probed for isolated GFP-tagged proteins, the associated HA-VAP-A and the input HA-VAP-A, as indicated. (b) Cryo-immuno-EM on HeLa cells expressing HA-LC3 and GFP-ORP1LΔORD, as detected by HA10nm and GFP15nm gold antibodies. Insets show ORP1L labeling in the membrane contact site between ER and autophagosome. The membranes of the ER are depicted in the bottom inset. Scale bar, 50nm. (c) Three-color superresolution image of an autophagosomal vesicle labelled by LC3 (green), ORP1L (blue) and the ER protein VAP-A (red). Scale bar, 500 nm (d) MelJuSo cells cultured either in lipid depleted serum or control medium were fixed and stained for LC3 and ER marker Calnexin. Scale bar, 10µm. Right panel: Manders coefficient for LC3 localization to the ER was calculated on at least 10 cells over three independent experiments. Bars indicate mean+SD. Student's t-test statistical analysis (**** $p < 0.0001$).*

brane of AVs, (Fig. 2e), which was confirmed by cryo-immuno-EM, where ORP1L was found to localize to single-membrane AVs, which defines them as amphisomes or autolysosomes (Fig. 2f). In support of this, all ORP1L marked AVs co-labelled for Rab7 (Fig. 2g and Supplementary Fig. 2d). Together, these data suggest that cholesterol as sensed by OPR1L dictates the intracellular position of Rab7-marked late autophagosomes.

Low cholesterol and ORP1L yield of ER-AV contact sites

When recruited to LE by Rab7, ORP1L has a conformational state allowing interactions with ER-protein VAP-A to establish a membrane contact site (MCS) between these two compartments. VAP-A then controls the binding of the dynein motor to RILP [33, 38]. This interaction with VAP-A is stabilized by mutating or deleting the ORD domain of ORP1L and is promoted by low cholesterol culture conditions ([38] and Fig. 3a). To assess whether ORP1L has the ability to form physical contacts between late autophagosomes and the ER, coincidence of ER marker calnexin and LC3 was detected as a function of ORP1L mutants. Robust distribution of (calnexin-positive) ER pockets to LC3+ structures occurred in the presence of either ORP1L or ORP1LΔORD, and could be prevented by eliminating the VAP-A binding site FFAT in the latter (by mutating Y477 and D478 into alanines, Fig. 3a). Typical MCSs are characterized by a spatial separation of less than 10-30nm between two compartments [39], which required analyses of these contact sites by EM and superresolution light microscopy. Cryo-immuno-EM showed long stretches of ER closely positioned to vesicles positive for both ORP1L and LC3 (Fig. 3b and Supplementary Fig. 3a). 3-Colour superresolution TIRF microscopy confirmed the existence of VAP-A – ORP1L contacts on LC3 positive structures, with AVs containing ORP1L significantly surrounded by ER protein VAP-A (Fig. 3c). At this level of resolution, ORP1L was again found at the limiting membrane and surrounded by VAP-A, covering major parts of the vesicle.

Similar to overexpression of ORP1L and ORP1LΔORD, cholesterol depletion profoundly stimulated re-distribution of the ER towards LC3 puncta, creating a distinct punctate ER contacting the LC3+ structures (Fig. 3d and Supplementary Fig. 3b). Notably, silencing of either ORP1L or VAP-A reduced these ER contacts with LC3 in the cell periphery, while perinuclear MCSs were only sensitive to silencing VAP-A (Supplementary Fig. 3c). This suggests that cholesterol controls the formation of ORP1L – VAP-A contact sites, as well as contact sites between VAP-A and a different autophagosomal protein. Together, these results visualized a novel membrane contact site, one between late autophagosomes and the ER.

RILP regulates transport of late autophagosomes

On LE/Ly, ORP1L forms a tripartite complex with Rab7 and RILP and controls binding of the dynein motor complex to RILP [33,40]. RILP is also found on AVs and its recruitment to Rab7 is enhanced under conditions that promote the autophagic flux [41], suggesting that RILP could also drive dynein acquisition on late autophagosomes—and is by extension sensitive to ORP1L. To assess this, we silenced RILP in MelJuSo cells, which yielded AV scattering and accumulation in the tips of the cell (Fig. 4a and 4b). Conversely, ectopic expression of RILP in HeLa cells produced

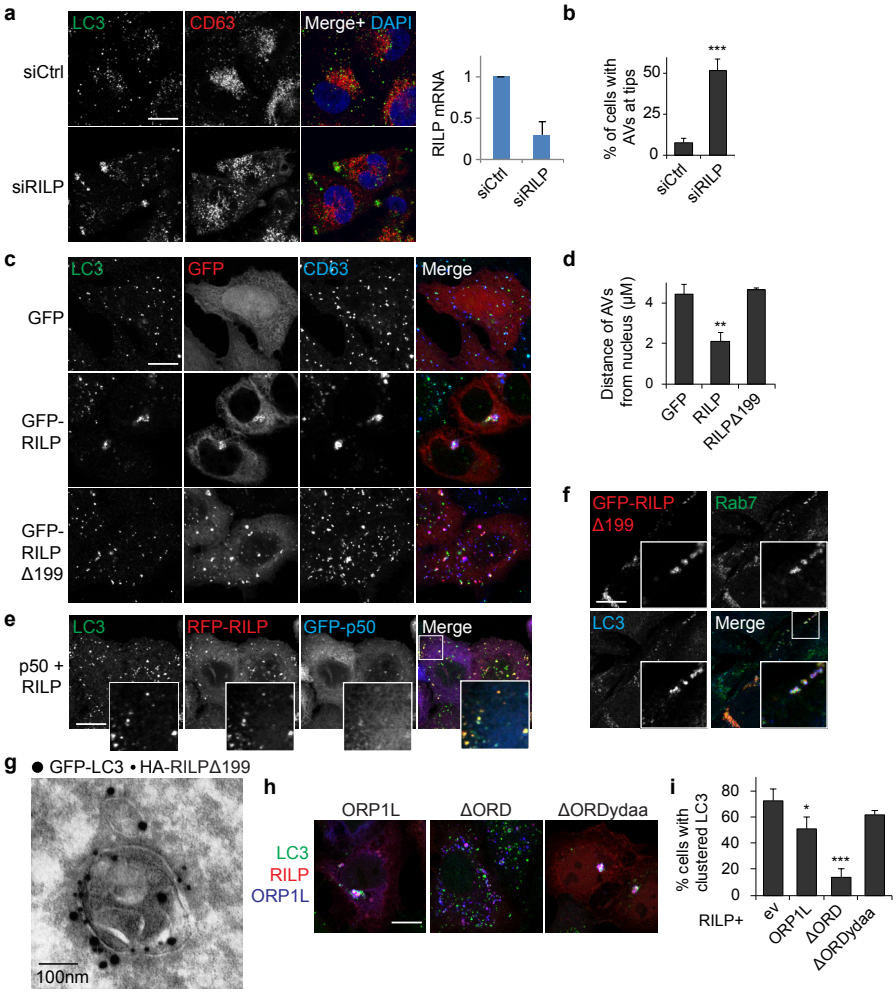


Figure 4. ORP1L controls RILP mediated transport of late autophagosomes. *(a) MelJuSo cells transfected with siCtrl or siRILP were stained for LC3, CD63 and DAPI. Scale bar, 10μm. Right panel; silencing efficiency of RILP was determined by qRT-PCR, RILP signal was normalized to GAPDH. Bars indicate mean+SD of three experiments. (b) Quantification of cells with AVs located at the tips of cells from a, >100 cells per experiment were quantified, bars show mean+SD of three independent replicates. Means were compared using Student's t-test (c) HeLa cells transfected with the indicated constructs were fixed and stained for LC3 and CD63, as indicated. Scale bar, 10μm. (d) Quantification of the average distance (μm) of AVs from the nucleus (by LasAF software) as shown in c, from >10 cells per experiment. Bars display mean+SD of three independent experiments, significance was calculated using Student's t-test. (e) HeLa cells transfected with the indicated constructs were stained for LC3. Scale bar, 10μm (f) MelJuSo cells expressing GFP-RILPΔ199 were stained for Rab7 and LC3. Scale bar, 10μm. (g) Immuno-electron micrograph of a HeLa cell expressing GFP-LC3 and HA-RILPΔ199, detected with 15 nm and 10 nm gold, respectively. Note the single membrane around the LC3 positive structure. Scale bar, 100nm (h) HeLa cells expressing GFP-RILP and HA-tagged ORP1L constructs were fixed and stained for HA and LC3. Scale bar, 10μm. (i) quantification of the number of cells with perinuclear accumulation of LC3 positive structures from h. Quantified >100 cells per experiment. Bars indicate mean+SD from independent triplicate experiments. Student's t-test statistical analysis. * p < 0.05, ** p < 0.01, *** p < 0.001. ev. empty vector control.*

strong clustering of AVs in the perinuclear region (Fig. 4c and 4d), while a RILP mutant deficient in dynein-dynactin interactions [40] (Δ199) left the AVs scattered in the cell periphery. Furthermore, RILP induced recruitment of the dynein-dynactin subunit p150glued to AVs (Supplementary Fig. 4a). RILP-mediated AV repositioning is dynein dependent, as disruption of the dynein motor complex by ectopically expressing p50dynamitin [42], which by itself accumulated AVs at the tips of cells (Supplementary Fig. 4b), negated the perinuclear clustering induced by RILP (Fig. 4e). RILP localized to a fraction of the LC3+ vesicles (Fig. 4e), constituting the Rab7 marked late autophagosomal pool (Fig. 4f). This was further supported by immuno-EM analysis that showed RILP(Δ199) (full length RILP strongly clustered AVs, LEs and Lys in the perinuclear region, thus preventing proper analyses) localizing to the limiting membrane of single membrane autophagosomes (amphisomes and autolysosomes [43]) (Fig. 4g). These data suggest that the Rab7 effector RILP recruits dynein for minus-end transport of mature autophagosomes.
To assess the effect of ORP1L on RILP-mediated transport, we co-expressed RILP with ORP1L. While overexpression of ORP1L had only minor effects on RILP-induced perinuclear clustering of AVs (Fig. 4h and 4i), ORP1LΔORD completely eliminated this clustering, an effect dependent on its ability to bind VAP-A, since mutating the interacting FFAT motif in ORP1LΔORD restored RILP-induced perinuclear clustering. Similar to this, recruitment of dynactin subunit p150glued to AVs was blocked by co-expression of RILP with ORP1LΔORD (Supplementary Fig. 4a). These data indicate that Rab7-effector RILP recruits the dynein motor to late autophagosomes for minus-end transport, and that ORP1L further controls this transport via the formation of ER-contact sites with VAP-A.

ORP1L controls autophagosome maturation

Since transport of AVs is associated to their maturation, we reasoned that ORP1L might inhibit the autophagic flux. Consistent with this, ORP1L silencing reduced the number of LC3+ structures in cells (Fig. 2a and 5a), as well as overall LC3B-II and p62 levels (Fig. 5b). This decrease was negated by blocking lysosomal degradation (Fig. 5b), illustrating that ORP1L depletion spurs the autophagic flux. Decreased p62 levels could imply that ORP1L also controls clearance of ubiquitinated protein aggregates. Aggregate-like induced structures (ALIS) are formed upon cellular stress and recognized by selective autophagy receptors, including p62, for targeting to the autophagic pathway. While ORP1L knockdown had no effect on the generation of puromycin-induced ALIS, the number of cells containing ubiquitinated aggregates at 4h and 6h following puromycin washout was reduced when compared to control cells (Fig. 5c). At these time points most remaining aggregates stained positive for LC3, indicating effective targeting to the autophagosomal pathway. Thus, silencing of ORP1L increases the autophagic flux and the rate of protein aggregate degradation.
Conversely, ectopic expression of ORP1L increased the number of AVs in cells, which was more pronounced by expressing ORP1LΔORD (Fig. 5d). This phenotype was largely corrected for by mutating the VAP-A interacting FFAT motif in ORP1LΔORD. Co-staining with the LE/Ly marker CD63 revealed that overexpression of either ORP1L or ORP1LΔORD increased the numbers of both early (LC3+CD63-) and late

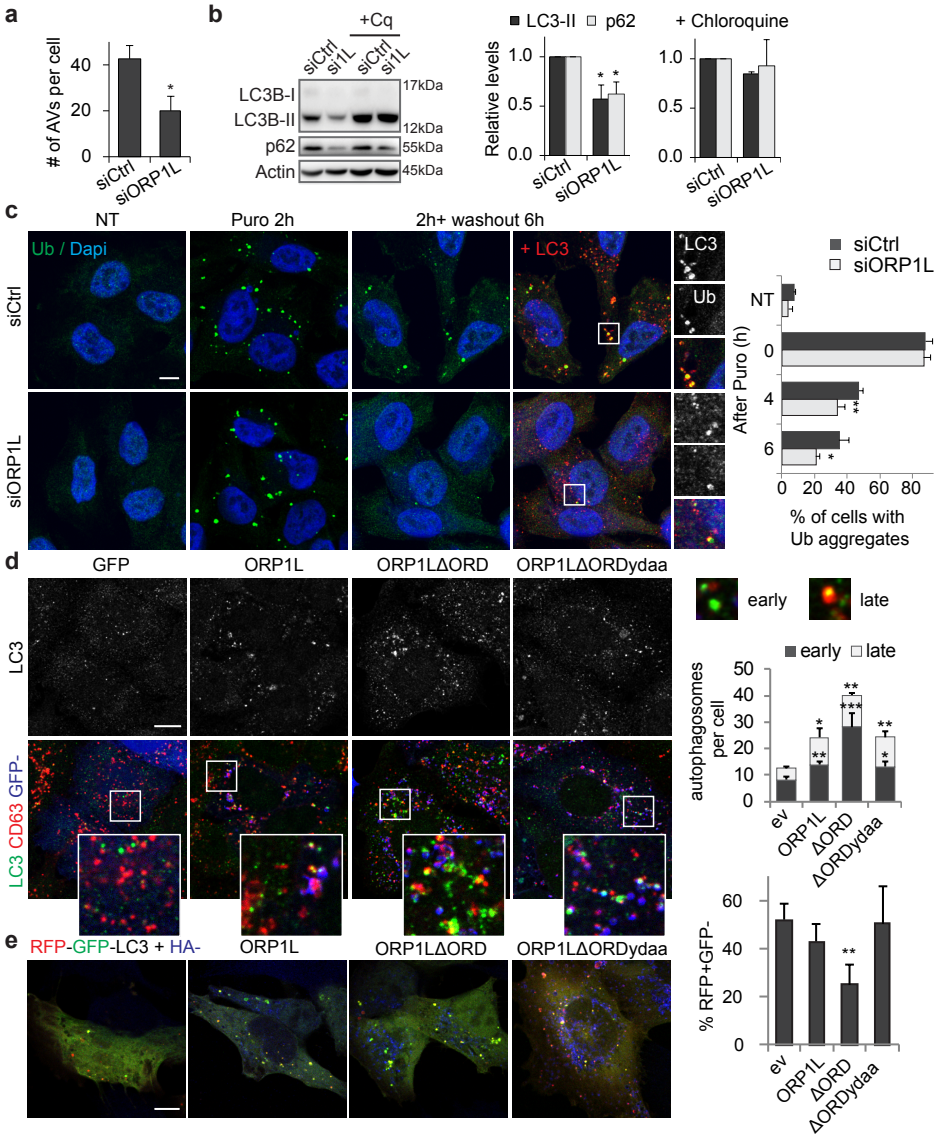


Figure 5. ORP1L controls autophagosome maturation. *(a) Quantification of the number of autophagosomes in MelJuSo cells transfected with siCtrl or siORP1L, from figure 2a. Number of LC3 structures was quantified in >10 cells per experiment, bars show mean+SD from three independent replicates. Means were compared using Student's t-test (b) MelJuSo cells transfected with siCtrl or siORP1L were either or not exposed to 50μM chloroquine for 4h, lysed and analyzed by SDS-PAGE and Western blotting for p62, LC3B and actin. Right panels, quantification of signals for p62 and LC3B-II, corrected for loading (actin) and normalized to siCtrl, untreated (left) and chloroquine treated (right). Bars correspond to mean+SD of three experiments, significance was calculated using Student's t-test. (c) MelJuSo cells transfected with siCtrl or siORP1L were left untreated (NT) or treated with 4μg/ml puromycin for 2hrs. Then, cells were washed and left to recover for the indicated time points before fixation and staining for ubiquitin (Ub), LC3 and DAPI. Scale bar, 10μm. Right panel; quantification of percentage of cells with cytosolic Ub aggregates, >100 cells per experiment and bars represent mean+SD of three independent experiments. Means were compared using Student's t-test (continues on the next page).*

(LC3+CD63+) autophagosomes. Surprisingly, the most significant difference was observed for the early (ORP1L negative) autophagosomes, suggesting that in addition to fine-tuning dynein motor-driven transport, ORP1L controls autophagosome fusion with the LE/Ly. To test this, we used the tandem mRFP-GFP-LC3B construct that contains a pH insensitive mRFP and a pH sensitive GFP molecule to distinguish early (GFP+RFP+) from late (GFP-RFP+) more acidic autophagosomes [12]. Following amino acid starvation to accelerate the autophagic flux, cells expressing the low cholesterol mimic ORP1LΔORD harbored a significantly elevated fraction of early autophagosomes when compared to cells expressing wild-type ORP1L and vector control (Fig. 5e). Thus, ORP1L induced ER contact sites are able to modulate autophagosome maturation.

We then tested whether cholesterol depletion or accumulation would also affect the autophagic flux. Whereas cholesterol lowering conditions did not yield measurable changes in autophagic flux (Supplemental Fig. 5a and b), in agreement with others [44,45], we found that increased lysosomal cholesterol levels prevented autophagosome-LE/Ly fusion (positioning them in very close proximity, Supplementary Fig. 5a and 5b). Since cholesterol reduction affects many cellular processes, it could be that compensatory mechanisms are in place, or that the cholesterol reduction is not strong enough to observe an effect on autophagic flux. Yet, the observed block in fusion with ORP1LΔORD suggests a role for endosomal cholesterol in autophagosome maturation.

ORP1L controls recruitment of PLEKHM1 and HOPS to Rab7-RILP

The observations that ORP1L blocks autophagosome-LE/Ly fusion, together with the preferential localization of ORP1L to Rab7-positive compartments, suggest that ORP1L likely affects fusion between autophagosomes and LE/Lys from the latter side. Recent work has implicated the Rab7 effector PLEKHM1 as pertinent to this fusion step [17]. To test a possible functional interplay between ORP1L and PLEKHM1, we co-expressed GFP-tagged PLEKHM1 with ORP1L and its mutants. Strikingly, ectopic expression of ORP1LΔORD inhibited distribution of PLEKHM1 to Rab7, yielding cytosolic PLEKHM1 instead (Fig. 6a). Mutating the VAP-A interacting FFAT motif of ORP1L restored acquisition of PLEKHM1 by Rab7, suggesting that ORP1L does not simply compete with PLEKHM1 for Rab7 binding space, but rather actively informs PLEKHM1 recruitment in a manner dependent on the association with the ER protein VAP-A.

To mediate fusion, PLEKHM1 binds the HOPS complex, a multiprotein complex organizing the SNARE proteins for fusion [46], likely through a direct interaction with

*Figure 5 (continued) (d) HeLa cells expressing theindicated GFP-tagged constructs were fixed and stained for LC3, CD63 and DAPI. Scale bar, 10μm. Right panel; quantification of LC3+CD63- (early, green) and LC3+CD63+ (late, yellow) autophagosomes detected in cells with indicated expressed proteins. Quantification of at least 10 cells per experiment, bars represent mean+SD of three independent experiments. Significance calculated using Student's t-test (e) MelJuSo cells expressing the indicated HA-tagged constructs in combination with the mRFP-GFP-LC3 tandem construct were starved for 4hrs, fixed and stained for HA. Scale bar, 10μm. Right panel: quantification of percentage of RFP-only LC3 structures relative to total LC3 labeled structures. Quantification of at least 10 cells per experiment is shown. Bars indicate mean+SD from independent triplicate experiments, statistical analysis using Student's t-test. * $p < 0.05$, ** $p < 0.01$, *** $p < 0.001$. ev: empty vector.*

HOPS subunit VPS39 [17]. Whether this interaction drives recruitment of the entire HOPS complex to Rab7 is unknown. To test this, we expressed several HOPS subunits in combination with PLEKHM1. While all subunits tested were cytosolic when expressed on their own, co-expression of PLEKHM1 relocalized both VPS39 and

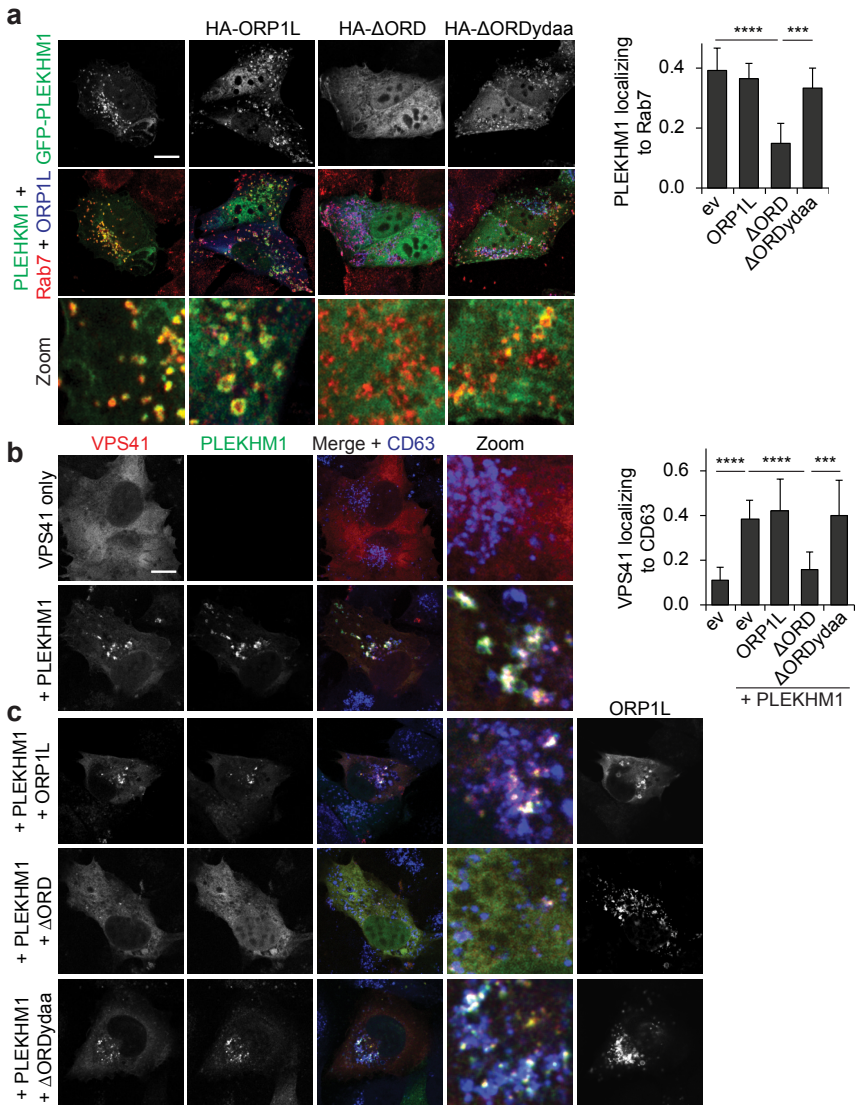


Figure 6. ORP1L regulates recruitment of PLEKHM1 and HOPS to Rab7 positive vesicles. *(a) MelJuSo cells expressing GFP-tagged PLEKHM1 and the indicated HA-tagged ORP1L mutants were fixed and stained for Rab7. Scale bar, 10µm. Right panel: Manders coefficient for PLEKHM1 localization to Rab7, as determined for >10 cells in three experiments. Bars represent mean+SD and significance calculated using Student's t-test. (b-c) MelJuSo cells were transfected with GFP-tagged PLEKHM1, mRFP-VPS41 and the indicated HA-tagged ORP1L mutants and stained for CD63. Manders coefficient for VPS41 localization to CD63 was determined for >10 cells in three experiments. Bars display mean+SD, means were compared using Student's t-test. *** p < 0.001, **** p < 0.0001. ev: empty vector.*

VSPS41 to LEs/Lys (Fig. 6b and Supplementary Fig. 6a). No recruitment was observed for an alternate HOPS complex member, VPS33b [16,20] (Supplementary Fig. 6b), implying that PLEKHM1 specifically recruits the HOPS core complex to Rab7. Introduction of ORP1LΔORD blocked membrane distribution of both VPS39 and VPS41, as well as PLEKHM1 in a manner dependent on the FFAT motif (Fig. 6c and Supplementary Fig. 6a). At the same time, ORP1LΔORD had no effect on localization of fusion factor VAMP8 (Supplementary Fig. 6c). These data support the premise that ORP1L-mediated ER-contact sites orchestrate tethering of autophago-

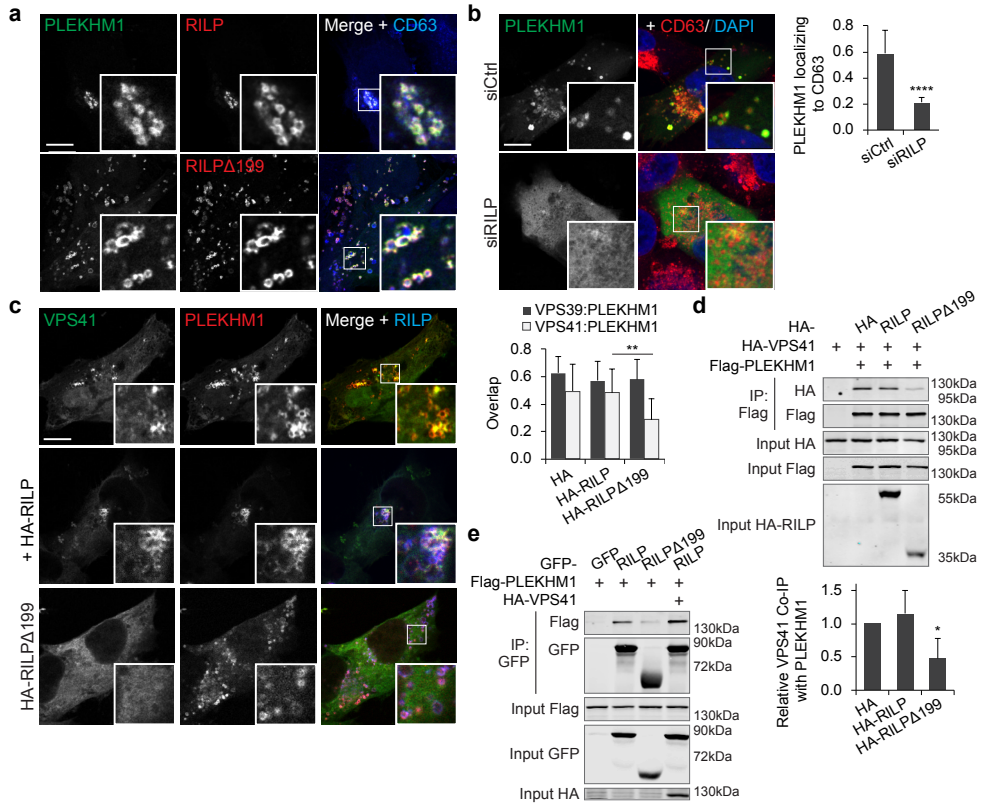


Figure 7. Rab7 effectors PLEKHM1 and RILP cooperate in HOPS complex recruitment. *(a) MelJuSo cells were transfected with GFP-PLEKHM1 and HA-RILP or HA-RILPΔ199 and stained for CD63, as indicated. Scale bar, 10μm. (b) MelJuSo cells silenced for siCtrl or siRilp were transfected with GFP-PLEKHM1 and stained for CD63. Manders coefficient for PLEKHM1 localization to CD63 was calculated for >10 cells over three experiments. Bars display mean+SD, significance determined using Student's t-test. Scale bar, 10μm. (c) MelJuSo cells were transfected with GFP-PLEKHM1 and mRFP-VPS41, together with HA-RILP or HA-RILPΔ199 when indicated. Manders coefficient for VPS39 (Supplementary Fig. 6c) or VPS41 localization to PLEKHM1 was calculated for >10 cells in three individual experiments. Bars represent mean+SD and significance was calculated using Student's t-test. Scale bar, 10μm. (d) Co-immunoprecipitation for Flag-PLEKHM1 and HA-VPS41 in the presence of HA-RILP or HA-RILPΔ199. HEK293T cells were transfected with the indicated constructs and immunoprecipitated for Flag. Bottom: quantification of co-immunoprecipitated HA-VPS41 signal corrected for input and normalized to control, n=4. Bars display mean+SD, means were compared using Student's t-test. (e) Immunoprecipitation for GFP or GFP-tagged RILP constructs in HEK293T cells co-expressing Flag-PLEKHM1 with or without HA-VPS41, as indicated. * p < 0.05, ** p < 0.01, *** p < 0.001, **** p < 0.0001.*

somes with LE/Ly by modulating recruitment of the autophagic effector PLEKHM1, and subsequently that of HOPS, to Rab7.
Besides PLEKHM1, also RILP can recruit the HOPS complex to Rab7, through a direct interaction with VPS41 [15,19]. This begs the question whether both Rab7 effectors—RILP and PLEKHM1—mediate fusion of different vesicular subpopulations, or rather cooperate to recruit HOPS, the latter possibility supported by the requirement for both adaptors in ensuring efficient access of endocytosed EGFR to the LE/Ly compartment [17,47]. RILP and PLEKHM1 robustly co-localized on the same vesicles (Fig. 7a and Supplementary Fig 7a), and silencing RILP relegated PLEKHM1 to the cytosol (Fig. 7b), implying a functional interplay between the two effectors. The latter was not related to the HOPS recruitment capacity of RILP, since the RILPΔ199 mutant (which fails to recruit HOPS15) did not affect endosomal membrane targeting of PLEKHM1 (Fig. 7a and Supplementary Fig. 7a). Furthermore, expression of constitutively active Rab7(Q67L) restored membrane targeting of PLEKHM1 (Supplementary Fig. 7b), indicating that the phenotype is likely a result of an altered activated Rab7 state, as observed previously for effector silencing or overexpression [18,28]. While in the presence of RILPΔ199, PLEKHM1 was still able to recruit VPS39 (Fig. 7c and Supplementary Fig 7c), it poorly recruited VPS41 to endosomes (Fig. 7c). Co-immunoprecipitation experiments confirmed that the interaction between PLEKHM1 and VPS41 was attenuated by RILPΔ199 (Fig. 7d), implying that functional RILP is required for PLEKHM1 to mobilize VPS41 and thus the entire HOPS complex. RILP and PLEKHM1 physically associated with each other, which was strongly reduced by using RILPΔ199, and more efficient when co-expressing VPS41 (Fig. 7e), suggesting that RILP and PLEKHM1 form a complex via HOPS. Together, these observations suggest that the HOPS complex is jointly recruited to LE/Lys by the Rab7 effectors PLEKHM1 and RILP, where PLEKHM1 binds to HOPS subunit VPS39 and RILP to VPS41. Whereas RILP remains associated to Rab7 following formation of ORP1L-VAP-A contact sites by ORP1LΔORD [15], PLEKHM1 and the HOPS complex are released, obstructing fusion of autophagosomes with LEs/Lys (Fig. 8).

Discussion

Autophagic proteolysis of bulky cargoes acquired in the cytosol necessitates their entry into the endocytic system for degradation by lysosomal hydrolases. Endosomes present a challenging target, as they traverse different maturation stages, all while moving quickly between the peripheral and interior regions of the cell. How fusion and transport of autophagosomes are negotiated within this dynamic vesicle network in space and time is poorly understood. Here, we show that maturing autophagosomes hijack late endosomal fusion and transport machinery to access the lysosomal compartment, and in doing so, become subject to endosome-centric regulatory mechanisms. Among these, we identify a negative regulator of autophagosome fusion with the LE/Ly— which functions as a cholesterol sensor poised on receiving vesicles to either license or refute autophagic progression.
Enclosure of cytosolic substrates within LC3+ double-membranes gives rise to early autophagosomes, which mature by fusion with lysosomes or endosomes harboring late characteristics. For fusion to take place, the autophagic membrane-bound

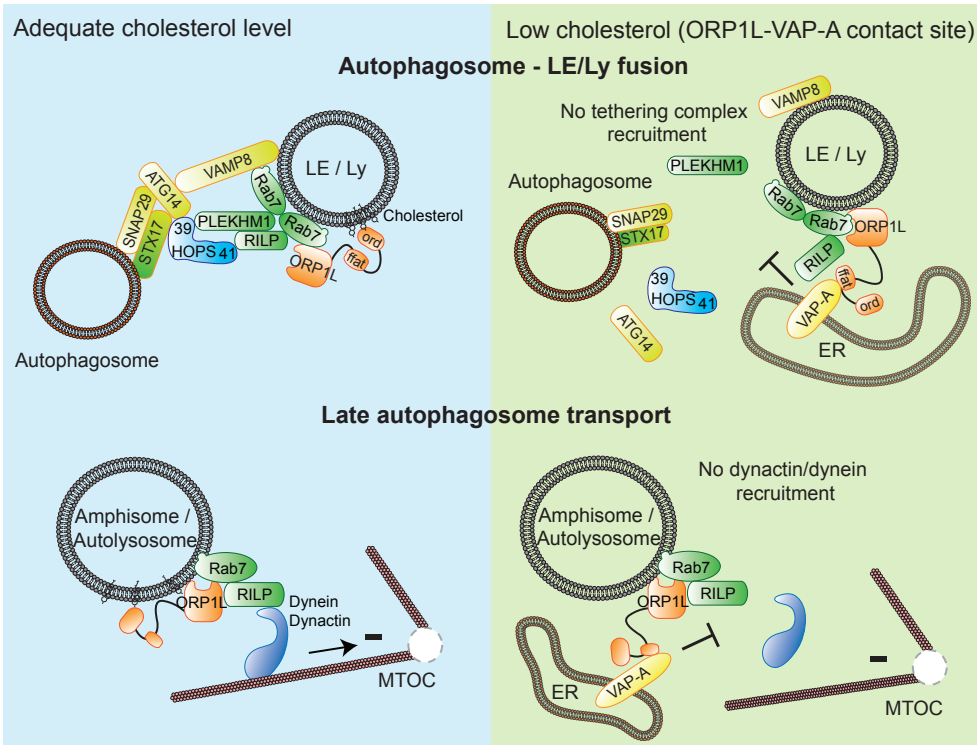


Figure 8. Model for ORP1L mediated control of autophagosome – LE/Ly fusion and late autophagosome transport. *SNARE proteins for fusion are depicted in yellow, tethering factors in green and the HOPS complex in blue. Tethering of autophagosomes with LE is orchestrated by two Rab7 molecules binding to two effectors PLEKHM1 and RILP, that respectively bind the VPS39 and VPS41 subunits of the HOPS tethering complex. From the autophagosome side, the SNARE Syntaxin 17 binds HOPS and mediates fusion together with the SNAREs SNAP29 and VAMP8, and ATG14. Under low cholesterol conditions, the ORD domain of ORP1L is released from the membrane, exposing the FFAT motif which interacts with ER protein VAP-A. This membrane contact site prevents recruitment of PLEKHM1 and HOPS to Rab7-RILP and hereby tethering and fusion. Once fusion does occur, RILP recruits dynactin-dynein to amphisomes to promote minus-end transport. Here, ORP1L can also form a contact site with VAP-A, which prevents dynactin recruitment and blocks minus-end transport. Thus, conformational changes in the cholesterol-sensor ORP1L time the fusion and transport of AVs. LE; late endosome, Ly; lysosome, 39; VPS39, 41; VPS41.*

SNARE protein STX17 [6] needs to contact the endosome-associated HOPS tethering complex [13,14]. On the LE/Ly side of the merger, the small GTPase Rab7 recruits its effectors PLEKHM1 and RILP, capable of respectively binding the VPS39 and VPS41 components of HOPS. Our data suggest that these effectors jointly recruit the same HOPS complex, which is analogous to yeast, where the Rab7 homologue YPT7 acquires HOPS by binding to both VPS39 and VPS41 [48,49]. Since RILP and PLEKHM1 bind the same motif on Rab7 [18], two Rab7 molecules probably associate to the two different effector proteins –RILP and PLEKHM1- which associate to two subunits of one tethering HOPS complex.

In addition to PLEKHM1 and RILP, Rab7 recruits another effector, the cholesterol-sensor ORP1L, which binds Rab7 in the presence of RILP [40] and engages di-

rectly with ER-located VAP-A. Genetic manipulation of underlying interaction determinants casts AV/LE fusion as subordinate to complex formation between ORP1L and VAP-A. In support of this, we find that in the presence of ORP1L predisposed to binding VAP-A, PLEKHM1 becomes relegated to the cytosol, while RILP remains associated to Rab7 but releases HOPS. This results in diminished entry of LC3+ compartments into the acidified luminal LE environment and expansion of the now arrested early autophagosomal repertoire. Given that ORP1L mediated ER-contact sites are modulated by cholesterol or oxysterols as recognized by the ORD domain of ORP1L, cholesterol on the cytosolic leaflet of Rab7-ORP1L compartments could control the autophagic flux. While the effects of the different ORP1L mutants on the autophagic flux revealed a clear and interpretable effect, this was less so for lipid manipulation of cells. This could be due to the milder nature of cholesterol manipulation, the multitude of other pathways that are affected by cholesterol, or another unknown factor controlling ORP1L contact site formation. However, our data with the ORP1L mutants suggest that cholesterol is instrumental for the autophagic flux, and demonstrate that the interplay between ORP1L and VAP-A determines whether a given AV/LE encounter will result in fusion, and by extension maturation of the autophagosome en route to proteolysis.

Following AV/LE fusion, the resulting amphisome needs to reach the lysosome in order to fulfill proteolysis of its contents. A large share of motor-based transport of autophagic vesicles is accounted for by amphisomes [21,24,50], and several transport adaptors, including DIC (dynein intermediate chain)-interacting proteins Snapin [24,51] and Huntingtin [52,53] are common between amphisomes and LEs. We demonstrate that LC3+ amphisomes retain both transport and regulatory determinants of its parent LE, all converging onto the small GTPase Rab7. Upon RILP engagement with amphisomes, the dynein – dynactin complex can be recruited for minus-end-directed transport towards lysosomes, typically congregating near the MTOC. Concomitant association of ORP1L to the Rab7-RILP complex adds an additional layer of regulation, involving a novel membrane contact site between amphisomes and the ER. Superresolution fluorescence imaging and immuno-EM revealed ORP1L on single-membrane-enclosed LC3+ amphisomes, juxtaposed against VAP-A on the ER, indicating an interaction occurring in trans rather than resulting from possible ERGIC-derived VAP-A spillover into nascent autophagosomes [54]. Formation of the amphisome-ER contact site is cholesterol dependent, advocating that via ORP1L, cholesterol can toggle decisions regarding transport of amphisomes. Why cholesterol is used to mark this step in autophagosome maturation is unclear. Possibly ORP1L confines the active transport machinery to defined regions on a vesicle, cholesterol-enriched subdomains. If so, decisions regarding transport are restricted to a few locations on a vesicle, so-called transport-nodes, which potentially simplifies regulation of bidirectional transport. In support of this theory, it was recently shown that on phagosomes Rab7 and the dynein motor are recruited specifically to cholesterol-enriched subdomains to control minus-end transport [55]. Interestingly, plus-end transport of amphisomes depends on PI(3)P binding by FYCO1 [31], suggesting a broader role for lipids in the regulation of amphisome transport. ORP family members have been demonstrated to also bind phosphoinositides within their ORD domain [56-58], which may also apply for the ORD domain

of ORP1L. The physiological role for transport regulation by cholesterol or other putative ligands of ORP1L is unclear, but it is possible that it functions as a timer, where older amphisomes can be recognized from a distinct lipid composition of their cytosolic leaflet, leading to minus-end transport and subsequent fusion with the lysosome. On top of the transport regulating ORP1L-VAP-A contact sites, we also observed cholesterol- and VAP-A-dependent but ORP1L-independent AV/ER contact sites. These could be facilitated by other ORP family members harboring the FFAT motif, or afforded by the divergent cholesterol-binding proteins STARD3 or STARD3NL [38,59,60], and will be subject for further study. Thus, via ORP1L, the ER and lipids in the limiting membranes of endosomes regulate late autophagosome transport, illustrating its complexity and intercompartmental control.
In addition to their role in autophagy induction through the regulation of mTOR activity [30,61], our data implicate LE/Ly as potent drivers of autophagic flux, capable of imposing restrictions on acceptance of autophagic vesicles into its fold. Fusion is thus not simply imposed by the autophagosome, but is also subject to license by the LE. This mechanism can be exploited on the individual endosome basis and activated on a specific set of LE/Ly, for example melanosomes or exocytic LEs/Lys, to prevent incoming cargo. Alternatively, ORP1L could serve as a quality control switch on LE/Ly to prevent incoming traffic when the endosome is not equipped to handle additional cargo, for example just after acquiring autophagosomal cargo. Following autophagic lysosome reformation [62], revitalized endosomes could inactivate ORP1L to take on a new degradation cycle. Given that starvation enhances AV/LE fusion [63], it will be interesting to investigate a potential interplay between mTOR signaling and ORP1L activity.
Collectively, our data suggest (Fig. 8) that the cholesterol sensor ORP1L regulates AV/LE fusion, and attenuates recruitment of PLEKHM1 and HOPS to Rab7-RILP complexes. Rab7 effectors PLEKHM1 and RILP then jointly attract HOPS for fusion. Following fusion, the resulting amphisome utilizes Rab7-RILP-associated dynein motor machinery for minus-end-directed transport, which is also under control of the very same ORP1L, through a novel type of MCS engaging late autophagosomal structures with the ER. These data provide a molecular basis for the potential role of a major dietary lipid, cholesterol, in controlling autophagosome transport and degradation of its content in lysosomal compartments [64,65].

Methods

Cell culture and constructs

MelJuSo cells were cultured in IMDM supplemented with 10% FCS, HeLa and HEK 293T cells in DMEM with 10% FCS. All cells were checked for contamination by other cells (using morphological analysis and surface marker expression) and were regularly tested for mycoplasma contamination. Constructs for expression of ORP1L, Rab7, RILP, p50, VPS39, VPS41, VPS33b, VAMP8 and VAP-A were described previously [15,33]. HA-ORP1L and mutants were obtained by swapping GFP in the GFP-C1 vector for a 2xHA tag. ORP1LΔORDydaa was generated by mutating the residues Y477 and D478 into alanines using the primers: 5'-gaggacgagttcgctgcggcgctgtcagattccg-3' and 5'-tctgacagcgccgcagcgaactcgtcctcgctaag-3'. Both residues

were mutated because a minor interaction with VAP-A was still observed in the D478A single amino acid mutant. PLEKHM1-GFP was a kind gift from Wim van Hul (Department of Medical Genetics, University of Antwerp, Belgium) [66] and was recloned into 2Flag-N1 using XhoI and HindIII. mRFP-mGFP-LC3 was generated by cloning mGFP and LC3 into an mRFP-C1 vector, mCherry-LC3 by cloning LC3 into an mCherry-C1 vector. All constructs were sequence verified.

Reagents and antibodies

Lipid depletion was carried out by incubating cells in DMEM/IMDM medium supplemented with 5% delipidized bovine serum (Pel-Freez Biologicals) in the presence of 50μM lovastatin (Millipore) to inhibit cholesterol production and 230μM Mevalonate (Sigma-Aldrich) to supply essential non-sterol isoprenoids. For endosomal cholesterol accumulation, cells were treated with 3μg/ml U-18666A (Cayman Chemicals), for lysosomal staining Lysotracker green (Molecular probes) was used. Starvation, used for the mRFP-mGFP-LC3 experiment, was performed by culturing cells in EBSS (ThermoScientific) for the indicated time. Puromycin (Gibco) was used at 4μg/ml. Antibodies used: rabbit anti-LC3B (Novus Biologicals NB100-2220, used for all experiments except co-staining with endogenous Rab7, microscopy 1:400, western blot 1:1000), mouse anti-LC3B (Cosmo Bio LC3-1703, only used for co-staining with Rab7, 1:100), rabbit anti-ORP1L (1:1000), rabbit anti-GFP (1:1000), mouse anti-CD63 (1:500) and rabbit anti-CD63 (1:100) (all described in [15]), rabbit anti-PDI (1:10, as described in [67]), mouse anti-HA (Covance 16B12, 1:1000), rat anti-HA 3F10 (Roche, 1:200), mouse anti-p62 D3 (1:500), goat anti-calnexin C-20 (1:40), goat anti-VAP-A K15 (microscopy 1:40, Western blot 1:500), mouse anti-Ubiquitin P4D1 (1:50) (all Santa Cruz), rabbit anti-Rab7 D95F2 (Cell Signaling Technologies, 1:100), and mouse anti-p150glued (BD Biosciences 610473, 1:100), rabbit anti-Flag F7425 and mouse anti-Flag M2 (Sigma, 1:1000). Secondary antibodies (goat anti-mouse Alexa 405/488/568/647, goat anti-rabbit Alexa 488/568/647, donkey anti-goat Alexa 488/568, donkey anti-mouse Alexa 488/555/647 and donkey anti-rabbit Alexa 488/647) were purchased from Life Technologies and donkey anti-rat CF568 from Biotium (all 1:200).

Transfections

For expression studies, MelJuSo and HeLa cells were transfected using Effectene (Qiagen) according to the manufacturer's instructions. Cells were transfected one day before fixation or lysis. For siRNA mediated depletion, cells were reverse transfected with DharmaFECT transfection reagent #1 and 50 nM siRNA (catalog numbers: siCtrl: D00120613-20, siORP1L: D008350-(01,05,18,19), siVAP-A: D021382-(01,02,03,04), siRILP D008787-(01,02,03,04) of the Human siGenome SMARTpool, Dharmacon) according to the manufacturer's protocol. Briefly, siRNAs and DharmaFECT were mixed and incubated for 20 minutes in a culture well, after which cells were added and left to adhere (reverse transfection). Three days later, cells were fixed and stained or lysed for biochemical analysis.

Co-immunoprecipitation and Western blotting

For co-immunoprecipitation experiments, cells were lysed in lysis buffer (0.5% NP-40, 5% glycerol, 150mM NaCl, 50mM Tris-HCl pH8.0, 5mM MgCl2 supplemented with complete EDTA-free Protease Inhibitor Cocktail (Roche)) and cleared by centrifugation. Lysates were incubated with GFP-Trap beads (Chromotek) or protein

G-Sepharose 4 FF resin with the indicated antibodies and after incubation washed extensively with lysis buffer before addition of sample buffer (2% SDS, 10% glycerol, 5% β-mercaptoethanol, 60mM Tris-HCl pH 6.8 and 0.01% bromophenol blue).
For whole cell lysate analyses, cells were lysed directly in sample buffer. Proteins were separated by SDS-PAGE and transferred to Western Blot filters. Blocking of the filter and antibody incubations were done in PBS supplemented with 0.1 (v/v)% Tween and 5% (w/v) milk powder. Blots were imaged using the Odyssey Imaging System (LI-COR) or ChemiDoc (Bio-Rad).

cDNA synthesis and qPCR

RNA isolation, cDNA synthesis and quantitative RT-PCR were performed according to the manufacturer's (Roche) instructions. Signal was normalized to GAPDH and calculated using the Pfaffl formula. Primers used for detection of GAPDH and RILP were: GAPDH fw: 5'-TGTTGCCATCAATGACCCCTT-3', GAPDH rv: 5'-CTCCACGACGTACTCAGCG-3', RILP fw: 5'- AAGCAGCGGAAGAAGATCAA-3', RILP rv: 5'-TTGTCATCGGAGAGCAGGAT-3'.

Confocal microscopy

Cells were seeded on coverslips, transfected 18 hours later and treated as indicated. 24 hrs later, cells were fixed in 3.7% formaldehyde for 10 min and permeabilized in ice-cold methanol for 2minutes. Staining was performed with the antibodies mentioned above and DAPI (Invitrogen) to stain DNA or Filipin (Cayman Chemicals) to detect cholesterol. Images were acquired using a Leica TCS SP5 confocal microscope (Leica Microsystems, Wetzlar, Germany) at 63x magnification. For live-cell imaging, the microscope was equipped with a climate control chamber and cells were imaged for 8 minutes with ~5 frames per minute. Images were quantified using Image J plugin Jacob for Mander's coefficient calculations or FIJI's Trackmate plugin for live-cell imaging and processed using Adobe Photoshop and Illustrator.

Cryo-immunoelectron microscopy

Transfected HeLa cells were fixed for 2 hours in 2% paraformaldehyde + 0,2% glutaraldehyde in 0.1 M PHEM buffer (60 mM PIPES, 25 mM HEPES, 2 mM MgCl2, 10 mM EGTA, pH 6.9) and then processed for ultrathin cryosectioning. Briefly, 50-nm cryosections were cut at -120°C using diamond knives in a cryoultramicrotome (Leica Aktiengesellschaft, Vienna, Austria) and transferred with a mixture of sucrose and methylcellulose onto formvar-coated copper grids. The grids were placed on 35-mm petri dishes containing 2% gelatine. Ultrathin frozen sections were incubated at room temperature with primary antibody and then incubated with 10nm protein A-conjugated colloidal gold (EM Lab, Utrecht University, Netherlands) as described [68]. For double labeling, the sections were first washed and then fixed for another 10 minutes in 1% glutaraldehyde, blocked and incubated with the second primary antibody and 15nm gold labeled protein A. The sections were embedded in a mixture of methylcellulose and uranyl acetate and examined with a Philips CM10 electron microscope (FEI, Eindhoven, The Netherlands).

Superresolution microscopy

Super-resolution microscopy was performed with a Leica SR GSD microscope (Leica Microsystems, Wetzlar, Germany) mounted on a Sumo Stage (#11888963) for drift free imaging. Collection of images was done with an EMCCD Andor iXon camera (Andor Technology, Belfast, UK) and an oil immersion objective (HCX PL

Apo 100X, NA 1.47). Laser characteristics were 405nm/30mW, 488 nm/300mW and 647nm/500mW, with the 405nm laser used for back pumping and the others for wide field/TIRF imaging. Ultra clean coverslips (cleaned and washed with base and acid overnight) were used for imaging. The number of recorded frames was variable between 10,000 to 50,000, with a frame rate of 100Hz. The data sets were analyzed with the Thunder Storm analysis module [69] and images were reconstructed with a detection threshold of 70 photons, sub pixel localization of molecules and uncertainty correction, with a pixel size of 10nm.

Statistical analysis and experimental set-up

All experiments shown in the paper are performed independently at least three times and images are representative of at least 10 cells viewed per individual experiment. For colocalization quantification, numerical values of individual cells were used for calculations, while for population quantifications the averages per experiment were used. Statistical significance was calculated using an unpaired Student's T-test, except for normalized signals, for which a paired T-test was done. Statistical values are as following: * $p < 0.05$, ** $p < 0.01$, *** $p < 0.001$, **** $p < 0.0001$.

Data availability

All data supporting the findings in this study are included in the article, either in the main figures or the supplemental data.

Acknowledgements

We thank the NKI Digital Microscopy Facility for support, members of the Neefjes group for critical discussions, Nico Ong for developing electron micrographs and Wim van Hul for providing the PLEKHM1 construct. This work was supported by the Institute of Chemical Immunology (ICI), an NWO Gravitation project funded by the Ministry of Education, Culture and Science of the government of the Netherlands and a European Research Council (ERC) advanced grant awarded to J.N.

Author contributions

R.W. and J.N. designed experiments, R.W. performed experiments, I.B. performed the live-cell imaging experiments, H.J. performed the Immuno-EM experiments, L.N. and K.J. performed the superresolution microscopy experiments and L.J. cloned constructs. R.W., I.B. and J.N. wrote the manuscript with input from all authors.

Competing financial interests

The authors declare no competing financial interests.

References

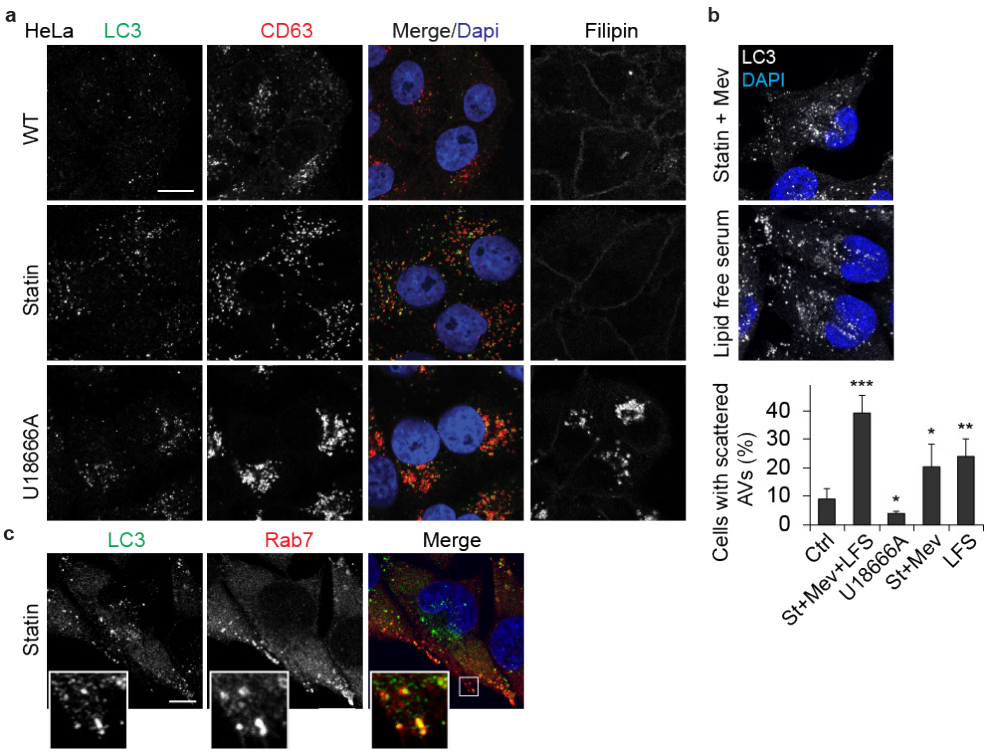
1. Yang, S. et al. Pancreatic cancers require autophagy for tumor growth. Genes Dev 25, 717-729 (2011).
2. Blum, R. & Kloog, Y. Metabolism addiction in pancreatic cancer. Cell Death Dis 5, e1065 (2014).
3. Rubinsztein, D.C., Bento, C.F. & Deretic, V. Therapeutic targeting of autophagy in neurodegenerative and infectious diseases. J Exp Med 212, 979-990 (2015).
4. Gordon, P.B. & Seglen, P.O. Prelysosomal convergence of autophagic and endocytic pathways. Biochem Biophys Res Commun 151, 40-47 (1988).
5. Diao, J. et al. ATG14 promotes membrane tethering and fusion of autophagosomes to endolys-

osomes. Nature 520, 563-566 (2015).
6. Itakura, E., Kishi-Itakura, C. & Mizushima, N. The hairpin-type tail-anchored SNARE syntaxin 17 targets to autophagosomes for fusion with endosomes/lysosomes. Cell 151, 1256-1269 (2012).
7. Takats, S. et al. Autophagosomal Syntaxin17-dependent lysosomal degradation maintains neuronal function in Drosophila. The Journal of cell biology 201, 531-539 (2013).
8. Shen, H.M. & Mizushima, N. At the end of the autophagic road: an emerging understanding of lysosomal functions in autophagy. Trends Biochem Sci 39, 61-71 (2014).
9. Gutierrez, M.G., Munafo, D.B., Beron, W. & Colombo, M.I. Rab7 is required for the normal progression of the autophagic pathway in mammalian cells. Journal of cell science 117, 2687-2697 (2004).
10. Jager, S. et al. Role for Rab7 in maturation of late autophagic vacuoles. Journal of cell science 117, 4837-4848 (2004).
11. Ganley, I.G., Wong, P.M., Gammoh, N. & Jiang, X. Distinct autophagosomal-lysosomal fusion mechanism revealed by thapsigargin-induced autophagy arrest. Mol Cell 42, 731-743 (2011).
12. Kimura, S., Noda, T. & Yoshimori, T. Dissection of the autophagosome maturation process by a novel reporter protein, tandem fluorescent-tagged LC3. Autophagy 3, 452-460 (2007).
13. Takats, S. et al. Interaction of the HOPS complex with Syntaxin 17 mediates autophagosome clearance in Drosophila. Molecular biology of the cell 25, 1338-1354 (2014).
14. Jiang, P. et al. The HOPS complex mediates autophagosome-lysosome fusion through interaction with syntaxin 17. Molecular biology of the cell 25, 1327-1337 (2014).
15. van der Kant, R. et al. Late endosomal transport and tethering are coupled processes controlled by RILP and the cholesterol sensor ORP1L. Journal of cell science 126, 3462-3474 (2013).
16. Wartosch, L., Gunesdogan, U., Graham, S.C. & Luzio, J.P. Recruitment of VPS33A to HOPS by VPS16 Is Required for Lysosome Fusion with Endosomes and Autophagosomes. Traffic 16, 727-742 (2015).
17. McEwan, D.G. et al. PLEKHM1 regulates autophagosome-lysosome fusion through HOPS complex and LC3/GABARAP proteins. Mol Cell 57, 39-54 (2015).
18. McEwan, D.G. et al. PLEKHM1 regulates Salmonella-containing vacuole biogenesis and infection. Cell Host Microbe 17, 58-71 (2015).
19. Lin, X. et al. RILP interacts with HOPS complex via VPS41 subunit to regulate endocytic trafficking. Sci Rep 4, 7282 (2014).
20. van der Kant, R. et al. Characterization of the mammalian CORVET and HOPS complexes and their modular restructuring for endosome specificity. The Journal of biological chemistry 290, 30280-30290 (2015).
21. Jahreiss, L., Menzies, F.M. & Rubinsztein, D.C. The itinerary of autophagosomes: from peripheral formation to kiss-and-run fusion with lysosomes. Traffic 9, 574-587 (2008).
22. Kimura, S., Noda, T. & Yoshimori, T. Dynein-dependent movement of autophagosomes mediates efficient encounters with lysosomes. Cell Struct Funct 33, 109-122 (2008).
23. Ikenaka, K. et al. dnc-1/dynactin 1 knockdown disrupts transport of autophagosomes and induces motor neuron degeneration. PLoS One 8, e54511 (2013).
24. Cheng, X.T., Zhou, B., Lin, M.Y., Cai, Q. & Sheng, Z.H. Axonal autophagosomes recruit dynein for retrograde transport through fusion with late endosomes. The Journal of cell biology 209, 377-386 (2015).
25. Kochl, R., Hu, X.W., Chan, E.Y. & Tooze, S.A. Microtubules facilitate autophagosome formation and fusion of autophagosomes with endosomes. Traffic 7, 129-145 (2006).
26. Maday, S., Wallace, K.E. & Holzbaur, E.L. Autophagosomes initiate distally and mature during transport toward the cell soma in primary neurons. The Journal of cell biology 196, 407-417 (2012).
27. Stenmark, H. Rab GTPases as coordinators of vesicle traffic. Nature reviews. Molecular cell biology 10, 513-525 (2009).
28. Jordens, I. et al. The Rab7 effector protein RILP controls lysosomal transport by inducing the recruitment of dynein-dynactin motors. Current biology : CB 11, 1680-1685 (2001).
29. Wijdeven, R.H., Jongsma, M.L., Neefjes, J. & Berlin, I. ER contact sites direct late endosome transport. Bioessays 37, 1298-1302 (2015).
30. Korolchuk, V.I. et al. Lysosomal positioning coordinates cellular nutrient responses. Nature cell biology 13, 453-460 (2011).
31. Pankiv, S. et al. FYCO1 is a Rab7 effector that binds to LC3 and PI3P to mediate microtubule plus end-directed vesicle transport. The Journal of cell biology 188, 253-269 (2010).
32. Lebrand, C. et al. Late endosome motility depends on lipids via the small GTPase Rab7. Embo

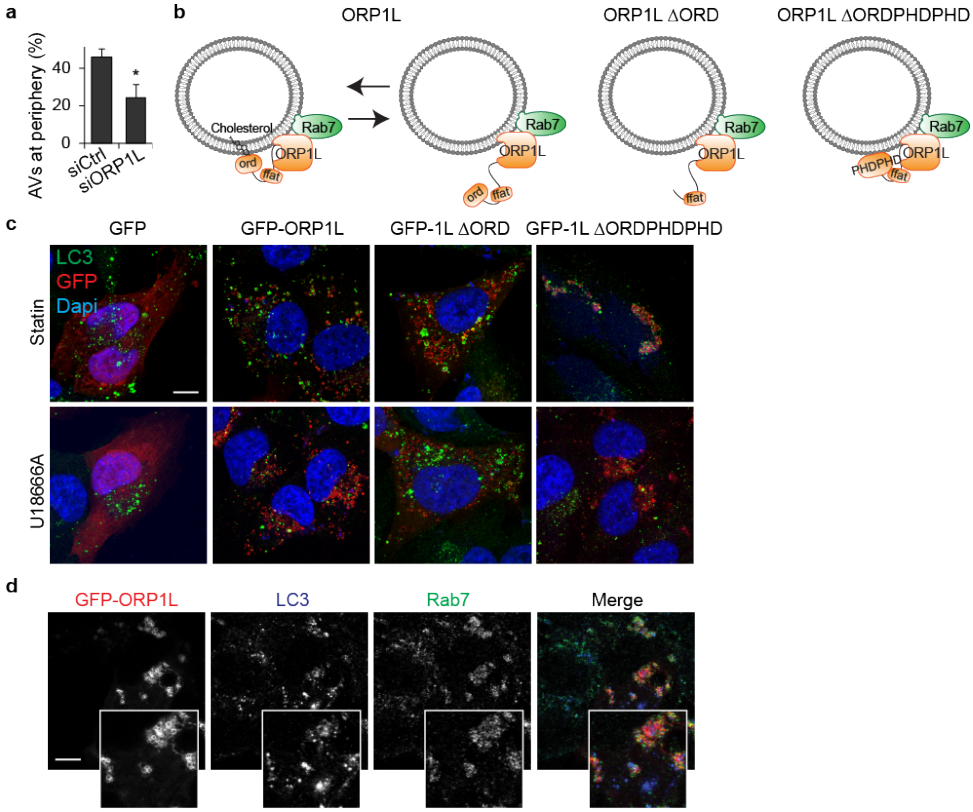
j 21, 1289-1300 (2002).
33. Rocha, N. et al. Cholesterol sensor ORP1L contacts the ER protein VAP to control Rab7-RILP-p150 Glued and late endosome positioning. The Journal of cell biology 185, 1209-1225 (2009).
34. Sugii, S. et al. Roles of endogenously synthesized sterols in the endocytic pathway. The Journal of biological chemistry 281, 23191-23206 (2006).
35. Lu, F. et al. Identification of NPC1 as the target of U18666A, an inhibitor of lysosomal cholesterol export and Ebola infection. Elife 4 (2015).
36. Hansen, T.E. & Johansen, T. Following autophagy step by step. BMC Biol 9, 39 (2011).
37. Vihervaara, T. et al. Sterol binding by OSBP-related protein 1L regulates late endosome motility and function. Cellular and molecular life sciences : CMLS 68, 537-551 (2011).
38. Weber-Boyvat, M., Kentala, H., Peranen, J. & Olkkonen, V.M. Ligand-dependent localization and function of ORP-VAP complexes at membrane contact sites. Cellular and molecular life sciences : CMLS 72, 1967-1987 (2015).
39. Helle, S.C. et al. Organization and function of membrane contact sites. Biochim Biophys Acta 1833, 2526-2541 (2013).
40. Johansson, M. et al. Activation of endosomal dynein motors by stepwise assembly of Rab7-RILP-p150Glued, ORP1L, and the receptor betalll spectrin. The Journal of cell biology 176, 459-471 (2007).
41. Bains, M., Zaegel, V., Mize-Berge, J. & Heidenreich, K.A. IGF-I stimulates Rab7-RILP interaction during neuronal autophagy. Neurosci Lett 488, 112-117 (2011).
42. Burkhardt, J.K., Echeverri, C.J., Nilsson, T. & Vallee, R.B. Overexpression of the dynamitin (p50) subunit of the dynactin complex disrupts dynein-dependent maintenance of membrane organelle distribution. The Journal of cell biology 139, 469-484 (1997).
43. Klionsky, D.J., Eskelinen, E.L. & Deretic, V. Autophagosomes, phagosomes, autolysosomes, phagolysosomes, autophagolysosomes... wait, I'm confused. Autophagy 10, 549-551 (2014).
44. Sarkar, S. et al. Impaired autophagy in the lipid-storage disorder Niemann-Pick type C1 disease. Cell Rep 5, 1302-1315 (2013).
45. Fraldi, A. et al. Lysosomal fusion and SNARE function are impaired by cholesterol accumulation in lysosomal storage disorders. Embo j 29, 3607-3620 (2010).
46. Balderhaar, H.J. & Ungermann, C. CORVET and HOPS tethering complexes - coordinators of endosome and lysosome fusion. Journal of cell science 126, 1307-1316 (2013).
47. Progida, C. et al. RILP is required for the proper morphology and function of late endosomes. Journal of cell science 120, 3729-3737 (2007).
48. Plemel, R.L. et al. Subunit organization and Rab interactions of Vps-C protein complexes that control endolysosomal membrane traffic. Molecular biology of the cell 22, 1353-1363 (2011).
49. Ostrowicz, C.W. et al. Defined subunit arrangement and rab interactions are required for functionality of the HOPS tethering complex. Traffic 11, 1334-1346 (2010).
50. Fu, M.M., Nirschl, J.J. & Holzbaur, E.L. LC3 binding to the scaffolding protein JIP1 regulates processive dynein-driven transport of autophagosomes. Dev Cell 29, 577-590 (2014).
51. Cai, Q. et al. Snapin-regulated late endosomal transport is critical for efficient autophagy-lysosomal function in neurons. Neuron 68, 73-86 (2010).
52. Caviston, J.P., Zajac, A.L., Tokito, M. & Holzbaur, E.L. Huntingtin coordinates the dynein-mediated dynamic positioning of endosomes and lysosomes. Molecular biology of the cell 22, 478-492 (2011).
53. Wong, Y.C. & Holzbaur, E.L. The regulation of autophagosome dynamics by huntingtin and HAP1 is disrupted by expression of mutant huntingtin, leading to defective cargo degradation. J Neurosci 34, 1293-1305 (2014).
54. Ge, L., Melville, D., Zhang, M. & Schekman, R. The ER-Golgi intermediate compartment is a key membrane source for the LC3 lipidation step of autophagosome biogenesis. Elife 2, e00947 (2013).
55. Rai, A. et al. Dynein Clusters into Lipid Microdomains on Phagosomes to Drive Rapid Transport toward Lysosomes. Cell 164, 722-734 (2016).
56. de Saint-Jean, M. et al. Osh4p exchanges sterols for phosphatidylinositol 4-phosphate between lipid bilayers. The Journal of cell biology 195, 965-978 (2011).
57. Mesmin, B. et al. A four-step cycle driven by PI(4)P hydrolysis directs sterol/PI(4)P exchange by the ER-Golgi tether OSBP. Cell 155, 830-843 (2013).
58. Tong, J., Yang, H., Yang, H., Eom, S.H. & Im, Y.J. Structure of Osh3 reveals a conserved mode of phosphoinositide binding in oxysterol-binding proteins. Structure 21, 1203-1213 (2013).
59. van der Kant, R., Zondervan, I., Janssen, L. & Neefjes, J. Cholesterol-binding molecules

MLN64 and ORP1L mark distinct late endosomes with transporters ABCA3 and NPC1. J Lipid Res 54, 2153-2165 (2013).
60. Alpy, F. et al. STARD3 or STARD3NL and VAP form a novel molecular tether between late endosomes and the ER. Journal of cell science 126, 5500-5512 (2013).
61. Sancak, Y. et al. Ragulator-Rag complex targets mTORC1 to the lysosomal surface and is necessary for its activation by amino acids. Cell 141, 290-303 (2010).
62. Yu, L. et al. Termination of autophagy and reformation of lysosomes regulated by mTOR. Nature 465, 942-946 (2010).
63. Guo, B. et al. O-GlcNAc-modification of SNAP-29 regulates autophagosome maturation. Nature cell biology 16, 1215-1226 (2014).
64. Miettinen, T.P. & Bjorklund, M. Mevalonate Pathway Regulates Cell Size Homeostasis and Proteostasis through Autophagy. Cell Rep 13, 2610-2620 (2015).
65. Tamura, A. & Yui, N. beta-Cyclodextrin-threaded biocleavable polyrotaxanes ameliorate impaired autophagic flux in Niemann-Pick type C disease. The Journal of biological chemistry 290, 9442-9454 (2015).
66. Van Wesenbeeck, L. et al. Involvement of PLEKHM1 in osteoclastic vesicular transport and osteopetrosis in incisors absent rats and humans. J Clin Invest 117, 919-930 (2007).
67. van der Wel, N. et al. M. tuberculosis and M. leprae translocate from the phagolysosome to the cytosol in myeloid cells. Cell 129, 1287-1298 (2007).
68. Calafat, J. et al. Human monocytes and neutrophils store transforming growth factor-alpha in a subpopulation of cytoplasmic granules. Blood 90, 1255-1266 (1997).
69. Ovesny, M., Krizek, P., Borkovec, J., Svindrych, Z. & Hagen, G.M. ThunderSTORM: a comprehensive ImageJ plug-in for PALM and STORM data analysis and super-resolution imaging. Bioinformatics 30, 2389-2390 (2014).

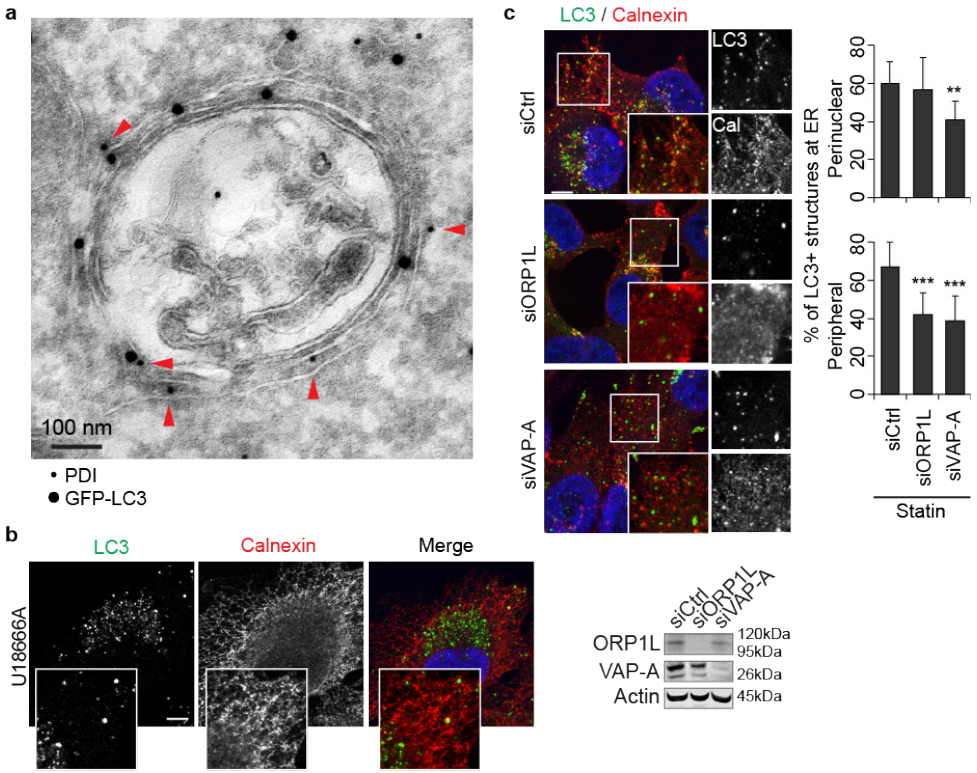
Supplementary Information



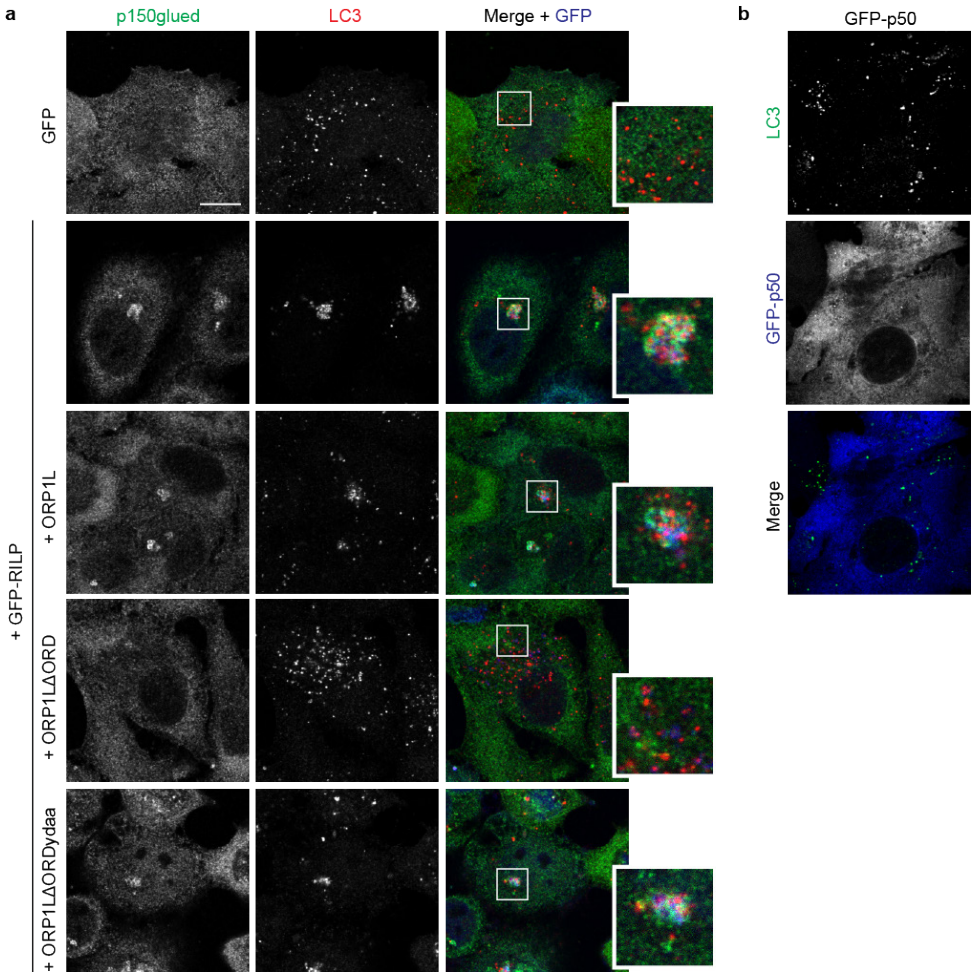
Supplementary Figure 1: cholesterol manipulation alters the positioning of autophagosomes in cells, related to figure 1. *(a) HeLa cells were treated for 24h under conditions reducing cholesterol (50μM Lovastatin, 5% lipid free serum and 230μM Mevalonate) or with 3μM U18666A to enrich for endosomal cholesterol and stained for the indicated markers. Filipin staining was performed on different slides to verify cholesterol depletion or accumulation following the respective treatments. Bar= 10 μm. (b) MelJuSo cells were treated for 24h with statin and mevalonate (Statin + Mev) or lipid free serum to reduce cholesterol and stained for the indicated markers. Lower panel: quantification of the percentage of cells showing peripheral accumulation of autophagosomes, treatments as in Fig 1b and S1b. >100 cells per experiments were counted. Bars indicate mean + SD from independent triplicate experiments and means were compared using Student's t-test. (c) Staining of cholesterol-reduced MelJuSo cells for LC3 and Rab7. Scale bar, 10μm. (* $p < 0.05$, ** $p < 0.01$, *** $p < 0.001$).*



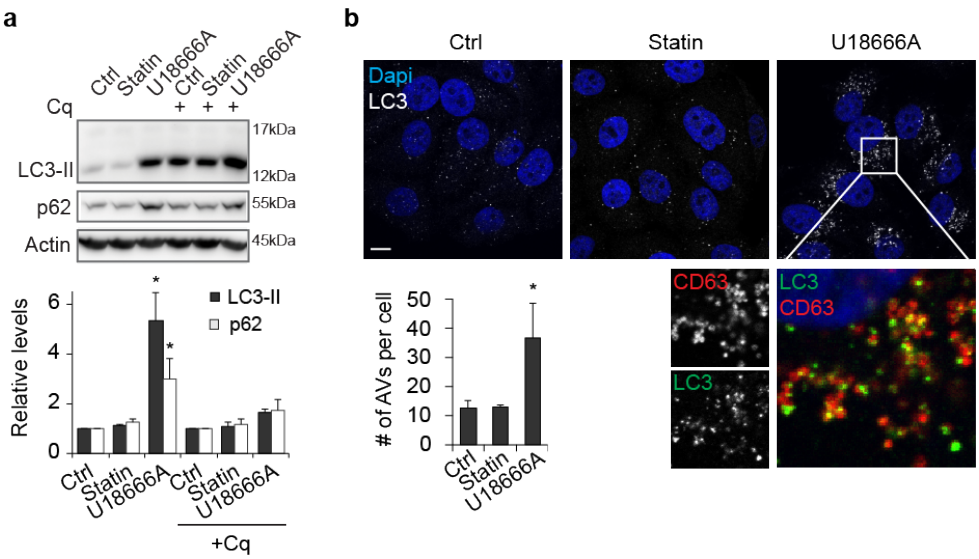
Supplementary Figure 2: ORP1L localizes to Rab7 positive autophagosomes and controls their positioning, related to figure 2. *(a) Quantification of the number of LC3 structures in the peripheral region, from Figure 2a. Autophagosomes outside the perinuclear region, relative to the total number of LC3 vesicles per cell were quantified. Quantification on >10 cells per experiment, bars represent mean+SD of independent triplicates. Student's t-test statistical analysis. (b) Model of ORP1L and its mutants. ORP1L binds cholesterol from the cytosolic leaflet of endosomal membranes by its ORD domain, which covers the FFAT motif. When not interacting with the membrane (low cholesterol conditions), ORP1L (like ORP1LΔORD) has its FFAT motif exposed to interact with ER protein VAP-A. The tandem PHD domains of ORP1LΔORDPHDPHD associate to the membrane and cover its FFAT motif, mimicking the high cholesterol condition. (c) MelJuSo cells transfected with the indicated constructs were cultured under cholesterol manipulating conditions and stained for LC3 and DAPI. (d) MelJuSo cells expressing GFP-ORP1L were stained for Rab7 and LC3. Bar= 10 µm. (* $p < 0.05$).*



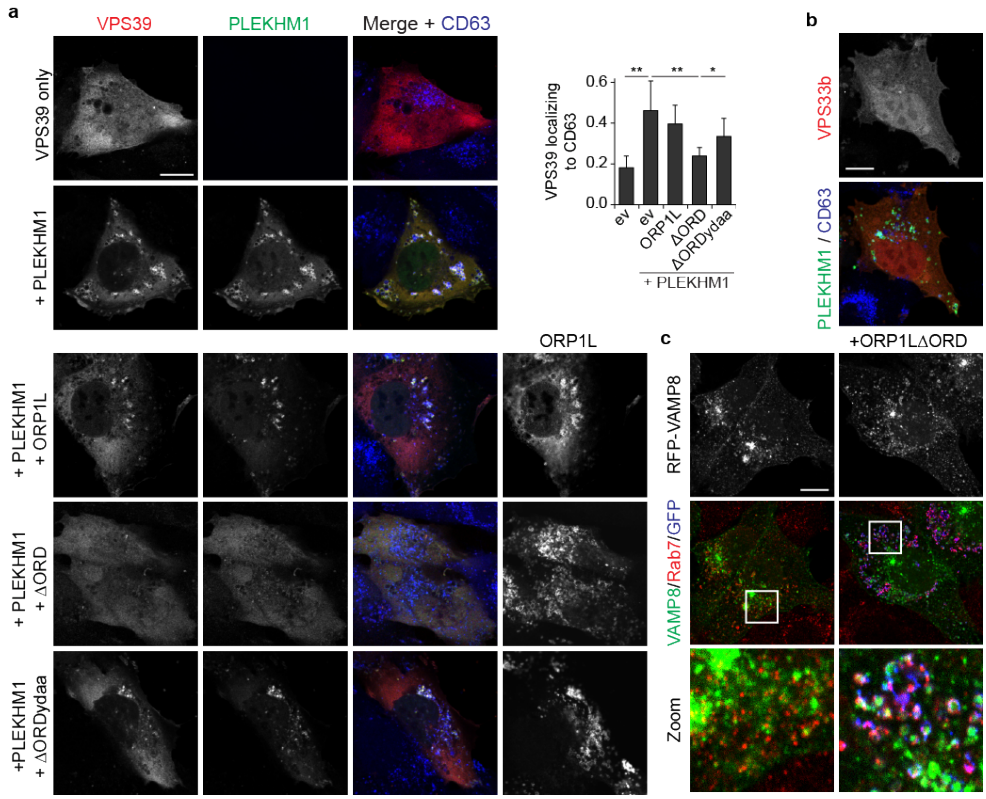
Supplementary Figure 3: ORP1L induces the formation of ER-autophagosome contact sites, related to figure 3. *(a) Immuno-EM on HeLa cells expressing GFP-LC3 and HA-ORP1LΔORD. Cells were stained for GFP and the luminal ER marker PDI. The double membrane surrounding autophagosomes stained positive for PDI (red arrowheads), illustrating ER contact sites with autophagosomes. Bar= 100nm (b) MelJuSo cells enriched for cholesterol by exposure to U18666A were stained for LC3 to mark autophagosomes and Calnexin to label the ER. Bar= 10 µm.(c) MelJuSo cells transfected with siCtrl, siORP1L or siVAP-A were depleted for cholesterol and stained for LC3 and Calnexin. Bar= 10 µm. Fraction of peripheral or perinuclear autophagosomes co-localizing with the ER were quantified manually in >10 cells per experiment over three experiments. Bars indicate mean+SD from independent triplicate experiments. Efficient silencing of VAP-A and ORP1L was confirmed by Western blot. Molecular weight is indicated on the right. Student's t-test statistical analysis (** $p < 0.01$, *** $p < 0.001$).*



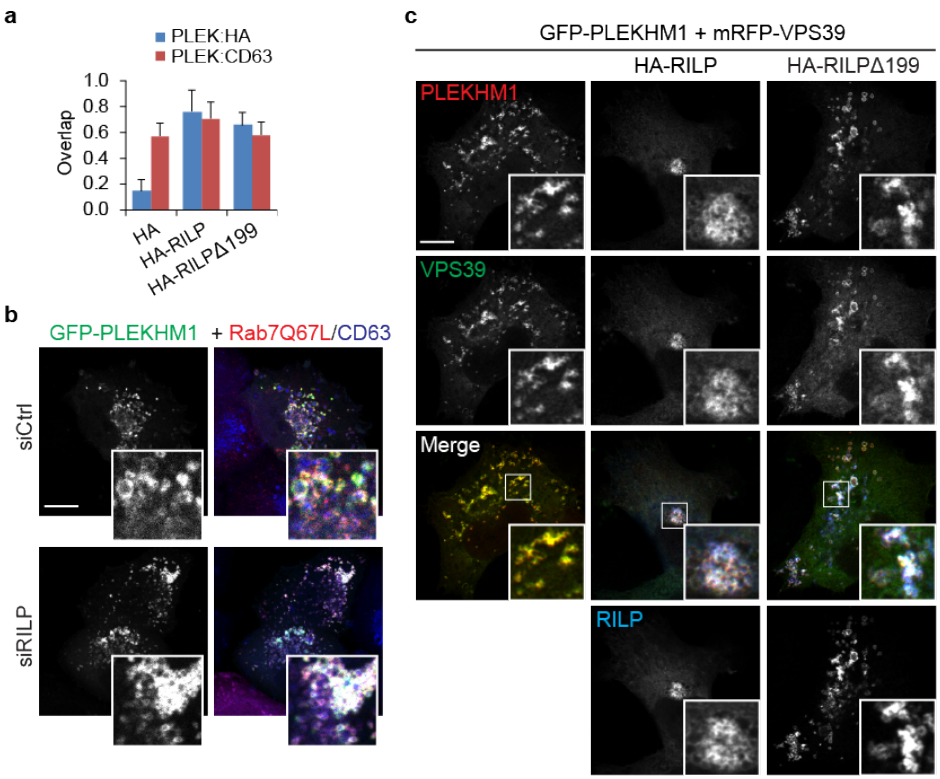
Supplementary Figure 4: RILP recruits the dynein-dynactin motor to AVs for minus-end transport, which is controlled by ORP1L, related to figure 4. *(a) HeLa cells overexpressing GFP, GFP-RILP, or GFP-RILP and HA-tagged ORP1L constructs (as indicated) were stained for LC3 and p150glued. Right: zoom-in of the indicated region. (b) HeLa cells transfected with GFP-P50dynamitin were stained for LC3 (red). Bar= 10 µm.*



Supplementary Figure 5: effects of cholesterol manipulation on the autophagic flux. *(a) HeLa cells were reduced (statin) or enriched (U18666A) for cholesterol for 24h and incubated for the last 4h with chloroquine (cq) when indicated. After lysis, samples were analyzed by SDS-PAGE and Western blot for the indicated proteins. Bottom: signal relative to actin was normalized to the Ctrl cells (with or without chloroquine). Bars represent mean+SD of three independent experiments, means are compared by Student's t-test. (b) HeLa cells were treated for 24h under conditions reducing cholesterol (50μM Lovastatin, 5% lipid free serum and 230μM Mevalonate) or with 3μM U18666A to enrich for endosomal cholesterol and stained for the indicated markers. Bar= 10 μm. Numbers of AVs per cell were quantified for >10 cells per experiment. Bars indicate mean+SD from independent triplicate experiments and significance was analyzed using Student's t-test statistical analysis. (* p < 0.05).*



Supplementary Figure 6: ORP1L controls recruitment of PLEKHM1 and HOPS to Rab7, related to figure 6. *(a) MelJuSo cells were transfected with GFP-tagged PLEKHM1, mRFP-VPS39 and the indicated HA-tagged ORP1L mutants and stained for CD63. Bar= 10 µm. Right: Manders coefficient for VPS39 localization to CD63 was determined for >10 cells over three independent experiments, bars represent mean+SD. Student's t-test statistical analysis. (b) PLEKHM1 fails to recruit VPS33b to membranes. MelJuSo cells were transfected with GFP-tagged PLEKHM1 and mRFP-VPS33b and stained for CD63. Bar= 10 µm. (c) ORP1L does not affect the localization of VAMP8. MelJuSo cells were transfected with either mRFP-VAMP8 or with mRFP-VAMP8 and GFP-ORP1LΔORD and stained for Rab7. Bar= 10 µm. Zoom-in from indicated region. ev: empty vector. (* $p < 0.05$, ** $p < 0.01$).*



Supplementary Figure 7: RILP controls PLEKHM1 recruitment by Rab7, related to figure 7. *(a) Quantification of Fig. 7a. Manders coefficient for PLEKHM1 localization to CD63 or HA was calculated for >10 cells over three independent experiments, bars represent mean+SD. (b) MelJuSo cells silenced with siCtrl or siRilp were transfected with GFP-PLEKHM1 and Myc-Rab7Q67L and stained for CD63. Bar= 10 µm. (c) MelJuSo cells were transfected with GFP-PLEKHM1 and mRFP-VPS39, together with HA-RILP or HA-RILPΔ199 when indicated. Bar= 10 µm. For all quantification experiments: bars indicate mean + SD from independent triplicate experiments.*

Chapter 3: ER-associated pathway draws the endosomal system's architecture for controlled cargo transport

Marlieke L.M. Jongsma[*,1,3], Ilana Berlin[*,1], Ruud H.M. Wijdeven[1], Lennert Janssen[1], George M.C. Janssen[2], Malgorzata A. Garstka[1], Hans Janssen[1], Mark Mensink[1], Peter A. van Veelen[2], Robbert M. Spaapen[3] and Jacques Neefjes[1,4].

[1] Division of Cell Biology, The Netherlands Cancer Institute, Plesmanlaan 121, 1066 CX Amsterdam, The Netherlands
[2] Department of Immunohematology and Blood Transfusion, Leiden University Medical Centre, PO Box 9600, 2300 RC Leiden, The Netherlands
[3] Department of Immunopathology, Sanquin Research and Landsteiner Laboratory AMC/UvA, Plesmanlaan 125, 1066 CX Amsterdam, The Netherlands
[4] Department of Chemical Immunology, Leiden University Medical Centre, PO Box 9600, 2300 RC Leiden, The Netherlands
[*] These authors contributed equally to this work

Cell. 2016 June 30; 166(1)

Abstract

Through a network of progressively maturing vesicles, the endosomal system connects the cell's interior with extracellular space. Intriguingly, this network exhibits a bilateral architecture, comprised of a relatively immobile perinuclear vesicle 'cloud' and a highly dynamic peripheral contingent. How this spatiotemporal organization is achieved and what function(s) it curates is unclear. Here we reveal the ER-located ubiquitin ligase RNF26 as the global architect of the entire endosomal system, including the TGN. To specify perinuclear vesicle coordinates, catalytically competent RNF26 recruits and ubiquitinates the scaffold p62/SQSTM1, in turn attracting ubiquitin-binding domains (UBDs) of various vesicle adaptors. Consequently, RNF26 restrains fast transport of diverse vesicles through a common molecular mechanism operating at the ER membrane, until the deubiquitinating enzyme USP15 opposes RNF26 activity to allow vesicle release into the cell's periphery. By drawing the endosomal system's architecture, RNF26 orchestrates endosomal maturation and trafficking of cargoes, including signaling receptors, in space and time.

Introduction

Visual inspection of a typical cell reveals canonical arrangements of membrane-enclosed organelles. Generally, the endoplasmic reticulum (ER) wraps around the nucleus, extending throughout the cytoplasmic space, while the mammalian Golgi stacks cluster between the nucleus and the microtubule-organizing center (MTOC) (1-3). From here, the trans-Golgi network (TGN) vesicles disseminate biosynthetic cargoes to their sites of function throughout the cell. (4). On the other side of vesicle traffic, endosomes originating from the plasma membrane carry internalized cargoes to the lysosome for degradation, or spare them through diversion to recycling (5). The roads traveled by endosomes time intracellular signaling cascades (6) and tune specialized functions, such as antigen processing and pathogen clearance in immune cells (7). To fulfill its myriad responsibilities, the collective endo- and exocytic pathway connects distant organelles (8) through a progressively maturing network of vesicles (9). How cells sense and manipulate the location of individual vesicles in space and time to suit their global housekeeping and environmental demands is unclear.

Intriguingly, the bulk of lysosomes, early and late endosomes, as well as vesicles of the TGN locates quiescently in the perinuclear region of the cell (10-14), poised towards the cell's periphery. Only select vesicles escape this 'perinuclear (PN) cloud' to become subject to fast bidirectional transport (15) by dynein (16-18) and kinesin motors (19, 20). What governs acceptance of vesicles into—and their release from—the PN cloud is unknown. Gaining fundamental insights into the way such decisions are made in molecular terms is pivotal to understanding regulation of transport programs in the cell.

The ER is the only intracellular organelle that occupies every corner of cytosolic space. Not surprisingly, it has been shown to participate in various functional contacts with other membranous compartments, mediating exchange of metabolites and controlling transport and fusion processes (21). Currently, contact sites between the ER and endosomes are emerging as potent regulatory hubs for vesicle transport (19, 22), fusion (23) and fission (24) events. Here we describe how an ER-associ-

ated protein network, organized by the E3 ubiquitin ligase Ring finger protein 26 (RNF26), serves as a platform for perinuclear positioning of the entire endosomal system. Localized in the ER membrane, RNF26 extends its catalytic determinants into the cytosol, restricting fast microtubule-based transport of early, recycling and late endosomes/lysosomes and the TGN. We show that RNF26 utilizes the ubiquitin scaffold p62/Sequestosome 1 (SQSTM1) as its substrate to attract UBDs of various vesicle membrane adaptors. The resulting molecular bridge restrains cognate vesicles in the perinuclear region and organizes the endosomal pathway for efficient cargo transfer and ligand-induced clearance of signaling receptors. Vesicles can then be released for fast transport into the cell's periphery from their perinuclear positions by way of RNF26-associated deubiquitinating enzyme (DUB) USP15, thus completing the dynamic cycle. Collectively, the RNF26-based protein network elucidates a key paradigm for functional control of intracellular architecture and organelle dynamics, highlighting the importance of inter-compartmental regulation in membrane cell biology.

Results

RNF26 regulates endocytic compartment architecture and dynamics

Across cell types, a wide variety of endosomal maturation stages—late (CD63, Figure 1A), early (EEA1) and recycling (TrfR) endosomes, as well as the vesicular arm of the TGN (TGN46) (Figure S1)—tend to cluster into a 'cloud' near the nucleus, with only a fraction of each subset extending into the cell's periphery. How such organization is established and controlled and what purpose it may serve is largely unknown. Given that late endosomes (LEs) constitute central nodes within the endo- and exocytic vesicular network (9), we mined a genome-wide siRNA-based screen for novel factors controlling LE biology (25), where silencing the RING finger ubiquitin ligase RNF26 was shown to severely disrupt the intracellular LE organization, leading to marked dispersion of LEs throughout the cytoplasm and even to the tips of cells, without significantly impacting cell shape (Figures 1B-D; Movies S1A and S1B (movies can be downloaded from the online version: http://www.sciencedirect.com/science/article/pii/S0092867416307255). These observations cast RNF26 as a potent candidate for control of the LE compartment architecture, prompting us to investigate the role of RNF26 in the organization and function of the perinuclear (PN) cloud.

In live cells, we observed a striking relationship between the LE compartment architecture and its dynamics. The majority of acidified vesicles marked by Lysotracker (LTVs) were positionally restricted to the PN cloud, while the sparsely populated periphery (PP) remained dynamic over time (Figure 1F, top right panels; Movie S2A). On the contrary, cells depleted of RNF26 exhibited an expanded periphery and increased mobility of the LTV contingent relative to control, thus blurring the PN/PP distinction (Figures 1E and 1F, bottom right panels; Movies S2B and S2C, Lysotracker; Movies S2D and S2E, mCherry-CD63).

To test whether other components of the endo- and exocytic vesicular repertoire also fall under the RNF26 purview, we investigated the effect of RNF26 silencing on distribution of various vesicle markers. Without exception, localization of all post-Golgi vesicles examined was susceptible to RNF26 depletion in two different cell lines test-

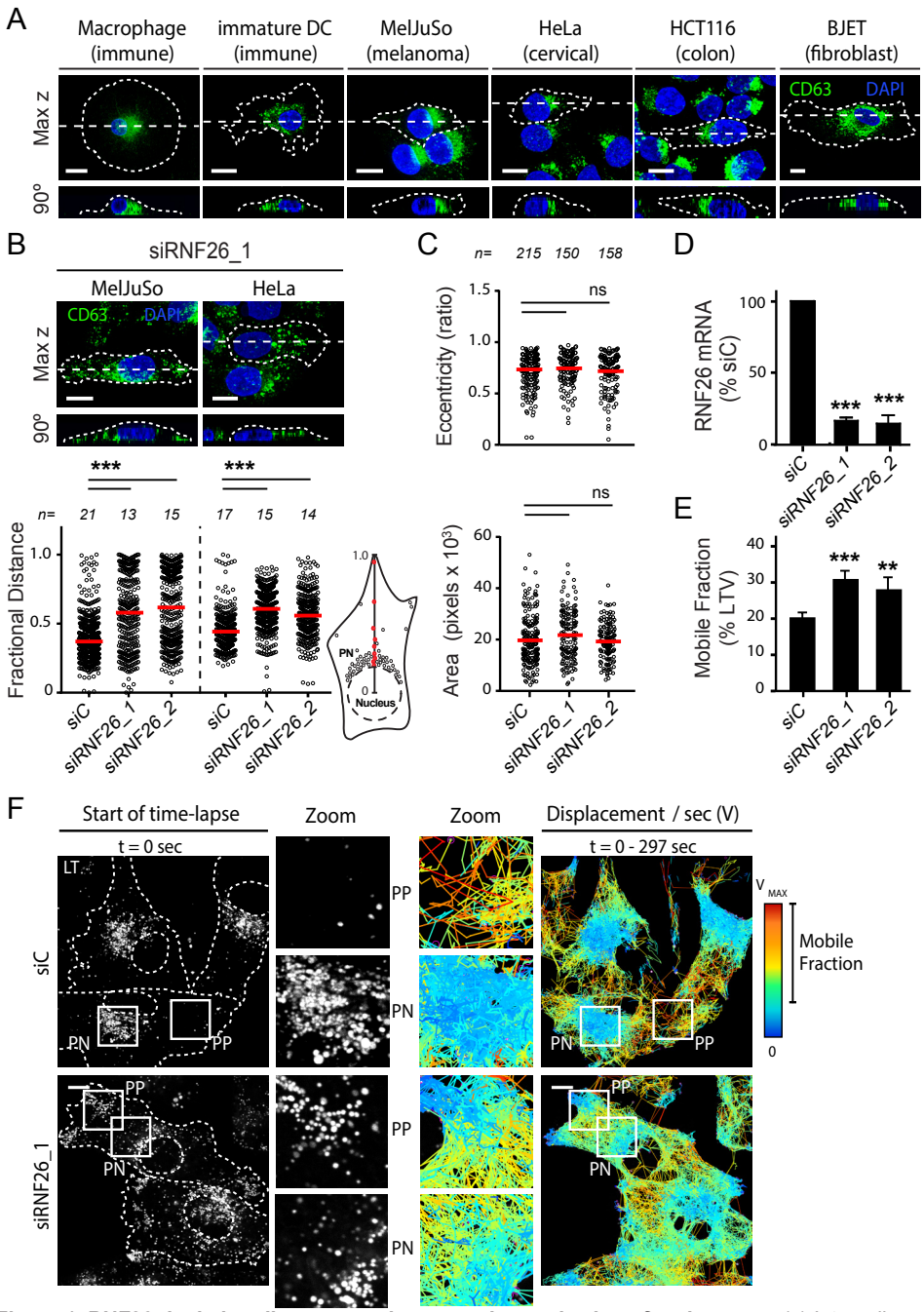


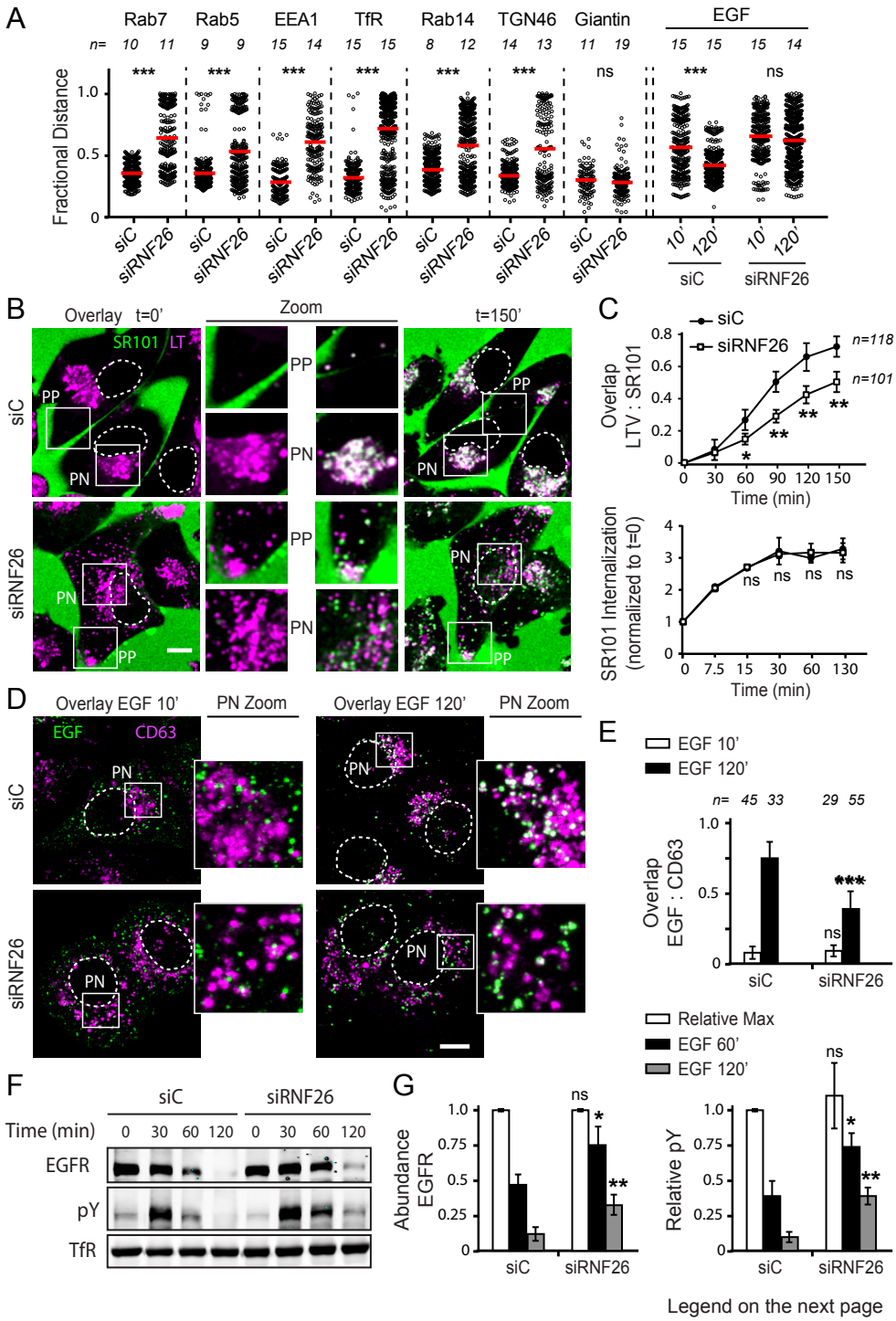
Figure 1. RNF26 depletion disrupts spatiotemporal organization of endosomes. *(a) Intracellular distribution of LEs (CD63, green) in various cell lines. Representative maximum z-projection (3D) overlays with nuclear DAPI (blue) and their corresponding z-cross sections along the demarcated line are shown. Cell boundaries are depicted in dashed lines. For other markers see Figure S1. Legend continues on next page*

ed, while distribution of the Golgi remained unaffected (Figures 2A, S2A and S2B; Movies S3A-S3D). Given that intracellular organization and its associated compartmentalization of transport apply across diverse vesicle types, we hypothesized that the PN cloud may serve as a meeting hub for maturation and cargo exchange. In support of this, we found that vesicles endocytosed by fluid-phase (as monitored using uptake of the extracellular dye sulforhodamine (SR101, (Wubbolts et al., 1996)) readily encountered LT-positive structures residing primarily in the PN cloud. By contrast, acquisition of SR101 by the disorganized acidified compartments in RNF26 depleted cells was markedly restrained (Figures 2B and 2C; Movies S4A and S4B), while SR101 internalization rate remained unaffected (Figure 2C), suggesting that endosomes mature in the PN cloud. We further explored whether trafficking of specific cargoes to the proteolytic compartment is affected by the endosomal system's architecture. Following acute stimulation with EGF, ligand-containing vesicles distributed to the PN cloud over time in control cells, but not in those compromised for RNF26 (Figure 2A). In the latter case, trafficking of EGF-positive vesicles to the LE compartment was severely impaired (Figures 2D and 2E), while availability of EGF receptor (EGFR) on the cell surface, as well as total receptor levels, remained unaffected (Figures S2C and S2E). Consistent with the above, ligand-induced degradation of EGFR was attenuated with RNF26 depletion, leaving activated receptors (detected as pY) to linger at late time-points following stimulation (Figures 2F and 2G). Taken together with the SR101 experiments, these findings imply that the PN cloud and its architect RNF26 facilitate efficient vesicle maturation and transit of cargo through the endosomal system, with implications for ligand-induced receptor signaling.

ER localization and ubiquitin ligase activity of RNF26 mediate endosomal positioning

Having determined that loss of RNF26 incurs detrimental effects on endosomal organization and function, we turned to ask whether this ER-located ubiquitin ligase (26) actively positions endosomes in the PN cloud. Ectopic expression of full length RNF26, but not its catalytic RING domain (ΔRING) truncation, substantially restricted mobility of LT-positive vesicles (Figures 3A and 3B). Mirroring the PN position of the vesicle cloud, RNF26 localized predominantly to the region of the ER proximal to the nucleus, while its ΔRING mutant distributed throughout the ER (Figures 3C and

(b) Effect of RNF26 depletion on distribution of LEs, represented as fractional distances of CD63 vesicles from center of nucleus (distance of pixels from nucleus = faction of distance from nucleus to the plasma membrane (1.0); mean shown in red). For 3D view, see Movies S1A and S1B. (c) Cell shape analysis for samples in (b), showing total cell area and eccentricity calculated in an automated fashion as described in the Extended Materials and Methods. (d) mRNA levels of RNF26 targeted by 2 different siRNAs (siRNF26_1 and siRNF26_2) as assessed by qPCR are expressed relative to siC; N=3. (e) Quantification of the mobile fraction of acidified Lysotracker (LT)-positive vesicles (LTVs) as a function of RNF26; N=3. For details, refer to the Extended Materials and Methods. (f) Organization and dynamics of LTVs (white) in control (siC) versus RNF26-depleted (siRNF26_1) MelJuSo cells. Left panels: representative single confocal plane fluorescence images taken at the start of time-lapse. Right panels: vesicle displacement rates (blue = immobile, red = max mobility) observed over the 297 sec time interval. Nuclei and cell boundaries are depicted in dashed lines, and zoom-ins highlight peripheral (PP) and perinuclear (PN) boxed regions. Quantification appears in (e). For LT time-lapses see Movies S2A-S2C. For CD63 time-lapses see Movies S2D and S2E. Scale bars = 10 μm. For all figures: n= # of cells analyzed per condition, N= # independent experiments, error bars = SD.



Legend on the next page

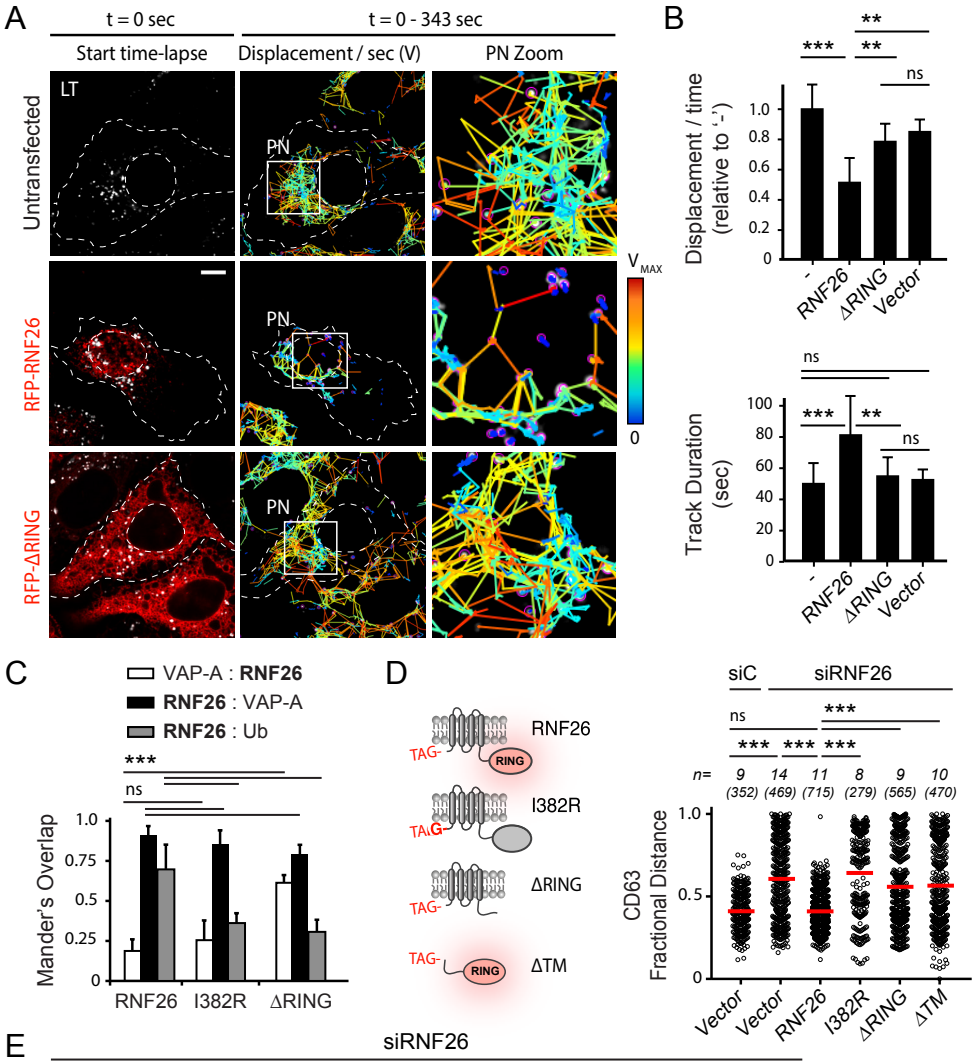
S3A-S3C; ER marked by VAP-A), indicating that the RING domain drives retention of the ligase in the perinuclear ER subdomain.

To explore the contribution of catalytic activity to RNF26 localization and function, we mutated a conserved Isoleucine 382 to Arginine (I382R, Figure S3A), thereby inhibiting expected interactions with E2 enzyme(s) without incurring deleterious effects on RING domain architecture, such as by mutating key Zn+2 coordinating modules (27). RNF26-I382R markedly reduced the enzyme's ubiquitin ligation capacity (Figure S3B), similar to the previously reported C401S mutant (26). Ubiquitin ligase activity was further illustrated by strong colocalization of wild type RNF26 with ubiquitinated species, relative to its catalytically dead mutants showing only marginal overlap with ubiquitin (Figures 3C and S3C). We next tested whether ubiquitin ligase activity afforded by RNF26 is critical to perinuclear endosome positioning. The RNF26 depletion phenotype, scored on the basis of LE scattering away from the nucleus, was robustly rescued by re-expression of RNF26, but not its mutants deficient in either ubiquitination or ER transmembrane segments (Figures 3D and 3E), implying that RNF26-mediated ubiquitination must take place at the ER membrane to effectively position vesicles in the PN cloud.

RNF26 interacts with a network of vesicle-associated adaptor proteins

To understand how an ER-located protein exerts control over the endosomal system and the TGN, we sought out interacting partners of the cytosolic tail of RNF26. Mass spectrometric analysis of proteins co-precipitating with either GST-ΔTM or GST-RING (Figures 4A, S4A) identified three membrane-associated adaptor proteins functioning in sorting and trafficking of endo- or exocytic vesicles—EPS15 (28), T6BP/TAX1BP1 (29) and TOLLIP (30), a ubiquitin scaffold p62/SQSTM1 (31) known for its role in autophagy (32) and a DUB USP15, which localizes to the nucleus and cytosol, targeting the TGFβ and NF-κB pathways (33, 34). Collectively, cargo specificities of the three former proteins afford broad coverage of both endocytic and

Figure 2. RNF26 promotes cargo trafficking and endosome maturation in the perinuclear cloud. *(a) Intracellular distribution of various markers and cargoes in MelJuSo cells in response to RNF26 depletion, presented as fractional distances with mean shown in red, as in Figure 1b. Late endosomes: Rab7; early endosomes: EEA1, Rab5 and Rab14; recycling endosomes: Transferrin receptor (TfR); TGN: TGN46; Golgi: Giantin; ligand-mediated endocytosis: EGF. See also Figures S2A, S2B and 2D and Movies S3A-S3D. (b) Trafficking of fluid phase dye SR101 (green) to the acidified compartment (LT, magenta). Single confocal plane fluorescence overlays with PP and PN zooms at t=0 and t=150 min following addition of SR101 to control or RNF26-depleted MelJuSo cells are shown. See also Movies S4A and S4B. (c) Top graph: quantification (Mander's overlap) of SR101 entry into LTVs as a function of time (min) in control MelJuSo cells or those silenced for RNF26. N=2. Bottom graph: total uptake of SR101 in control or RNF26-depleted MelJuSo cells as measured by flow cytometry, expressed as fold increase normalized to t = 0 as a function of time; N=3. (d) Effect of RNF26 depletion on receptor-mediated trafficking of EGF-555 (green) to the late endosome compartment (CD63, magenta). Representative z-projection (3D) overlays at 10 min (left panels) and 120 min (right panels) following stimulation (100 ng/ml) are shown with PN zooms for control and RNF26-depleted HeLa cells. (e) Colocalization (Mander's overlap) of EGF with CD63 at 10 min (white) and 120 min (black) following ligand stimulation; N=2. (f) EGFR degradation in control versus RNF26-depleted HeLa cells. Immunoblots against total (EGFR) and phosphorylated (pY) EGFR, as well as TfR (loading control) along a time-course following 20 ng/ml EGF addition (min) are shown (lane corresponding to t=10 min was excised from siC panel). For analysis of surface and total EGFR levels see Figures S2C and S2E, respectively. (g) Quantification of total (left graph, relative to t=0) and activated (right graph, pY relative to siC at t=30') EGFR as a function of time following EGF addition; N=3. Scale bars = 10 μm.*



Legend on the next page

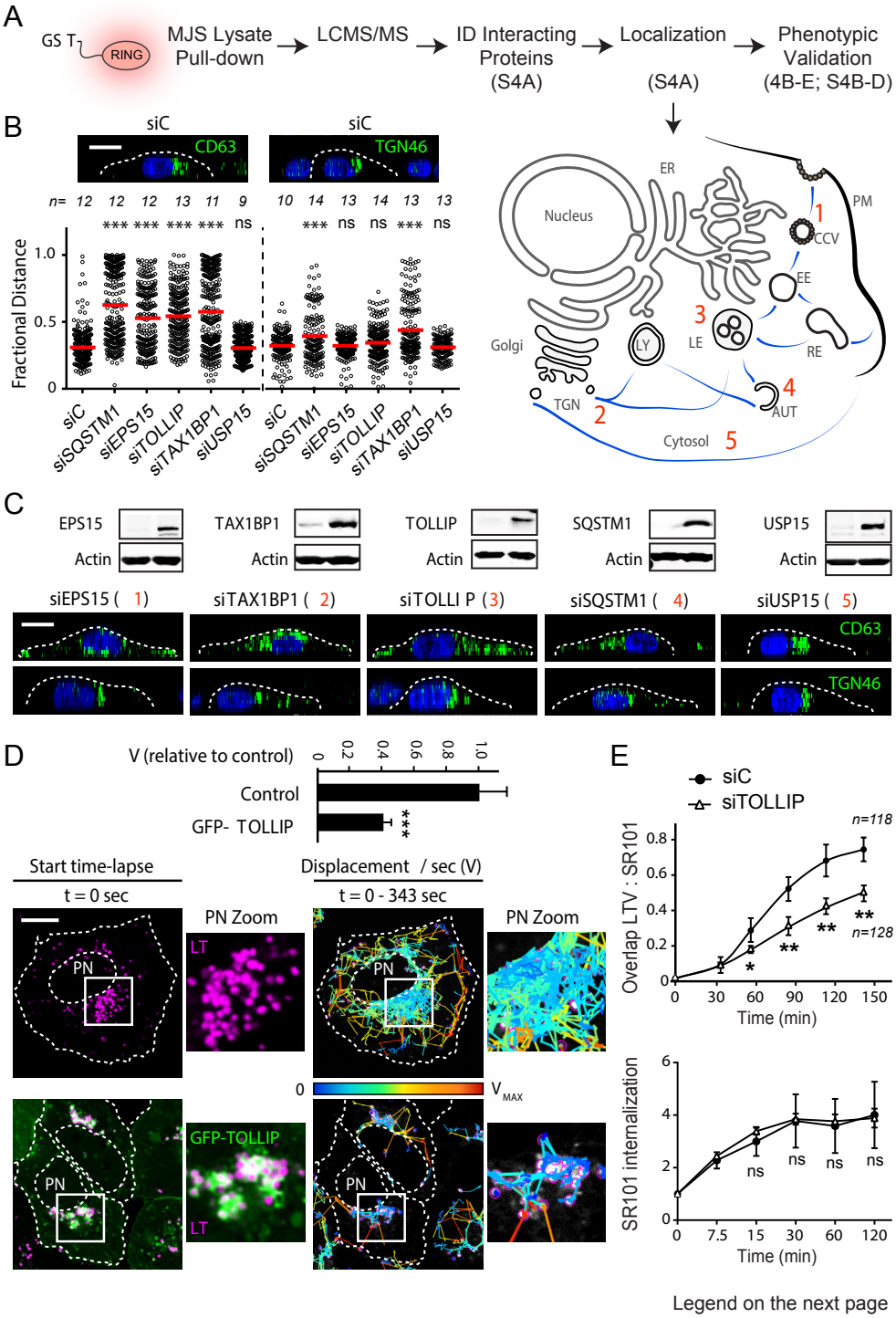
biosynthetic vesicle trajectories (Figures 4A and S4A), implying that by association with different vesicle-targeting adaptors, RNF26 may influence positioning of a wide range of endosomes and the TGN. Silencing the above proteins (excluding USP15) produced marked LE dispersion (Figures 4B and 4C). By contrast, TGN vesicle dispersion resulted only from depletion of the TGN-associated adaptor TAX1BP1 and SQSTM1, but not of endocytic adaptors EPS15 and TOLLIP (Figures 4B and 4C), and overall cell shape parameters were profoundly altered only by depletion of TAX1BP1 (Figure S4B). Further, co-silencing multiple adaptors resulted in additive effects on CD63 distribution (Figure S4C), underscoring the contribution of multi-directional traffic to the global architecture of the LE compartment.

To assess whether specific adaptors can influence localization and dynamics of their cognate vesicles, we followed the mobility of LTVs in cells ectopically expressing GFP-TOLLIP. Double-positive vesicles were found to localize primarily in the PN cloud (Figure 4D), and overall LTV movement was dramatically restricted relative to control (Figure 4D; Movies S5A and S5B). Additionally, exogenous TOLLIP restored PN localization of vesicles marked by CD63 in an exceptional cell line (RKO, Figure S4D), which exhibits natural dispersion of the LE compartment (Figure S1). Mirroring the dysfunction in endosomal maturation incurred by depletion of RNF26 (Figures 2B and 2C), silencing TOLLIP inhibited access of SR101-containing endosomes to the acidified compartments, without affecting the internalization rate (Figure 4E). Taken together, the above observations illustrate the capacity of a specific adaptor to position its chosen vesicles in the PN cloud.

Catalytically active RNF26 attracts ubiquitin-binding domains of endocytic adaptors

To dissect the molecular basis of communication between RNF26 and its partners, we interrogated their respective interaction determinants. Without exception, EPS15, TAX1BP1, TOLLIP, USP15 (Figure 5A) and SQSTM1 (Figure 5B, right panels) exhibited a strong binding preference for catalytically competent RNF26, relative to the inactive I382R mutant. Given the critical role of RNF26 ubiquitination activity in the

Figure 3. ER-associated ubiquitin ligase activity of RNF26 organizes the PN cloud and controls vesicle dynamics. *(a) Effect of RNF26 on vesicle dynamics. Left panels: representative single confocal plane fluorescence overlays of LT (white) in control (untransfected; focal plane through the nucleus) HeLa cells or those ectopically expressing (red) RFP-RNF26 (focal plane just above the nucleus) or its ΔRING mutant (focal plane through the nucleus) at the start of time-lapse are shown. Middle panels: corresponding vesicle displacement rates (blue = immobile, red = max mobility) observed during the 343 sec time interval. Right panels: zooms of boxed PN regions. (b) Quantification of displacement rates (relative to untransfected cells) and track duration times (sec) for data presented in (a); N=4. (c) Colocalization (Mander's overlap) of RNF26 or its mutants I382R and ΔRING with the ER protein VAP-A or ubiquitin. White bars: overlap VAP-A with RNF26; black bars: overlap RNF26 with VAP-A; gray bars: overlap RNF26 with ubiquitin; n=10 per sample per experiment, N=3. See also Figures S3A-S3C.(d) Rescue of RNF26 depletion phenotype (siRNF26 targeting 3'UTR) by re-expression of wild type HA-RNF26, its RING domain mutants I382R and ΔRING, its trans-membrane truncation ΔTM or empty vector. Late endosome (LE) fractional distance analysis of CD63 in MelJuSo cells is shown (mean in red), along with a schematic overview of RNF26 constructs used. For cell shape analysis of ectopic RNF26 expression, see Figure S3D. (e) Selected representative maximum z-projection (3D) image overlays of CD63 (green) with nuclear DAPI (blue) corresponding to quantification in (d) are shown, together with their z-cross sections along the demarcated line. Single confocal slices in top panels show HA-tagged expression. Scale bars = 10 μm.*



Legend on the next page

establishment of endosomal system's architecture described in Figure 3, we proceeded to investigate ubiquitin-mediated recognition in this context. Most interacting partners of RNF26 described here harbor ubiquitin-binding domains (UBDs) (Figure 5C), and point mutations targeting the CUE domain of TOLLIP (35), UIM domain of EPS15 (36), and UBZ2 domain of TAX1BP1 (but not UBZ1, which is incapable of ubiquitin interactions (37)) strongly affected association of these proteins with wild type RNF26 (Figures 5B, left panels and S5A). Moreover, the UBD-dependent loss of binding was comparable to that observed between wild-type adaptors and mutant RNF26 (Figure 5D). Strikingly, SQSTM1 did not follow suit, displaying no significant reliance on its UBA domain for productive interaction with RNF26 (Figures 5B, right panels and 5D). Mechanistically, these observations set SQSTM1 apart from the other adaptors within the RNF26 network.

Because the known specificity of SQSTM1 for autophagic membranes is unlikely to account for its broad effects on positioning of both endocytic and biosynthetic systems of vesicles (Figures 4A-4C and S4A), we hypothesized that it may instead function by attracting ubiquitin-dependent partners to RNF26. To test this, we investigated spatial localization of SQSTM1 versus the RNF26-interacting vesicle adaptors relative to the ligase and its associated ubiquitin signals. As expected based on the Co-IP data, the LE adaptor GFP-TOLLIP readily colocalized with RNF26 at the corresponding sites of endogenous ubiquitin accumulation, while its ubiquitin-binding deficient point-mutant (CUE*) did not (Figures 5E). Importantly, lack of its recruitment to the ligase had no discernable effect on ubiquitin enrichment at RNF26 (Figures 5E and 5F). By contrast, UBA domain truncation of SQSTM1 (ΔUBA) was still able to occupy RNF26-positive structures, but significantly suppressed accumulation of associated ubiquitinated species (Figures 5G and 5H), thus implicating SQSTM1, along with its ubiquitin interactions, in the assembly of ubiquitinated spe-

Figure 4. Protein network associated with the RING domain of RNF26. *(a) Workflow scheme for the identification and validation of proteins interacting with the cytosolic domain of RNF26. RING-associated RNF26 proteome consists of membrane-associated adaptor proteins and a DUB USP15 (for proteomic analysis details, see Figure S4A). Localization of RNF26-interacting proteins EPS15, TOLLIP, TAX1BP1, SQSTM1 and USP15 are depicted schematically (for representative marker overlays see Figure S4A). CCV: clathrin-coated vesicle, EE: early endosome, RE: recycling endosome, LE: late endosome, Ly: lysosome, TGN: trans-Golgi network, AUT: autophagosome, PM: plasma membrane. (b) Intracellular distribution (fractional distance analysis, mean shown in red) of LEs (CD63) and TGN (TGN46) in MelJuSo cells as a function of indicated siRNA perturbations. For cell shape analysis, see Figure S4B. For combinatorial silencing of vesicle adaptors, see Figure S4C. (c) Representative z-cross section (3D) image overlays of CD63 (green, upper panels) or TGN46 (green, bottom panels) with nuclear DAPI (blue) in MelJuSo cells are shown with the corresponding protein levels of silenced targets (left lanes) as compared to the control (right lanes). (d) Effect of GFP-TOLLIP (green) overexpression on the organization and dynamics of acidified vesicles (LTVs, magenta) in HeLa cells. Left panels: representative single confocal plane fluorescence image overlays taken at the start of the time-lapse. Right panels: corresponding vesicle displacement rates (blue = immobile, red = max mobility) observed during the 343 sec time interval; zoom-ins highlight boxed PN regions. Quantification of LTV dynamics (displacement / sec relative to untransfected cells) as a function of TOLLIP is shown above the images; N=2. See also Movies S5A and S5B. See also Figure S4D. (e) Top graph: quantification (Mander's overlap) of SR101 entry into acidified vesicles (LTVs) as a function of time (min) in control MelJuSo cells (siC; control data set in common with Figure 2C) versus those depleted of TOLLIP (siTOLLIP). N=2. Bottom graph: total uptake of SR101 in control or TOLLIP-depleted MelJuSo cells as measured by flow cytometry, expressed as fold increase normalized to t = 0 as a function of time; N=3. Scale bars = 10 μm.*

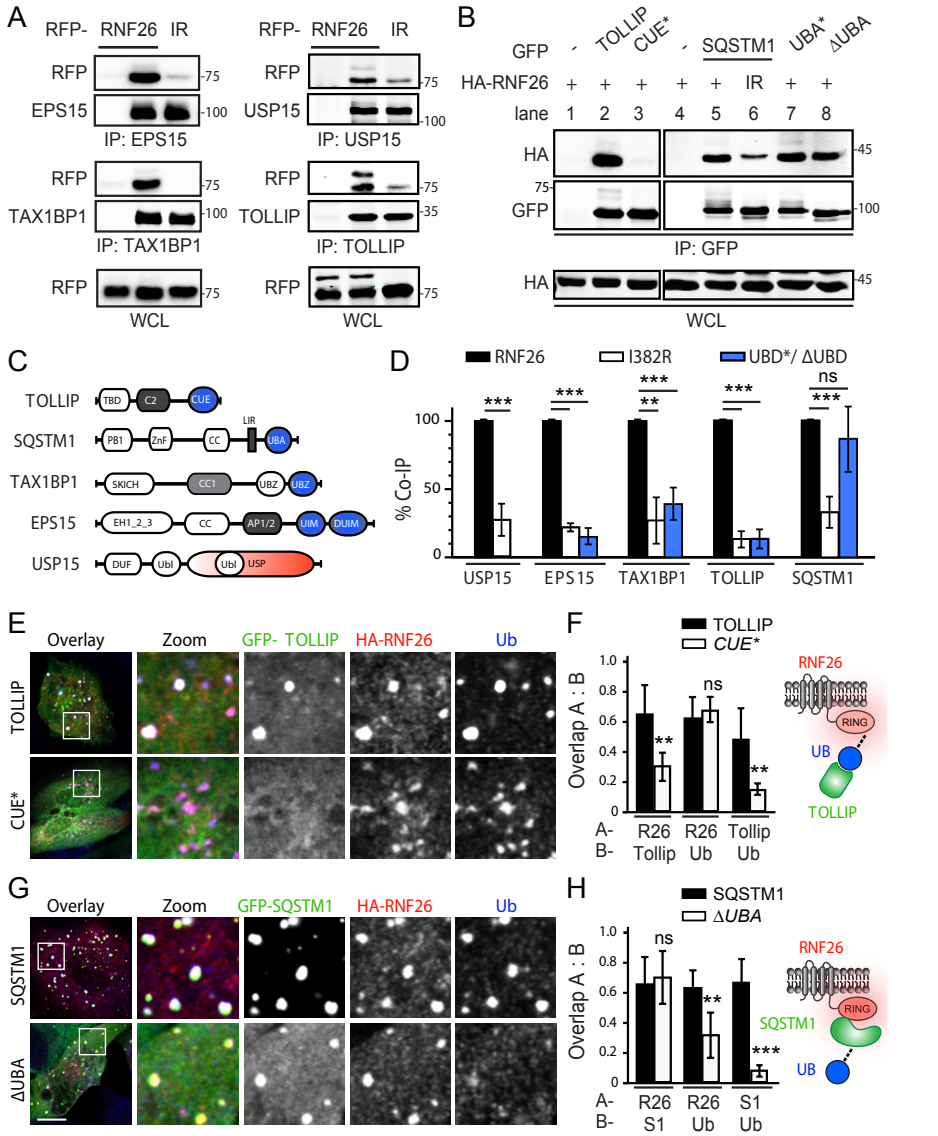


Figure 5. RNF26 couples to ubiquitin-binding domains of specific membrane adaptors. *(a) Interactions (assayed by Co-IP) between RNF26 versus its inactive mutant I382R (IR) and endogenous EPS15, TAX1BP1, TOLLIP and USP15 in HEK293T cells. WCL: whole-cell lysate. (b) Effects of mutations in ubiquitin-binding domains (UBDs) of TOLLIP and SQSTM1 on interaction with RNF26 in HEK293T cells (extraneous lanes between 4 and 5, as well as 6 and 7 were excised). For TAX1BP1 and EPS15, see Figure S5A. (c) Schematic: domain organization of RNF26-interacting proteins, highlighting membrane-targeting domains (gray), UBDs (blue), and USP (red). (d) Quantification of interactions (normalized as % of WT/WT Co-IP, black bars) as a function of RNF26 inactivation (I382R white bars) or loss of UBD capabilities (UBA*/ΔUBA, blue bars) for each pair of proteins; N=3. (e-h) Colocalization of GFP-tagged (green) (e) TOLLIP (quantified in (f); N=2) and (g) SQSTM1 (quantified in (h); N=2) or their UBD mutants (CUE* and ΔUBA, respectively) with HA-RNF26 (red) and endogenous ubiquitin (blue) in MelJuSo cells. Representative single confocal plane fluorescence overlays and single-channel zooms are shown. Summary is illustrated schematically at the right. Scale bars = 10 μm.*

cies at RNF26.

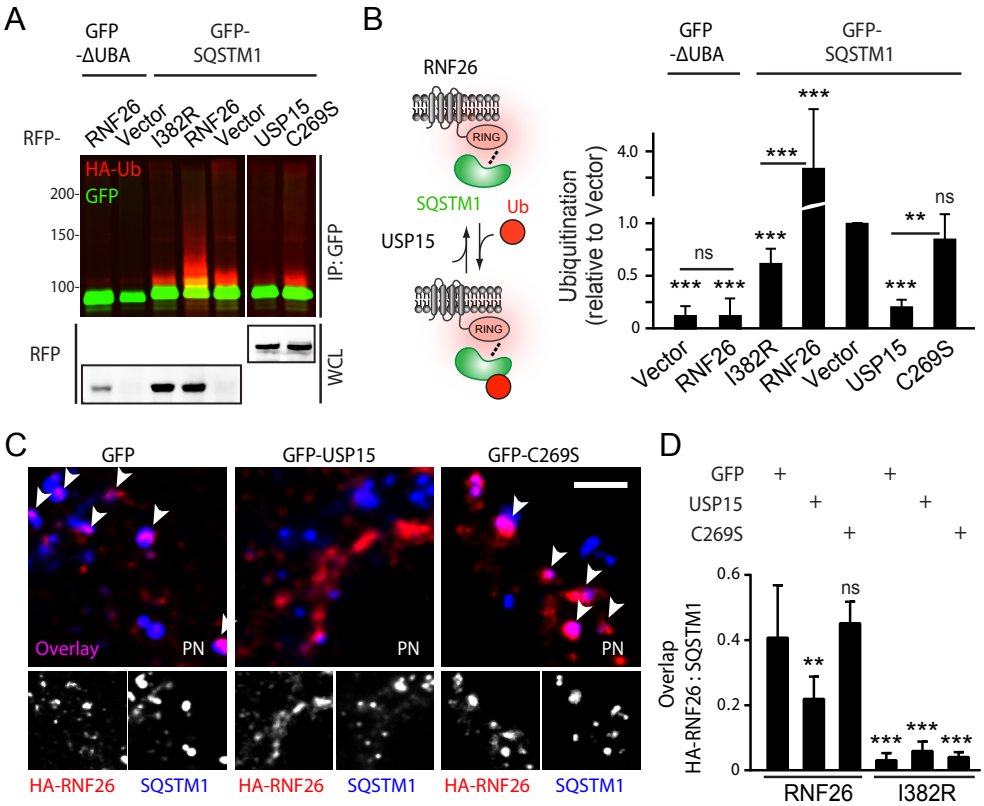
RNF26 and the DUB USP15 share a substrate in SQSTM1

To elucidate the unique mechanism of SQSTM1 function within the RNF26 protein network, we delved into the contribution of its UBA domain. Given previously reported connections between ubiquitin binding and ubiquitination of UBD-containing proteins (38), we considered whether SQSTM1 constitutes a substrate for RNF26. Indeed, major enhancement in short ubiquitin conjugates on SQSTM1 was observed in response to ectopic expression of wild type but not catalytically inactive RNF26 relative to vector control (Figures 6A and 6B). Importantly, RNF26 was unable to ubiquitinate truncated SQSTM1 lacking its UBA domain (Figures 6A and 6B), indicating that only SQSTM1 in possession of its ubiquitin-binding faculties can serve as a substrate for the ER-located ubiquitin ligase. Taken together with the findings presented in Figure 5, the above evidence suggests that ubiquitinated SQSTM1 comprises the Ub-rich signals observed at sites of RNF26 activity.

If ubiquitination afforded by RNF26 restricts vesicles in the PN cluster, a deubiquitinating activity may then complete the biochemical cycle to allow release of vesicles for rapid transit in the cell's periphery. This function could be served by USP15, which preferentially associates with catalytically competent RNF26 (Figures 5A and 5D). We therefore tested whether USP15 deubiquitinates the RNF26 substrate, SQSTM1. Indeed, overexpression of wild type USP15 dramatically decreased short-chain modification of SQSTM1 with ubiquitin in a manner dependent on its catalytic Cys 269 residue (Figures 6A and 6B). Furthermore, expression of wild type (but not inactive) USP15 reduced the degree of colocalization of RNF26 with SQSTM1 (Figures 6C, 6D and S5B), indicating that USP15 activity modulates occupancy of ligase-positive sites. Consistent with the notion that USP15 functionally rivals RNF26, silencing USP15 essentially ablated the highly mobile peripheral contingent marked by Lysotracker (Figure 6E; Movies S5A and S5C), resulting in an overall decrease in mobility of acidified organelles (Figure 6F)—a phenotype opposite to that observed with depletion of RNF26 (Figures 1E and 1F). As expected, based on their catalytic opposition, co-depletion of USP15 and RNF26 partially restored the PN/PP balance (Figure 6G), implying that USP15 promotes release of vesicles captured and restrained by the active RNF26 complex.

The ER-located RNF26/SQSTM1 complex controls vesicle positioning and dynamics

Consistent with the proposed role of SQSTM1 in bridging adaptor-selected vesicles to catalytically competent RNF26, we observed colocalization of all three specific membrane adaptors—EPS15, TAX1BP1 and TOLLIP—with endogenous SQSTM1 at sites of wild type, but not inactive RNF26 (Figures S6A and S6B). Additionally, the interaction between TOLLIP and SQSTM1 was exquisitely sensitive to mutation in the UBD domain of the former (Figure S6C), recapitulating ubiquitin-mediated recognition of RNF26 complexes by adaptor proteins (Figure 5). Importantly, structures positive for RNF26 and SQSTM1 (or its fragments) did not overlap with the autophagy marker LC3 (Figure S6A, right panels), indicating that the function of SQSTM1 in this context is unrelated to autophagy.



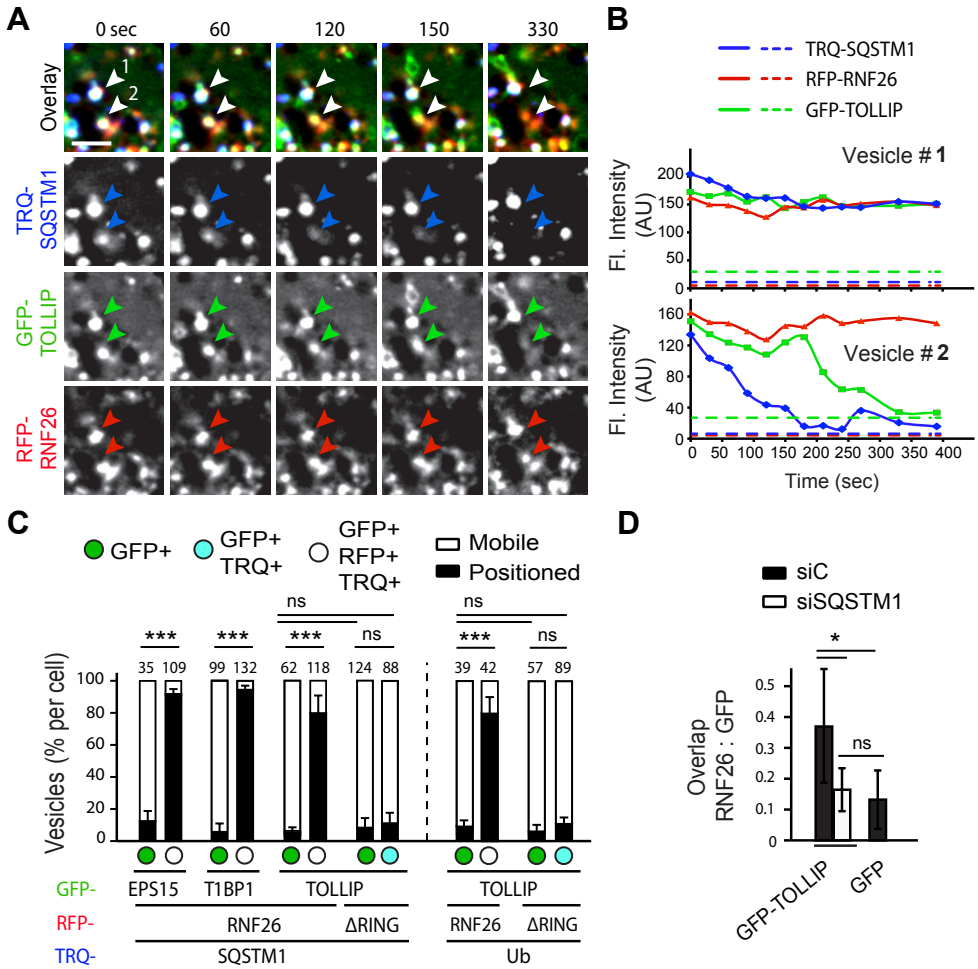
Legend on the next page

To test whether SQSTM1 dictates endosome positioning at RNF26, we monitored vesicle dynamics via specific membrane adaptors in living cells co-expressing fluorescent SQSTM1. We observed stable PN contacts between GFP-Adaptors ('green') and RFP-RNF26 ('red') that were overwhelmingly positive for TRQ-SQSTM1 ('blue'; Figure S7A; Movie S6A), with tripartite complex formation (appearing 'white' in the overlay) strongly correlated to fixed positional residence of vesicles marked by EPS15, TAX1BP1, and TOLLIP (Figures 7A-7C). By contrast, the vast majority of only GFP-positive 'green' vesicles remained subject to fast transport (Figure 7C; Movie S6A). As expected, RNF26 lacking its RING domain could not mediate stable contacts with TRQ-SQSTM1 and failed to stabilize vesicles in position over time (Figures 7C and S7A, Movie S6B). Similar to TRQ-SQSTM1, TRQ-ubiquitin was found at contracts between GFP-TOLLIP-positive vesicles retained by RFP-RNF26 (but not RFP-ΔRING), while highly mobile vesicles were free of ligase and ubiquitin contacts (Figures S7B and 7C).

Interestingly, while most 'white' vesicles stayed docked at the RNF26/SQSTM1 complex over time, occasional release was observed following disappearance of TRQ-SQSTM1 (Figures 7A and 7B, vesicles #1 and #2, respectively; Movie S7), and depletion of SQSTM1 markedly reduced distribution of TOLLIP-positive structures to RNF26 (Figure 7D). Considering diminished RNF26 occupancy by SQSTM1 in the presence of USP15 (Figures 6C and 6D), these findings suggest that assembly of SQSTM1 contacts at sites of RNF26 positions vesicles in the PN cloud, while disintegration of such complexes mediates vesicle release.

Taken together with the interaction and functional studies, the observations described above are consistent with the following order of molecular events: catalytically competent RNF26 recruits SQSTM1, which becomes subject to UBA-dependent ubiquitination by the ligase. This ubiquitin-rich RNF26/SQSTM1 complex is then poised to attract UBDs of endocytic adaptors (and the DUB USP15) to the PN cloud (proposed model depicted in Figure 7E). Subsequently, deubiquitination by USP15 at these sites determines release of the SQSTM1/Ub/Adaptor complex from the ER membrane, allowing transport of vesicles into the cell periphery). Collectively, our findings illustrate that by attracting diverse membrane-associated vesicle adaptors

Figure 6. SQSTM1 is a substrate for RNF26 and the DUB USP15. *(a) Ubiquitination status of SQSTM1 as a function of catalytic activities of RNF26 and USP15. GFP-SQSTM1 (or -ΔUBA) was isolated from HEK293T cells overexpressing HA-Ub in the presence of vector, RFP-RNF26 versus its catalytic mutant I382R, or USP15 versus its catalytic mutant C269A. Ubiquitination status of GFP-substrate (green) was assessed by immunoblots against HA (red). (b) Quantification of the ubiquitination assay in A; N=4. Schematic on the left depicts proposed catalytic opposition between RNF26 and USP15. (c) Effect of USP15 on localization of SQSTM1 (blue) at RNF26-positive sites (red) in the PN area. Representative single confocal plane fluorescence overlays of PN regions are shown with their corresponding single channel images (HeLa cells). For a full image panel, see Figure S5B. Scale bar = 2.5 µm. (d) Quantification of RNF26 or I382R occupancy by SQSTM1 (Mander's overlap) as a function of USP15 catalytic activity; N=2. (e) Organization and dynamics of acidified LT-positive vesicles (LTVs, white) in control (siC) versus USP15 depleted (siUSP15) HeLa cells. Left panels: representative single confocal plane fluorescence images at the start of time-lapse are shown. Right panels: corresponding vesicle displacement rates (blue = immobile, red = max mobility) observed during the 343 sec time interval; zoom-ins highlight boxed PP and PN regions. For time-lapses, see Movies S5A and S5C. Scale bar = 10 µm. (f) Effect of USP15 depletion on LTV dynamics (displacement / sec relative to cells transfected with control siRNA); N=2. (g) Functional interplay between siUSP15 and siRNF26. Quantification of mobile LTV fraction as a function of indicated siRNA perturbations (+) in MelJuSo cells; N=2.*



Legend on the next page

through a common mechanism, the RNF26/SQSTM1 complex controls the positioning and dynamics of endosomal vesicle transport, and so designs the architecture of the endo- and exosomal system.

Discussion

Proper control of the biosynthetic and endocytic membrane networks is crucial to normal functioning of cells and organisms, and failures therein are known to result in neuronal diseases (39) and obstructed immune responses (40), as well as contribute to a variety of cancers (41). The biology of endosomes (and the TGN) relies on cargo acquisition and vesicle transport working together to ensure accurate and timely delivery of select materials to their destinations. While we understand various aspects of cargo selection and vesicle transport, we know very little of the molecular decisions required to negotiate their arrivals and departures in the busy 3D environment of the cell. In the present study we explored the functional relationship between the endosomal system's architecture and dynamics, exposing its molecular underpinnings.

Cells organize a wide variety of their endosomal flavors (including vesicles of the TGN) into a PN cloud positioned near the MTOC. When in the cloud, vesicles exhibit restricted mobility, with only a fraction of each subtype traveling fast to and from the cell's periphery at any given time. We show that the central player governing this spatiotemporal integrity—the ER-located E3 ligase RNF26—retains endosomes on location of its choice through post-translational modification with ubiquitin. Residing in the subdomain of the ER proximal to the nucleus, RNF26 draws the perinuclear architecture of the complex vesicle network suggestive of a cargo bazaar—a meeting place accessible from all corners of the cell, where efficient exchange can take place. We show that vesicles, internalized by either fluid-phase or ligand-mediated endocytosis, are targeted to the PN cloud, where they meet the late endosomal contingent. Loss of RNF26 function inhibits these encounters, slowing maturation of endosomes acquired in the periphery, without affecting the internalization rate. Furthermore, RNF26 depletion delays degradation of activated—i.e. signaling-competent—EGFR following ligand exposure, substantiating the notion that the spatiotemporal control afforded by the PN cloud facilitates vesicle maturation and cargo

Figure 7. RNF26/SQSTM1 complex positions and retains adaptor-selected vesicles. *(a) Overlay zooms of frames selected from a time-lapse (Movie S7) of vesicles marked by GFP-TOLLIP (green) in the presence of TRQ-SQSTM1 (blue) and RFP-RNF26 (red) in HeLa cells. Arrowheads point to two vesicles profiled in B. Scale bar = 2.5 µm. (b) Plots of signal intensities over time corresponding to a positioned vesicle #1 (top graph) and a released vesicle #2 (bottom graph) as observed in A. Dashed lines show background signal for each channel. (c) Quantification of adaptor-selected vesicle dynamics (mobile = white; positioned = black) expressed as % of vesicles per category (# counted given above each bar). GFP-marked vesicles (green); vesicles colocalizing with RFP-RNF26/-ΔRING and/or TRQ-SQSTM1 (white and cyan, respectively). See also Figures S6 and S7; Movies S6A, S6B. (d) Co-localization (Mander's overlap) between RNF26 and GFP-TOLLIP in control (siC) and SQSTM1 depleted (siSQSTM1) MelJuSo cells. (e) Model of vesicle positioning in the PN cloud by the RNF26 system. (1) Adaptor-selected (green) vesicles are subject to fast microtubule-based transport when unanchored by RNF26. (2) Catalytically competent RNF26 (light red) recruits SQSTM1 (blue) and mediates ubiquitin ligation (red), which serves to attract UBDs of specific vesicle-associated adaptors. Upon engagement, this multi-protein complex positions cognate vesicles (early, recycling and late endosomes, and TGN) in the perinuclear space. (3) Dissociation of the RNF26/SQSTM1 complex, promoted by the DUB USP15 (yellow), releases target vesicles for (4) fast transport into the cell periphery.*

trafficking. Taken together with a recent report connecting a lysosome's pH with its distance from the nucleus (42), our findings argue that spatial information is intimately connected to function within the endosomal system.

To uncover the molecular mechanism responsible for PN cloud integrity, we identified RNF26-interacting proteins involved in the establishment and regulation of the PN cloud. Enabled by its catalytic activity, RNF26 employs ubiquitin-based communication with several membrane-associated ubiquitin-binding vesicle adaptors—TOLLIP (30), EPS15 (28) and TAX1BP1 (29)—each exhibiting unique compartment selectivity. Importantly, all of the above adaptors in question are critical modulators of different signal transduction pathways. While EPS15 is phosphorylated by EGFR (43), TAX1BP1 binds TRAF6 downstream of TLRs and IL-1R (44), and TOLLIP interacts with TLR2/4 to inhibit innate immune response signaling (Zhang, Ghosh, JBC 2002). Given that RNF26 silencing attenuates ligand-mediated receptor clearance by the endocytic pathway (as shown here for EGFR), the ER-located ubiquitin ligase may influence diverse signaling pathways emanating downstream of cell surface receptors when the latter are targeted by cognate adaptors to the PN cloud.

To signal vesicle recruitment, catalytically competent RNF26 attracts and ubiquitinates SQSTM1, which then serves as a platform for downstream ubiquitin/UBD-mediated complex assembly. These findings add a new dimension to the functional repertoire of SQSTM1, apart from its established role as an autophagic substrate adaptor (32) and its recently reported involvement in dynein-mediated transport (45). Thus, through ubiquitin-based recognition, the ER controls the location and influences the dynamics of different vesicles with distinct biological functions. Given that TOLLIP, EPS15 and TAX1BP1 were isolated from a human melanoma cell line using a proteomic approach, it stands to reason that other vesicle-associated adaptor proteins expressed in other cell types could exhibit a similar relationship with RNF26. Indeed, the endocytic system is notoriously rich in UBD-containing adaptors (5, 46), and some of these could in principle read positional signals from RNF26 as well.

If RNF26-associated machinery could only catch vesicles without being able to let go, the dynamic integrity of the system would be abolished. The breadth of ubiquitin-based recognition in dynamic biological processes (47) is due in large part to its controlled reversibility, with DUB activities often functionally accompanying ubiquitin ligation (48). We show that RNF26 interacts with the DUB USP15, which influences occupancy of RNF26 by their common substrate, SQSTM1. Through their catalytic opposition, the two enzymes negotiate the delicate architectural/dynamic balance between the PN cloud and the periphery. How USP15 selects vesicles to be released is at present unclear, but may involve targeted localization or activation of its deubiquitinating functionality at specific RNF26-SQSTM1-adaptor complexes cleared for release.

It is becoming increasingly clear that the cell biology of endosomes and associated vesicle repertoires is modulated by their proximity to other membranes, and contacts with the ER feature prominently in this regard (19, 21, 22). The sheer expansiveness of the ER provides a broadly available docking platform—an intracellular 3D grid—whereupon the RNF26 system could be uniquely capable of facilitating various aspects of vesicle biology. This is gleamed from our observations on delays in endosomal progression and cargo trafficking under conditions of PN cloud break-

down afforded by silencing RNF26. Furthermore, as a consequence of temporarily restricting vesicle mobility, the ER-located RNF26 could assist in the logistics of complex molecular processes, such as fission and/or fusion, both reportedly dependent on ER-endosome contact sites (24, 39). Our findings take a key step toward understanding how cells determine and manipulate the location of their highly mobile endosomal constituents and unveil a new facet of influence the ER exerts over the endosomal system.

Materials and Methods

Light Microscopy

Samples were prepared as described in the supplemental Extended Experimental Procedures. Fixed and live samples were imaged using 63x lenses on Leica SP5 confocal microscopes adapted with a climate control chamber. To calculate fractional distances, fluorescent intensities along multiple line ROIs (assessed on maximum z-projections using the line profile tool in LAS-AF software) were background corrected based on signal thresholds and normalized to median. Fractional distances were reported relative to the maximum distance from the centre of the nucleus to the cell perimeter along a given trajectory. Vesicle tracking during time-lapses was performed using TrackMate for Fiji. Fluid phase endocytosis was performed using SR101 as previously described (Wubbolts et al., 1996). Colocalization was reported as Mander's coefficients calculated using JACoP for ImageJ. All error bars correspond to SD of the mean. Statistical evaluations report on Student's T Test (analysis of two groups) or one-way ANOVA analyses (analysis of three or more groups), with *p<0.05, **p<0.01, ***p<0.001, and ns = not significant.

Cell Lines and Culturing

MelJuSo (human melanoma cell line), BJET (human fibroblast), HCT116 (human colon carcinoma) and RKO (human colon carcinoma) cells were cultured in IMDM (Gibco) supplemented with 7.5% fetal calf serum (FCS, Greiner). Human HEK293T cells and HeLa cells were cultured in DMEM (Gibco) supplemented with 7.5% fetal calf serum (FCS, Greiner). Monocytes were isolated from human blood using CD14 microbeads, and differentiated into macrophages (M-CSF, 50ng/ml, for 9 days) and immature dendritic cells (IL4 (800U/ml), GM-CSF (1000U/ml) for 6 days) by A. Thielen, A. Zaal and A. Saris (Sanquin Research). A MelJuSo cell line stably expressing TGN46-GFP was used in relevant live cell experiments.

Antibodies and fluorescent dyes

(Confocal Microscopy) Rabbit anti-HC (NKI), mouse anti-HC10 (NKI), rabbit anti-human HLA-DR (Neefjes et al., 1990), mouse anti-TrfR (Invitrogen 905963A), mouse anti-EEA1 (mAb 610457, BD transduction laboratories), mouse anti-CD63 NKI-C3 (Vennegoor and Rumke, 1986), mouse anti-clathrin (X22 CP45, Calbiochem), rabbit anti-TGN46 (Thermo Scientific, PA5-23568), rabbit anti-Giantin (Covance PRB-114C), mouse anti-M6PR (ab2733, Abcam), mouse anti-ubiquitin (mAb, P4D1, sc-8017, Santa Cruz), rabbit anti-LC3 (Novus Biologic), mouse anti-SQSTM1 (mAb, sc-28359, Santa Cruz), goat anti-VAP-A (Santa Cruz), and Rat anti-HA (3F10, Roche) were used to stain MHC class I, HLA-DR (Late endosomes/MVBs), EEA1 (Early endosomes), CD63 (Late endosomes), clathrin, TGN46 (Trans Golgi Network), Gian-

tin (Golgi), M6PR (secretory vesicles), ubiquitin, LC3 (autophagosomes), SQSTM1, VAP-A and HA-tagged proteins respectively, followed by secondary anti-Rabbit/ Mouse/Rat Alexa-dye coupled antibodies (Invitrogen) for detection by confocal microscopy. DAPI (Sigma), Lysotracker deep red (Life Technologies) and Lysotracker green (DND-260, Molecular probes; 0.1μM added for 15-30min before fixation) were used to stain the nucleus and lysosomes for detection by confocal microscopy. Sulforhodamine 101 (SR101, Sigma), 25μg/ml; Wubbolts et al, 1996) and EGF-Alexa555 (100ng/ml, Invitrogen) were used in endocytosis assays. (Flow cytometry) anti-HLA-DR (APC) (347403, BD), EGFR (Alexa647) (528, sc-120 Santa Cruz) and anti-CD63 (NKI-C3) (DyLight647 conjugated, Thermo Scientific) were used to stain MHC class II, EGFR and CD63 at the cell surface. (Western Blotting) mouse anti TfR (905963A, Invitrogen), rabbit anti-EGFR (Millipore), mouse anti-phosphotyrosine (pY; 4G10 Millipore), mouse anti-HLA DRα (1B5, NKI), mouse anti-SQSTM1 (mAb, sc-28359, Santa Cruz), rabbit anti-Rab9A (NKI), mouse anti-LAMP1 (BD, 611042), rabbit anti-USP15 (Bethyl, A300-923A), goat anti-TOLLIP (sc27315, Santa Cruz), rabbit anti-TAX1BP1 (A303-791A, Bethyl), rabbit anti-EPS15 (pAb, sc-1840, Santa Cruz), rabbit anti-mGFP (Rocha et al., 2009), mouse anti-HA (HA.11 (16B12), Covance MMS-101R), anti-mRFP (Rocha et al., 2009), rabbit anti-FLAG (F7425, Sigma), mouse anti-FLAG M2 (F3165, Sigma) and mouse anti B-actin (AC-2 15, Sigma) followed by secondary Rabbit anti-Mouse-PO (P0161, Dako) or HRP-Protein A (10-1023, Invitrogen) were used for detection of endogenous or overexpressed proteins by Western blot. Secondary IRDye 680LT Donkey anti-Goat IgG (H+L) (926-68024, Li-Cor), IRDye 800CW Goat anti-rabbit IgG (H+L) (926-32211, Li-COR), IRDye 800CW Goat anti-mouse IgG (H+L) (926-32210, Li-COR), IRDye 680LT Goat anti-rabbit IgG (H+L) (926-68021, Li-COR) and IRDye 680LT Goat anti-mouse IgG (H+L) (926-68020, Li-COR) were used for detection using the Odyssey Classic imager (Li-Cor). (Immuno-precipitation) rabbit anti-Tollip (Sigma), rabbit anti-mGFP (Rocha et al., 2009), rabbit anti-FLAG (F7425, Sigma), rabbit anti-TAX1BP1 (A303-791A, Bethyl), rabbit anti-USP15 (Bethyl, A300-923A), mouse anti-SQSTM1 (mAb, sc-28359, Santa Cruz) and rabbit anti-EPS15 (pAb, sc-1840, Santa Cruz) were used for immuno-precipitation of tagged or endogenous proteins.

Constructs

RNF26 was amplified from IMAGE: 3507662 and cloned into mRFP-C1, mGFP-C1 and 2HA-C1 vectors by EcoRI/BamH1 restriction sites. Inactive mutants of RNF26 (I382R and C401S) were created by site directed mutagenesis. RNF26 ΔTM (aa 246-433) and RNF26 ΔRING (aa1-352) was amplified from the full length construct and cloned into mRFP-C1, mGFP-C1 and/or 2HA-C1 via EcoRI/BamHI Restriction sites. GST-RNF26 ΔTM (aa246-433) and GST-RNF26 RING (aa363-433) were cloned into pRP265 using BamHI/HindIII restriction sites and used for protein production. TOLLIP was cloned into mGFP-C1 and 2xFLAG-C1 by KpnI/HindIII restriction sites. GFP- and FLAG-TOLLIP M240A/F241A (CUE*) was created from the full-length construct by site directed mutagenesis. GFP-SQSTM1 and GFP-SQSTM1 ΔUBA (aa1-401) were amplified from Addgene plasmid #28027 and cloned into mGFP-C1 or mTurqoise-C1 (Goedhart et al., 2012) using EcoRI/XhoI restriction sites. GFP-SQSTM1 P392L (UBA*) was made from the full-length construct by site directed mutagenesis. TAX1BP1 (IMAGE: 100001732) was cloned into mGFP-C1 using

the restriction enzymes Asp718 and BamHI, GFP-TAX1BP1 F737A (UBZ1*) and F764A (UBZ2*) were made from the full-length construct by site directed mutagenesis. GFP-EPS15, FLAG-EPS15 and FLAG-EPS15 L883A/L885A (UIM*) in pMT2SM were a gift from J. Borst (NKI, Amsterdam). USP15 (Addgene plamid #22570) was cloned into mRFP-C1 and mGFP-C1 using the restriction enzymes HinDIII and MluI. The inactive mutant USP15 C269A was generated from the full-length construct by site-directed mutagenesis. HA-ubiquitin in pcDNA3.1 was a generous gift from I. Dikic (Institute for Biochemie II, Frankfurt). mTurquoise-Ub was cloned into mTurquoise-C1 (Goedhart et al., 2012) using HindIII/Asp718I restriction sites. TGN46-GFP was amplified from IMAGE: 53117823 and cloned into mGFP-N1 by EcoRI/BamH1 restriction sites. GFP-Rab14 was cloned into eGFP-C1 (Kuijl et al., 2013). GFP-Rab7 was described before (I. Jordens et al., 2001). GFP-Rab5 was previously described (Jordens et al., 2001). All constructs were sequence verified.

Site directed Mutagenesis

Forward en reverse primers containing the desired mutations were created. A mixture containing template DNA, 1x Pfu buffer, 20mM dNTPs, 0.6µM forward primer, 0.6µM reverse primer, 1µl Turbo Pfu Polymerase filled to 50µl with DEPC was amplified using the following program: 95°C 2min; (95°C 30s; 52°C 30s; 68°C 13min + 2min/Kb) x 20 cycles; 68°C 20min; 4°C forever. 20µl amplified product was incubated with 2µl DpnI (Thermo scientific) for 4hrs at 37°C to digest the template DNA. The mutated DNA was transformed into DH5α using 2xYT medium to increase the amount of the mutated constructs.

siRNA transfection

Sequences of the siRNA oligos targeting RNF26 used in this study are given in the table below. In all cases siRNF26_1 was used unless otherwise indicated. For rescue experiments, siRNF26 3'UTR was used. Gene silencing was performed in a 24 well plate using 50µl siRNA (500nM stock) mixed with 0.75µl DharmaFECT1 #1 (Dharmacon) diluted in 49.25µl IMDM. Transfections performed in other dish/well volumes were scaled up according to media volume appropriate for standard culturing. In case of double or triple siRNA transfections a final concentration of 50nM in a 1:1 (or 1:1:1) ratio of the different siRNA duplexes was used. The mixture was incubated for 20min on a shaker followed by the addition of 28,000 MelJuSo cells in IMDM and cultured for three days at 37°C and 5%CO2 before analysis. Non-targeting siRNA (siCTRL, D-001206-13-20, Dharmacon) was used as a negative control. RNF26 interacting proteins EPS15, TAX1BP1, TOLLIP, SQSTM1 and USP15 were silenced using siRNAs from the siGenome SMARTpool library (Dharmacon).

Gene	siRNA sequence (sense)
RNF26_1 (siGENOME D-007060-17)	GAGAGGAUGUCAUGCGGCU
RNF26_2 (siGENOME D-007060-04)	GCAGAUCAGAGGCAGAAGA
RNF26 3'UTR (Custom, Thermo Sci)	CAGGAGGGAUAACCGGAUUUU

Author Contributions

M.J. and I.B. designed, conducted and interpreted the majority of the experiments and prepared the manuscript. R.H.W. performed the experiments in Figures 3C and S3C and advised on data presentation throughout the manuscript. P.V. and G.J. per-

formed mass spectrometry on prepared samples. L.J. and M.M. provided technical support, H.J. advised on endosome morphology, and M.G. contributed to the study of TOLLIP function on late endosomes. R.S. discussed the results throughout the project. J.N. supervised the project, and all authors edited the manuscript.

Acknowledgments

We thank Jannie Borst for valuable discussions and critical reading of the manuscript and B. van den Broek for help with the Cell Profiler software. We also thank the NKI Protein Production Facility and L. Oomen and L. Brocks for Microscopy Facility support, and particularly L. Oomen for advice on TrackMate software. This work was supported by the ICI, an NWO Gravitation project funded by the Ministry of Education, Culture and Science of the Netherlands and an ERC Advanced Grant awarded to J.N.; I.B. and M.G. were recipients of long-term EMBO fellowships.

References

1. R. M. Rios, M. Bornens, The Golgi apparatus at the cell centre. Curr Opin Cell Biol 15, 60-66 (2003).
2. J. Thyberg, S. Moskalewski, Role of microtubules in the organization of the Golgi complex. Exp Cell Res 246, 263-279 (1999).
3. F. Valderrama et al., Actin microfilaments are essential for the cytological positioning and morphology of the Golgi complex. Eur J Cell Biol 76, 9-17 (1998).
4. S. Waguri et al., Visualization of TGN to endosome trafficking through fluorescently labeled MPR and AP-1 in living cells. Mol Biol Cell 14, 142-155 (2003).
5. C. Raiborg, H. Stenmark, The ESCRT machinery in endosomal sorting of ubiquitylated membrane proteins. Nature 458, 445-452 (2009).
6. G. Scita, P. P. Di Fiore, The endocytic matrix. Nature 463, 464-473 (2010).
7. J. S. Blum, P. A. Wearsch, P. Cresswell, Pathways of antigen processing. Annu Rev Immunol 31, 443-473 (2013).
8. L. M. Traub, J. S. Bonifacino, Cargo recognition in clathrin-mediated endocytosis. Cold Spring Harb Perspect Biol 5, a016790 (2013).
9. J. Huotari, A. Helenius, Endosome maturation. The EMBO journal 30, 3481-3500 (2011).
10. L. A. Sadacca, J. Bruno, J. Wen, W. Xiong, T. E. McGraw, Specialized sorting of GLUT4 and its recruitment to the cell surface are independently regulated by distinct Rabs. Mol Biol Cell 24, 2544-2557 (2013).
11. S. E. Reed et al., A role for Rab14 in the endocytic trafficking of GLUT4 in 3T3-L1 adipocytes. J Cell Sci 126, 1931-1941 (2013).
12. I. Rojo Pulido et al., Myosin Va acts in concert with Rab27a and MyRIP to regulate acute von-Willebrand factor release from endothelial cells. Traffic 12, 1371-1382 (2011).
13. C. Wasmeier, A. N. Hume, G. Bolasco, M. C. Seabra, Melanosomes at a glance. J Cell Sci 121, 3995-3999 (2008).
14. N. Anikeeva, Y. Sykulev, Mechanisms controlling granule-mediated cytolytic activity of cytotoxic T lymphocytes. Immunol Res 51, 183-194 (2011).
15. R. Wubbolts et al., Opposing motor activities of dynein and kinesin determine retention and transport of MHC class II-containing compartments. J Cell Sci 112 (Pt 6), 785-795 (1999).
16. C. M. Schroeder, J. M. Ostrem, N. T. Hertz, R. D. Vale, A Ras-like domain in the light intermediate chain bridges the dynein motor to a cargo-binding region. Elife 3, e03351 (2014).
17. I. Jordens et al., The Rab7 effector protein RILP controls lysosomal transport by inducing the recruitment of dynein-dynactin motors. Current biology : CB 11, 1680-1685 (2001).
18. G. Cantalupo, P. Alifano, V. Roberti, C. B. Bruni, C. Bucci, Rab-interacting lysosomal protein (RILP): the Rab7 effector required for transport to lysosomes. The EMBO journal 20, 683-693 (2001).
19. C. Raiborg et al., Repeated ER-endosome contacts promote endosome translocation and neurite outgrowth. Nature 520, 234-238 (2015).
20. C. Rosa-Ferreira, S. Munro, Arl8 and SKIP act together to link lysosomes to kinesin-1. Dev Cell 21, 1171-1178 (2011).
21. S. C. Helle et al., Organization and function of membrane contact sites. Biochim.Biophys.Acta

1833, 2526-2541 (2013).
22. N. Rocha et al., Cholesterol sensor ORP1L contacts the ER protein VAP to control Rab7-RILP-p150 Glued and late endosome positioning. J.Cell Biol. 185, 1209-1225 (2009).
23. R. van der Kant et al., Late endosomal transport and tethering are coupled processes controlled by RILP and the cholesterol sensor ORP1L. J Cell Sci 126, 3462-3474 (2013).
24. A. A. Rowland, P. J. Chitwood, M. J. Phillips, G. K. Voeltz, ER contact sites define the position and timing of endosome fission. Cell 159, 1027-1041 (2014).
25. P. Paul et al., A Genome-wide multidimensional RNAi screen reveals pathways controlling MHC class II antigen presentation. Cell 145, 268-283 (2011).
26. Y. Qin et al., RNF26 temporally regulates virus-triggered type I interferon induction by two distinct mechanisms. PLoS pathogens 10, e1004358 (2014).
27. R. J. Deshaies, C. A. Joazeiro, RING domain E3 ubiquitin ligases. Annual review of biochemistry 78, 399-434 (2009).
28. A. Benmerah, M. Bayrou, N. Cerf-Bensussan, A. Dautry-Varsat, Inhibition of clathrin-coated pit assembly by an Eps15 mutant. Journal of cell science 112 (Pt 9), 1303-1311 (1999).
29. B. Morriswood et al., T6BP and NDP52 are myosin VI binding partners with potential roles in cytokine signalling and cell adhesion. Journal of cell science 120, 2574-2585 (2007).
30. G. Ankem et al., The C2 domain of Tollip, a Toll-like receptor signalling regulator, exhibits broad preference for phosphoinositides. Biochem.J. 435, 597-608 (2011).
31. B. Ciani, R. Layfield, J. R. Cavey, P. W. Sheppard, M. S. Searle, Structure of the ubiquitin-associated domain of p62 (SQSTM1) and implications for mutations that cause Paget's disease of bone. J Biol Chem 278, 37409-37412 (2003).
32. M. Lippai, P. Low, The Role of the Selective Adaptor p62 and Ubiquitin-Like Proteins in Autophagy. Biomed.Res.Int. 2014, 832704 (2014).
33. K. Schweitzer, P. M. Bozko, W. Dubiel, M. Naumann, CSN controls NF-kappaB by deubiquitinylation of IkappaBalpha. EMBO J 26, 1532-1541 (2007).
34. P. J. Eichhorn et al., USP15 stabilizes TGF-beta receptor I and promotes oncogenesis through the activation of TGF-beta signaling in glioblastoma. Nat Med 18, 429-435 (2012).
35. S. Mitra, C. A. Traughber, M. K. Brannon, S. Gomez, D. G. Capelluto, Ubiquitin interacts with the Tollip C2 and CUE domains and inhibits binding of Tollip to phosphoinositides. J Biol Chem 288, 25780-25791 (2013).
36. E. Klapisz et al., A ubiquitin-interacting motif (UIM) is essential for Eps15 and Eps15R ubiquitination. J Biol Chem 277, 30746-30753 (2002).
37. H. Iha et al., Inflammatory cardiac valvulitis in TAX1BP1-deficient mice through selective NF-kappaB activation. EMBO J 27, 629-641 (2008).
38. A. Sorkin, Ubiquitination without E3. Mol Cell 26, 771-773 (2007).
39. R. van der Kant, J. Neefjes, Small regulators, major consequences - Ca(2)(+) and cholesterol at the endosome-ER interface. J.Cell Sci. 127, 929-938 (2014).
40. C. Watts, The endosome-lysosome pathway and information generation in the immune system. Biochim Biophys Acta 1824, 14-21 (2012).
41. I. Mellman, Y. Yarden, Endocytosis and cancer. Cold Spring Harb Perspect Biol 5, a016949 (2013).
42. D. E. Johnson, P. Ostrowski, V. Jaumouille, S. Grinstein, The position of lysosomes within the cell determines their luminal pH. J Cell Biol 212, 677-692 (2016).
43. F. Fazioli, L. Minichiello, B. Matoskova, W. T. Wong, P. P. Di Fiore, eps15, a novel tyrosine kinase substrate, exhibits transforming activity. Mol Cell Biol 13, 5814-5828 (1993).
44. L. Ling, D. V. Goeddel, T6BP, a TRAF6-interacting protein involved in IL-1 signaling. Proc Natl Acad Sci U S A 97, 9567-9572 (2000).
45. L. Calderilla-Barbosa et al., Interaction of SQSTM1 with the motor protein dynein--SQSTM1 is required for normal dynein function and trafficking. J Cell Sci 127, 4052-4063 (2014).
46. S. B. Shields et al., ESCRT ubiquitin-binding domains function cooperatively during MVB cargo sorting. J Cell Biol 185, 213-224 (2009).
47. C. M. Pickart, Ubiquitin enters the new millennium. Mol Cell 8, 499-504 (2001).
48. M. J. Clague, H. Liu, S. Urbe, Governance of endocytic trafficking and signaling by reversible ubiquitylation. Developmental cell 23, 457-467 (2012).

Supplementary Figures

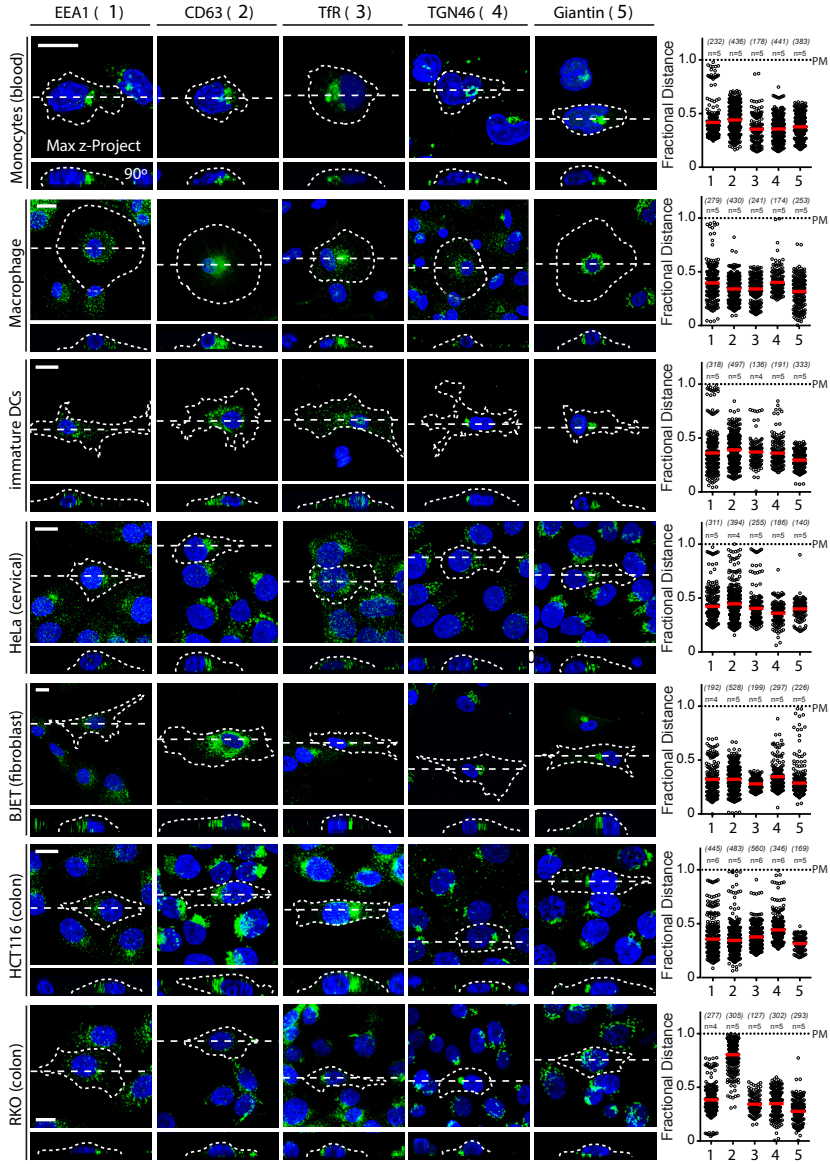


Figure S1. A wallpaper showing endosomal and Golgi distribution in various cell types, related to Figure 1. *Intracellular distribution of early endosomes (EEA1 (1), green), LEs/Lysosomes (CD63 (2), green), recycling endosomes (TfR (3), green), Trans-Golgi network (TGN46 (4), green), and Golgi (Giantin (5), green) in various cell lines (3 human primary immune cells (monocytes, macrophages and immature dendritic cells and 4 human cell lines including the primary BJET fibroblast cell line). Representative maximum z-projection (3D) overlays with nuclear DAPI (blue) and their corresponding z-cross sections along the demarcated line are shown below the X-Y images. Cell boundaries are depicted in dashed lines. Fractional distance analysis of marked vesicles in various cell lines are shown (right panels) reported as distance of pixels from nucleus = faction of distance from nucleus to the plasma membrane (max 1.0); mean shown in red. Numbers below the figure relate to the marker proteins indicated above the microscopy images; N=2. Scale bars = 10 µm; n= # of cells analyzed per condition, with # of data points analyzed per condition given in parenthesis.*

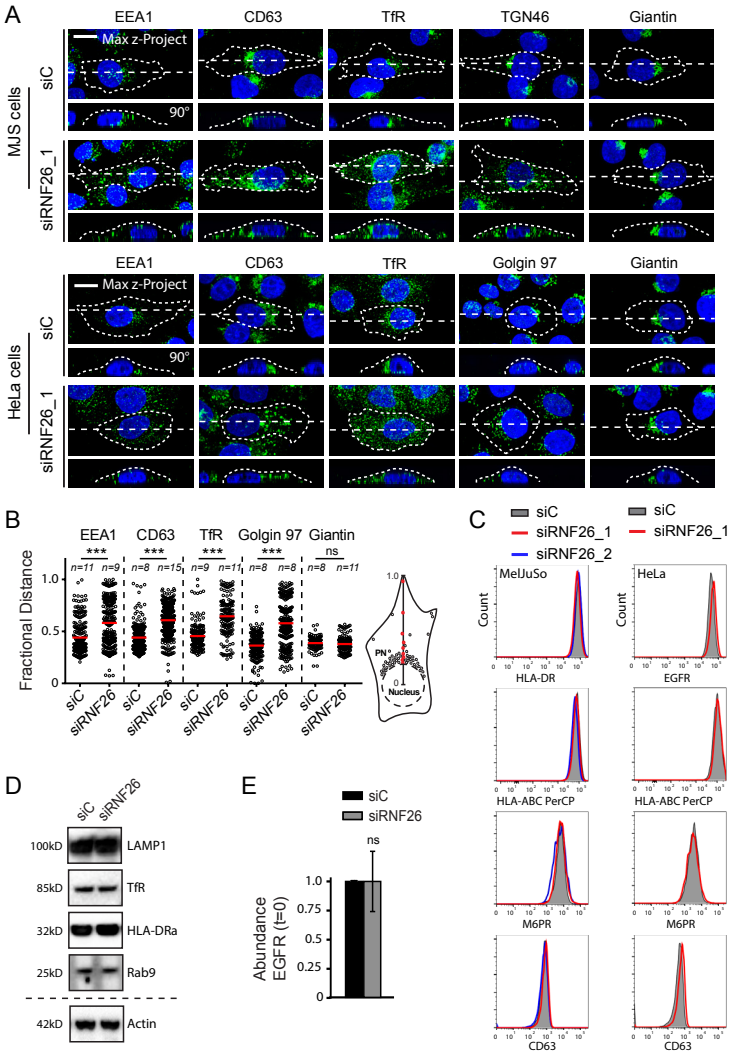


Figure S2. Effect of RNF26 depletion on the expression and distribution of various marker proteins, related to Figure 2. *(a) MelJuSo cells (top panels) and HeLa cells (bottom, panels) transfected with siRNA against RNF26 (siRNF26_1) or control siRNA (siC), as indicated. Intracellular distribution of Early endosomes (EEA1, green), LEs/Lysosomes (CD63, green), recycling endosomes (TfR, green), Trans-Golgi network (TGN46, green) and the Golgi (Giantin, green) are shown. Representative maximum z-projection (3D) overlays with nuclear DAPI (blue) and their corresponding z-cross sections along the demarcated line are shown below the X-Y images. Cell boundaries are depicted in dashed lines; N=2. (b) Intracellular distribution of various markers and cargoes in HeLa cells in response to RNF26 depletion (siRNF26), shown in A, presented as fractional distances with mean shown in red. For MelJuSo cells, see Figure 2a. (c) Cell surface expression of various markers in RNF26-depleted MelJuSo cells (left panels, MHC class II (HLA-DR), MHC class I (HLA-ABC), M6PR and CD63) or HeLa cells (right panels, EGFR, MHC class I (HLA-ABC), M6PR and CD63) analyzed by flow cytometry; N=3. (d) Total levels of endosomal marker proteins and cargoes in MelJuSo cells depleted of RNF26 (siRNF26) compared to control cells (siC) analyzed by SDS-PAGE and WB using Actin as loading control. Lysosomes (LAMP1); recycling endosomes (TfR); MIIC (MHC class II: HLA-DRa) and (late)-endosomes (Rab9). (e) Total cellular abundance of EGFR in HeLa cells depleted of RNF26 (siRNF26) compared to control cells (siC) analyzed by SDS-PAGE and WB using TfR as loading control; N=3. Scale bars = 10 µm; n= # of cells analyzed per condition, N= # independent experiments, error bars = SD*

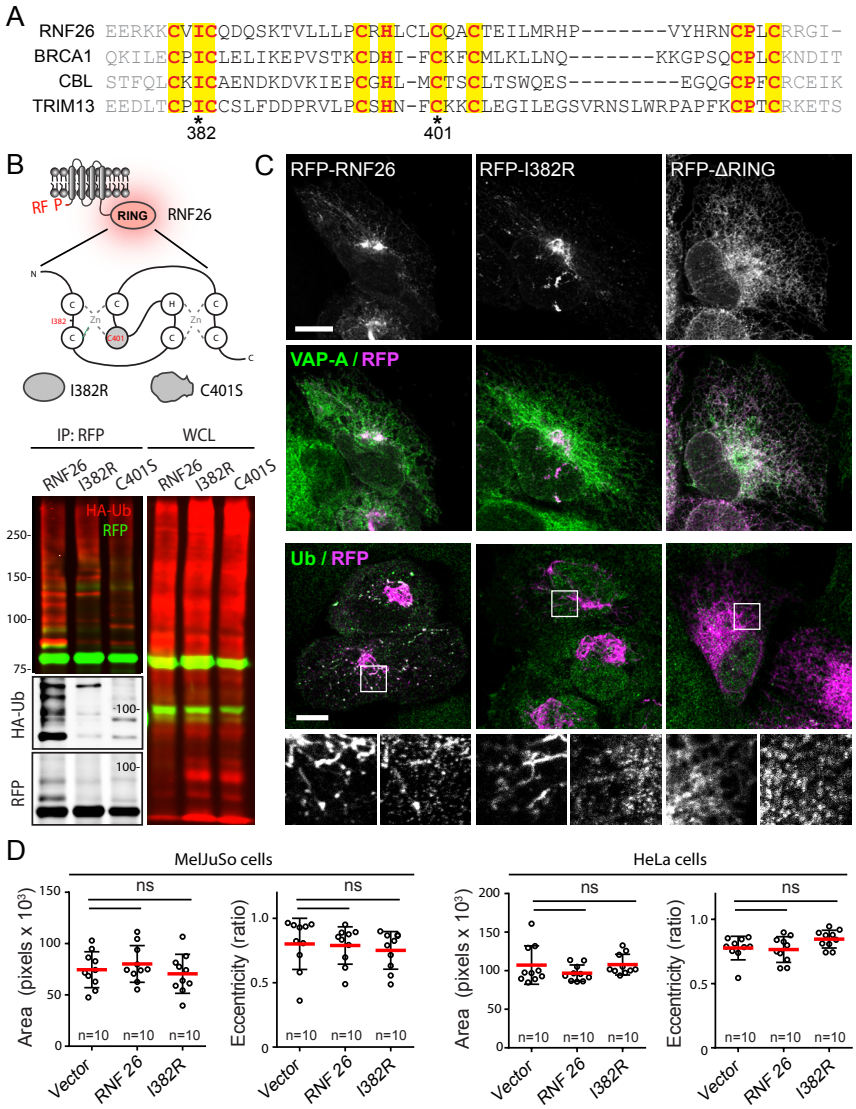


Figure S3. The RING domain of RNF26 mediates its localization and function, related to Figure 3. *(a) Sequence comparison of the RNF26 RING domain with the RING domains of three other structurally related E3-ligases (BRCA1, CBL and TRIM13). The amino acids required for the Zn2+ positioning are indicated in yellow; amino acids mutated to inactivate RNF26 are indicated with * (Iso 382 and Cys 401). (b) (top) Schematic overview of the RNF26 RING domain: residues Iso382 and Cys401 mutated in this study are indicated in red. (bottom) RFP-RNF26 and its inactive mutants, co-expressed with HA-Ubiquitin in HEK293 cells, were immunoprecipitated under harsh lysis conditions, separated by SDS-PAGE and analyzed by WB to visualize the associated modifications with HA-Ub (left panel). Whole-cell lysate (WCL) controls are shown on the right. (c) RFP-RNF26 or the indicated mutants (magenta) were expressed in MelJuSo cells and co-stained for VAP-A (green) to label the ER or with Ubiquitin (green). Zoom-in of the indicated region illustrates effective co-labeling of WT, but not catalytically incompetent RNF26 with Ub. (d) Effect of ectopical expression of RNF26 or its inactive mutant I382R on the size and eccentricity in either MelJuSo (left panels) or HeLa cells (right panels) (mean shown in red); N=2. n= # of cells analyzed per condition, N= # independent experiments, error bars = SD. Scale bar = 10 µm.*

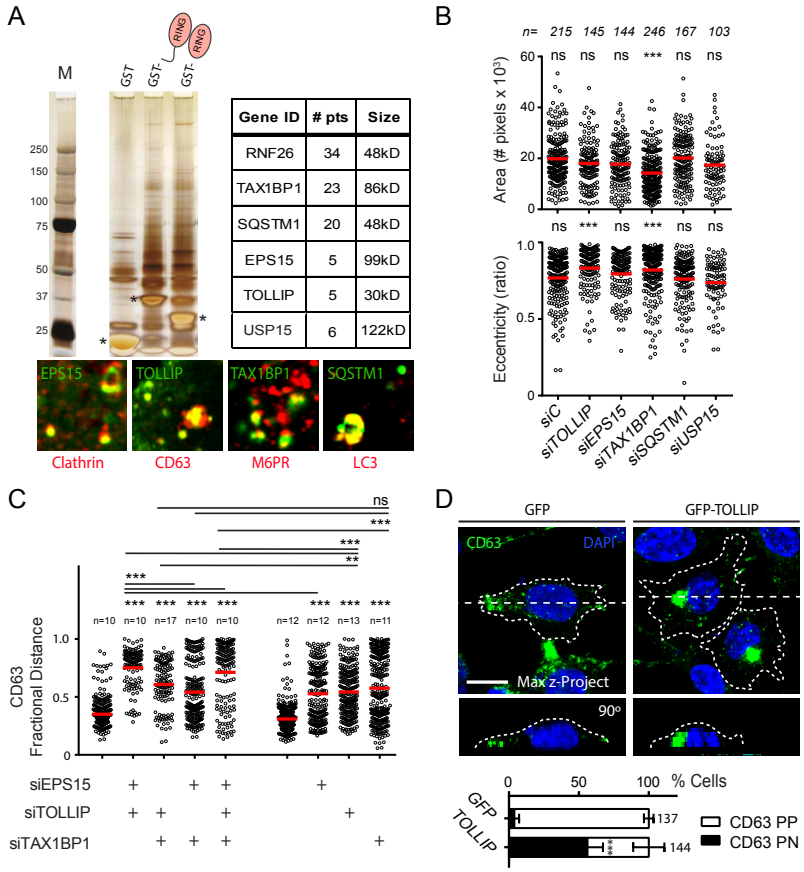


Figure S4. Isolation and characterization of proteins associated to the RNF26 cytoplasmic domain, related to Figure 4 *(a) (left) Isolation and characterization of RNF26 associated proteome interacting with its RING domain. Two GST-tagged RNF26 tails (aa304-433 and aa363-433) including the RING domain were used (last two lanes) and compared to GST-tag only as a control (first lane). The Silver-stained gel (including marker lane) with bands isolated and identified by mass spectrometry marked as indicated. (right) Table showing the number of unique identified peptides (#pts) corresponding to RNF26 and its interacting partners TAX1BP1, SQSTM1, EPS15, TOLLIP and USP15 that were absent in the GST-only control lane. (bottom) Zoom-in of identified endogenous proteins along with marker proteins for their vesicular localization in MelJuSo cells. EPS15 (green) marks clathrin-coated vesicles (clathrin, red); TOLLIP (green) locates to late endosomes (CD63, red); TAX1BP1 partially co-localizes with secreted M6PR (red) and SQSTM1 locates to autophagosomes (LC3, red). (b) Effect of protein depletion (identified in A) on cell size and shape (eccentricity) in MelJuSo cells compared to control cells (siC) with mean shown in red; N=2. (c) Fractional distance analysis of CD63 marked late endosomes in MelJuSo cells after silencing one or multiple ubiquitin adaptors identified. Mean in red and statistical significance relative to the control (siC) are indicated. (d) In contrast to other cell types analyzed, RKO tumor cell line displayed unusual distribution of CD63 (green, upper panel, see also Figure S1). Overexpression of GFP-TOLLIP in these cells re-clusters CD63 positive vesicles (green, bottom panel). Representative maximum z-projection (3D) overlays with nuclear DAPI (blue) and their corresponding z-cross sections along the demarcated line are shown below the X-Y images. Cell boundaries are depicted in dashed lines. GFP signal was omitted from the presented image, but use to define the transfected cells. Quantification of perinuclear (PN) and peripheral (PP) positioning of CD63 positive vesicles following GFP or GFP-TOLLIP expression; N=2. Scale bars = 10 µm; n= # of cells analyzed per condition, N= # independent experiments, error bars = SD*

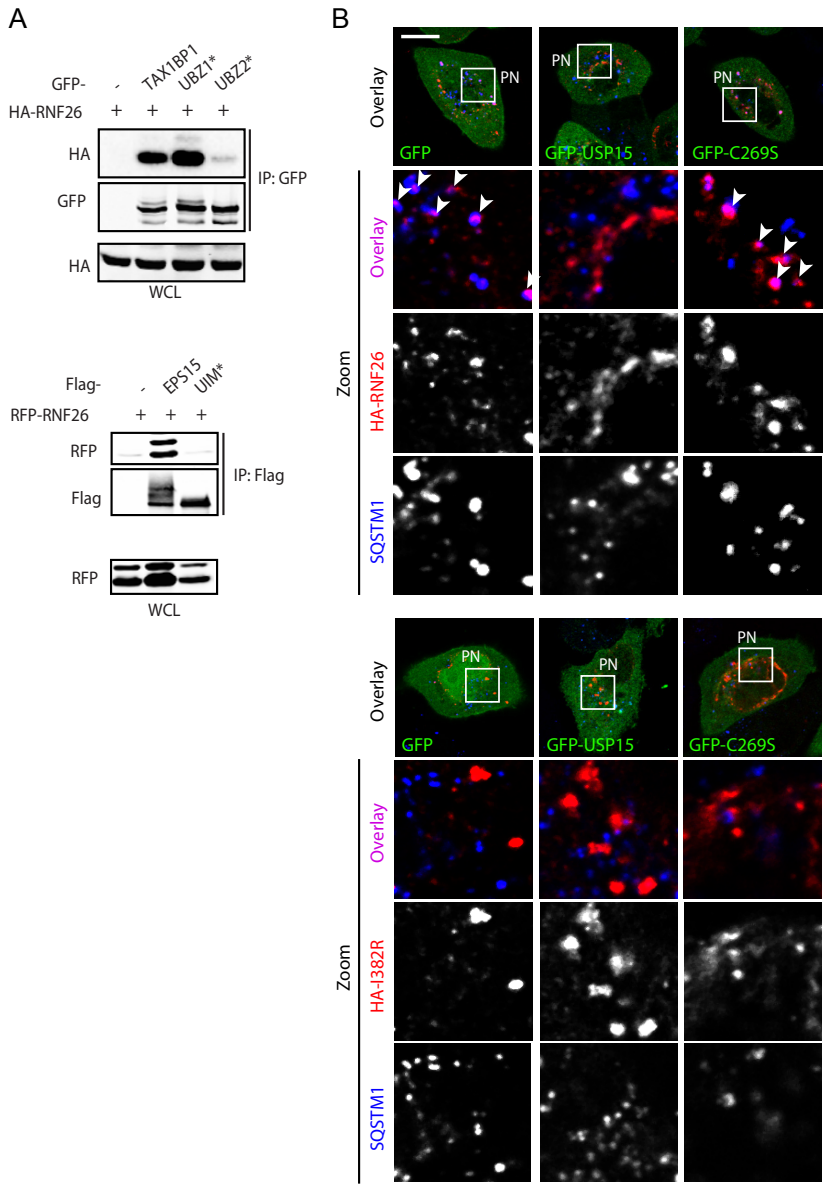


Figure S5. RNF26 interacts with ubiquitin-binding domains of vesicle adaptors, and USP15 reduces co-localization of RNF26 and SQSTM1, related to Figures 5 and 6, respectively. *(a) (Top panel) Complex formation between HA-RNF26 and either GFP-TAX1BP1 or its mutants UBZ* and UBZ2*. (bottom panel) Complex formation between RFP-RNF26 and either FLAG-EPS15 or its mutant UIM*. WCL: whole-cell lysate. For quantification of complex formation under the above and other conditions, see Figure 5D. (b) HeLa cells expressing active (top panel) or inactive (bottom panel) HA-RNF26 (red) along GFP-USP15 or its inactive mutant GFP-C269A (green) were stained for endogenous SQSTM1 (blue). A three-color overlay of a representative cell is shown in the top image for each condition and a zoom-in of the indicated perinuclear (PN) region for SQSTM1 and HA-RNF26 or its mutants is indicated below. Arrows point towards locations of colocalization of RNF26 and SQSTM1. Quantification appears in Figure 6D; N=2, scale bar = 10 μm.*

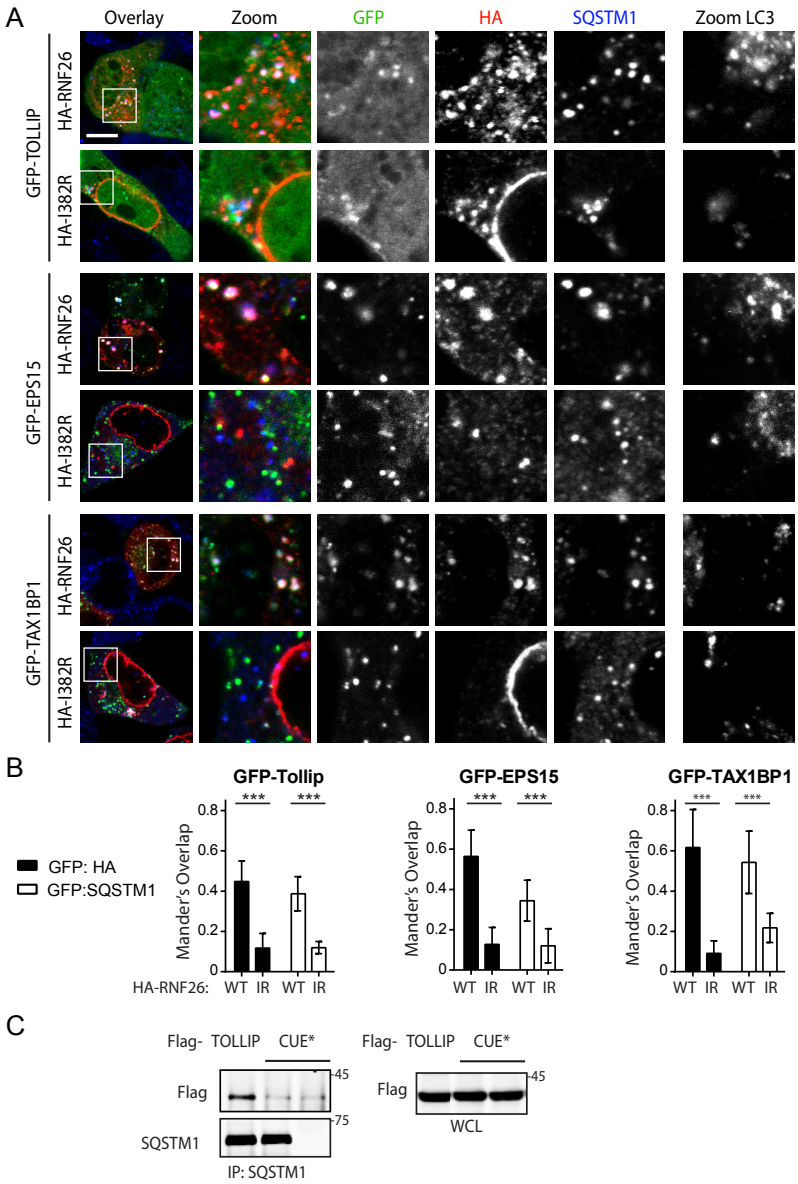


Figure S6. Vesicle Adaptors EPS15, TOLLIP and TAX1BP1 colocalize with SQSTM1 at RNF26-Positive Sites on the ER, related to Figure 7. *(a) Co-localization of GFP-TOLLIP (top panels), GFP-EPS15 (middle panels) or GFP-TAX1BP1 (bottom panels) with wild-type HA-RNF26 (red) versus catalytically inactive I382R (red) and SQSTM1 (blue) is shown as representative 3-color overlays and insets with their corresponding individual channels. Co-staining against LC3 is shown to the right. For dynamics of adaptor-selected vesicles associated with the RNF26/SQSTM1 complex see Figures 7 and S7. (b) Quantification of (a) Co-localization (Mander's overlap) of either RNF26 (HA, black bars) or SQSTM1 (white bars) with GFP-TOLLIP (left), GFP-EPS15 (middle) or GFP-TAX1BP1 (right) is given for cells expressing the active (WT) or inactive (IR) form of RNF26. N=2. (c) Complex formation between endogenous SQSTM1 and either FLAG-TOLLIP or its mutant CUE*. WCL: Whole-cell lysate. Scale bars = 10 μm; N= # independent experiments; shown are the mean + error bars = SD*

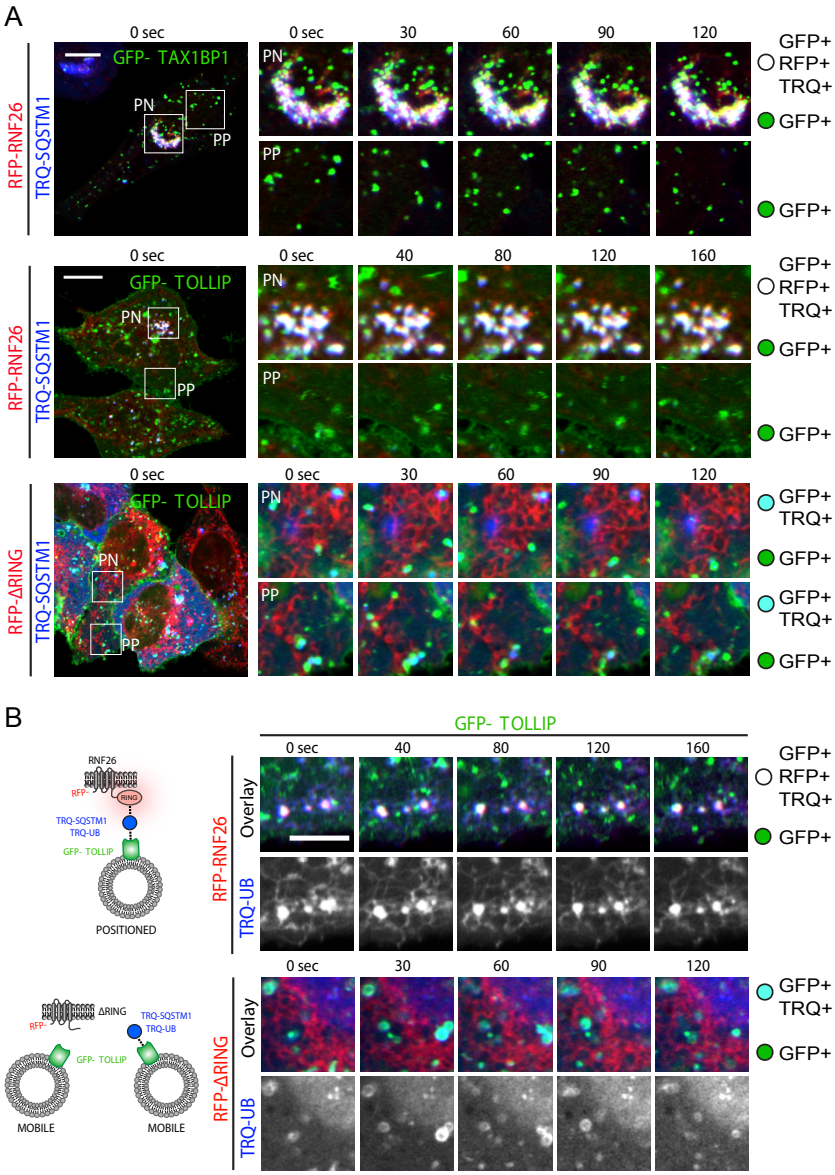


Figure S7. RNF26/SQSTM1 Complex Retains Adaptor-Selected Vesicles in the Perinuclear Cloud, related to Figure 7. *(a) Overlay confocal frame insets of selected perinuclear (PN) and peripheral (PP) regions from time-lapses of HeLa cells co-expressing TRQ-SQSTM1 (blue) and GFP-TAX1BP1 (top, green), GFP-TOLLIP (middle and bottom, green) in the presence of either RFP-RNF26 (red) or RFP-ΔRING (red), as indicated. Quantification appears in Figure 7C. See also Movies S6A and S6B. (b) Schematic illustration of the suggested interaction between RNF26 and RNF26-ΔRING with SQSTM1 and the adaptors on vesicles. Colors correspond to the proteins as shown in (a). Snap shots of HeLa cells expressing RFP-RNF26 (top panels, red) or mutant RFP-RNF26ΔRING (bottom panel, red), TRQ-ubiquitin (blue) and GFP-TOLLIP (green). Three-color zoom-ins and Ubiquitin single (gray) images of a time lapse of the perinuclear region are shown. Quantification appears in Figure 7C. Scale bars = 10μm.*

Chapter 4:
Identification of DUBs controlling MHCII biology and endosome dynamics.

Ruud H. Wijdeven[1,2], Ilana Berlin[1,2], George Jansen[3], Hans Janssen[2], Peter van Veelen[3], Jacques Neefjes[1,2]

[1] Department of Chemical Immunology, LUMC, Leiden, the Netherlands
[2] Department of Cell Biology, Netherlands Cancer Institute, Amsterdam, the Netherlands
[3] Department of Immunohematology and Blood Transfusion, LUMC, Leiden, the Netherlands.

Abstract

For efficient antigen loading and presentation at the cell surface, MHC class II molecules (MHCII) traverse an extensive part of the endocytic pathway. Interference with the latter could be used as means to manipulate MHCII antigen presentation, and hereby the activation of CD4+ T-cells. Here, by performing an RNAi screen for de-ubiquitinating enzymes (DUBs), we identified novel functions in the MHCII pathway for several of these enzymes. One of these, OTUD1, regulates transcription of MHCII and is required for proper perinuclear localization of the early and late endosomal compartment. Furthermore, loss of OTUD1 impairs the processing of endocytic cargo, as measured by decreased degradation of endocytosed EGFR. Together, our work provides a framework for future studies on the role of several DUBs in the endocytic pathway and describes a function for OTUD1 in the regulation of the early and late endosomal compartment.

Introduction

Antigen presenting cells (APCs) activate CD4+ helper T-cells to initiate an adaptive immune response by presenting antigens on their Major Histocompatibility Complex class II molecules (MHCII) (1, 2). Improper antigen presentation or undesired stimulation of autoreactive CD4+ T-cells underlies many autoimmune diseases, and multiple MHCII alleles associate to specific autoimmune disorders, for example HLA-DRB1 and rheumatoid arthritis and HLA-DR4 to Type I Diabetes (3, 4). Expression of MHCII is limited to professional APCs like dendritic cells and B-cells, but other cell types can also express MHCII upon cytokine stimulation or oncogenic transformation. Transcription of the MHCII complex (consisting of an alpha and beta chain, as well as the invariant chain (Ii) that is required for peptide loading and endosomal trafficking) is controlled by transcriptional activator CIITA, which recruits the necessary transcription factors to initiate transcription (5). After synthesis in the ER, MHCII associates with Ii, followed by transport via the trans-Golgi network (TGN) to multi-vesicular late endosomes, also called MHCII compartments (MIIC). Alternatively, MHCII is first transported towards the plasma membrane and subsequently endocytosed to reach the MIIC. Here, the invariant chain is cleaved by various proteases including cathepsin S and SPPL2a (6, 7), leaving only a small fragment termed CLIP in the MHCII peptide-binding groove. Subsequent association of CLIP-bound MHCII with chaperone HLA-DM facilitates exchange of CLIP for an external peptide (8). Most peptides are generated in endosomes, but cytosolic and even nuclear peptides are presented by MHCII, usually after they entered the MIIC by autophagy (9, 10). After loading, MHCII is transported to the cell surface, where the peptide is presented.

While the basic principles of antigen presentation are set, the underlying processes ensuring proper expression and transport of MHCII are understood less well. Furthermore, as it utilizes major parts of the endocytic pathway, MHCII is an excellent marker for the identification of novel members of this cellular trafficking system. A group of enzymes that could control these processes are de-ubiquitinating enzymes (DUBs), which counteract post-translational modification (PTM) of proteins by ubiquitin (11). Ubiquitination is one of the most prevalent PTMs and is involved in almost every cellular process, ranging from targeting proteins for proteasomal

degradation to signal transduction (12). Proteins can be modified on a lysine with a single ubiquitin (mono-ubiquitination), which can further be ubiquitinated, leading to the formation of ubiquitin chains (poly-ubiquitination). Depending on the lysine on ubiquitin that is modified, this yields chains with different structures and functions. DUBs cleave off the ubiquitin (chain), thereby preventing protein degradation or terminating the ubiquitin-based signal. Given the reversible and flexible nature of PTMs in the endocytic pathway, DUBs perform essential functions in trafficking, reaching beyond modulation of protein abundance (13, 14). As MHCII molecules traverse nearly the entire endocytic network, DUBs implicated in endocytic trafficking, including USP8 and AMSH (15), could influence MHCII expression. Also, many DUBs are poorly studied and some may be involved in endocytic trafficking or transcription of MHC-related genes. Their enzymatic nature makes them attractive drug targets to modulate the magnitude of antigen presentation.
To identify novel regulators of MHCII expression and endocytic transport in general, we performed an RNAi screen for the different de-ubiquitinating enzymes. Using this screen, we identified several DUBs that control MHCII surface expression, either by regulating transcription or endocytic trafficking. One of these DUBs, OTUD1, was studied in more detail. OTUD1 is required for transcription of MHCII, as well as for proper localization of the late endosomal/lysosomal (LE/Ly) compartment, suggesting a pleiotropic function for this lysine-63 specific DUB.

Results

RNAi screen for DUBs in control of MHCII expression

Cell surface levels of MHCII are regulated by a plethora of factors, with many of them uncovered by a genome-wide RNAi screen performed in our lab (16). However, only few DUBs were identified in this screen, likely due to its stringent selection criteria and large scale. As some DUBs implicated in endocytic trafficking were not identified, we performed a more targeted screen using a library of siRNAs targeting all known DUBs. As a model for MHCII expression the MelJuSo melanoma cell line was used, which constitutively expresses the MHCII transcriptional regulator CIITA at high levels and is transfectable. DUBs were silenced for three days to allow sufficient knockdown, after which cell surface levels of peptide loaded MHCII were measured using flow cytometry (Fig. 1a).
Silencing of 9 DUBs increased MHCII expression (z-score >2.5), whereas depletion of 11 DUBs yielded a decrease in MHCII cell surface levels (Fig. 1b). To assess whether any of these DUBs are in control of MHCII transcription, the DUBs were silenced and cells were subjected to qRT-PCR analysis for MHCII subunit HLA-DRα. Depletion of USP9x, USP42, as well as the OTU-domain DUBs OTUD1 and OTUD4 decreased HLA-DRα transcription (Fig. 1c). Of these four DUBs, only depletion of OTUD1 quenched HLA-DRα expression induced by the cytokine IFNγ (Fig. 1d). Transcription of Ii, which is co-regulated with OTUD1, or CIITA and IRF1, were not affected by OTUD1 knockdown, suggesting that OTUD1 is specifically involved in transcription of HLA-DRα.
MHCII extensively traverses the endocytic network and some DUBs may affect its surface levels by altering transport. Confocal microscopy for MHCII, as well as GFP-tagged ubiquitin to investigate ubiquitin dynamics, revealed that whereas the

perinuclear accumulation of MHCII remained intact after silencing of most DUBs, silencing of some DUBs severely affected the localization or size of the MIIC compartment (Fig. 1e). Depletion of USP8 induced swelling of the MIIC, which was heavily labeled with ubiquitin, consistent with the known role for USP8 in trafficking of receptors through the endocytic compartment (17, 18). Loss of USP34 yielded hyperclustering of the MIICs, while USP54 silenced cells had hyperclustered MIICs in combination with increased plasma membrane staining, which agrees with the Flow Cytometry data. Increased plasma membrane staining was also observed for depletion of VCPIP. Finally, loss of USP9x and OTUD1 resulted in scattering of MHCII throughout the cell, as well as the appearance of ubiquitin aggregates in the cytosol, which were also visible when USP54 was silenced. The decreased MHCII surface levels as a result of OTUD1 knockdown were a result of impaired MHCII transcription and not trafficking, as total MHCII levels were also altered, overexpression of GFP-tagged HLA-DRα driven by a CMV promotor rescued MHCII surface levels, and cell surface expression of CD63, which also localizes to LE/Lys, was not affected by OTUD1 silencing (Fig. 1f). Thus, we identified several novel DUBs that control transcription and/or transport of MHCII.

OTUD1 is required for late endosome positioning

One of the interesting hits was OTUD1, a DUB specifically cleaving lysine-63 poly-ubiquitin linkages (19) and overexpressed in early stages of thyroid cancer (20). However, its cellular function is unknown. The re-localization of MHCII upon silencing of OTUD1 suggests that this DUB might be involved in trafficking of LE/Lys. Indeed, silencing of OTUD1 using two different siRNAs resulted in a profound scattering of CD63-positive compartments in both HeLa and MelJuSo cells (Fig. 2a). Overexpression of Rab7-effector RILP re-established the perinuclear localization of CD63 (Fig. 2b), suggesting that the peripheral re-localization is not the result of defective minus-end transport towards the perinuclear region. Increased scattering was accompanied by an increase in the number of LE/Lys as stained by CD63 and Lysotracker (Fig. 2c), instilling the idea that OTUD1 is required for proper organization of the endosomal compartment. To address whether these scattered endosomes are a consequence of increased plus-end transport or peripheral stabilization, we labeled these endosomes with lysotracker and followed them by time lapse imaging. Vesicles in the peripheral region did not undergo increased fast microtubule-based transport, indicating that the peripheral re-localization is not a result of increased plus-end transport. Rather, they appeared static and mostly immobile, as if docked to a cellular structure (Fig. 2d and 2e). Thus, OTUD1 affects the organization of the LE/Ly compartment and its loss results in a collapse of the perinuclear region, without increasing actual endosome transport.

Proper endocytic functioning requires OTUD1

To address the effect of OTUD1 on the endosomal pathway as a whole, we stained cells either or not silenced for OTUD1 with markers for different endosomal compartments. Excessive scattering was also observed for early endosomes (detected by EEA1) but not the trans-Golgi network (Mannose-6-phosphate receptor) (Fig. 3a), indicating that OTUD1 acts as a regulator of the early and late endocytic network, but not the entire endocytic pathway that includes TGN.

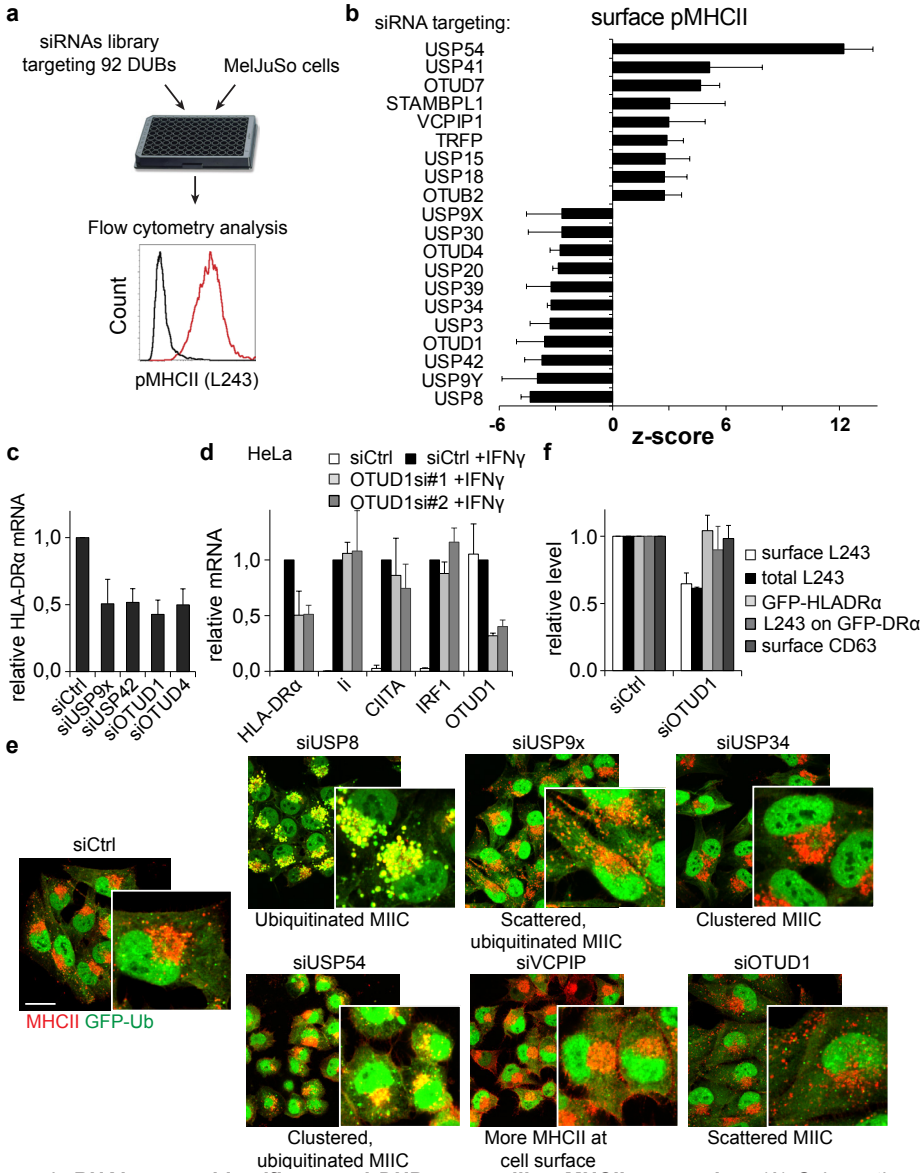


Figure 1: RNAi screen identifies novel DUBs controlling MHCII expression. *(A) Schematic overview of the screen (B) Hits from the screen with a Z-score > 2.5 or < -2.5. Z-scores represent amount of standard deviations away from the control. (C) MelJuSo silenced for hits from the screen were analysed for mRNA expression of HLA-DRα using qRT-PCR. Silencing of four DUBs had a significant effect and are shown. (D) HeLa cells transfected with the indicated siRNAs were stimulated with 100ng/mL IFNγ for 24h and expression of the indicated mRNAs was analyzed using qRT-PCR. (E) MelJuSo cells expressing GFP-Ubiquitin were transfected with the indicated siRNAs and fixed and stained three days later for MHCII. Representative images are shown. Scale bar, 10µm. (F) MelJuSo cells transfected with siCtrl or siOTUD1 were stained for surface pMHCII, CD63 or first fixed and permeabilized to stain for total pMHCII levels. Alternatively, MelJuSo cells expressing GFP-tagged HLA-DRα were stained with L243 and analyzed by flow cytometry for GFP and surface pMHCII levels. All graphs represent mean + SD of three independent experiments.*

Perinuclear localization of endosomes aides the efficient encounter of early endosomes and LE/Lys and hereby times the degradation of cargo, for example activated growth receptors (21). Therefore, we tested the participation of OTUD1 in the timely degradation of the Epidermal Growth Factor Receptor (EGFR). In line with the disorganized endosome localization, ligand-induced degradation of EGFR was delayed upon depletion of OTUD1, which was accompanied by prolonged presence of phosphorylated EGFR (Fig. 3b). The setback in degradation was a result of impaired access of EGFR to the degradatory LE/Ly compartment, since co-localization between fluorescent EGF and CD63 was lower in cells lacking sufficient OTUD1 (Fig. 3c). Whereas in control cells EGF containing endosomes moved towards the perinuclear region, EGF containing endosomes remained dispersed over the cell following OTUD1 silencing, further supporting the notion that OTUD1 is involved in the positioning of endosomes.

OTUD1 is functionally linked to the actin cytoskeleton

Whereas the phenotype suggests an important function for OTUD1 in endosome biology, OTUD1 localized predominantly to the cytosol (Fig. 4c), suggesting an indirect effect on endosomes, possibly via adaptor proteins. An earlier study did not show any endosome associated target (22), therefore we performed mass spectrometry analyses of OTUD1 associated proteins. We isolated GFP-tagged OTUD1 from Hek 293T cells and analyzed interacting proteins by MS/MS. Besides all six reported proteins, peptides were identified corresponding to several novel interactors (Fig. 4a). However, none of these proteins were known to localize to endosomes. Therefore we focused on Filamin A (FLNA), an actin cross-linking protein, as it is described to be required for proper localization of the LE/Ly compartment (23). OTUD1 indeed interacted with Filamin A, via its alanine-rich N-terminal domain (Fig. 4b). Given the importance of endosome-localized actin filaments in endosome motility and positioning (24-27), we wondered whether OTUD1 is involved in actin organization and hereby controls endosome biology. This idea was corroborated by the notion that a small fraction of OTUD1 co-localized with actin and Filamin A at peripheral protrusion structures (Fig. 4c). Furthermore, OTUD1 depleted cells contained a vastly extended actin network, including more and smaller actin fibers, as if the actin organization was perturbed (Fig. 4d). Also, the morphology of these cells was altered, which was especially apparent in glioblastoma U118 cells, where many cells containing spikey but short protrusions (Fig. 4e), suggestive of a defect in cellular organization or altered migratory behavior. To address whether OTUD1-mediated actin reorganization and endosome positioning are coupled, we silenced FLNA, as well as Keap1, another actin-binding protein identified in the mass spec experiment, and analyzed its effect on endosome positioning. Whereas cells appeared more elongated in both cases, no striking effect was observed on endosome positioning (data not shown). Thus, OTUD1 is involved in actin dynamics and endosome positioning, the latter probably independently of FLNA and Keap1.

Discussion

Vesicle transport and delivery of associated cargo is tightly controlled by members

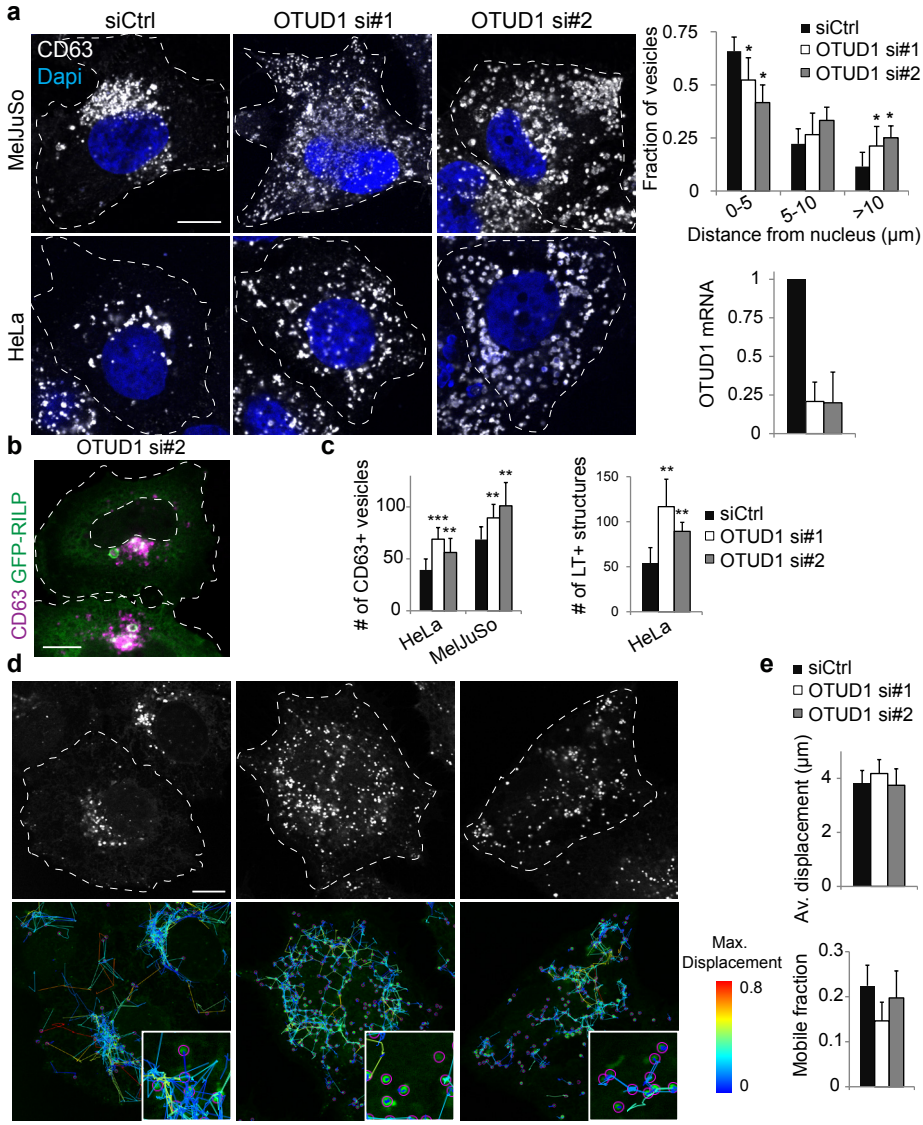


Figure 2: OTUD1 is required for late endosome positioning. *(A) MelJuSo and HeLa cells transfected with indicated siRNAs were fixed and stained for CD63 and DAPI. Bar = 10 µm. Quantification of CD63+ vesicle distance from the nucleus. Fraction of vesicles in each of the categories was quantified in at least 10 cells per experiment, n=3. Bottom right: silencing efficiency of OTUD1 in MelJuSo cells as detected by qRT-PCR. (B) siRNA transfected HeLa cells were transfected with GFP-RILP and fixed and stained for the indicated markers. (C) Amount of CD63+ (antibody staining) or Lysotracker+ (Live cell microscopy) structures in HeLa or MelJuSo cells transfected with the indicated siRNAs. At least 10 cells were counted from at least two independent experiments. (D) Dynamics of lysotracker marked vesicles in HeLa cells transfected with the indicated siRNAs. Confocal image at start of time-lapse is shown on the top, vesicle trajectories over a 240 sec interval are displayed below. Colors of individual vesicle trajectories are compared to the maximal displacement rate (blue=0, red=0.8 of control). Scale bar, 10 µm. (E) Average displacement (µm) for a vesicle during the 240 sec duration of the movie using trackmate. Bottom: quantification of the fraction of mobile vesicles. Vesicles with a total displacement of >5µm during the movie were considered immobile. For both quantifications over 5 fields of cells were imaged over 2 independent experiments.*

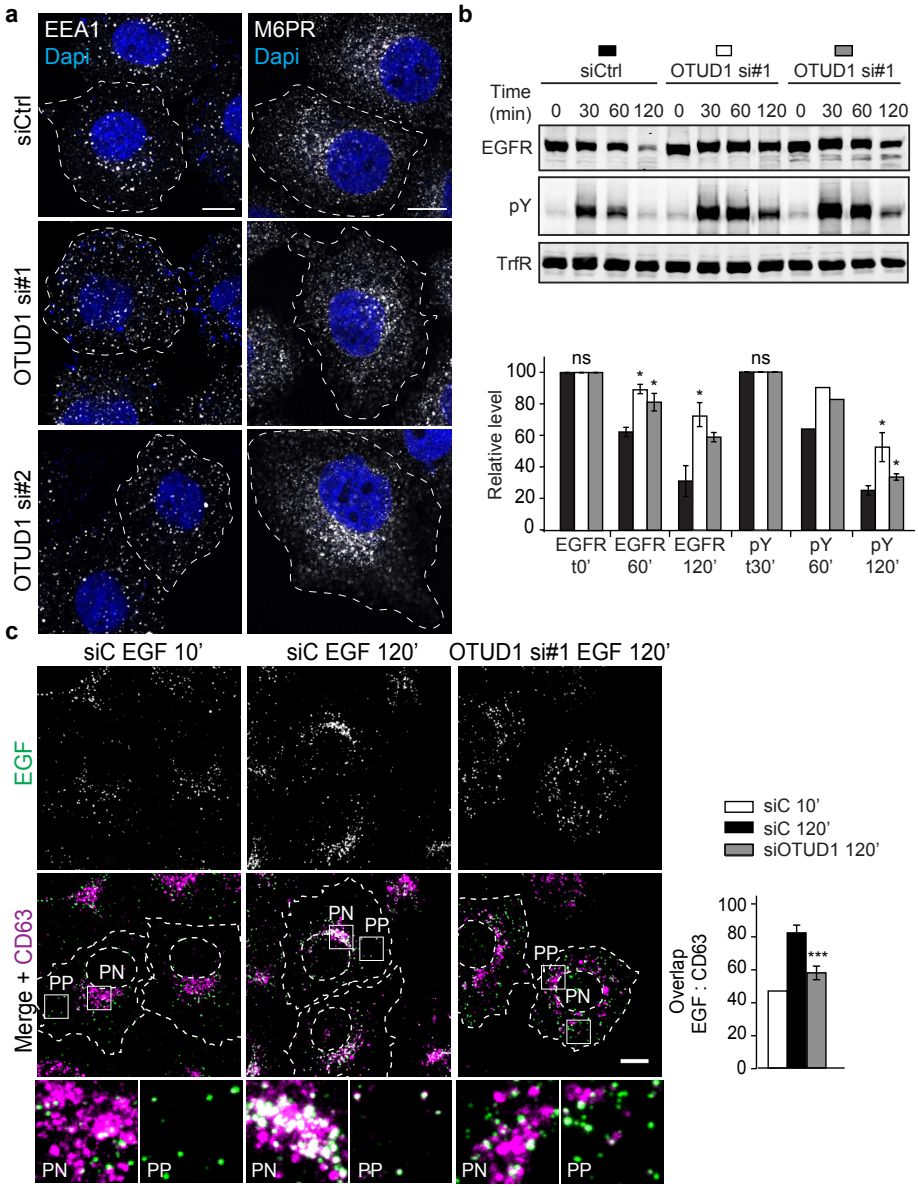
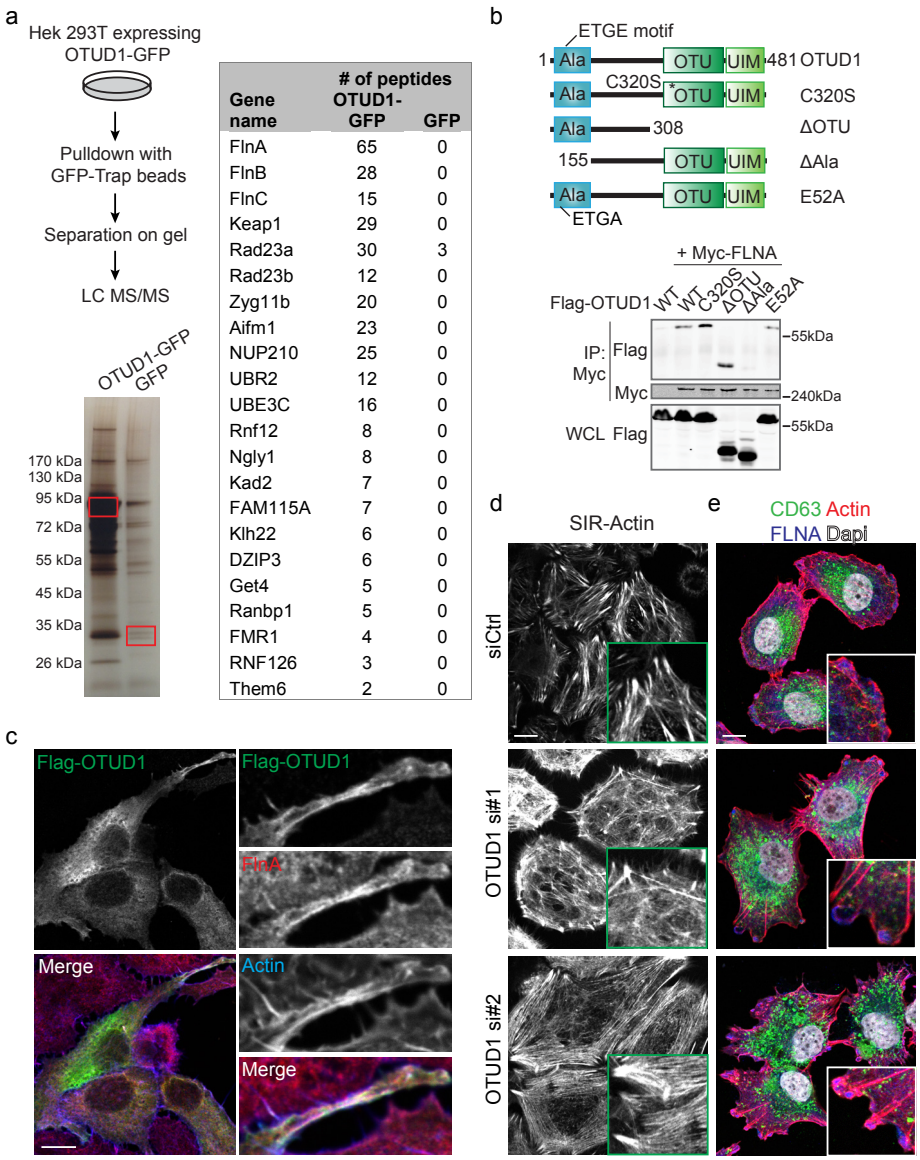


Figure 3: OTUD1 regulates early endosome positioning and EGFR degradation. *(A) HeLa cells were transfected with the indicated siRNAs and fixed and stained for EEA1 or Mannose-6-phosphate receptor (M6PR) and DAPI three days later. Bar = 10 µm. (B) EGFR degradation in control versus OTUD1-depleted HeLa cells. Immunoblots against total (EGFR) and phosphorylated (pY) EGFR, as well as TfR (loading control) along a time course following 20 ng/ml EGF addition (min) are shown. For quantification of EGFR, signal was normalized to corresponding t=0min. (C) Effect of OTUD1 depletion on receptor-mediated trafficking of EGF-555 (green) to the late endosome compartment (CD63, magenta). Representative z projection (3D) overlays at 10 min (left panels) and 120 min (right panels) following stimulation (100 ng/ml) are shown with perinuclear (PN) and peripheral (PP) zooms for control and OTUD1-depleted HeLa cells. Colocalization (Mander's overlap) of EGF with CD63 at 10 min (white) and 120 min (black) following ligand stimulation.*

of the endosomal system, as well as the cytoskeleton and external stimuli. Due to its specific spatiotemporal characteristics, where each vesicle should be controlled on an individual basis, the endocytic system is strongly regulated by dynamic post-translational modifications. Using an RNAi screen we identified novel DUBs that function in the endocytic system. One of these, OTUD1, is required for proper perinuclear localization of both early- and late endosomes and its loss impairs access of endocytosed material to the lysosome. Furthermore, OTUD1 interacts with actin-crosslinking protein FLNA and controls the actin cytoskeletal structure and cell morphology.

Timely delivery of growth receptors, adhesion complexes and autophagic cargo is facilitated by endosomal fusion, fission, sorting and transport events, materializing from different endosomal subsets. Organization of these events occurs at the cellular level by mechanisms regulating endosome positioning, such as the RNF26 system (21), as well as on the individual endosome basis, regulated by for example cargo itself (28). Our data show that loss of OTUD1 leads to a disorganized early- and late endosomal compartment, whereas other endocytic carriers such as the trans-Golgi network remain intact. Furthermore, the timely delivery of activated growth receptors like EGFR to the lysosomal compartment was perturbed, with EGFR accumulating in the early endosomal compartment. Whereas the molecular mechanism by which OTUD1 regulates these events is still unclear, our data suggest regulation at the interplay between the early- and late endosomal compartment, or alternatively of a protein complex that acts on both types of endosomes. Interestingly, the scattered endosome phenotype in combination with impaired degradation is reminiscent of a dysfunctional Rab5-Rab7 conversion, as HOPS perturbations provide a similar phenotype. However, we failed to identify any link between OTUD1 and co-isolated endocytic proteins in our mass spectrometry experiment, arguing for a transient interaction or an indirect effect. Therefore, it will be interesting to identify the substrates of OTUD1, by isolating ubiquitinated proteins accumulating after inactivation of OTUD1. We will then assess which of these proteins may link to the endosomal system, also using the data set that we generated in the earlier genome-wide siRNA screen for factors controlling MHC class II. This functional data set integration will allow unbiased hit selection for further experiments.

Besides controlling the integrity of the endosomal compartment, OTUD1 depleted cells displayed an altered morphology and actin cytoskeleton. OTUD1 knockdown cells contained an extended network of small actin fibers, compared to control cells having more focused, thick actin fibers. This could be the result of a functional interaction with the Filamin proteins, which are known to control actin crosslinking (29, 30). However, recent findings showed that OTUD1 restrains TGFβ-signaling by antagonizing RNF12-mediated ubiquitination of SMAD7, hereby increasing the levels of this inhibitory SMAD protein (Peter ten Dijke, personal communication). This in turn impairs migration and epithelial-to-mesenchymal transition, which is accompanied by extensive actin remodeling, suggesting that the effects of OTUD1 on the actin cytoskeleton are indirect, via alterations in the cellular differentiation state. Interestingly, SMAD7 localizes to endosomes to exert its negative regulation of the TGFβ-pathway (31), suggesting a potential coupling of SMAD signaling to



Gene name	# of peptides OTUD1-GFP	GFP
FlnA	65	0
FlnB	28	0
FlnC	15	0
Keap1	29	0
Rad23a	30	3
Rad23b	12	0
Zyg11b	20	0
Aifm1	23	0
NUP210	25	0
UBR2	12	0
UBE3C	16	0
Rnf12	8	0
Ngly1	8	0
Kad2	7	0
FAM115A	7	0
Klh22	6	0
DZIP3	6	0
Get4	5	0
Ranbp1	5	0
FMR1	4	0
RNF126	3	0
Them6	2	0

Figure 4: OTUD1 interacts and colocalizes with Filamin A and alters the actin cytoskeleton. *(A) Hek293T cells expressing GFP or OTUD1-GFP were lysed and immunoprecipitated for GFP using GFP-Trap beads. Associated proteins were visualized by silver stain and bands were subjected to MS/MS analysis. Red box corresponds to molecular weight of the GFP-tagged protein. Proteins identified by at least 2 peptides in the mass spectometer are depicted in the table. (B) Top: domain structure of OTUD1. Bottom: Co-immunoprecipitation for Filamin A (FLNA) with OTUD1. Myc-FLNA was isolated from lysates of HEK293T cells co-overexpressing indicated Flag-OTUD1 constructs using Myc-Trap beads. Western blot filters were probed for isolated Myc-tagged proteins, and the associated Flag-OTUD1. (C) HeLa cells transfected with Flag-OTUD1 were fixed and stained for the indicated markers. Bar = 10 µm. (D) HeLa cells transfected with the indicated siRNAs were imaged under the microscope using the SIR-actin probe. Still image is represented, bar = 10 µm. (E) U118 cells transfected with the indicated siRNAs were fixed and stained for the indicated markers. Bar = 10 µm.*

the effect of OTUD1 on the endosomal pathway. Alternatively, Filamin A has been shown to stimulate TGFβ-signaling by allowing phosphorylation of SMAD2 (32), which is antagonized by SMAD7 (33). Filamin A could thus interact with OTUD1 to prevent de-ubiquitination of SMAD7. Similarly, depletion of Keap1, another actin- and OTUD1-interacting protein, increases SMAD7 protein levels and attenuates TGFβ-signaling (34), raising the possibility that Keap1 inhibits OTUD1. It will be interesting to investigate the potential interplay between actin organizers and OTUD1 in relation to TGFβ-signaling, as well as the function of OTUD1 recruitment to different sites of action.

In summary, our experiments identify the DUB OTUD1 as critical in the organization and function of the endocytic compartment. Furthermore, MHC class II expression is controlled by OTUD1, as well as organization of the actin cytoskeleton. Additional experiments are required to dissect the underlying molecular mechanisms of action.

Materials and methods

Cell culture and constructs

MelJuSo cells and MelJuSo cells stably expressing GFP-Ubiquitin or GFP-HLA-DRα (35) were cultured in IMDM supplemented with 10% FCS, HeLa and Hek293T cells in DMEM with 10% FCS. The following constructs were obtained from addgene: Myc-FLNA (#8982), Flag-OTUD1 (#22553). GFP-RILP was described previously (36). OTUD1 and indicated mutants were cloned into a Flag-C1 vector.

Reagents and antibodies

For lysosomal staining Lysotracker green (Molecular probes) was used, for actin staining SIR-Actin (TeBu Bio). Antibodies used: rabbit anti-MHCII (1:100), rabbit anti-GFP (1:1000), mouse anti-CD63 (1:500) and rabbit anti-CD63 (1:100) (all described in (36)), mouse anti-HA (Covance 16B12, 1:1000), rat anti-HA 3F10 (Roche, 1:200), mouse anti-M6PR, rabbit anti-FLNA (all from Abcam, both 1:100), mouse anti-EEA1 , mouse anti-Transferrin receptor (Invitrogen, 1:100 confocal, 1:1000 western blot), rabbit anti-Flag F7425 and mouse anti-Flag M2 (Sigma, 1:1000), rabbit anti-EGFR (Millipore, 1:1000), mouse anti-phosphotyrosine (pY; 4G10 Millipore, 1:1000), actin was stained with Phalloidin-Alexa 647 (Life Technologies). Secondary antibodies (goat anti-mouse Alexa 405/488/568/647, goat anti-rabbit Alexa 488/568/647, donkey anti-goat Alexa 488/568, donkey anti-mouse Alexa 488/555/647 and donkey anti-rabbit Alexa 488/647) were purchased from Life Technologies and donkey anti-rat CF568 from Biotium (all 1:200).

Transfections

For expression studies, MelJuSo and HeLa cells were transfected using Effectene (Qiagen) according to the manufacturer's instructions. Cells were transfected one day before fixation or lysis. Hek293T cells were transfected using polyethylenimine (PEI). For siRNA mediated depletion, cells were reverse transfected with DharmaFECT transfection reagent #1 and 50 nM siRNA of the Human siGenome SMARTpool, Dharmacon, according to the manufacturer's protocol. siRNA sequences for OTUD1: #1 5'-ACGAAGAACTTGCCAAATC-3' and #2 5'-TATCATCGCTGCTGCCCCAA -3'. Briefly, siRNAs and DharmaFECT were mixed and

incubated for 20 minutes in a culture well, after which cells were added and left to adhere (reverse transfection). Three days later, cells were fixed and stained or lysed for biochemical analysis.

Flow Cytometry

Three days after siRNA transfections as described above, cells were trypsinized and stained with Cy3-labeled L243 antibody, described in (16), and analyzed using flow cytometry (BD FACSArray). For staining of total pMHCII levels, cells were fixed with 2% formaldehyde and permeabilized using 0.125% Saponin before staining, which was also used during antibody washes. Data were normalized to the control (siCtrl transfected cells) and z-scores were calculated using the standard deviations of the controls. All hits with z-scores > 2.5 were included in follow up analysis.

EGFR degradation assays

Ligand-mediated turnover of EGFR was assayed as previously described using 20ng/ml EGF (21). Receptor abundance at each indicated time-point following stimulation was quantified relative to Transferrin receptor and expressed as a fraction of EGFR at t=0 for each condition. Receptor phosphorylation was expressed relative to the maximal activation achieved in control cells (siC).

Co-immunoprecipitation and Western blotting

For co-immunoprecipitation experiments, Hek293T cells were lysed in lysis buffer (0.5% NP-40, 5% glycerol, 150mM NaCl, 50mM Tris-HCl pH8.0, 5mM MgCl2 supplemented with complete EDTA-free Protease Inhibitor Cocktail (Roche)) and cleared by centrifugation. Lysates were incubated with GFP-Trap beads (Chromotek) or protein G-Sepharose 4 FF resin with the indicated antibodies and after incubation washed extensively with lysis buffer before addition of sample buffer (2% SDS, 10% glycerol, 5% β-mercaptoethanol, 60mM Tris-HCl pH 6.8 and 0.01% bromophenol blue).

For whole cell lysate analyses, cells were lysed directly in sample buffer. Proteins were separated by SDS-PAGE and transferred to Western Blot filters. Blocking of the filter and antibody incubations were done in PBS supplemented with 0.1 (v/v)% Tween and 5% (w/v) milk powder. Blots were imaged using the Odyssey Imaging System (LI-COR) or ChemiDoc (Bio-Rad).

Mass spectrometry

Samples from immune-precipitated GFP-tagged proteins were separated by SDS-PAGE and were silver stained (Invitrogen). Selected bands (and the same region in the GFP control lane as negative controls) were cut from the silver stained gel and subjected to reduction with dithiothreitol, alkylation with iodoacetamide and in-gel trypsin digestion using a Proteineer DP digestion robot (Bruker). Tryptic peptides were extracted from the gel, lyophilized, dissolved in 95/3/0.1 v/v/v water/acetonitril/formic acid and subsequently analyzed by online nanoHPLC MS/MS using an 1100 HPLC system (Agilent Technologies), as previously described (Meiring et al., 2002). Peptides were trapped at 10 µl/min on a 15mm column (100µm ID; ReproSil-Pur C18-AQ, 3 µm, Dr. Maisch GmbH) and eluted to a 200 mm column (50µm ID; ReproSil-Pur C18-AQ, 3 µm) at 150 nl/min. All columns were packed in house. The column was developed with a 30min gradient from 0 to 50% acetonitrile in 0.1% formic acid. The end of the nanoLC column was drawn to a tip (5-µm ID),

from which the eluent was sprayed into a 7tesla LTQ-FT Ultra mass spectrometer (Thermo Electron). The mass spectrometer was operated in data-dependent mode, automatically switching between MS and MS/MS acquisition. Full scan MS spectra were acquired in the FT-ICR with a resolution of 25,000 at a target value of 3,000,000. The two most intense ions were then isolated for accurate mass measurements by a selected ion-monitoring scan in FT-ICR with a resolution of 50,000 at a target accumulation value of 50,000. Selected ions were fragmented in the linear ion trap using collision-induced dissociation at a target value of 10,000. In a post-analysis process, raw data were first converted to peak lists using Bioworks Browser software v3.2 (Thermo Electron), and then submitted to the Swissprot database version 51.6 (257,964 entries), using Mascot v. 2.2.04 (www.matrixscience.com) for protein identification. Mascot searches were with 2 ppm and 0.8 Da deviation for precursor and fragment mass, respectively, and trypsin as enzyme. Protein was finally sorted and compared using Scaffold software version 3.0.1 (www. proteomesoftware.com).

cDNA synthesis and qPCR

RNA isolation, cDNA synthesis and quantitative RT-PCR were performed according to the manufacturer's (Roche) instructions. Signal was normalized to GAPDH and calculated using the Pfaffl formula. Primers used for detection were: GAPDH fw: 5'-TGTTGCCATCAATGACCCCTT-3', GAPDH rv: 5'-CTCCACGACGTACTCAGCG-3', HLA-DRα fw: 5'- -3', HLA-DRα rv: 5'- -3', IRF1 fw: 5'-GCACCAGTGATCTGTACAAC-3', IRF1 rv: 5'-GCTCCTCCTTACAGCTAAAG-3', CIITA fw: 5'-CCTGCTGTTCGGGACCTAAA-3, CIITA rv: 5'-GGATCCGCACCAGTTTGG-3', OTUD1 fw: 5'-CCTAGTATTTGGCTCAGTTGG-3', OTUD1 rv: 5'-TTGTCGTACTCTGGGTTAGG-3'.

Confocal microscopy

Cells were seeded on coverslips, transfected 18 hours later and treated as indicated. 24 hrs later, cells were fixed in 3.7% formaldehyde for 10 min and permeabilized in ice-cold methanol (for LC3 stainings) for 2 minutes or in 0.1% Triton-X100 for 10 minutes. Alternatively, cells were fixed and permeabilized in ice-cold methanol for 2 minutes for Tubulin stainings. Staining was performed with the antibodies mentioned above and DAPI (Invitrogen) to stain DNA. Images were acquired using a Leica TCS SP5 confocal microscope (Leica Microsystems, Wetzlar, Germany) at 63x magnification. For live-cell imaging, the microscope was equipped with a climate control chamber and cells were imaged for 3 minutes with ~6 frames per minute. Images were quantified using Image J plugin Jacob for Mander's coefficient calculations or FIJI's Trackmate plugin for live-cell imaging and processed using Adobe Photoshop and Illustrator.

Acknowledgements

We thank the NKI and LUMC microscopy facility, the NKI FACS facility and the NKI Robotics and Screening facility, with special thanks to Ben Morris for all his help with hit validations. Also, members of the Neefjes group for critical discussions, Nico Ong for developing electron micrographs, Lennert Janssen for help with cloning. This work was supported by the Institute of Chemical Immunology (ICI), an NWO Gravitation project funded by the Ministry of Education, Culture and Science

of the government of the Netherlands and a European Research Council (ERC) advanced grant awarded to J.N.

References

1. J. Neefjes, M. L. Jongsma, P. Paul, O. Bakke, Towards a systems understanding of MHC class I and MHC class II antigen presentation. Nat Rev Immunol 11, 823-836 (2011).
2. R. H. Wijdeven, J. M. Bakker, P. Paul, J. Neefjes, Exploring genome-wide datasets of MHC class II antigen presentation. Molecular immunology 55, 172-174 (2013).
3. M. M. Fernando et al., Defining the role of the MHC in autoimmunity: a review and pooled analysis. PLoS Genet 4, e1000024 (2008).
4. E. R. Unanue, V. Turk, J. Neefjes, Variations in MHC Class II Antigen Processing and Presentation in Health and Disease. Annual review of immunology 34, 265-297 (2016).
5. W. Reith, S. LeibundGut-Landmann, J. M. Waldburger, Regulation of MHC class II gene expression by the class II transactivator. Nat Rev Immunol 5, 793-806 (2005).
6. J. Schneppenheim et al., The intramembrane protease SPPL2a promotes B cell development and controls endosomal traffic by cleavage of the invariant chain. J Exp Med 210, 41-58 (2013).
7. D. R. Beisner et al., The intramembrane protease Sppl2a is required for B cell and DC development and survival via cleavage of the invariant chain. J Exp Med 210, 23-30 (2013).
8. W. Pos et al., Crystal structure of the HLA-DM-HLA-DR1 complex defines mechanisms for rapid peptide selection. Cell 151, 1557-1568 (2012).
9. C. Paludan et al., Endogenous MHC class II processing of a viral nuclear antigen after autophagy. Science (New York, N.Y.) 307, 593-596 (2005).
10. D. Schmid, M. Pypaert, C. Munz, Antigen-loading compartments for major histocompatibility complex class II molecules continuously receive input from autophagosomes. Immunity 26, 79-92 (2007).
11. D. Komander, M. J. Clague, S. Urbe, Breaking the chains: structure and function of the deubiquitinases. Nature reviews. Molecular cell biology 10, 550-563 (2009).
12. O. Kerscher, R. Felberbaum, M. Hochstrasser, Modification of proteins by ubiquitin and ubiquitin-like proteins. Annual review of cell and developmental biology 22, 159-180 (2006).
13. R. C. Piper, I. Dikic, G. L. Lukacs, Ubiquitin-dependent sorting in endocytosis. Cold Spring Harbor perspectives in biology 6, (2014).
14. M. J. Clague, S. Urbe, Integration of cellular ubiquitin and membrane traffic systems: focus on deubiquitylases. The FEBS journal, (2017).
15. M. H. Wright, I. Berlin, P. D. Nash, Regulation of endocytic sorting by ESCRT-DUB-mediated deubiquitination. Cell Biochem Biophys 60, 39-46 (2011).
16. P. Paul et al., A Genome-wide multidimensional RNAi screen reveals pathways controlling MHC class II antigen presentation. Cell 145, 268-283 (2011).
17. I. Berlin, H. Schwartz, P. D. Nash, Regulation of epidermal growth factor receptor ubiquitination and trafficking by the USP8.STAM complex. The Journal of biological chemistry 285, 34909-34921 (2010).
18. I. Berlin, K. M. Higginbotham, R. S. Dise, M. I. Sierra, P. D. Nash, The deubiquitinating enzyme USP8 promotes trafficking and degradation of the chemokine receptor 4 at the sorting endosome. The Journal of biological chemistry 285, 37895-37908 (2010).
19. T. E. Mevissen et al., OTU deubiquitinases reveal mechanisms of linkage specificity and enable ubiquitin chain restriction analysis. Cell 154, 169-184 (2013).
20. A. P. Carneiro et al., A putative OTU domain-containing protein 1 deubiquitinating enzyme is differentially expressed in thyroid cancer and identifies less-aggressive tumours. British journal of cancer 111, 551-558 (2014).
21. M. L. Jongsma et al., An ER-Associated Pathway Defines Endosomal Architecture for Controlled Cargo Transport. Cell 166, 152-166 (2016).
22. M. E. Sowa, E. J. Bennett, S. P. Gygi, J. W. Harper, Defining the human deubiquitinating enzyme interaction landscape. Cell 138, 389-403 (2009).
23. G. Liu et al., Cytoskeletal protein ABP-280 directs the intracellular trafficking of furin and modulates proprotein processing in the endocytic pathway. The Journal of cell biology 139, 1719-1733 (1997).
24. M. Fernandez-Borja, L. Janssen, D. Verwoerd, P. Hordijk, J. Neefjes, RhoB regulates endo-

some transport by promoting actin assembly on endosomal membranes through Dia1. Journal of cell science 118, 2661-2670 (2005).
25. A. L. Zajac, Y. E. Goldman, E. L. Holzbaur, E. M. Ostap, Local cytoskeletal and organelle interactions impact molecular-motor- driven early endosomal trafficking. Current biology : CB 23, 1173-1180 (2013).
26. M. Anitei, B. Hoflack, Bridging membrane and cytoskeleton dynamics in the secretory and endocytic pathways. Nature cell biology 14, 11-19 (2011).
27. J. Taunton et al., Actin-dependent propulsion of endosomes and lysosomes by recruitment of N-WASP. The Journal of cell biology 148, 519-530 (2000).
28. J. Huotari, A. Helenius, Endosome maturation. The EMBO journal 30, 3481-3500 (2011).
29. G. M. Popowicz, M. Schleicher, A. A. Noegel, T. A. Holak, Filamins: promiscuous organizers of the cytoskeleton. Trends in biochemical sciences 31, 411-419 (2006).
30. F. Nakamura, T. P. Stossel, J. H. Hartwig, The filamins: organizers of cell structure and function. Cell adhesion & migration 5, 160-169 (2011).
31. G. M. Di Guglielmo, C. Le Roy, A. F. Goodfellow, J. L. Wrana, Distinct endocytic pathways regulate TGF-beta receptor signalling and turnover. Nature cell biology 5, 410-421 (2003).
32. A. Sasaki, Y. Masuda, Y. Ohta, K. Ikeda, K. Watanabe, Filamin associates with Smads and regulates transforming growth factor-beta signaling. The Journal of biological chemistry 276, 17871-17877 (2001).
33. H. Hayashi et al., The MAD-related protein Smad7 associates with the TGFbeta receptor and functions as an antagonist of TGFbeta signaling. Cell 89, 1165-1173 (1997).
34. I. G. Ryoo, H. Ha, M. K. Kwak, Inhibitory role of the KEAP1-NRF2 pathway in TGFbeta1-stimulated renal epithelial transition to fibroblastic cells: a modulatory effect on SMAD signaling. PloS one 9, e93265 (2014).
35. N. P. Dantuma, T. A. Groothuis, F. A. Salomons, J. Neefjes, A dynamic ubiquitin equilibrium couples proteasomal activity to chromatin remodeling. The Journal of cell biology 173, 19-26 (2006).
36. R. van der Kant et al., Late endosomal transport and tethering are coupled processes controlled by RILP and the cholesterol sensor ORP1L. Journal of cell science 126, 3462-3474 (2013).

Chapter 5:
USP54 is a novel regulator of cytoskeletal dynamics

Ruud H. Wijdeven[1,3,4], Ilana Berlin[1,3,4], George Jansen[2], Hans Janssen[3], Peter van Veelen[2], Jacques Neefjes[1,3]

[1] Department of Chemical Immunology, LUMC, Leiden, the Netherlands
[2] Department of Immunohematology and Blood Transfusion, LUMC, Leiden, the Netherlands.
[3] Department of Cell Biology, Netherlands Cancer Institute, Amsterdam, the Netherlands
[4] Contributed equally to this work

The endocytic pathway is critical for cellular organization, and spatiotemporally confined internalization from and recycling to specific plasma membrane sites is essential for the establishment of cell polarity. However, the molecular mechanisms underlying geographically restricted endosome transport and fusion are poorly understood. Here, we identified USP54 as an active DUB regulating cell-cell contact site integrity and endocytic transport. USP54 localizes to cell-cell contact sites and endosomes and traverses between these compartments. At these compartments, USP54 respectively co-localized and interacted with tight junction proteins including ZO-2 and select members of the HOPS tethering complex. Loss of USP54 decreased membrane localization of tight junction protein ZO-1 and induced peripheral re-localization and stabilization of microtubules, indicative of a cell polarity defect. Altered ZO-1 localization was also observed for HOPS depletion. Together, our data suggest that USP54 interacts with different complexes, including HOPS and tight junctions, to control trafficking of cell-cell contact proteins from endosomes to the cell surface and thus regulate the establishment of cell polarity.

The endocytic network is a highly dynamic arrangement of different carriers, each able to deliver or accept cargo from specific compartments. It serves as the primary means for communication with the extracellular environment, as well as with neighboring cells via physical contacts. These cell-cell contact sites are maintained by spatially restricted internalization and recycling of specific cell-cell contact proteins and are essential for the establishment of cell polarity (1, 2). Furthermore, the endocytic network controls specific cargo transport to the apical and basolateral sides of polarized cells, underscoring the diverse flavors of endosomes.
To identify novel regulators of the endocytic pathway, we used the results of an RNAi screen that we recently performed on the role of de-ubiquitinating enzymes (DUBs) in the MHCII pathway (Chapter 4). One of the hits was of particular interest, USP54. This mechanistically unstudied DUB is implicated in cell migration (3), a process involving cell polarization, and its loss yielded a strong clustering phenotype of the MHCII compartment, suggesting a function for this DUB in the transport dynamics of late endosomes. To assess whether this regulation is specific for MHCII or extends to the endocytic compartment as a whole, MelJuSo cells silenced for USP54 were analyzed by electron microscopy to determine the localization of membranous compartments. Strikingly, all endocytic vesicles, and even the mitochondria, clustered around the MTOC, leaving a nearly empty cytosolic peripheral space (Fig. S1a). Other cell types such as HeLa (cervical cancer) and U2OS (osteosarcoma) showed a more mixed phenotype, with cells showing strongly clustered organelles and other cells a more scattered phenotype. Thus, the clustering phenotype may be secondary to a different effect on cellular organization. Besides clustering of compartments, many cells lacking USP54 were bi- or multi-nucleated, suggesting defective mitosis or abscission (Fig. 1a). Consistent with this, the amount of cells with double the DNA-content was increased in these cells, both in MelJuSo and p53 pathway proficient U2OS cells (Fig. 1b and 1c). Given the presence of a Microtubule Interacting and Transport (MIT) domain in USP54 (Fig. 1d (4)), a microtubule-defect following USP54 silencing would be an option. Indeed, cells depleted for USP54 possessed

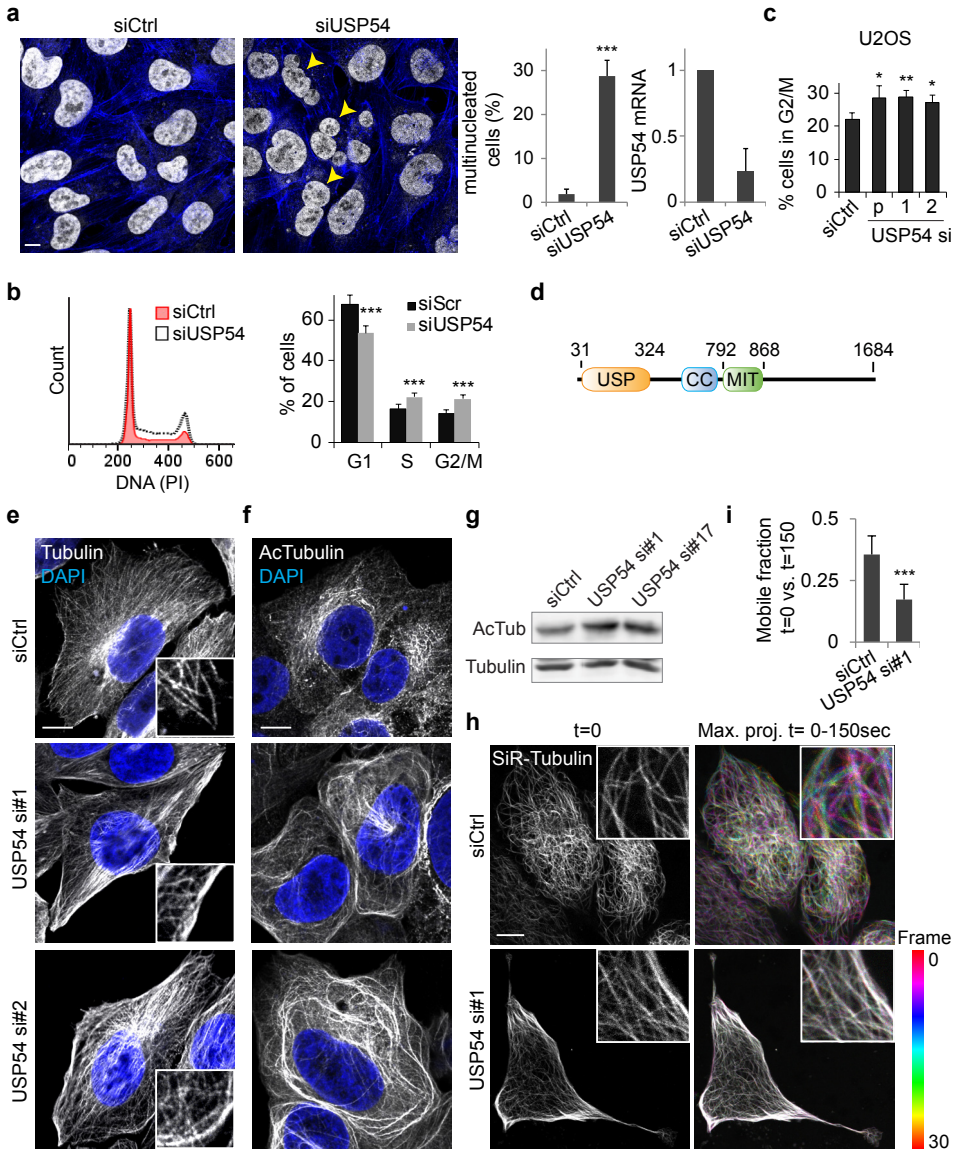


Figure 1: USP54 controls microtubule dynamics. *(A) MelJuSo cells transfected with the indicated siRNAs were fixed and stained with DAPI and Phalloidin (actin). Amount of cells with more than one DAPI-positive structure were counted for at least 50 cells per experiment, n=3. Right: silencing efficiency of USP54 was analyzed by qRT-PCR. (B) MelJuSo cells transfected with the indicated siRNAs were analyzed for cell cycle stage by flow cytometry using propidium iodide (PI). Left: representative FACS plot of PI intensity. Right: quantification of cells in different cell cycle stages. (C) U2OS cells transfected with the indicated siRNAs (USP54 pool of 4 siRNAs or specific siRNA sequences #1 and #2) were analyzed for cell cycle stage by flow cytometry using propidium iodide (PI). % of cells in G2/M phase was quantified. (D) USP54 domain structure. (E) MelJuSo transfected with the indicated siRNAs were fixed and stained with DAPI and Tubulin. (F) U2OS transfected with the indicated siRNAs were fixed and stained with DAPI and AcTubulin. Legend continues on next page*

a remarkably different microtubule structure, with a more peripheral localization of the bulk of the microtubules, sometimes following the edges of the cell (Fig. 1e and S1b). This was corroborated by an extended network of acetylated Tubulin (Fig. 1f), which labels relatively stable microtubules (5), implying these cells contain more static microtubules at the periphery. Overall levels of Acetylated Tubulin increased only marginally (Fig. 1g), hinting at a reorganization of the stable microtubule network. To address the mobility of the microtubule network, microtubule dynamics were followed using a fluorescent tubulin-binding compound (6) in cells either or not depleted for USP54. Again, we observed a massive microtubule network at the cellular edges and the microtubules were much more static compared to control cells, suggesting a defect in microtubule de-polymerization or docking at the plasma membrane (Fig. 1h and 1i). Together, these data establish a role for USP54 in cytoskeletal organization by influencing the dynamics of microtubules.

While containing a USP DUB-domain, USP54 was predicted to be catalytically inactive as it lacks a critical Histidine that assists the catalytic triad in conventional USP-domains (7). To assess whether this indeed prevented catalytic activity, we exposed USP54 to a DUB activity-based probe (8). Wild-type USP54, but not its counterpart missing the catalytic cysteine (C42S), reacted with the probe (Fig. 2a). However, the fraction of USP54 labelled by the activity-based probe was much lower than that for USP8 (and other active DUBs tested), suggesting slow reactivity, either because of the missing Histidine or because co-factors are required for full activity. Nevertheless, USP54 is a catalytically competent enzyme.

The presence of an MIT domain begged the question whether USP54 is in fact a microtubule-interacting protein that controls microtubule dynamics. However, we were unable to detect an interaction or co-localization between the MIT domain and tubulin. Rather, full-length USP54 exhibited three distinct localizations; the plasma membrane and more specifically cell-cell contact sites, actin filaments, and endosome-like structures (Fig. 2b). The cell-cell contact and endosome localization was primarily controlled by the C-terminal domain in USP54, since expression of the C-terminal 1432-1684 amino acids resembled the localization of the full length protein, albeit with a more spotted plasma membrane localization (Fig. 2c and 2d). These spots marked the locations where actin stress fibers between different cells were connected (Fig. 2e), usually the location of tight junctions (9). Time-lapse experiments showed that USP54 was immobile at these junctions for prolonged periods of time (Fig. 2f), suggesting USP54 is an integral part of the contact site. Fast, endosome-resembling mobility to and from the contact site was observed for USP54-positive structures (green arrows), indicating USP54 traffics to or from these

(G) Western blot analysis for the indicated markers on U2OS cells transfected with the indicated siRNAs. (H) Microtubules in U2OS cells transfected with the indicated siRNAs were followed in time using SIR-Tubulin. Left: still image at the start of the movie. Images were recorded for 150 seconds with an image every 5 seconds. Right: hyperstack of the individual frames, represented as a Spectrum image according to the legend on the right. Immobile microtubules appear white, mobile ones as a multicolor image. (I) Calculation of the percentage of mobile microtubule. Pearson's coefficient of the first and last image of the movies from (H) were calculated and coefficient was taken as percentage of immobile microtubule. Quantification of at least 10 cells over three independent experiments. For all experiments: bars indicate mean + SD from independent triplicate experiments. T-test statistical analysis ($p < 0.05$, ** $p < 0.01$, *** $p < 0.001$). For all experiments, bar = 10 µm.*

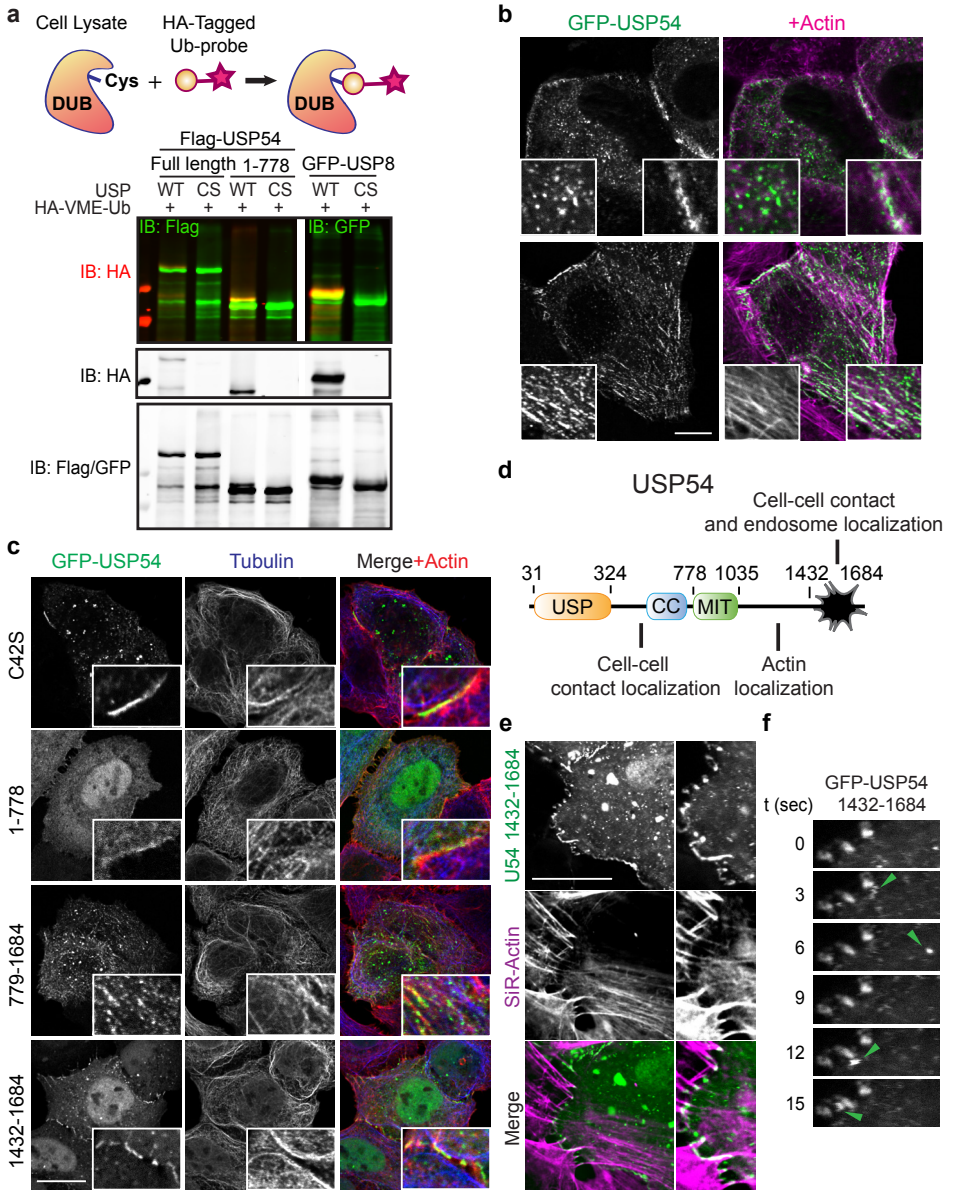


Figure 2: USP54 is a catalytically active DUB that localizes to membrane compartments. *(A) Ub-probe assay. Hek293T cells were transfected with the indicated plasmids (CS harbor a mutation in the catalytic site that renders the DUB inactive) and lysates were incubated with HA-VME-Ub for 30minutes. Samples were run on SDS-PAGE and analysed by western blot for HA (the probe) and Flag (the enzyme). (B) GFP-tagged USP54 was expressed in U2OS cells and cells were fixed and stained for actin. (C) GFP-tagged USP54 and mutants were expressed in HeLa cells and fixed and stained for actin and tubulin. (D) Overview of the localization determinants present in USP54 on the basis of experimets in (C) and (S2). (E) HeLa cells expressing GFP-USP54 1432-1684 were imaged together with SIR-Actin. Still image of a movie is shown. (F) Zoom-in of a movie made in (E), with different timepoints shown in separate frames. Green arrows indicate an endosome moving to or from the cell-cell contact site. For all experiments, bar = 10 µm.*

contact sites.
Extension of the C-terminal fragment, either 1035-1684 or 779-1684, redirected USP54 to actin fibers. This implies that the segment between the MIT domain and plasma membrane targeting domain likely interacts with actin-binding proteins (Fig. 2c and S2). The 1-778 and 1-1035 domains predominantly localized to the cytosol, although a small fraction localized to cell-cell contacts, indicating that the USP-domain and/or the coiled-coil domain contained some cell-cell contact localization determinants. Interestingly, cells ectopically expressing either the 1432-1684 or the catalytically inactive full-length enzyme (C42S) harbored a rounded microtubule structure resembling USP54 knockdown, suggesting that the catalytic activity of USP54 is required for its function, as well as the localization domain at the N-terminus. Thus, USP54 is an active DUB that localizes to cell-cell contact sites, endosomes and actin filaments. The different USP54 domains potentially regulate the interplay between these compartments.
Given its complex localization and domain structure, we set out to identify interacting proteins by immunoprecipitating different GFP-tagged USP54 domains and subjected interactors to mass spectrometry identification (Fig. 3a and 3b). This revealed that especially the coiled-coil domain and the C-terminal domain interact with a large array of proteins. The C-terminal fragment was associated with, among others, Plakoglobin/JUP/γ-Catenin, an integral component of desmosomes and adherens junctions, as well as several members of the HOPS complex (Fig. 3c). The extended C-terminal fragment, including the actin-localizing domain, isolated the actin-based motor proteins Myosin Heavy Chain 1 (MYH1), Myosin 1b and Myosin 1c, which could account for the actin localization. The coiled-coil domain precipitated a plethora of proteins, most notably: several members of tight and adherens junctions (most strongly ZO-1, ZO-2 and USP9x), multiple cilia proteins (predominantly IFT172), DOCK7 (a GEF for the RAC1 and CDC42 GTPases and involved in cell motility and polarity (10, 11)), HDAC6 (the deacetylase for αTubulin (12) and involved in adherens junction disassembly (13, 14)), SNX27 (a member of the sorting nexin family that mediates recycling of cargo from endosomes to the plasma membrane(15)), and STXBP4 (an inhibitor for STX4-mediated exocytosis (16)). Furthermore, strong co-immunoprecipitation was observed for several members of the 14-3-3 protein family of phosphorylation-binding proteins (17), suggesting that this USP54 domain harbors a phosphorylation site that is recognized by these proteins. Indeed, USP54 contains two canonical 14-3-3 binding RXXSXP sequences (18), and both localized in this isolated USP54-domain (amino acids 493-498 and 666-670). The USP-domain predominantly interacted with VCP/p97/TERA, a chaperone ATPase involved in the segregation of large protein complexes (19), and which also promotes sorting of Caveolin-positive endosomes towards the lysosome (20). Interestingly, this interaction occurred preferentially with the C42S variant. The MIT domain, besides its role in protein-protein interactions also known to interact with phospholipids such as PI3P and PI4P (21), interacted with the kinase DYRK1a and phosphatase PGAM5. Thus, we identified five domains in USP54, each with specific sets of interacting proteins.
During the formation of an epithelial cell layer, the establishment of apico-basal polarization is coupled to the formation of tight and adherens junctions, and this

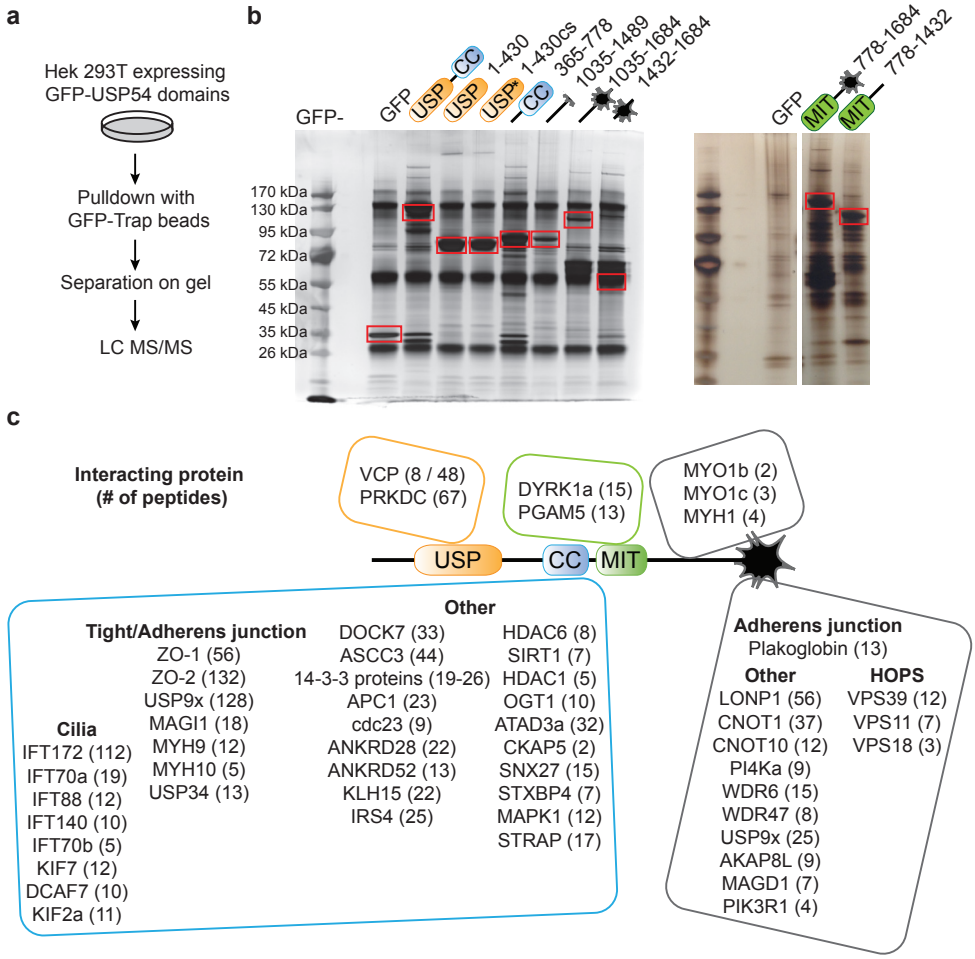


Figure 3: Identification of USP54-interacting proteins. *(A) Set-up of the mass spec experiment. Hek293T cells were transiently transfected with GFP or GFP-tagged USP54 domains and after lysis GFP was immunoprecipitated using GFP-Trap beads. Associated material was separated by SDS-PAGE and after silver staining the unique bands were subjected to MS/MS analysis. (B) Results of the silver stain and the constructs used. Red boxes indicate GFP-tagged proteins. (C) Selection of most relevant and abundant hits per domain, with the corresponding amount of peptides between brackets (). For VCP, number of peptides in respectively the active USP domain and inactive USP domain are shown. For fragment in between MIT and C-terminal domain, results from 1432-1684 were subtracted from the 1035-1684 domain. For MIT domain, 1035-1684 was subtracted from 779-1684.*

subsequently restructures the microtubule network towards a more peripheral texture (22-27). The strong immunoprecipitation of several tight / adherens junction proteins in conjunction with the described role for these junctions in cytoskeletal dynamics made us speculate that by interfering with the integrity of cell-cell contact sites or the formation of apical-basal lateral polarization, USP54 controls microtubule dynamics. USP54 at the cell-cell contact sites indeed co-localized with ZO-1, an integral member of both tight and adherens junctions (Fig. 4a). Co-immunoprecipitation experiments confirmed an interaction of USP54 with tight junction protein

ZO-2, but not ZO-1. Possibly ZO-1 interacts with ZO-2 and subsequently USP54. To address whether USP54 affects cell-cell contact site formation, we silenced USP54 and stained for ZO-1. Whereas in both U2OS and HeLa cells about half of the cells contained at least one ZO-1 positive cell-cell contact site, cells depleted for USP54 contained hardly any ZO-1 at the membrane (Fig. 4c and Fig. S3a). Most of the residual membranous ZO-1 was found on actin filaments running perpendicular to the plasma membrane (Fig. 4c, bottom inset). No effect was observed for the adherens junction members β-Catenin and y-Catenin (Fig. 4d and S3b), suggesting that USP54 controls the formation or stability of tight junctions but not adherens junctions.

Given the endosome-like localization of USP54, it could be involved in shuttling cargo from endosomes to cell-cell contact sites. The C-terminal domain of USP54 pulled-down three members of the HOPS complex, a tethering complex recruited to LE/Lys by Rab7 and Arl8b that mediates fusion and maturation of said endosomes (28-30), implying USP54 could be recruited to these structures. Indeed, USP54 co-localized with vesicle-localized VPS39, VPS11 and VPS18, but not with VPS41, another member of the HOPS core complex (Fig. 5a and S4a). In agreement with this and the mass spectrometry experiment, USP54 interacted with VPS39 and VPS18, but not with VPS41, or VPS33b, part of the HOPS-related VIPAR complex (31) (Fig. 5b), implying USP54 is recruited to only a segment of the HOPS complex. Interestingly, these VPS- and USP54-positive vesicles did not stain for CD63 (Fig. 5a), suggesting that the VPS-subunits interact with USP54 on a different type of endosome. Co-stainings with different endosomal markers did not show significant co-localization of USP54 with early endosomal Rab5, or to recycling endosomes marked by Rab11 and Transferrin receptor (Fig. S4b), although sometimes both endosomal structures were adjacent to each other and in close contact, as if somehow tethered. Whereas VPS11 and VPS18 are only known for their roles in the early endosomal CORVET and late endosomal HOPS tethering complexes, VPS39 can also be recruited by Rab2a to a specialized recycling endosome (32). Nevertheless, also Rab2a did not co-localize with USP54 (Fig. S4c). Thus, VPS39, VPS11 and VPS18 interact with the C-terminal tail of USP54 and co-localize on a yet undefined subset of endosomes (Fig. 5c).

To address whether VPS11, VPS18 and VPS39 are important for the function of USP54 in tight junction formation, we silenced the different subunits and addressed the localization of ZO-1. While membrane localization per se was not significantly impaired by VPS-knockdown, ZO-1 junctions often mislocalized to actin filaments perpendicular to the membrane or formed round structures, as if the junctions were ruptured in the middle and the cells detached from each other (Fig. 5d). Whereas not phenocopying USP54 silencing, both USP54 and the VPS-subunits appear to be involved in tight junction localization, possibly by acting in a large multi-protein complex.

Conclusions and future directions

Spatially confined internalization and recycling of cargo is crucial for the installment of polarity and cellular differentiation. However, the processes underlying this specific regulation are poorly understood. Here, we have identified USP54 as a novel fac-

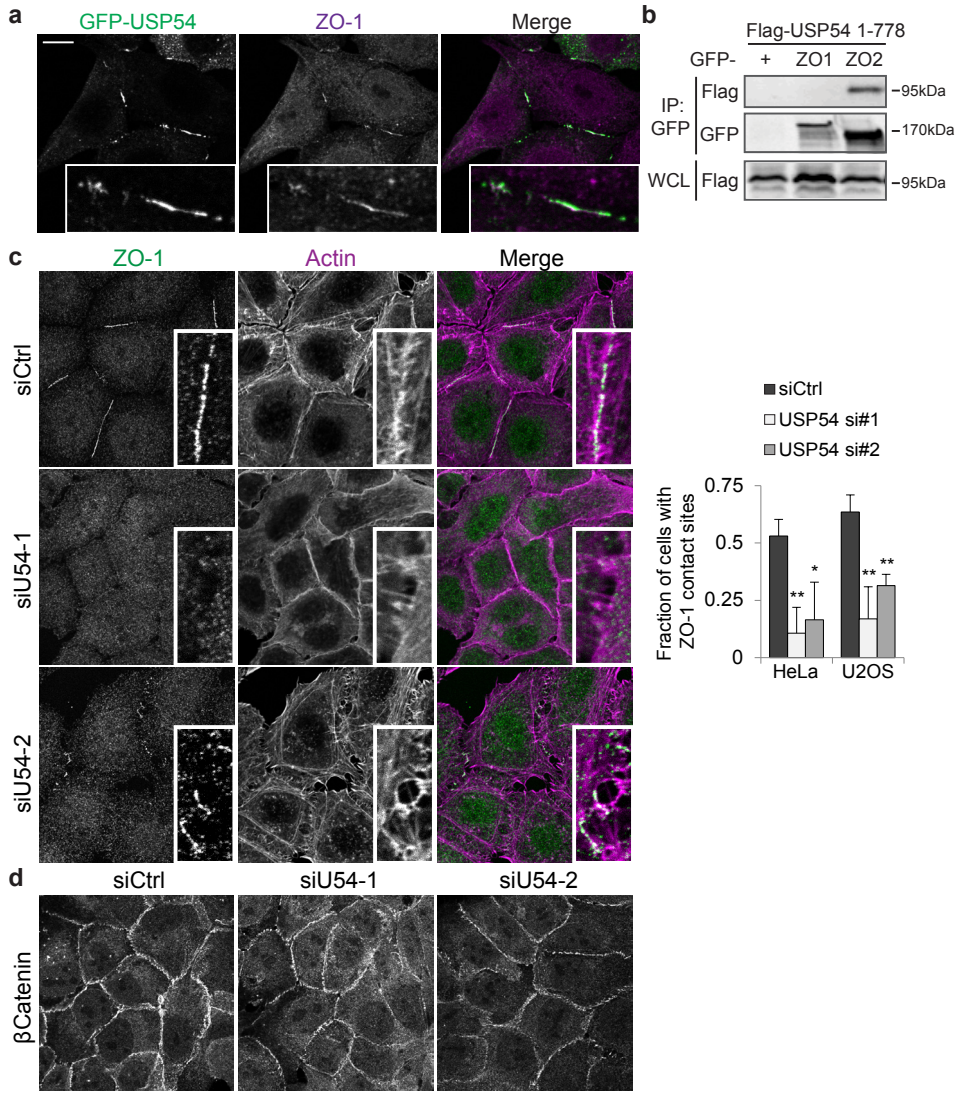


Figure 4: USP54 controls membrane localization of tight junction member ZO-1. *(A) USP54 co-localizes with ZO-1. HeLa cells transfected with GFP-USP54 were fixed and stained for ZO-1. (B) Co-immunoprecipitation for ZO-1 and ZO-2 with USP54. Indicated GFP-tagged construct was isolated from lysates of HEK293T cells co-overexpressing Flag-USP54 1-778 construct using GFP-Trap beads. Western blot filters were probed for isolated GFP-tagged proteins, and the associated Flag-USP54. (C) U2OS cells transfected with the indicated siRNAs were fixed and stained for ZO-1 and actin. Right: quantification of the amount of cells containing ZO-1 surface staining, quantified with at least 50 cells per experiment. (D) U2OS cells transfected with the indicated siRNAs were fixed and stained for β-Catenin. For all experiments, bar = 10 µm.*

tor that shuttles between endosomes and cell-cell contacts. USP54 is a catalytically competent DUB that resides at tight junction sites, actin filaments and endosomes. Functionally, loss of USP54 is accompanied by a shift in the microtubule structure towards a more peripheral and stable network, as well as loss in membrane localiza-

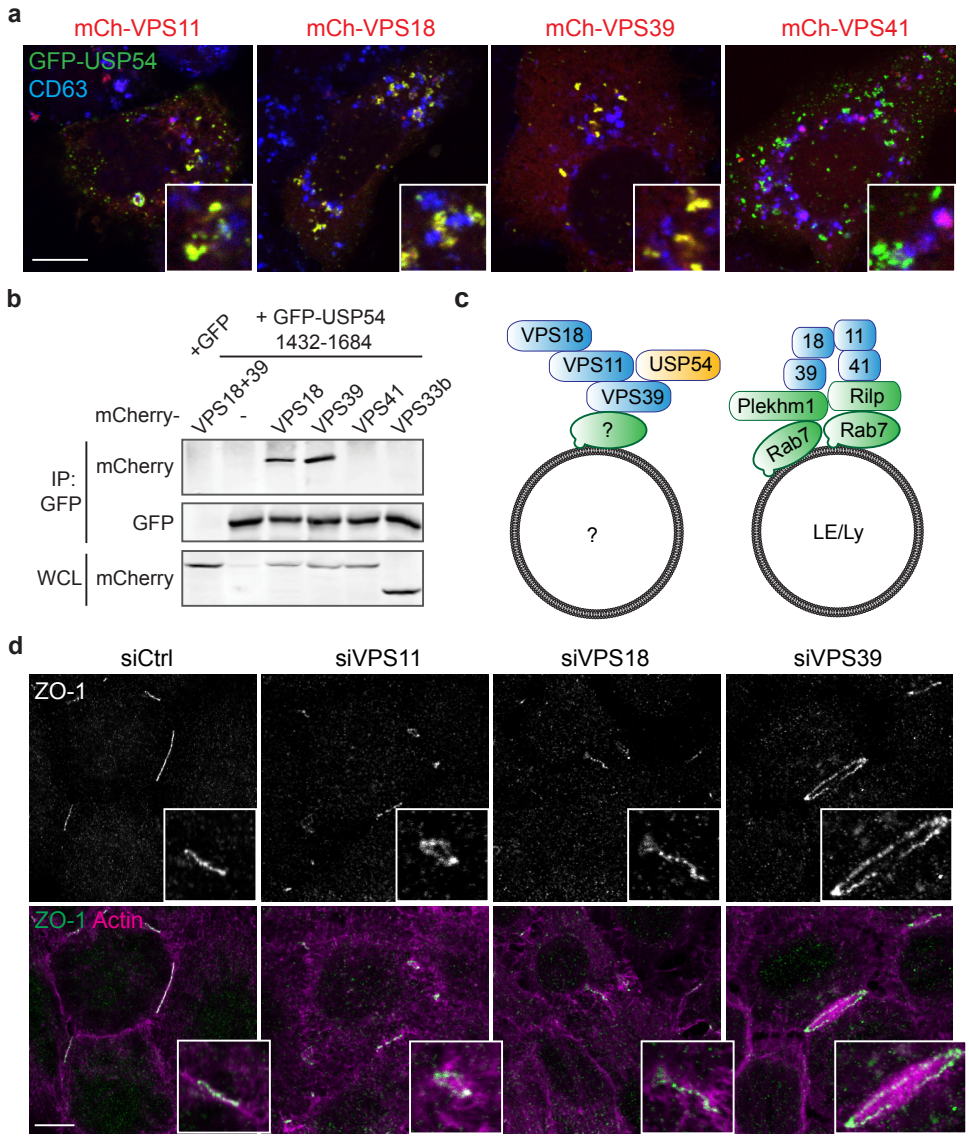


Figure 5: USP54 co-localizes and interacts with several subunits of the HOPS complex. *(A) USP54 co-localizes with select members of the HOPS complex. GFP-USP54 was co-transfected into HeLa cells with the indicated mCherry-VPS constructs, fixed and stained for CD63. (B) Co-immunoprecipitation in Hek293T cells for the indicated constructs. GFP-tagged USP54 1432-1684 was isolated using GFP-Trap beads and isolates were analyzed by western blot. Whole cell lysate (WCL) and IP samples were scanned on the same gel and are shown at the same scanning intensity. (C) Model for endosome recruitment of USP54 by HOPS subunits, versus the canonical HOPS recruitment to Rab7. (D) HeLa cells transfected with the indicated siRNAs were fixed and stained for ZO-1 and actin. For all experiments, bar = 10 µm.*

tion of junction protein ZO-1, suggesting USP54 plays a role in decisions regarding the polarity of cells.
The endocytic pathway contains a multitude of endosome sorting and recycling pathways, which are critical for cellular identity and tightly linked to cellular differentiation state and function. This is especially well described for polarized epithelial cells, where the integrity of the apical and basolateral sides are maintained by polarized endosomal recycling pathways (2). Specific recycling pathways control trafficking of endosomes towards the apical and basolateral sides, as well as towards the cilium and the lateral side where the tight junctions are formed (1). Our data suggest that USP54 localizes to a subset of recycling endosomes and is recycled to the plasma membrane at cell-cell contact sites. In agreement with this, cells grown individually, and thus lack cell-cell contact sites, display strictly endosomal or actin-localized USP54. These endosomes are not classical early or late endosomes, nor Rab2, Rab11 or Rab14 recycling endosomes. The mass spec experiment identified STXBP4/Synip as a possible USP54 interactor, which is an inhibitor of Syntaxin4- and Rab4-mediated recycling (16, 33, 34), suggesting that these endosomes could be Rab4+ recycling endosomes. Indeed, Rab4 and STX4 are implicated in recycling of tight and adherens junction proteins (35-37), and in polarized cells syntaxin-4 regulates recycling towards the basolateral membrane (38). Syntaxin-4 and STXBP4 are best studied for their role in recycling of the glucose uptake receptor GLUT4 in adipocytes (16, 39). Interestingly, a recent study showed that mice lacking USP54 are characterized by a strongly increased adipocyte mass (3), a phenotype that could arise from increased GLUT4-mediated glucose uptake by these cells (40-42). It would thus be interesting study the effect of USP54 on GLUT4 trafficking and STX4-mediated recycling of cargo.
USP54 has a very specific localization to different cellular structures, but what is its function? USP54 has been shown to be instrumental for cellular migration and is expressed at high levels in colon stem cells, but its actual function is unknown (3). Our data show that loss of USP54 resulted in altered microtubule organization, including enhanced formation or stabilization of peripheral microtubules, as well as the loss of tight junction protein ZO-1 from cell-cell contact sites. This altered microtubule cytoskeleton could arise from different sources. Firstly, USP54 could directly influence microtubule stability, for example by interacting with HDAC6, the microtubule deacetylase that was identified from the mass spec. Given its localization at the plasma membrane, it could mediate deacetylation specifically at these sites, which could lead to altered microtubule dynamics. However, given the limited role of microtubule acetylation in its stability (43-45), this is unlikely the primary function of USP54. Secondly, USP54 could recruit stabilizing or destabilizing factors, such as microtubule capping factors or interacting proteins. An interaction was found with microtubule capping enzyme CKAP5 (CH-TOG; identified by only 2 peptides), and some interactors or interacting complexes are linked to microtubule stabilizing or destabilizing factors, including DOCK7 (46), IFT proteins (47), and tight and adherens junctional proteins (24, 25). Alternatively, loss of USP54 perturbs the cellular differentiation and polarization process. Establishment of cell polarity is accompanied by changes in the microtubule network (26, 47), similar to that observed for USP54 knockdown. Furthermore, it instigates the formation of cell-cell contact sites, which

serve as physical barriers to separate the apical- and basolateral sides of polarized cells. Loss of ZO-1 membrane localization, but not adherens junction markers β- and γ-Catenin, after USP54 depletion suggests a defect in the formation of tight junctions which subsequently affects cell polarization. Besides junction proteins, another major group of USP54 interacting proteins identified by mass spec were cilia-associated factors, more specifically the intra-flagellar transport (IFT) proteins. Thus, it appears that USP54 localizes to multiple components of a polarized cell, the lateral side by virtue of the tight and adherens junctions, and the cilium via the IFT-proteins. Since the cells used in this study are incapable of full polarization and hardly contain cilia, it will be interesting to investigate the function of USP54 in polarity establishment in polarized cells such as HUVEC or MDCK. Our hypothesis would be that USP54 acts as a gatekeeper at different cellular sections to control their integrity (eg. Tight junctions and cilia), or regulates recycling of cargo specifically to these compartments.
Tight and adherens junctions are intimately connected to the actin cytoskeleton and actin connects junctions together to instigate tension formation between cells. Furthermore, endosome sorting and fission, as well as fusion with the plasma membrane, requires local actin (de)polymerization. Besides localizing to endosomes and cell-cell contacts, USP54 localizes to actin filaments via a domain at its C-terminus. Three actin-binding myosin motors were found to interact with this USP54 domain, Myosin 1b, 1c and MYH1. Of these, Myosin 1c is already known to interact with ZO-1 (48) and regulates GLUT4 exocytosis (49, 50) and adherens junction turnover (51), indicating a connection between actin and junction recycling, possibly controlled by USP54. Furthermore, USP54 interacts with DOCK7, a GEF for actin-polymerizing GTPases, and could hereby induce actin polymerization. Preliminary analysis indeed showed the appearance of polymerized actin on endosomes harboring full length catalytically inactive USP54, but not wild-type USP54 or the C-terminal tail alone, suggesting that the DUB domain inhibits actin polymerization. Via its slow catalytic activity, USP54 could act as a timer to regulate the turnover or activity of its cognate substrate. However, it is also possible that USP54 is strongly activated by substrate binding, for example by altering its catalytic fold. To gain full mechanistic understanding, it will be imperative to identify USP54 substrates using ubiquitin-proteomics. This would provide the framework for a more complete picture of the interacting proteins and substrates that in assembly determine the function of this fascinating DUB. Collectively, our work has identified an extensive set of interactors for the DUB USP54, arguing for a function in establishment of cell polarity and the recycling of specific endocytic cargo. Further research on this intriguing de-ubiquitinating enzyme will likely unravel novel and exciting biology, describing the regulation of cell polarity by the endocytic system.

Materials and methods

Cell culture and constructs

MelJuSo cells were cultured in IMDM supplemented with 10% FCS, U2OS, HeLa and Hek293T cells in DMEM with 10% FCS. The following constructs were obtained from addgene: GFP-ZO1 (#30313), GFP-ZO2 (#27422). GFP-RILP, mCherry-VPS and GFP-Rab constructs were described previously (29), as well as GFP-USP8 constructs (8). GFP-Rab2a was a kind gift from G. Scita (32). USP54 was ordered as a

custum synthesized gene and together with indicated truncation mutants re-cloned into the GFP-C1 and mRFP-C1 vectors.

Reagents and antibodies

For tubulin and actin staining respectively SIR-Tubulin and SIR-Actin (TeBu Bio) were used. Antibodies used: rabbit anti-GFP (1:1000), mouse anti-CD63 (1:500) and rabbit anti-CD63 (1:100) (all described in (29)), mouse anti-HA (Covance 16B12, 1:1000), rat anti-HA 3F10 (Roche, 1:200), rabbit anti-βCatenin, mouse anti-Tubulin and mouse anti-AcTubulin 6-11-B1 (both 1:100, Sigma), rabbit anti-ZO1, mouse anti-yCatenin A6 (all from Santa Cruz, both 1:100), actin was stained with Phalloidin-Alexa 647 (Life Technologies). Secondary antibodies (goat anti-mouse Alexa 405/488/568/647, goat anti-rabbit Alexa 488/568/647, donkey anti-goat Alexa 488/568, donkey anti-mouse Alexa 488/555/647 and donkey anti-rabbit Alexa 488/647) were purchased from Life Technologies and donkey anti-rat CF568 from Biotium (all 1:200).

Transfections

For expression studies, MelJuSo and HeLa cells were transfected using Effectene (Qiagen) according to the manufacturer's instructions. Cells were transfected one day before fixation or lysis. Hek293T cells were transfected using polyethylenimine (PEI). For siRNA mediated depletion, cells were reverse transfected with DharmaFECT transfection reagent #1 and 50 nM siRNA of the Human siGenome SMARTpool, Dharmacon, according to the manufacturer's protocol. siRNA sequences for USP54: #1 5'-GATAGAAGTTTGTCAGGTA-3' and #2 5'-GGTCACTGATAGAGCGCAA-3'. Briefly, siRNAs and DharmaFECT were mixed and incubated for 20 minutes in a culture well, after which cells were added and left to adhere (reverse transfection). Three days later, cells were fixed and stained or lysed for biochemical analysis.

Co-immunoprecipitation and Western blotting

For co-immunoprecipitation experiments, Hek293T cells were lysed in lysis buffer (0.5% NP-40, 5% glycerol, 150mM NaCl, 50mM Tris-HCl pH8.0, 5mM MgCl2 supplemented with complete EDTA-free Protease Inhibitor Cocktail (Roche)) and cleared by centrifugation. Lysates were incubated with GFP-Trap beads (Chromotek) or protein G-Sepharose 4 FF resin with the indicated antibodies and after incubation washed extensively with lysis buffer before addition of sample buffer (2% SDS, 10% glycerol, 5% β-mercaptoethanol, 60mM Tris-HCl pH 6.8 and 0.01% bromophenol blue).

For whole cell lysate analyses, cells were lysed directly in sample buffer. Proteins were separated by SDS-PAGE and transferred to Western Blot filters. Blocking of the filter and antibody incubations were done in PBS supplemented with 0.1 (v/v)% Tween and 5% (w/v) milk powder. Blots were imaged using the Odyssey Imaging System (LI-COR) or ChemiDoc (Bio-Rad).

Mass spectrometry

Samples from immune-precipitated GFP-tagged proteins were separated by SDS-PAGE and were silver stained (Invitrogen). Selected bands (and the same region in the GFP control lane as negative controls) were cut from the silver stained gel and subjected to reduction with dithiothreitol, alkylation with iodoacetamide and in-gel trypsin digestion using a Proteineer DP digestion robot (Bruker). Tryptic peptides were extracted from the gel, lyophilized, dissolved in 95/3/0.1 v/v/v water/acetonitril/formic acid and subsequently analyzed by online nanoHPLC MS/MS using an 1100

HPLC system (Agilent Technologies), as previously described (Meiring et al., 2002). Peptides were trapped at 10 µl/min on a 15mm column (100µm ID; ReproSil-Pur C18-AQ, 3 µm, Dr. Maisch GmbH) and eluted to a 200 mm column (50µm ID; Repro-Sil-Pur C18-AQ, 3 µm) at 150 nl/min. All columns were packed in house. The column was developed with a 30min gradient from 0 to 50% acetonitrile in 0.1% formic acid. The end of the nanoLC column was drawn to a tip (5-µm ID), from which the eluent was sprayed into a 7tesla LTQ-FT Ultra mass spectrometer (Thermo Electron). The mass spectrometer was operated in data-dependent mode, automatically switching between MS and MS/MS acquisition. Full scan MS spectra were acquired in the FT-ICR with a resolution of 25,000 at a target value of 3,000,000. The two most intense ions were then isolated for accurate mass measurements by a selected ion-monitoring scan in FT-ICR with a resolution of 50,000 at a target accumulation value of 50,000. Selected ions were fragmented in the linear ion trap using collision-induced dissociation at a target value of 10,000. In a post-analysis process, raw data were first converted to peak lists using Bioworks Browser software v3.2 (Thermo Electron), and then submitted to the Swissprot database version 51.6 (257,964 entries), using Mascot v. 2.2.04 (www.matrixscience.com) for protein identification. Mascot searches were with 2 ppm and 0.8 Da deviation for precursor and fragment mass, respectively, and trypsin as enzyme. Protein was finally sorted and compared using Scaffold software version 3.0.1 (www. proteomesoftware.com).

Ub-probe experiments

Assessment of catalytic activity was done using a HA-VME-Ub probe, which is covalently associated with a DUB when tries to cleave the modified thioester bond (8). Briefly, HEK293T cells were transfected with the indicated plasmids and lysed in mild lysis buffer (Tris pH 8.0 (50 mM), sucrose (250 mM), MgCl2 (5 mM), DTT (1 mM)) supplemented with CHAPS (0.5%) and NP40 (0.1%). After sonication, and centrifugation, the supernatant was incubated for 30minutes with 1µM HA-VME-Ub. After addition of sample buffer, cells were analyzed on an SDS-PAGE gel.

cDNA synthesis and qPCR

RNA isolation, cDNA synthesis and quantitative RT-PCR were performed according to the manufacturer's (Roche) instructions. Signal was normalized to GAPDH and calculated using the Pfaffl formula. Primers used for detection were: GAPDH fw: 5'-TGTTGCCATCAATGACCCCTT-3', GAPDH rv: 5'-CTCCACGACGTACTCAG-CG-3', HLA-DRα fw: 5'- -3', HLA-DRα rv: 5'- -3', IRF1 fw: 5'-GCACCAGTGATCT-GTACAAC-3', IRF1 rv: 5'-GCTCCTCCTTACAGCTAAAG-3', CIITA fw: 5'-CCTGCT-GTTCGGGACCTAAA-3, CIITA rv: 5'-GGATCCGCACCAGTTTGG-3', OTUD1 fw: 5'-CCTAGTATTTGGCTCAGTTGG-3', OTUD1 rv: 5'-TTGTCGTACTCTGGGT-TAGG-3'.

Confocal microscopy

Cells were seeded on coverslips, transfected 18 hours later and treated as indicated. 24 hrs later, cells were fixed in 3.7% formaldehyde for 10 min and permeabilized in ice-cold methanol (for LC3 stainings) for 2 minutes or in 0.1% Triton-X100 for 10 minutes. Alternatively, cells were fixed and permeabilized in ice-cold methanol for 2 minutes for Tubulin stainings. Staining was performed with the antibodies mentioned above and DAPI (Invitrogen) to stain DNA. Images were acquired using a Leica TCS SP5 confocal microscope (Leica Microsystems, Wetzlar, Germany) at 63x magnifi-

cation. For live-cell imaging, the microscope was equipped with a climate control chamber and cells were imaged for 3 minutes with ~12 frames per minute. Images were quantified using Image J plugin Jacob for Mander's or Pearson's coefficient calculations and processed using Adobe Photoshop and Illustrator.

Electron microscopy

Cells were fixed in Karnovsky fixative overnight. After washing with 0,1M Cacodylate buffer pH 7.2 the cells were postfixed with 1% Osmiumtetroxide, en-block stained with 0,5% uranylacetate (Ultrastain 1 from Leica, Austria) followed by dehydration series and embedding in Agar100/NMA/DDSA/BDMA (Aurion, the Netherlands). The sections were examined using a Tecnai12G2 microscope (FEI, the Netherlands).

Acknowledgements

We thank the NKI and LUMC microscopy facility, the NKI FACS facility and the NKI Robotics and Screening facility, with special thanks to Ben Morris for all his help with hit validations. Also, members of the Neefjes group for critical discussions, Nico Ong for developing electron micrographs, Lennert Janssen for help with cloning. This work was supported by the Institute of Chemical Immunology (ICI), an NWO Gravitation project funded by the Ministry of Education, Culture and Science of the government of the Netherlands and a European Research Council (ERC) advanced grant awarded to J.N.

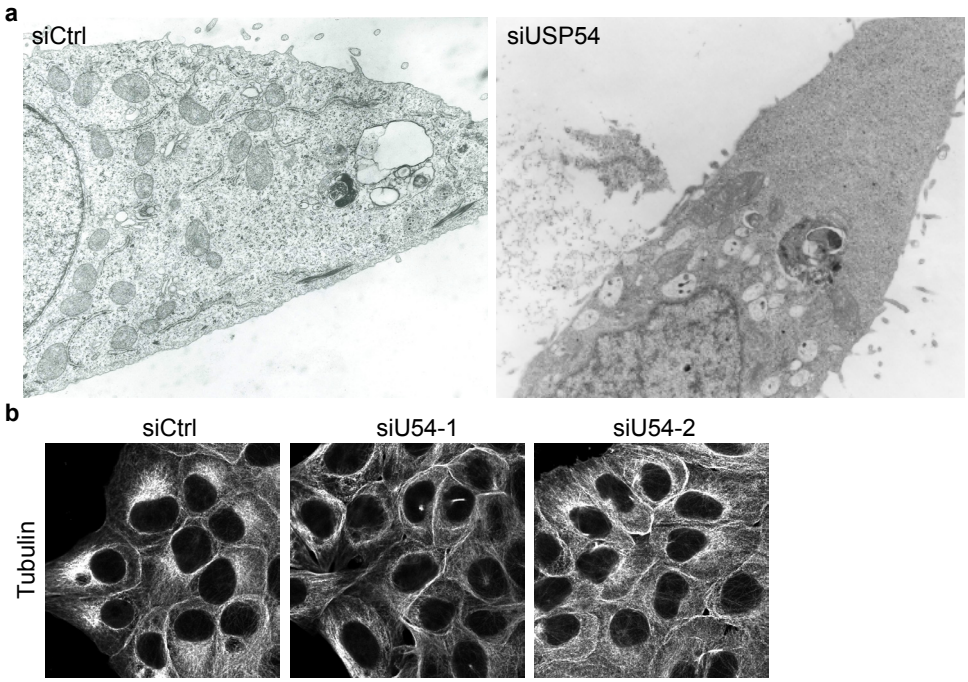
References

1. E. Rodriguez-Boulan, I. G. Macara, Organization and execution of the epithelial polarity programme. Nature reviews. Molecular cell biology 15, 225-242 (2014).
2. D. M. Bryant, K. E. Mostov, From cells to organs: building polarized tissue. Nature reviews. Molecular cell biology 9, 887-901 (2008).
3. J. M. Fraile, D. Campos-Iglesias, F. Rodriguez, Y. Espanol, J. M. Freije, The deubiquitinase USP54 is overexpressed in colorectal cancer stem cells and promotes intestinal tumorigenesis. Oncotarget 7, 74427-74434 (2016).
4. D. J. Rigden, H. Liu, S. D. Hayes, S. Urbe, M. J. Clague, Ab initio protein modelling reveals novel human MIT domains. FEBS letters 583, 872-878 (2009).
5. L. Li, X. J. Yang, Tubulin acetylation: responsible enzymes, biological functions and human diseases. Cellular and molecular life sciences : CMLS 72, 4237-4255 (2015).
6. G. Lukinavicius et al., Fluorogenic probes for live-cell imaging of the cytoskeleton. Nat Meth 11, 731-733 (2014).
7. V. Quesada et al., Cloning and enzymatic analysis of 22 novel human ubiquitin-specific proteases. Biochemical and biophysical research communications 314, 54-62 (2004).
8. A. de Jong et al., Ubiquitin-based probes prepared by total synthesis to profile the activity of deubiquitinating enzymes. Chembiochem : a European journal of chemical biology 13, 2251-2258 (2012).
9. C. Zihni, M. S. Balda, K. Matter, Signalling at tight junctions during epithelial differentiation and microbial pathogenesis. Journal of cell science 127, 3401-3413 (2014).
10. Y. Zhou, J. L. Johnson, R. A. Cerione, J. W. Erickson, Prenylation and membrane localization of Cdc42 are essential for activation by DOCK7. Biochemistry 52, 4354-4363 (2013).
11. G. Gadea, A. Blangy, Dock-family exchange factors in cell migration and disease. European journal of cell biology 93, 466-477 (2014).
12. C. Hubbert et al., HDAC6 is a microtubule-associated deacetylase. Nature 417, 455-458 (2002).
13. Y. Li, X. Zhang, R. D. Polakiewicz, T. P. Yao, M. J. Comb, HDAC6 is required for epidermal growth factor-induced beta-catenin nuclear localization. The Journal of biological chemistry 283, 12686-12690 (2008).
14. J. Yu, M. Ma, Z. Ma, J. Fu, HDAC6 inhibition prevents TNF-alpha-induced caspase 3 activation

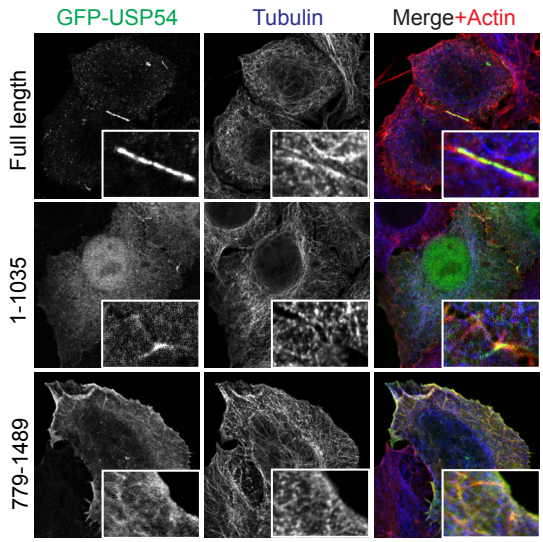
in lung endothelial cell and maintains cell-cell junctions. Oncotarget 7, 54714-54722 (2016).
15. F. Steinberg et al., A global analysis of SNX27-retromer assembly and cargo specificity reveals a function in glucose and metal ion transport. Nature cell biology 15, 461-471 (2013).
16. J. Min et al., Synip: a novel insulin-regulated syntaxin 4-binding protein mediating GLUT4 translocation in adipocytes. Molecular cell 3, 751-760 (1999).
17. Y. Aghazadeh, V. Papadopoulos, The role of the 14-3-3 protein family in health, disease, and drug development. Drug discovery today 21, 278-287 (2016).
18. C. Johnson et al., Bioinformatic and experimental survey of 14-3-3-binding sites. The Biochemical journal 427, 69-78 (2010).
19. H. Meyer, M. Bug, S. Bremer, Emerging functions of the VCP/p97 AAA-ATPase in the ubiquitin system. Nature cell biology 14, 117-123 (2012).
20. D. Ritz et al., Endolysosomal sorting of ubiquitylated caveolin-1 is regulated by VCP and UBXD1 and impaired by VCP disease mutations. Nature cell biology 13, 1116-1123 (2011).
21. N. Iwaya et al., MIT domain of Vps4 is a Ca2+-dependent phosphoinositide-binding domain. Journal of biochemistry 153, 473-481 (2013).
22. F. Martin-Belmonte, M. Perez-Moreno, Epithelial cell polarity, stem cells and cancer. Nature reviews. Cancer 12, 23-38 (2011).
23. C. Zihni, C. Mills, K. Matter, M. S. Balda, Tight junctions: from simple barriers to multifunctional molecular gates. Nature reviews. Molecular cell biology 17, 564-580 (2016).
24. L. A. Ligon, S. Karki, M. Tokito, E. L. Holzbaur, Dynein binds to beta-catenin and may tether microtubules at adherens junctions. Nature cell biology 3, 913-917 (2001).
25. M. N. Shahbazi et al., CLASP2 interacts with p120-catenin and governs microtubule dynamics at adherens junctions. The Journal of cell biology 203, 1043-1061 (2013).
26. D. A. Goldspink et al., The microtubule end-binding protein EB2 is a central regulator of microtubule reorganisation in apico-basal epithelial differentiation. Journal of cell science 126, 4000-4014 (2013).
27. D. Cohen, P. J. Brennwald, E. Rodriguez-Boulan, A. Musch, Mammalian PAR-1 determines epithelial lumen polarity by organizing the microtubule cytoskeleton. The Journal of cell biology 164, 717-727 (2004).
28. A. Spang, Membrane Tethering Complexes in the Endosomal System. Frontiers in cell and developmental biology 4, 35 (2016).
29. R. van der Kant et al., Late endosomal transport and tethering are coupled processes controlled by RILP and the cholesterol sensor ORP1L. Journal of cell science 126, 3462-3474 (2013).
30. D. Khatter et al., The small GTPase Arl8b regulates assembly of the mammalian HOPS complex on lysosomes. Journal of cell science 128, 1746-1761 (2015).
31. R. van der Kant et al., Characterization of the mammalian CORVET and HOPS complexes and their modular restructuring for endosome specificity. The Journal of biological chemistry 290, 30280-30290 (2015).
32. H. Kajiho et al., RAB2A controls MT1-MMP endocytic and E-cadherin polarized Golgi trafficking to promote invasive breast cancer programs. EMBO reports 17, 1061-1080 (2016).
33. L. Li, W. Omata, I. Kojima, H. Shibata, Direct interaction of Rab4 with syntaxin 4. The Journal of biological chemistry 276, 5265-5273 (2001).
34. L. J. Foster, A. Klip, Mechanism and regulation of GLUT-4 vesicle fusion in muscle and fat cells. American journal of physiology. Cell physiology 279, C877-890 (2000).
35. A. I. Ivanov, A. Nusrat, C. A. Parkos, Endocytosis of epithelial apical junctional proteins by a clathrin-mediated pathway into a unique storage compartment. Molecular biology of the cell 15, 176-188 (2004).
36. M. Matsuda, A. Kubo, M. Furuse, S. Tsukita, A peculiar internalization of claudins, tight junction-specific adhesion molecules, during the intercellular movement of epithelial cells. Journal of cell science 117, 1247-1257 (2004).
37. J. Torres, H. M. Funk, M. M. Zegers, M. B. ter Beest, The syntaxin 4 N terminus regulates its basolateral targeting by munc18c-dependent and -independent mechanisms. The Journal of biological chemistry 286, 10834-10846 (2011).
38. E. Reales, N. Sharma, S. H. Low, H. Folsch, T. Weimbs, Basolateral sorting of syntaxin 4 is dependent on its N-terminal domain and the AP1B clathrin adaptor, and required for the epithelial cell polarity. PloS one 6, e21181 (2011).
39. H. Yu, S. S. Rathore, J. Shen, Synip arrests soluble N-ethylmaleimide-sensitive factor at-

tachment protein receptor (SNARE)-dependent membrane fusion as a selective target membrane SNARE-binding inhibitor. The Journal of biological chemistry 288, 18885-18893 (2013).
40. P. R. Shepherd et al., Adipose cell hyperplasia and enhanced glucose disposal in transgenic mice overexpressing GLUT4 selectively in adipose tissue. The Journal of biological chemistry 268, 22243-22246 (1993).
41. M. A. Herman et al., A novel ChREBP isoform in adipose tissue regulates systemic glucose metabolism. Nature 484, 333-338 (2012).
42. J. M. Rutkowski, J. H. Stern, P. E. Scherer, The cell biology of fat expansion. The Journal of cell biology 208, 501-512 (2015).
43. S. C. Howes, G. M. Alushin, T. Shida, M. V. Nachury, E. Nogales, Effects of tubulin acetylation and tubulin acetyltransferase binding on microtubule structure. Molecular biology of the cell 25, 257-266 (2014).
44. J. Asthana, S. Kapoor, R. Mohan, D. Panda, Inhibition of HDAC6 deacetylase activity increases its binding with microtubules and suppresses microtubule dynamic instability in MCF-7 cells. The Journal of biological chemistry 288, 22516-22526 (2013).
45. K. Sadoul, S. Khochbin, The growing landscape of tubulin acetylation: lysine 40 and many more. The Biochemical journal 473, 1859-1868 (2016).
46. M. Watabe-Uchida, K. A. John, J. A. Janas, S. E. Newey, L. Van Aelst, The Rac activator DOCK7 regulates neuronal polarity through local phosphorylation of stathmin/Op18. Neuron 51, 727-739 (2006).
47. A. A. Bizet et al., Mutations in TRAF3IP1/IFT54 reveal a new role for IFT proteins in microtubule stabilization. Nature communications 6, 8666 (2015).
48. S. E. Goldblum et al., The active Zot domain (aa 288-293) increases ZO-1 and myosin 1C serine/threonine phosphorylation, alters interaction between ZO-1 and its binding partners, and induces tight junction disassembly through proteinase activated receptor 2 activation. FASEB journal : official publication of the Federation of American Societies for Experimental Biology 25, 144-158 (2011).
49. M. F. Yip et al., CaMKII-mediated phosphorylation of the myosin motor Myo1c is required for insulin-stimulated GLUT4 translocation in adipocytes. Cell metabolism 8, 384-398 (2008).
50. A. Bose et al., Unconventional myosin Myo1c promotes membrane fusion in a regulated exocytic pathway. Molecular and cellular biology 24, 5447-5458 (2004).
51. H. Tokuo, L. M. Coluccio, Myosin-1c regulates the dynamic stability of E-cadherin-based cell-cell contacts in polarized Madin-Darby canine kidney cells. Molecular biology of the cell 24, 2820-2833 (2013).

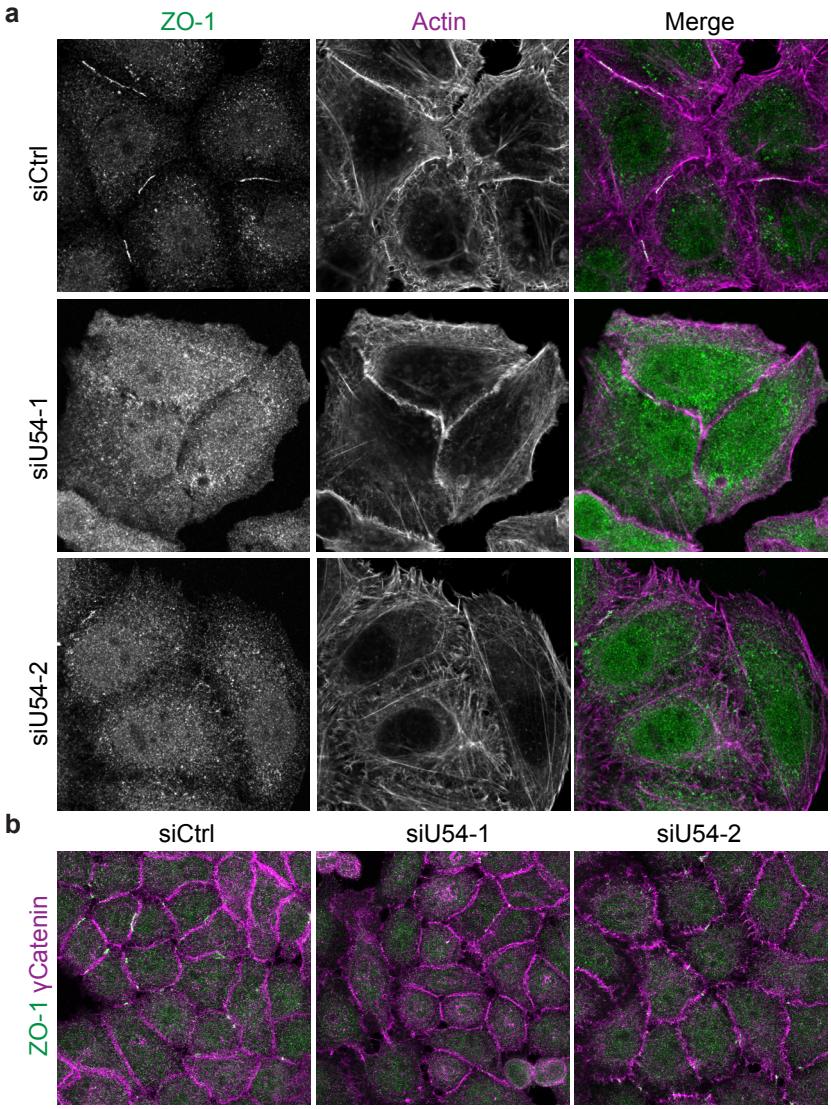
Supplementary Figures



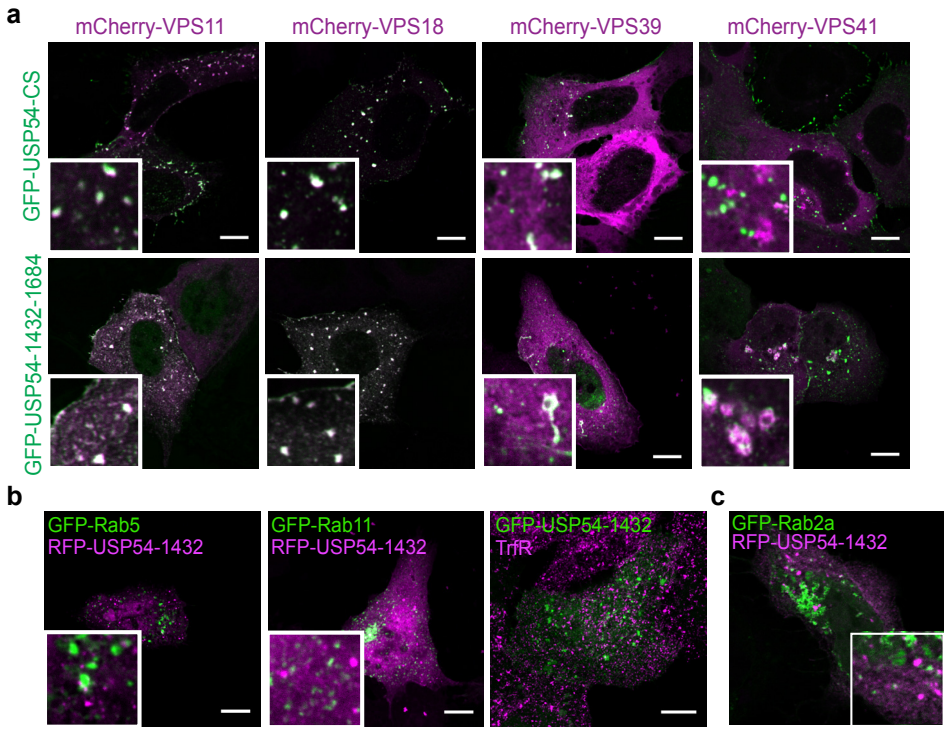
Supplementary Figure S1: USP54 controls microtubule dynamics. *(A) Electron micrograph of Mel-JuSo cells transfected with the indicated siRNAs. Note the absence of peripheral endosomal structures in the siUSP54 condition. (B) siRNA transfected U2OS cells were fixed and stained for the indicated markers.*



Supplementary Figure S2: localization determinants for USP54. *HeLa cells were transfected with the indicated GFP-tagged USP54 constructs, fixed and stained for Actin and Tubulin.*



Supplementary Figure S3: USP54 mediates ZO-1 membrane localization. *(A) siRNA transfected HeLa cells were stained for the indicated markers. (B) siRNA transfected HeLa cells were stained for the indicated markers. Image represents maximum Z-projection of multiple images.*



Supplementary Figure S4: USP54 co-localizes with members of the HOPS complex. *(A) HeLa cells transfected with the indicated constructs were fixed and imaged. (B) HeLa cells transfected with the indicated constructs were fixed, stained and imaged. (C) HeLa cells transfected with GFP-Rab2a, RFP-USP54 1432-1684 and Flag-VPS39 were fixed, stained and imaged. For all experiments, bar = 10 µm.*

Chapter 6:
Exploring genome-wide datasets of MHC class II antigen presentation

Ruud H Wijdeven[1,2], Jeroen M Bakker[1,2], Petra Paul[1], Jacques Neefjes[1]

[1] Division of Cell Biology, the Netherlands Cancer Institute, Plesmanlaan 121, 1066CX Amsterdam, the Netherlands
[2] These authors contributed equally to this work

Molecular Immunology 55 (2013), pp. 172-174

Abstract
MHC class II molecules (MHCII) are critical for presenting antigens to CD4+ T-cells. They control ignition of CD4+ T cells and are as such involved in most auto-immune diseases. To define proteins and pathways controlling MHCII antigen presentation and expression, we performed a genome-wide flow cytometry based RNAi screen. Hits were subsequently classified by two screens that monitored the intracellular distribution and transcription of MHCII. This multi-dimensional approach allowed sub-classification of hits into functional groups as a first step to defining new pathways controlling MHCII antigen presentation. The datasets from this screen are used as a template for several follow-up studies. This review focuses on how data from genome-wide screens can be used for target-lead identification, data mining, systems biology and systematic cell biology.

Introduction
Antigen presenting cells (APCs) activate CD4+ helper T-cells by presenting antigens on their Major Histocompatibility Complex class II molecules (MHCII). Many auto-immune diseases are caused by improper antigen presentation or undesired stimulation of autoreactive CD4+ T-cells and MHCII is the strongest genetic link to most auto-immune diseases (1). Expression of MHCII is limited to professional APCs like dendritic cells, macrophages and B-cells. Other cell types only express MHCII after cytokine stimulation, hereby contributing to local immune responses.
Transcription of MHCII is controlled by a transcriptional 'master regulator' called CIITA (2). After translation and synthesis in the ER, MHCII associates with the invariant chain (Ii) for transport to late endosomes, called MHCII compartments (MIIC). Here, the chaperone protein HLA-DM enhances the actual peptide loading. Resident proteases degrade the MHCII-associated invariant chain, leaving only a small Ii fragment termed CLIP in the peptide binding groove of MHC II (3). Endocytosed antigens are also digested and trimmed by proteases in the MIIC and the resulting fragments compete with CLIP to fill the peptide binding groove. Ultimately MHCII is transported to the plasma membrane for antigen presentation. This transport involves motor proteins and is under control of pathways that are poorly understood (4).
Many direct players in MHCII antigen presentation are defined but how these fit into pathways is unclear. For example it is known that CIITA is expressed in a tissue specific manner, but it remains unclear how the transcription factors regulating this expression are activated. This addresses a general biological question: how tissue selective expression is imposed. In principle, genome-wide data sets should contain the information on these (and other) issues, but it is unclear how to extract them. We discuss findings of how MHC class II expression and transport are regulated and ways to systematically use large datasets for solving such biological questions.

Current status
To identify genes controlling MHCII expression, a genome wide siRNA screen was performed. After knockdown of every annotated gene, a two color high throughput flow cytometry analysis was performed to examine effects on MHCII expression. Two monoclonal antibodies were used to visualize correctly loaded MHCII on the

plasma membrane (L243) and MHCII bound to the CLIP fragment (CerCLIP), which represents inefficient loading of MHCII with correct antigenic peptides. After multiple rounds of screening, 276 genes were identified that affected MHCII expression (L243) and/or peptide loading (CerCLIP). The set of genes included most already known factors in the MHCII antigen presenting pathway, such as CIITA, DM and the HLA-DRA and -DRB chains. By using two antibodies probing different conformations of one protein, genes could be divided as being involved in controlling expression or peptide loading of MHCII molecules using flow cytometry.
To extract genes controlling MHCII expression at the transcriptional level, all hits were analyzed for their effect on MHCII transcription. mRNA levels of MHCII, the invariant chain and CIITA were determined by qPCR to select the genes involved in controlling MHCII and/or CIITA transcription. Nine candidates were identified including CIITA. From these data,we were able to define a transcriptional network that controls MHCII expression.
Still, the majority of the hits were not functionally assigned and possibly regulated intracellular trafficking of MHCII. To study this intracellular localization of GFP-tagged MHCII was visualized using confocal microscopy after knockdown of the hits. Using Cellprofiler software the phenotypes were clustered into different groups. These effects included vesicle enlargement, clustering or dispersion of vesicles and a redistribution of MHCII to the cell surface. This information was combined with the flow cytometry and qPCR data and used for a data-based integrative bioinformatic approach to predict functional relationships of the candidates and build pathways and networks of genes controlling MHCII functioning.
Next we tried to use these data to extract new biology. Several hits from the screen gave a redistribution of MHCII to the cell surface after knockdown, resembling a mature dendritic cell phenotype where the intracellular pool of MHCII is exported to the cell surface. The biology of this massive but regulated export is poorly understood. By analyzing microarray expression data of immature and mature dendritic cells it was found that 11 of the genes that gave redistribution of MHCII to the cell surface were actually downregulated upon maturation. These genes were silenced in dendritic cells using shRNAs and MHCII expression and distribution were analyzed by flow cytometry and confocal microscopy. Silencing of six hits generated immature dendritic cells with a mature phenotype in terms of MHCII expression and distribution. Without the use of unbiased screening these genes would not have been linked to MHCII transport, illustrating the power of RNAi screening (5).

Future prospects

RNAi screening data can be used as a data mining tool. The advantage of siRNA screening is that every gene is a datapoint and can be treated as such. This makes it possible to compare different screens and to integrate different types of large scale analyses like expression data and mass-spec studies. This is very important as siRNA screens miss hits due to ineffective silencing or redundancy among genes. Yet, they represent a major step forward by adding a functional component that allows for identification of new proteins and pathways. Furthermore siRNA datasets can be used for drug discovery and the identification of new inhibitors for known genes. Here we discuss the use of our dataset for these purposes and speculate how screens in

general can be used for new data-based Systems Biology.

Data-based Systems Biology

siRNA-based screens provide a powerful tool for studying cell biological processes. Potential interacting proteins can be selected based on overlapping phenotypes, which represents shared pathways. This is a first step in the definition of a scaffold of pathways, which then has to be experimentally tested.

We exploited this route to identify proteins involved in controlling transport of MHCII containing vesicles to the plasma membrane in dendritic cells following maturation signals. Amongst the selected genes that control MHCII transport in immature dendritic cells is a small GTPase called Arl14 or Arf7. Arl14/ARF7 is a newly identified protein and is located on MIIC. Silencing Arl14/ARF7 in immature dendritic cells redistributes MHCII to the plasma membrane, a phenotype that is typically observed in mature dendritic cells. These observations were used as a starting point for building a pathway explaining the control of MHCII transport in dendritic cells.

Again, various sets of information were used to predict interacting proteins with Arl14/ARF7. A GEF, which activates Arl14/ARF7, was identified as these have so-called SEC7 domains. We screened our siRNA data sets for proteins with this domain and the same phenotype as Arl14/ARF7 silencing (ie upregulation of MHCII) and identified two candidates. In vitro testing revealed that only one, PSD4, activated Arl14/ARF7. The effector of Arl14/ARF7 was identified by performing a yeast two-hybrid. This provided one unknown protein, now called ARF7EP, which was then used as a bait to identify interaction proteins by mass spec. This yielded a myosin motor called Myo1e which is involved in the anchoring of vesicles to the actin cytoskeleton. Eliminating this pathway then allows the MIIC (and thus MHCII) to leave the intracellular location for surface deposition. This exemplifies how large data sets can be used to build new networks involved in biologically relevant processes, like MHCII transport in dendritic cells. This can be further expanded as the GAP and the proteins controlling the activity of the GEF are not identified. They may hide in the siRNA generated data sets and have to be found.

The siRNA screen yielded a wide variety of proteins; kinases, ring- and zinc finger proteins, proteins involved in the ubiquitination pathway, controllers of transcription etc. However, almost half of the hits represented new and unknown proteins. The latter are possibly the most interesting ones and yet the most difficult one to place in functional networks. The approach discussed above represents an unbiased selection allowing placing unknown proteins in networks. Using data-based Systems Biology approaches as described here enables the construction of new pathways based around single hits thus constructing new cell biology.

Data mining to feed Systems Biology

Another relevant use for screens involves data mining. Many labs check new screening datasets for the phenotype of their proteins of interest. This is helpful to place proteins in pathways and emphasizes the importance of a uniform publication format. It calls for an online database for uploading screening data (including the primary data) to allow easy and open access. In addition, it will be very important to arrive at proper statistical methods to assess the quality of screens (such as z-factors). Such open

networks would allow broad use of data sets and accelerate cell biology and can be set up like the GEO database at the NCBI website for microarray information.
A common data format would also allow data-based Systems Biology at a higher level. The results from different screens can be compared and used to construct pathways by combining the information. By for example comparing data sets where effects on cell surface receptors were measured, genes involved in different aspects of endocytosis can be clustered and used to extract pathways. By including negative data (a gene that does not give a phenotype) branches in pathways may be determined. For example when protein A and B belong to the same pathway in one screen while only protein A shows up in another screen, A and B should have different functions and pathways. By using a scoring system and comparing multiple screens, this may result in a more functional approach to elucidate branching of pathways in the cell. Obviously, such approaches will only allow prediction of pathways and these have to be experimentally tested.
Systems Biology usually integrates literature and microarray datasets. The advantage of including siRNA data is its functional and unbiased approach. With the publication of more siRNA datasets in the public domain, Systems Biology will convert into a data-based Systems Biology which improves the quality of predicted pathways.

Applying data sets to define new drug targets and new drug off-target effects

New proteins regulating MHCII expression provide new drug targets to manipulate MHCII antigen presentation. This is of interest for vaccines and treatment of auto-immune diseases that are related to MHCII. Usually enzymes and receptors are considered druggable targets. Some of our hits have defined inhibitors such as the kinase DYRK1a. DYRK1a is a kinase important in Down's syndrome and has never been linked to antigen presentation. DYRK1a depletion with siRNAs results in lower MHCII surface expression and this is expected for chemical inhibition of DYRK1a as well. By using genome wide screening data as a source for new targets, we are selecting compounds to manipulate MHCII antigen presentation.
Besides predicting inhibitors on the basis of the hit list, the genome wide screen can also be used as a template to identify new targets for drugs already used in the clinic. The effect of drugs can be placed in the siRNA data sets after phenotypic comparison of drug and siRNA in a multidimensional manner (combining flow cytometry, qPCR and microscopy). Drugs affecting MHCII expression were identified by screening a library containing 1500 FDA-approved drugs in a setting similar as the RNAi screen. Using this approach, several clinically used compounds were identified that affect MHCII expression and that have never been linked to manipulation of antigen presentation. By comparing the phenotypes of the drugs to these of the siRNAs, only a limited number of siRNA hits give a corresponding phenotype. These are the potential targets of the drugs. With this approach, we identified an inhibitor of CIITA. By using target prediction programs, target-lead combinations were made and current work focuses on validating these predictions to identify a new target for this drug.
These two approaches illustrate how genetic screening data can be used to improve drug discovery without prior definition of the target, only based on the biological

effect.

Conclusions

Genome-wide RNAi screening data can provide important insights into cell biological pathways and processes and identify genes that would otherwise not have been considered. A functional dataset can be used for many other purposes and should be accessible to the scientific community. This requires a common format and platform at which datasets can be uploaded and analyzed. Only then the data will be used at its maximum potential and serve system biologists, drug finders, immunologists and cell biologists to accelerate their research.

References

1. D. D. Chaplin, M. E. Kemp, The major histocompatibility complex and autoimmunity. Year Immunol 3, 179-198 (1988).
2. C. H. Chang, S. Guerder, S. C. Hong, W. van Ewijk, R. A. Flavell, Mice lacking the MHC class II transactivator (CIITA) show tissue-specific impairment of MHC class II expression. Immunity 4, 167-178 (1996).
3. J. M. Riberdy, J. R. Newcomb, M. J. Surman, J. A. Barbosa, P. Cresswell, HLA-DR molecules from an antigen-processing mutant cell line are associated with invariant chain peptides. Nature 360, 474-477 (1992).
4. J. Neefjes, M. L. Jongsma, P. Paul, O. Bakke, Towards a systems understanding of MHC class I and MHC class II antigen presentation. Nat Rev Immunol 11, 823-836 (2011).
5. P. Paul et al., A Genome-wide multidimensional RNAi screen reveals pathways controlling MHC class II antigen presentation. Cell 145, 268-283 (2011).

Chapter 7: Chemical and genetic control of IFNγ-induced MHCII expression

Ruud H. Wijdeven[1], Marvin M. van Luijn[2], Peter J. van den Elsen[3], Rogier Q. Hintzen[2], Jacques Neefjes[1]

[1] Department of Chemical Immunology, LUMC, Leiden, the Netherlands
[2] Department of Immunology and MS Center ErasMS, Erasmus MC University Medical Center, Rotterdam, The Netherlands.
[3] Department of Immunohematology and Blood Transfusion, LUMC, Leiden, the Netherlands.

Under review

Abstract

The cytokine Interferon-γ (IFNγ) can induce expression of MHC class II (MHCII) on non-hematopoietic cells, leading to antigen presentation to CD4+ T-cells and immune activation, which has been linked to anti-tumour immunity and graft-versus-host disease. The extent of MHCII upregulation by IFNγ is highly variable between cell types and under extensive control by epigenetic regulators and signalling pathways. Here, we identified novel determinants in the control of MHCII expression. Loss of the oxidative stress sensor Keap1 and autophagy adaptor p62/SQSTM1 impaired IFNγ-mediated MHCII expression, by decreasing the levels of histone acetylation. A similar phenotype was observed for arsenite, an oxidative stressor, and these phenotypes could be reversed by inhibition or depletion of histone deacytelase 1/2, suggesting that oxidative stress conditions are translated into epigenetic alterations that affect MHCII expression. This is further illustrated by dimethylfumarate, an antioxidant used for the treatment of several autoimmune diseases, which impairs the IFNγ response. Using an integrated chemical genetics approach, we identified novel pathways and associated drugs controlling IFNγ-mediated MHCII expression, which provides a molecular basis for the treatment of MHCII associated auto-immune diseases.

Introduction

Antigen presentation by Major Histocompatibility Complex class II (MHCII) molecules is critical for the initiation of an adaptive CD4+ helper T-cell response (1). Many MHCII alleles are correlated to specific autoimmune disorders, for example HLA-DRB1*1501 to multiple sclerosis (2, 3), and it is anticipated that MHCII antigen presentation sensitizes to particular autoimmune diseases. Expression of MHCII is limited to professional antigen presenting immune cells such as dendritic cells and B-cells. However, normal tissue cells can also express MHCII, usually under inflammatory condition following release of various cytokines, predominantly interferon gamma (IFNγ), thus resulting in antigen presentation by non-hematopoietic cells (4). The relevance of non-immune cell mediated antigen presentation is highlighted by its important role in the onset of graft-versus-host disease (GVHD)(5, 6), transplant rejection (7, 8), some autoimmune diseases (9), as well as its potential for T-cell priming on tumour cells (10, 11).

Transcription of MHCII, as well as the associated invariant chain (Ii), which aides MHCII trafficking and occupies the peptide binding groove before antigen loading, is governed by transcriptional master regulator CIITA (12, 13). CIITA does not bind the MHCII promoter directly, but rather assembles a complex of transcription factors at the MHCII promoter, which includes RFX5, CREB and NF-Y (14). Furthermore, CIITA alters the chromatin environment by recruiting chromatin remodelling factors such as BRG-1, histone acetyltransferases (HATs) and deacetylates (HDACs)(15-17), as well as via its intrinsic HAT activity (18). In its turn, CIITA is transcribed from different promoters in different cell types, with its IFNγ-induced isoform being initiated by transcription factor IRF-1 (19).

Besides upregulating MHC class II antigen presentation, IFNγ induces a pro-inflammatory gene signature in both immune and non-immune cells and is important for clearance of viral and bacterial infections (20). Furthermore, recent findings have

demonstrated that cancer cells promote resistance to immunotherapy by altering their IFNγ signalling pathway (21, 22), illustrating the importance of an intact IFNγ response for immune recognition. As for MHCII, sustained IFNγ signalling can lead to uncontrolled activation of the immune system, causing MHCII-dependent transplant rejection (23) as well as autoimmunity, albeit its importance in the disease pathology for different autoimmune diseases is ambiguous (24-27). Molecularly, engagement of the IFNγ receptor by IFNγ leads to the activation of JAK kinases, which phosphorylate and stimulate nuclear translocation of transcription factor STAT1 (28). STAT1 subsequently induces transcription of IRF-1, which stimulates expression of many pro-inflammatory genes, along with CIITA (29). While the central pathway leading to transcription of IRF-1, CIITA and MHCII is conserved in most cells, many IFNγ-induced genes are expressed cell-type specifically upon activation (15, 30-32), suggesting major regulation by epigenetic modifiers and additional signalling pathways to steer the response. This is in agreement with the notion that HDAC inhibitors increase the expression of IFNγ-target genes in different tumours, hereby sensitizing tumour cells to immune checkpoint inhibition (33, 34). Understanding the factors regulating the IFNγ-response could thus provide novel means of interfering with this important signalling pathway.

Here, we identified two novel regulators of IFNγ-mediated expression of MHCII, the oxidative stress sensor Keap1 and autophagy adaptor p62. Both proteins positively control histone acetylation, and their loss can be compensated by inhibition of HDACs. Furthermore, immunotoxic agent arsenite, as well as anti-autoimmunity drug dimethylfumarate, impinge on the MHCII pathway, providing an additional mechanism of action for these compounds.

Results

Keap1 regulates IFNγ-induced expression of MHCII

Previously, we identified OTUD1 as a novel regulator of MHCII transcription (Chapter 4). To gain insight into the molecular basis for this, a secondary siRNA screen was performed for potential interactors of OTUD1, as previously identified in a mass-spec interaction screen (35). The siRNA screen identified Keap1 as a novel regulator of IFNγ-induced MHCII expression (Fig. 1a and 1b), however, no effect was observed on constitutive MHCII expression in MelJuSo cells (data not shown). Keap1 is involved in many processes and best studied for its inhibitory role in the oxidative stress response by facilitating Cullin3 dependent ubiquitination and degradation of Nrf2, a transcription factor for antioxidant genes (36). In addition, Keap1 regulates NFκB signalling (37, 38), autophagy (39), DNA repair (40), drug resistance (41), and cell migration (42), via binding to a variety of substrates. However, a role for Keap1 in IFNγ-induced MHCII expression has not been reported.

We continued by testing how Keap1 controls MHCII expression. qPCR analyses of different genes in HeLa cells stimulated with IFNγ for 24 hours indicated that Keap1 silencing inhibited the expression of HLA-DRα, as well as Ii, but not CIITA (Fig. 1c), suggesting a different mechanism of regulation from OTUD1. To assess whether Keap1 controls the activity of CIITA or the associated transcription factors, a luciferase construct under control of the MHCII promoter was utilized. In contrast to the control knockdown of STAT1, depletion of Keap1 had no effect on MHCII pro-

moter activity (Fig. 1d), indicating Keap1 does not control any of the factors involved in promoter activation. Furthermore, Keap1 did not affect the stability of HLA-DRα transcripts, since a pulse chase for mRNA degradation using Actinomycin D did not yield any difference in degradation rates (Fig. 1e). Thus, Keap1 is a novel regulator of MHCII transcription, independently of promoter activation or mRNA stability.

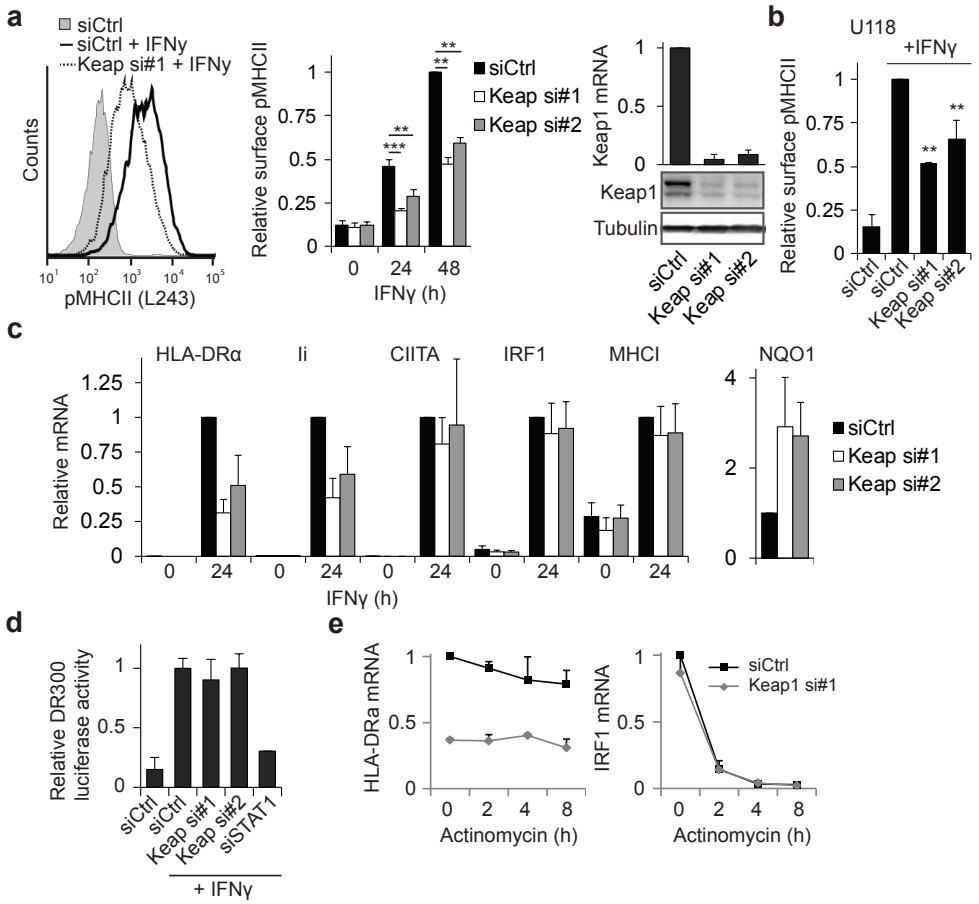


Figure 1: Keap1 positively regulates IFNγ mediated MHCII expression. *(A) HeLa cells were transfected with siCtrl or siRNAs targeting Keap1 and stained 72h later for peptide loaded MHCII (L243-cy5), stimulated or not with 100ng/ml IFNγ for the indicated time. Representative histogram and quantification are shown. Right: Keap1 silencing was determined by Western blot analysis (bottom) and qRT-PCR (top, normalized to GAPDH). (B) U118 cells were analysed for pMHCII levels according to the same protocol as in (A). (C) HeLa cells transfected with siCtrl or siKeap1 were stimulated or not with IFNγ for 24h and mRNA expression of the indicated genes was analysed using qRT-PCR. (D) MHCII promoter activity was analysed using a Luciferase under control of the MHCII promoter (DR300) in cells transfected with the indicated siRNAs and treated with IFNγ when indicated. siSTAT1 was used as a positive control and signals were normalized to a Renilla control plasmid. (E) Cells transfected with siCtrl or siKeap1 were treated with IFNγ for 24h and lysed, or Actinomycin D (2uM) was added and cells were lysed 2, 4 or 8h later. mRNA expression level of HLA-DRα and IRF1 was analysed using qRT-PCR, IRF1 was used as a control for effectivity of Actinomycin D. Experiments shown represent mean +SD of at least three independent experiments (except D, n=2). Statistical significance was calculated as compared to control cells (* p < 0.05, ** p < 0.01, *** p < 0.001).*

Keap1 regulates MHCII expression epigenetically via HDAC1/2

The discrepancy between the effect of Keap1 on endogenous MHCII transcription versus exogenous MHCII promoter activity proposes a role for epigenetic regulation controlled by Keap1 to influence IFNγ-induced MHCII transcription. MHCII expression is controlled by various epigenetic markers, including H3K27me3, DNA methylation, and histone deacetylation (17, 43, 44). Treatment of cells with inhibitors of EZH2, which prevent H3K27me3 modifications(45, 46), as well as HDAC inhibitors, indeed induced MHCII expression in HeLa cells (Fig. 2a), whereas inhibition of DNA methylation using Decitabine had no effect (data not shown). Whereas the relative effect of Keap1 depletion remained intact upon treatment with EZH2-inhibitors, all three HDAC inhibitors corrected the inhibition of IFNγ-induced MHCII expression following Keap1 silencing, implying that Keap1 controls MHCII via histone acetylation/deacetylation.

SAHA is a pan-HDAC inhibitor, MGCD0103 specifically targets HDAC1/2 and MS-

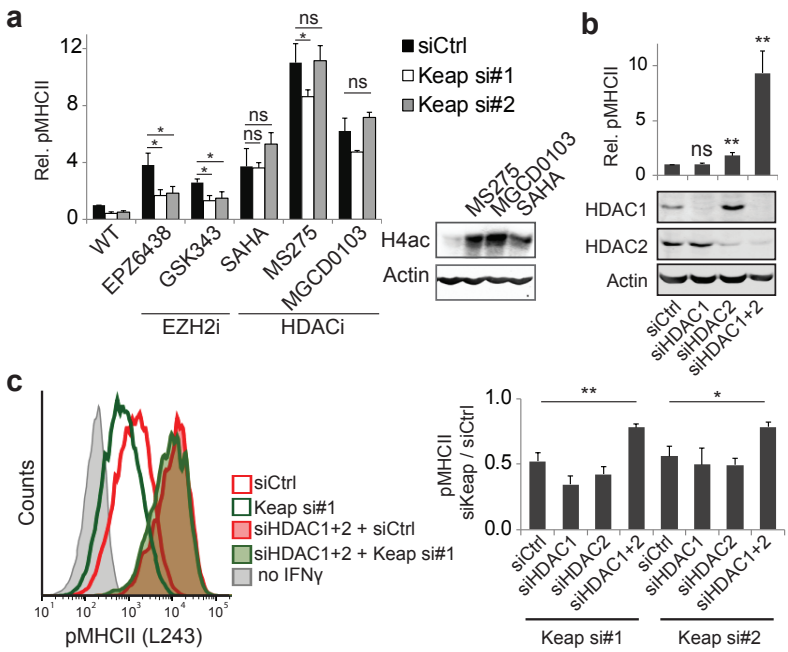


Figure 2: Keap1 regulates MHCII expression via HDACs. *(A) HeLa cells transfected with the indicated siRNAs were treated for 48h with IFNγ and inhibitors and expression of pMHCII was analysed by flow cytometry. Maximum non-toxic doses of the inhibitors were used: EPZ6438 (2μM), GSK343 (10μM), SAHA (5μM), MS-275 (0.1μM) and MGCD0103 (1μM). Right: Western blot for H4ac, to test effectivity of the HDAC inhibitors. (B) Cells transfected with siCtrl (75nM), siHDAC1 (37.5nM siHDAC1 +37.5nM siCtrl), siHDAC2 (37.5nM siHDAC2 +37.5nM siCtrl), or siHDAC1+2 (37.5nM siHDAC1+37.5nM siHDAC2) were stimulated for 48h with IFNγ and expression of pMHCII was analysed by flow cytometry. Bottom: silencing efficiency was evaluated using Western blot. (C) Cells transfected with the indicated siRNAs (37.5nM HDAC1, 37.5nM HDAC2 and 37.5nM Keap1 or siCtrl) were stimulated for 48h with IFNγ and expression of pMHCII was analysed by flow cytometry. Signal for siKeap1 was normalized to the respective siCtrl. All experiments shown represent mean +SD of at least three independent experiments. Statistical significance was calculated compared to control cells (* p < 0.05, ** p < 0.01).*

275 inhibits HDAC1 and to a minor extent HDAC2 (47), arguing that HDAC1 or HDAC2 is the primary regulator of MHCII expression, which is in line with data that overexpression of HDAC1 or HDAC2 represses MHCII expression (17). However, silencing of HDAC1 did not upregulate MHCII expression, while knockdown of HDAC2 had only a minor effect (Fig. 1b and 1c). HDAC1 and HDAC2 have partly overlapping functions and can compensate for each other (48), therefore we also silenced both HDACs together. This strongly increased IFNγ-induced MHCII expression, and decreased the sensitivity of cells to Keap1 depletion (Fig. 2b and 2c). Thus, HDAC1 and HDAC2 together inhibit IFNγ-induced MHCII expression in a pathway that is antagonized by Keap1.

Keap1 regulates histone acetylation levels

The rescue of Keap1-mediated regulation of MHCII expression by HDAC inhibitors implies that Keap1 controls MHCII expression by controlling histone acetylation. Indeed, cells silenced for Keap1 displayed reduced acetylation of H3 and H4, which was independent of addition of IFNγ (Fig. 3a), indicating Keap1 regulates global histone acetylation. This effect was observed in multiple cell types (Fig. 3b), suggesting broad regulation of steady state histone acetylation by Keap1. Inhibition of HDAC1/2 mostly compensated for reduced histone acetylation (Fig. 3c), suggesting that Keap1 inhibits HDAC activity rather than promoting histone acetyl transferase (HAT) activity. HDAC1/2 levels were not increased by loss of Keap1 (Fig. 3a), and total HDAC activity in the cells was unaltered by Keap1 silencing (Fig. 3d). Thus, Keap1 does not affect total HDAC activity but does affect histone acetyl modification and hereby MHCII expression.

P62/SQSTM1 interacts with Keap1 and controls histone acetylation and MHCII expression

How do Keap1 and HDACs intermingle to modify MHCII expression in non-APC? Keap1 mainly serves as a substrate adaptor for Cul3 and binds many interactors, including Nrf2 and other substrates containing an ETGE motif, via its Kelch-domain, to properly position it for Cul3-mediated ubiquitination (49). Two point mutations of Keap1 were generated, one that renders Keap1 unable to bind ETGE motif containing proteins (Y572A)(50) and one that eliminates ubiquitin transfer to substrate proteins (G186R)(51). Stable expression of wild-type RNAi resistant Keap1 allowed rescuing IFNγ-induced MHCII expression upon Keap1 silencing, confirming that the effect of the siRNAs indeed relied on Keap1 depletion. In contrast, the effects on MHCII expression were not rescued by either point mutant of Keap1 (Fig. 4a and 4b), indicating a role for both substrate binding and ubiquitination in IFNγ-induced MHCII expression by Keap1. This effect was independent of the canonical substrate Nrf2, as co-depletion of Nrf2 did not restore IFNγ-induced MHCII expression to normal levels (Fig. 4c).

To identify proteins that cooperate with Keap1 to control IFNγ-induced MHCII transcription, we performed an RNAi screen targeting all described Keap1 interactors. Using this screen, BPTF/FALZ and p62/SQSTM1 were identified as additional partners in the regulations of IFNγ-induced MHCII expression (Fig. 4d). BPTF is a chromatin remodeler that binds histone modifications H3K4me3 and H4K16ac and

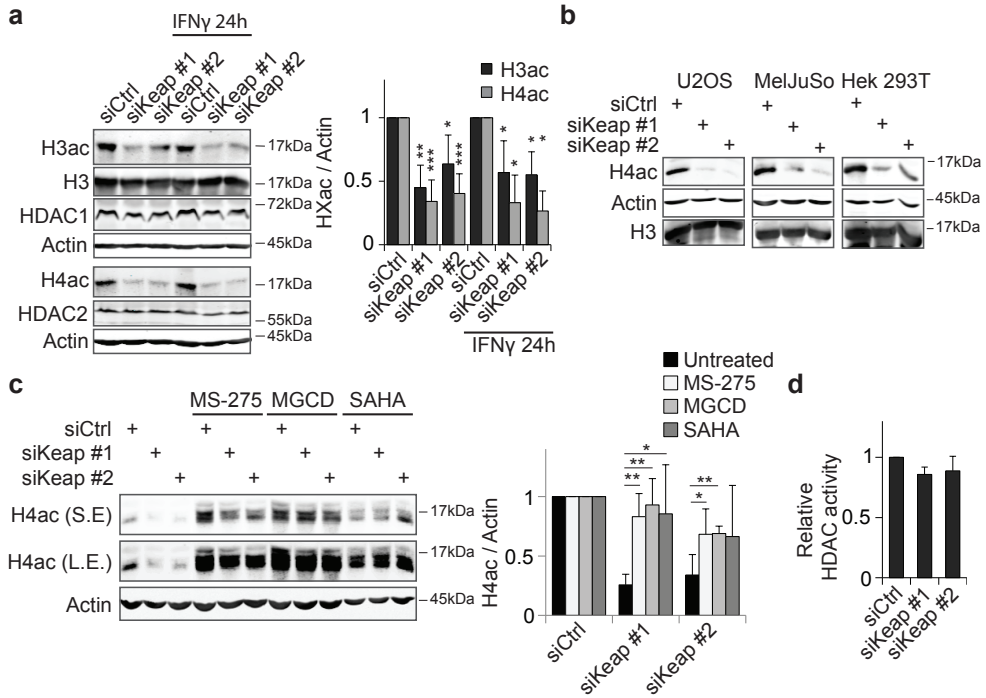


Figure 3: Keap1 regulates histone acetylation. *(A) Western blot analysis for the indicated proteins from HeLa cells transfected with the indicated siRNAs and treated for 24h with IFNγ when indicated. Right: quantification of H3ac and H4ac signals relative to corresponding siCtrl and normalized for actin. (B) HeK293T, MelJuSo and U2OS cells transfected with the indicated siRNAs were lysed and analysed by Western Blot for the indicated proteins. (C) HeLa cells transfected with siRNAs were treated with HDAC inhibitors when indicated and subjected to Western Blot analysis. Bottom: quantification of H4ac signals relative to corresponding siCtrl and normalized for actin. All experiments shown represent mean +SD of at least three independent experiments. Statistical significance was calculated compared to control cells (* p < 0.05, ** p < 0.01, *** p < 0.001).*

unwinds the local chromatin to allow transcription (52, 53), while p62 is an adaptor protein involved in autophagy, endosome positioning and cell signalling (54-56). p62 interacts with Keap1 in a ETGE-motif dependent manner and can promote its degradation via autophagy (57), while BPTF does not contain an ETGE(-like) motif but does bind the Kelch domain of Keap1 (58). Whereas depletion of BPTF did not decrease histone acetylation as detected by H4ac, p62 depletion reduced histone acetylation (Fig. 4e), suggesting Keap1 cooperates with p62 to drive MHCII expression. In agreement, p62 knockdown decreased the transcription and expression of MHCII and Ii, but not CIITA (Fig. 4f). In addition, the reduced histone acetylation levels following p62 depletion could be restored by inhibition of HDACs (Fig. 4g), analogous to earlier observations with Keap1 depletion. Thus, p62 is somewhere in the Keap1 controlled pathway of histone acetylation that modifies IFNγ-induced MHCII expression in non-immune cells.

Arsenite regulates IFNγ-induced MHCII expression

Keap1 contains several exposed cysteine residues that are modified during oxida-

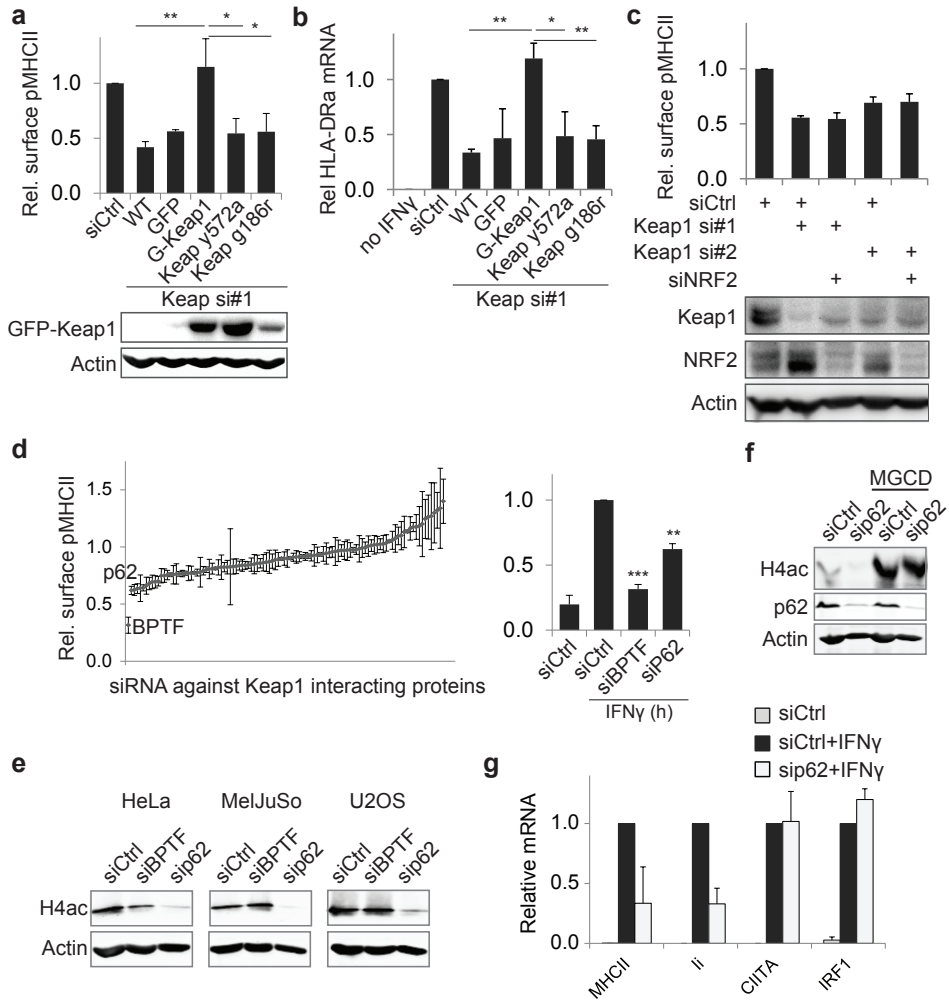


Figure 4: Keap1 cooperates with p62 to regulate histone acetylation. *(A) HeLa cells stably expressing GFP or RNAi resistant GFP-Keap1 with the indicated mutations were transfected with the indicated siRNAs and stimulated with IFNγ for 48h and analysed by flow cytometry. Below: Western Blot for expression of the indicated GFP-Keap1 constructs. (B) HeLa cells from (A) were stimulated for 24 hours with IFNγ and mRNA levels of HLA-DRα were measured using qRT-PCR. (C) pMHCII levels on HeLa cells transfected with the indicated siRNAs and stimulated with IFNγ for 48h were measured using flow cytometry. Bottom: Western blot for expression of the indicated proteins (D) Screen for effect of silencing Keap1 interacting proteins on MHCII surface levels. HeLa cells transfected with 106 different siRNAs targeting Keap1-interacting proteins were stimulated with IFNγ for 48h and analysed by flow cytometry. Right: summary of the independent triplicate experiment data for siRNAs targeting BPTF and p62. (E) p62 or BPTF was silenced in the indicated cell line and expression of the indicated proteins was assessed using Western blot. (F) HeLa cells transfected with the indicated siRNAs were treated with 1μM MGCD0103 for 24 hours and analysed for the indicated proteins by Western Blot. (G) HeLa cells transfected with the indicated siRNAs were stimulated for 24 hours with IFNγ and mRNA levels were measured using qRT-PCR. All experiments shown represent mean +SD of at least three independent experiments. Statistical significance was calculated compared to control cells (* p < 0.05, ** p < 0.01, *** p < 0.001).*

tive stress, rendering it inactive and hereby facilitating the NRF2-dependent expression of antioxidant genes. This raises the possibility that by inactivating Keap1, oxidative stress impairs IFNγ-induced MHCII expression. Interestingly, in vivo exposure to AS(III), an oxidative stressor that activates NRF2, has already been reported to decrease the expression of different MHCII-alleles and is linked to an impaired immune response (59, 60). To assess a direct role for AS(III) in IFNγ-induced MHCII expression, HeLa cells were exposed to different concentrations of sodium arsenite (AS(III)) during stimulation with IFNγ. A dose-dependent decrease in MHCII expression was observed, indicating a direct role for AS(III) in the regulation of IFNγ-induced MHCII expression (Fig. 5a). Similar to Keap1 depletion, this decrease was transcription-dependent and confined to MHCII and Ii, but not CIITA (Fig. 5b). As for Keap1 depletion, treatment with HDAC-inhibitor MGCD0103 fully restored IFNγ-induced MHCII expression (Fig. 5a). However, as reported earlier (61), no decrease was observed in global histone acetylation levels upon treatment with AS(III) (Fig. 5c), arguing against AS(III)-mediated inhibition of Keap1. AS(III) is also known to directly target the H4K16-specific histone acetyltransferase MYST1 (61), suggesting it could exert its effect via MYST1. In support of this, MYST1 knockdown reduced

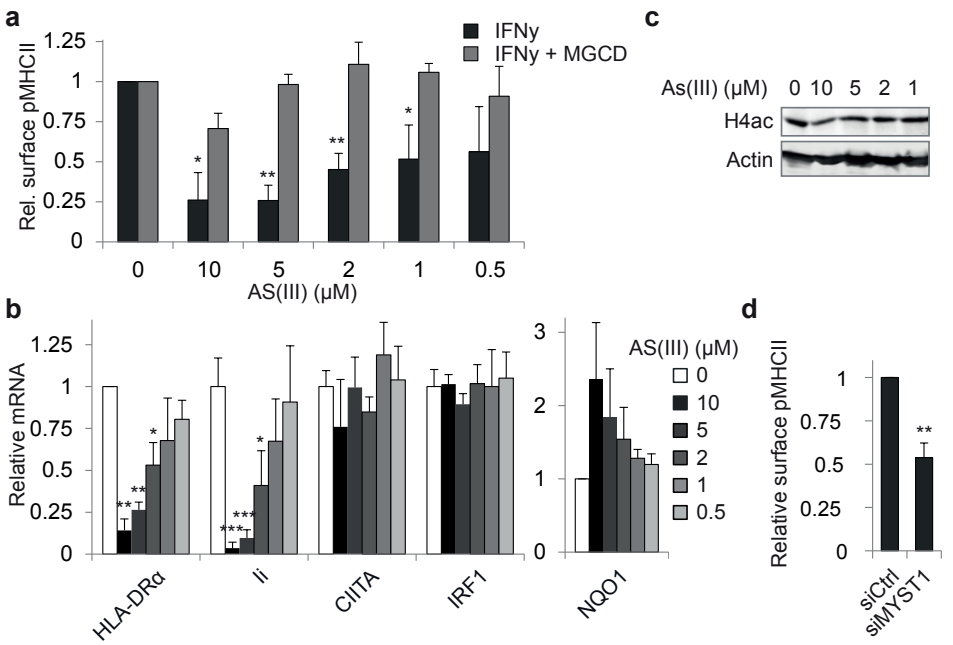


Figure 5: Arsenite controls histone acetylation dependent MHCII expression. *(A) HeLa cells were stimulated with IFNy for 48 hours in combination with the indicated concentration of NaAs2O3 and or 1μM MGCD0103 were analysed for pMHCII expression using flow cytometry. MGCD0103-treated samples were normalized to its corresponding no NaAs2O3 treatment sample. (B) HeLa cells treated or not with NaAs2O3 were stimulated for 24 hours with IFNy and mRNA levels were measured using qRT-PCR. (C) HeLa cells treated or not with NaAs2O3 for 24h were subjected to analysis of the indicated proteins by Western Blot. (D) pMHCII levels on HeLa cells transfected with the indicated siRNAs and stimulated with IFNy for 48h were measured using flow cytometry. All experiments shown represent mean +SD of at least three independent experiments. Statistical significance was calculated compared to control cells (* p < 0.05, ** p < 0.01, *** p < 0.001).*

IFNγ-induced MHCII expression (Fig. 5d). Thus, sodium arsenite impairs IFNγ-mediated MHCII expression, probably by targeting specific histone acetylation at H4K16 by MYST1, and this effect could be negated by HDAC-inhibitors.

Antioxidants control IFNy-induced MHCII expression

Keap1 senses oxidative stress and is a primary target for antioxidants such as tert-butylhydroquinone (tBHQ) and dimethyl fumarate (DMF) (36, 62). Both of these drugs display immunomodulatory activity, with their mechanism of action not fully defined (63, 64). DMF has been approved by the FDA for the treatment of psoriasis and multiple sclerosis (MS) (65-67). Interestingly, both of these autoimmune diseases have been linked to IFNy and activation of CD4+ T-cells (25, 68, 69), implying a possible role for IFNy-induced MHCII expression in disease pathology. To address whether DMF, like Keap1 inhibition, reduces IFNy-induced MHC class II expression, we treated various cells with IFNy in the absence or presence of DMF. In all these cells, DMF reduced IFNy-induced MHCII expression in a dose dependent manner, whereas constitutive MHCII expression on monocyte-like THP-1 cells was unaffected (Fig. 6a). Similarly, tBHQ specifically reduced IFNy-induced MHCII expression (Fig. 6a). In multiple sclerosis (MS), as well as experimental autoimmune encephalomyelitis (EAE, a mouse model that mimics MS), macrophages play an important role in the initiation of the inflammatory response(70). To assess whether DMF also affects MHCII expression on these cells, monocyte derived macrophages (MDMs), as well as MDMs that were cultured in the presence of myelin to generate foamy macrophages, which are present in brain lesions of MS patients (71), were treated with different doses of DMF. In both types of macrophages, DMF caused a dose dependent decrease in IFNy-induced MHCII expression but not constitutive MHCII expression (Fig. 6b and c).
mRNA analysis of these macrophages revealed that the effect was transcriptional, since levels of HLA-DRα and Ii transcripts were reduced (Fig. 6d). No significant decrease was observed for IRF1, whereas the response of CIITA was highly variable. As reported before for keratinocytes and peripheral blood mononuclear cells (PBMCs) (72), DMF also reduced the expression of the pro-inflammatory chemokines CXCL9 and CXCL10 in macrophages, suggesting a broad reduction of the IFNy-induced pro-inflammatory signature following DMF treatment (Fig. 6d). To our surprise, the inhibitory effect of DMF (and tBHQ) was independent of histone acetylation, as this inhibition could not be relieved by HDAC-inhibitors (Fig. 6e), histone acetylation levels were not affected by DMF (Fig. 6f), and the activity of the DR300-luciferase construct was affected by DMF (Fig. 6g). Thus, DMF inhibits IFNy-induced MHCII and chemokine expression via a mechanism independent of Keap1, possibly aiding its anti-inflammatory properties.

Discussion

Cytokine stimulated non-hematopoietic cells have often been discarded as functional contributors to MHCII-dependent immune activation, due to their lack of co-stimulatory receptors. However, several reports have recently challenged this dogma by demonstrating that tumour recognition, transplantation rejection, graft-versus-host disease and specific autoimmune diseases rely on MHCII expression by non-profes-

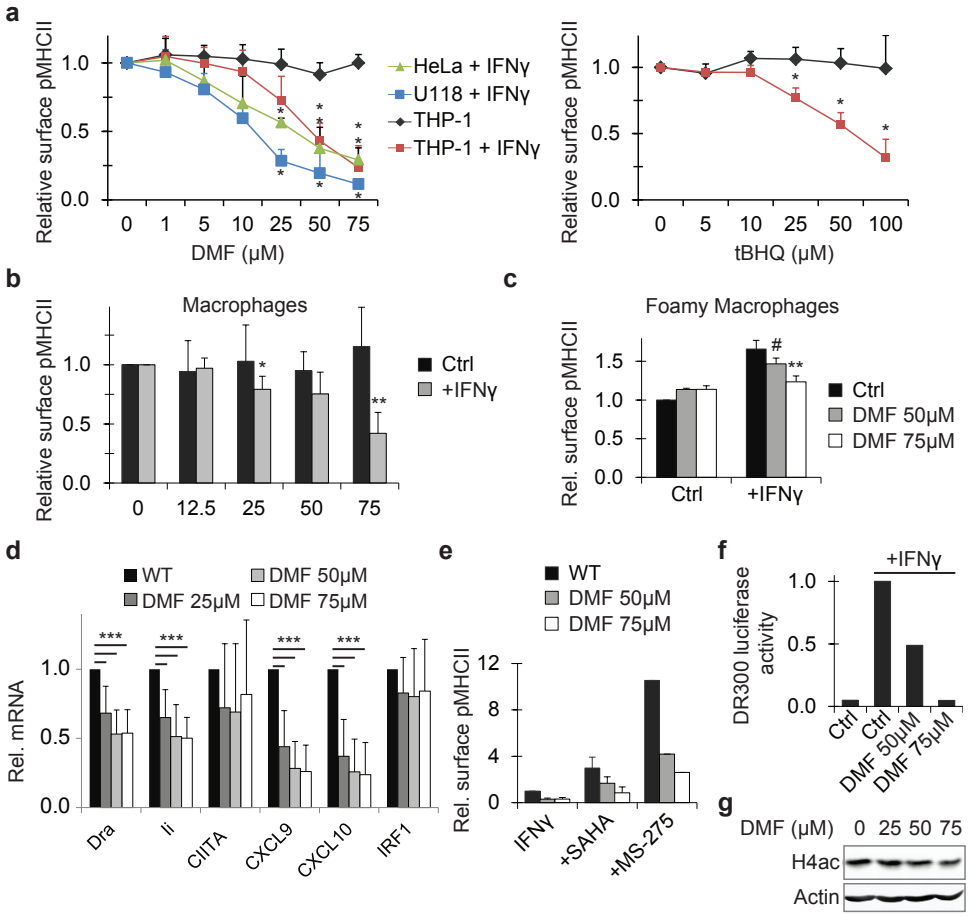


Figure 6: Dimethylfumarate inhibits IFNγ-induced MHCII and chemokine expression. *(A) THP-1, HeLa and U118 cells were treated with the indicated concentration of DMF or tBHQ as well as IFNγ for 48h when indicated and pMHCII expression was analysed using flow cytometry. For THP-1+IFNγ samples, signal for THP-1 without IFNγ was subtracted to correct for upregulation by IFNγ. n=3. (B) Macrophages were treated with the indicated concentration of DMF as well as IFNγ for 48h when indicated and pMHCII expression was analysed using flow cytometry. For IFNγ treated samples, the signal of wt macrophages was subtracted. n=4. (C) Foamy macrophages were treated with the indicated concentration of DMF as well as IFNγ for 24h when indicated and pMHCII expression was analysed using flow cytometry. n=3. (D) Macrophages were treated with the indicated concentration of DMF as well as IFNγ for 24h and mRNA expression of the indicated proteins was analysed using qRT-PCR, using GAPDH as loading control. n=8. (E) HeLa cells were stimulated for 48h with IFNγ and inhibitors and expression of pMHCII was analysed by flow cytometry. Concentrations: SAHA (5μM), MS-275 (0.1μM). (F) MHCII promoter activity (DR300) was analysed in HeLa cells treated or not with IFNγ and the indicated concentration of DMF. (G) HeLa cells were treated with DMF as indicated and analysed by Western Blot for the indicated proteins. Statistical significance was calculated compared to control cells (# p = 0.069, * p < 0.05, ** p < 0.01, *** p < 0.001).*

sional APCs, sparking interest in modulating this process. Here, we identify factors and compounds that interfere with IFNγ-induced MHCII expression in non-immune cells. We show that oxidative stress sensor Keap1 and autophagy adaptor p62 uphold global histone acetylation levels to facilitate IFNγ-induced MHCII expression

(Fig. 7). Their loss can be compensated for by inhibition of HDACs, arguing for a role in the epigenetic regulation of MHCII expression. Furthermore, we identify DMF, an antioxidant used in the treatment of psoriasis and MS, as an inhibitor of the IFNγ response, suggesting an additional mechanism of action for this immunomodulatory drug.

Dimethylfumarate (DMF) has recently been FDA approved for the treatment of relapsing-remitting MS, but its exact mechanism of action is still unresolved (73, 74). Several immunomodulatory actions have been ascribed to this drug, including skewing dendritic cell differentiation to a protective type II subset (75, 76), inhibition of dendritic cell and monocyte maturation (64, 77), inhibition of T-cell activation (78), and skewing T-cells to a Th2 subtype(79, 80). In addition, other modes of proposed action include inhibition of leukocyte infiltration and migration (81). Many of these cellular outcomes are key to the pro-inflammatory action of IFNγ, as this cytokine induces CXCL9 and CXCL10 production to induce T-cell migration and attraction, as well as MHCII expression to facilitate activation of CD4+ T-cells. We show that DMF inhibits IFNγ-induced chemokine expression in macrophages, as also shown for keratinocytes and PBMCs (72). The inhibitory effect of DMF extents to IFNγ-induced expression of MHCII, indicating that DMF acts to dampen antigen presentation and immune cell recruitment in both hematopoietic and non-hematopoietic origin. Since DMF did not affect constitutive expression of MHCII on macrophages and B-cells, it probably acts as a context-specific inhibitor of MHCII expression. The sensitivity of different cell types to DMF varied, with non-hematopoietic cell types significantly reducing MHCII expression at concentrations as low as 10μM, while macrophages required at least 50μM DMF for a similar response. This could be the result of the higher expression of antioxidant genes in macrophages, which help quench DMF (82). While the exact mechanism of action for DMF remains unclear, recent data in

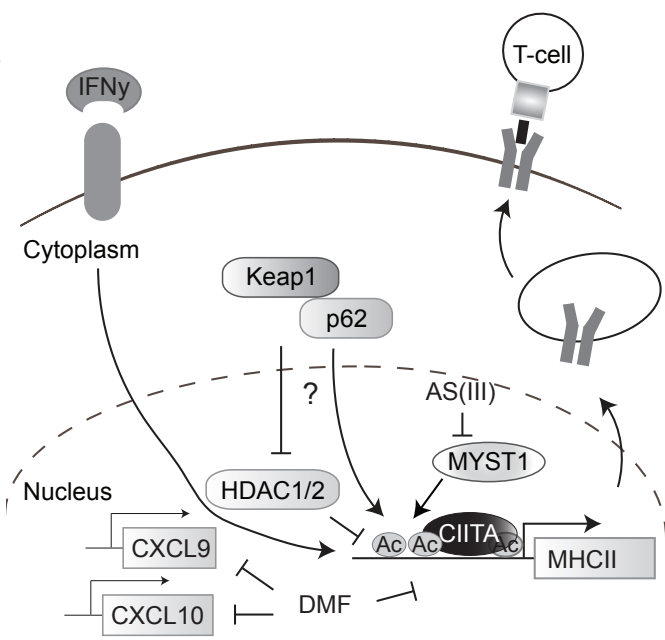


Figure 7: Model for the regulation of transcription of IFNγ-induced MHCII expression by Keap1, p62, arsenite and DMF. *Transcription of MHCII genes is regulated by CIITA and histone acetylation. HDAC1/2 represses histone acetylation, while p62, Keap1 and MYST1 promote it. Arsenite inhibits MYST1 and hereby impairs MHCII expression. Dimethyfumarate inhibits IFNγ-induced expression of MHCII, as well as CXCL9 and CXCL10, via a yet undefined mechanism.*

a mouse model for MS suggest that the immunomodulatory and protective activity of DMF does not involve NRF2 (64). This observation is in line with our data that suggest that the effect of DMF on the IFNγ-axis is independent of the Keap1-NRF2 antioxidant response pathway. Since many proteins are targeted by DMF (78), its immunomodulatory action could result from interfering with multiple pathways.
Besides antioxidants, we also tested a role for oxidative stressor arsenite in IFNγ-induced MHCII expression. Arsenic contamination of drinking water is a persistent problem in many countries and can lead to carcinogenesis and immunotoxicity (83). Our data suggest that the latter could in part be mediated via impaired IFNγ-induced expression of MHCII. This is corroborated by in vivo data where a decrease in MHCII expression on leukocytes was observed in mice exposed to arsenite, as well as people living in areas with high arsenic levels in drinking water (59, 60). Interestingly, arsenic alleviates graft-versus-host-disease (GVHD) and transplantation rejection of MHCII-mismatched donors (84, 85), which could arise from decreased IFNγ-induced expression of MHCII on respectively host and donor cells. Quenched IFNγ-induced MHCII expression was restored by inhibition of HDAC1/2, arguing that arsenite alters epigenetic regulation of MHCII expression. In agreement with this, arsenite reduces global histone acetylation levels in drosophila (86), as well as H3K9 and H4K16, but not global, histone acetylation in human cells (87, 88), the latter by targeting the histone acetyltransferase MYST1 (61). Depletion of MYST1 also impaired IFNγ-induced MHCII expression, suggesting that arsenite inhibits MYST1 to control MHCII expression. Thus, arsenic controls IFNγ-mediated MHCII expression via epigenetic regulation, possibly contributing to its immunosuppressive activity.
Apart from chemical modulators of MHCII expression, our data indicate a function for Keap1 and p62/SQSTM1 in control of IFNγ-induced MHCII expression. Keap1 and p62 instil their effects by modulating the epigenetic environment of the MHCII locus, as no significant effect of their loss was observed on an ectopically introduced MHCII promoter or expression of CIITA. Depletion of Keap1 and p62 was accompanied by a reduction in global histone acetylation levels, which could be restored by inhibition of HDAC1 and HDAC2. Thus, Keap1 and p62 either inhibit HDAC1/2 or activate HATs. p62 is known to inhibit HDAC6 (89) via a direct interaction. However, we failed to detect an interaction of either Keap1 or p62 with HDAC1. Loss of Keap1 did not change total HDAC activity in the cell, nor did it alter the localization of HDAC1 (data not shown), raising the possibility that HDAC targeting to the DNA via recruitment factors is affected. The predominantly cytosolic nature of Keap1 and p62 versus the nuclear localization of HDAC1 presuppose that this regulation is indirect. In assembly, Keap1 and p62 alter the epigenetic histone acetylation landscape to facilitate expression of MHCII after IFNγ stimulation.
Physiologically, many stimuli regulate global cellular histone acetylation levels, either via HATs (as in the case of NFκB signalling (90)), or via HDACs (in the case of cell cycle related kinase CK2, nuclear actin and sumoylation (89, 91, 92)). Keap1 and p62 could be involved in histone acetylation regulation due to their role as stress sensors, respectively being degraded by oxidative stress and autophagy. This would translate extracellular conditions to epigenetic effects. The notion that overall histone acetylation levels are decreased upon removal of Keap1 and p62 infers that the transcriptional changes are not limited to MHCII. For Keap1, this could function to

minimize expression of novel proteins that are subjected to oxidation, whereas for p62 this could attenuate transcription of MHCII and other genes to favour the expression of autophagy-related genes, as observed for mTOR inhibition, which inhibits H4K16ac to drive autophagy gene expression (93). This integrates regulation of histone acetylation into the stress response that is activated following downregulation of Keap1 and p62.

Mutations in or depletion of Keap1 and p62 potentially impairs MHCII expression by tumour cells, subsequently hampering immune recognition. In agreement with this, epigenetic silencing of IFNγ target genes in tumours has been widely observed, and its reversal by HDAC-inhibitors aides immunotherapy treatment in several mouse models (33, 34). Keap1 is frequently mutated in lung cancer (94), providing a rationale for treatment selection with HDAC-inhibitors in lung patients. However, we observed no clear correlation between expression of Keap1-target NRF2 and MHCII in lung tumour tissues from the Human Protein Atlas database (95). Furthermore, both Keap1 mutant and wild-type lung cancer cell lines are sensitive to HDAC-inhibitors (34), indicating that multiple factors are involved in the epigenetic silencing of IFNγ target genes. Nevertheless, our data support the notion that HDAC-inhibitors, specifically HDAC1 and HDAC2 inhibitors, are interesting tools to stimulate immune recognition of tumour cells.

Collectively, our data identify several novel regulators of IFNγ-induced MHCII expression, as occurs in inflamed tissue. Two stress-related proteins, Keap1 and p62, induce histone acetylation and IFNγ-mediated MHCII expression in non-immune cells. Mutation of the p62-binding site in Keap1 failed to restore expression of MHCII, implying that Keap1 and p62 functionally cooperate in this process. Arsenite, an immunosuppressive compound that induces oxidative stress, also controls IFNγ-mediated MHCII expression. The effects of Keap1 or p62 depletion and arsenite on MHCII expression could be overcome by HDAC-inhibitors, implying epigenetic regulation by these factors. Finally we demonstrate that the drug dimethylfumarate (DMF) specifically impairs IFNγ-induced MHCII expression, providing an additional mechanism of action for this drug that is used for the treatment of autoimmune diseases.

Acknowledgements

We thank members of the Neefjes group for critical discussions and the NKI Flow Cytometry Facility and Robotics Facility for support, with special thanks to Ben Morris. This work was supported by the Institute of Chemical Immunology, an NWO Gravitation project funded by the Ministry of Education, Culture and Science of the government of the Netherlands awarded to J.N.

Materials and Methods

Cell culture, treatments and constructs

HeLa, U118, U2OS and Hek293T cells were cultured in DMDM supplemented with 10% FCS, MelJuSO cells in IMDM with 10% FCS. For IFNγ stimulation, cells were stimulated with 100 ng/ml IFNγ (Ebioscience) for the indicated time. For genera-

tion of stable cell lines, Keap1 was cloned into a GFP-C1 vector and mutagenized to avoid targeting by Keap1 siRNA#1 using the primers: fw 5'-ggggctttgacgggacaaatcgtctaaactcagctgagtgttac-3', rv 5'- gggtagtaacactcagctgagtttagacgatttgtcccgtcaaagc-3'. Subsequent mutagenesis was performed using the following primers: Y572A fw: 5'-ctacgtccttggaggcgctgatggtcacacgttc-3', Y572A rv: 5'-actgtccaggaacgtgtgaccatcagcgcctccaaggacg-3' G186R fw: 5'-cccagcaatgccatccgcatcgccaacttcg-3', G186R rv: 5'-gctcagcgaagttggcgatgcggatggcattg-3'. GFP and GFP-Keap1 mutants were recloned into a retroviral pMX vector and upon retroviral transduction cells selected using Puromycin (4µg/ml, Gibco).

Transfections

For expression studies, HeLa cells were transfected using Effectene (Qiagen) according to the manufacturer's instructions. For siRNA mediated depletion, cells were reverse transfected according to the manufacturer's protocol with DharmaFECT transfection reagent #1 and 50 nM siRNA (except for double and triple transfections). Briefly, siRNAs and DharmaFECT were mixed and incubated for 20 minutes in a culture well, after which cells were added and left to adhere. Three days later, cells were used for analysis. Catalog numbers: siCtrl: D00120613-20, siSTAT1 D-003543, siHDAC1 D-003493, siHDAC2 D-003495, siBPTF M-004025-01-0005, sip62 D-010230 of the Human siGenome SMARTpool, Dharmacon. siRNA sequences targeting Keap1: #1 GGACAAACCGCCUUAAUUC and #2 GGGCGUGGCUGUCCUCAAU, siRNA sequences targeting p62: #1 and #2 , all from Dharmacon.

Reagents and antibodies

Rabbit αHDAC1 NB100-56340 (Novus Biologicals), Rabbit αHDAC2 SC-7899, mouse αp62 SC-28359 (both from Santa Cruz), Rabbit αH3ac 06599 (Millipore), rabbit αH4ac ab177790, rabbit αH3 ab1791 (both from Abcam), mouse αKeap1, mouse αActin (both from Sigma), rabbit αGFP (as described before (96)). Sodium (meta)Arsenite and Dimethylfumarate were acquired from Sigma.

Flow Cytometry

Three days after siRNA transfection, HeLa cells were trypsinized and stained with Cy5-labeled L243 antibody(97), before analysis using flow cytometry (BD FACSArray, or BD FACS Calibur for GFP co-detection).

Co-immunoprecipitation and Western blotting

For protein expression analysis, cells were directly lysed in sample buffer and proteins were separated by SDS-PAGE and transferred to Western Blot filters. Antibody incubations and blocking were done in PBS supplemented with 0.1 (v/v)% Tween and 5% (w/v) milk powder. Blots were imaged using the Odyssey Imaging System (LI-COR) or Chemidoc (Biorad).

cDNA synthesis and qPCR

RNA isolation, cDNA synthesis and quantitative RT-PCR were performed according to the manufacturer's (Roche) instructions. Signal was normalized to GAPDH and calculated using the Pfaffl formula. Primers used for detection were: GAPDH fw: 5'-TGTTGCCATCAATGACCCCTT-3', GAPDH rv: 5'-CTCCACGACGTACTCAGCG-3', HLA-DRα fw: 5'-CATGGGCTATCAAAGAAGAAC-3', HLA-DRα rv: 5'-CTTGAGCCTCAAAGCTGGC-3', Ii fw: 5'-CACCTGCTCCAGAATGCTG-3', Ii rv: 5'-CAGTTCCAGTGACTCTTTCG-3', IRF1 fw: 5'-GCACCAGTGATCTGTACAAC-3', IRF1 rv: 5'-GCTCCTCCTTACAGCTAAAG-3', CIITA fw: 5'-CCTGCTGTTCGG-

GACCTAAA-3, CIITA rv: 5'-GGATCCGCACCAGTTTGG-3', Keap1 fw: 5'-CTG-GAGGATCATACCAAGCAGG-3', Keap1 rv: 5'-GAACATGGCCTTGAAGACAGG-3', NQO1 fw: 5'-GGGCAAGTCCATCCCAACTG-3', NQO1 rv: 5'-GCAAGTCAGG-GAAGCCTGGA-3', CXCL9 fw: 5'- GTGGTGTTCTTTTCCTCTTG-3', CXCL9 rv: 5'-GTAGGTGGATAGTCCCTTGG-3', CXCL10 fw: 5'- TGATTTGCTGCCTTATCT-TTCTGA-3', CXCL10 rv: 5'- CAGCCTCTGTGTGGTCCATCCTTG-3'.

Luciferase assays

HeLa cells reverse transfected with the indicated siRNAs were transfected the next day with a luciferase construct under the control of the MHCII locus (DR300), as well as a SV40-Renilla pGL3 reporter construct. A day later, cells were stimulated with IFNγ when indicated and lysed and analysed the day after using the Dual Luciferase Reporter Assay (Promega). Data were normalized to Renilla luciferase signal.

HDAC activity assay

Three days after transfection, HDAC activity in HeLa cells were analysed using the Fluor de Lys assay (Enzo Life Sciences) according to the manufacturer's instructions. Read-out was performed on the BMG Labtech Clariostar.

References

1. J. Neefjes, M. L. Jongsma, P. Paul, O. Bakke, Towards a systems understanding of MHC class I and MHC class II antigen presentation. Nat Rev Immunol 11, 823-836 (2011).
2. M. M. Fernando et al., Defining the role of the MHC in autoimmunity: a review and pooled analysis. PLoS Genet 4, e1000024 (2008).
3. J. D. Rioux et al., Mapping of multiple susceptibility variants within the MHC region for 7 immune-mediated diseases. Proceedings of the National Academy of Sciences of the United States of America 106, 18680-18685 (2009).
4. T. Kambayashi, T. M. Laufer, Atypical MHC class II-expressing antigen-presenting cells: can anything replace a dendritic cell? Nat Rev Immunol 14, 719-730 (2014).
5. M. Koyama et al., Recipient nonhematopoietic antigen-presenting cells are sufficient to induce lethal acute graft-versus-host disease. Nature medicine 18, 135-142 (2011).
6. K. P. MacDonald, W. D. Shlomchik, P. Reddy, Biology of graft-versus-host responses: recent insights. Biology of blood and marrow transplantation : journal of the American Society for Blood and Marrow Transplantation 19, S10-14 (2013).
7. J. Kim et al., Roles of Host Nonhematopoietic Cells in Autoimmunity and Donor Cell Engraftment in Graft-versus-host Disease. Immune network 10, 46-54 (2010).
8. P. Abrahimi et al., Blocking MHC class II on human endothelium mitigates acute rejection. JCI insight 1, (2016).
9. C. Thelemann et al., Absence of nonhematopoietic MHC class II expression protects mice from experimental autoimmune myocarditis. European journal of immunology 46, 656-664 (2016).
10. R. Meazza, A. Comes, A. M. Orengo, S. Ferrini, R. S. Accolla, Tumor rejection by gene transfer of the MHC class II transactivator in murine mammary adenocarcinoma cells. European journal of immunology 33, 1183-1192 (2003).
11. D. B. Johnson et al., Melanoma-specific MHC-II expression represents a tumour-autonomous phenotype and predicts response to anti-PD-1/PD-L1 therapy. Nature communications 7, 10582 (2016).
12. V. Steimle, L. A. Otten, M. Zufferey, B. Mach, Complementation cloning of an MHC class II transactivator mutated in hereditary MHC class II deficiency (or bare lymphocyte syndrome). Cell 75, 135-146 (1993).
13. K. Masternak et al., CIITA is a transcriptional coactivator that is recruited to MHC class II promoters by multiple synergistic interactions with an enhanceosome complex. Genes Dev 14, 1156-1166 (2000).
14. W. Reith, S. LeibundGut-Landmann, J. M. Waldburger, Regulation of MHC class II gene expression by the class II transactivator. Nat Rev Immunol 5, 793-806 (2005).
15. R. Mudhasani, J. D. Fontes, The class II transactivator requires brahma-related gene 1 to activate transcription of major histocompatibility complex class II genes. Mol Cell Biol 22, 5019-5026 (2002).

16. G. W. Beresford, J. M. Boss, CIITA coordinates multiple histone acetylation modifications at the HLA-DRA promoter. Nature immunology 2, 652-657 (2001).
17. E. Zika, S. F. Greer, X. S. Zhu, J. P. Ting, Histone deacetylase 1/mSin3A disrupts gamma interferon-induced CIITA function and major histocompatibility complex class II enhanceosome formation. Mol Cell Biol 23, 3091-3102 (2003).
18. A. Raval et al., Transcriptional coactivator, CIITA, is an acetyltransferase that bypasses a promoter requirement for TAF(II)250. Molecular cell 7, 105-115 (2001).
19. P. J. van den Elsen, Expression regulation of major histocompatibility complex class I and class II encoding genes. Frontiers in immunology 2, 48 (2011).
20. J. R. Schoenborn, C. B. Wilson, Regulation of interferon-gamma during innate and adaptive immune responses. Advances in immunology 96, 41-101 (2007).
21. J. Gao et al., Loss of IFN-gamma Pathway Genes in Tumor Cells as a Mechanism of Resistance to Anti-CTLA-4 Therapy. Cell 167, 397-404.e399 (2016).
22. J. M. Zaretsky et al., Mutations Associated with Acquired Resistance to PD-1 Blockade in Melanoma. The New England journal of medicine 375, 819-829 (2016).
23. G. H. Ring et al., Interferon-gamma is necessary for initiating the acute rejection of major histocompatibility complex class II-disparate skin allografts. Transplantation 67, 1362-1365 (1999).
24. K. M. Pollard, D. M. Cauvi, C. B. Toomey, K. V. Morris, D. H. Kono, Interferon-gamma and systemic autoimmunity. Discovery medicine 16, 123-131 (2013).
25. G. Arellano, P. A. Ottum, L. I. Reyes, P. I. Burgos, R. Naves, Stage-Specific Role of Interferon-Gamma in Experimental Autoimmune Encephalomyelitis and Multiple Sclerosis. Frontiers in immunology 6, 492 (2015).
26. S. Oon, N. J. Wilson, I. Wicks, Targeted therapeutics in SLE: emerging strategies to modulate the interferon pathway. Clinical & translational immunology 5, e79 (2016).
27. J. L. Harden et al., Humanized anti-IFN-gamma (HuZAF) in the treatment of psoriasis. The Journal of allergy and clinical immunology 135, 553-556 (2015).
28. L. C. Platanias, Mechanisms of type-I- and type-II-interferon-mediated signalling. Nat Rev Immunol 5, 375-386 (2005).
29. K. Schroder, P. J. Hertzog, T. Ravasi, D. A. Hume, Interferon-gamma: an overview of signals, mechanisms and functions. J Leukoc Biol 75, 163-189 (2004).
30. H. Kamma, T. Yazawa, T. Ogata, H. Horiguchi, T. Iijima, Expression of MHC class II antigens in human lung cancer cells. Virchows Archiv. B, Cell pathology including molecular pathology 60, 407-412 (1991).
31. J. M. Wroblewski, D. L. Bixby, C. Borowski, J. R. Yannelli, Characterization of human non-small cell lung cancer (NSCLC) cell lines for expression of MHC, co-stimulatory molecules and tumor-associated antigens. Lung cancer (Amsterdam, Netherlands) 33, 181-194 (2001).
32. M. Hiroi, Y. Ohmori, Constitutive nuclear factor kappaB activity is required to elicit interferon-gamma-induced expression of chemokine CXC ligand 9 (CXCL9) and CXCL10 in human tumour cell lines. The Biochemical journal 376, 393-402 (2003).
33. A. C. West et al., An intact immune system is required for the anticancer activities of histone deacetylase inhibitors. Cancer research 73, 7265-7276 (2013).
34. H. Zheng et al., HDAC Inhibitors Enhance T-Cell Chemokine Expression and Augment Response to PD-1 Immunotherapy in Lung Adenocarcinoma. Clinical cancer research : an official journal of the American Association for Cancer Research 22, 4119-4132 (2016).
35. M. E. Sowa, E. J. Bennett, S. P. Gygi, J. W. Harper, Defining the human deubiquitinating enzyme interaction landscape. Cell 138, 389-403 (2009).
36. K. Taguchi, H. Motohashi, M. Yamamoto, Molecular mechanisms of the Keap1-Nrf2 pathway in stress response and cancer evolution. Genes to cells : devoted to molecular & cellular mechanisms 16, 123-140 (2011).
37. D. F. Lee et al., KEAP1 E3 ligase-mediated downregulation of NF-kappaB signaling by targeting IKKbeta. Molecular cell 36, 131-140 (2009).
38. J. E. Kim et al., Suppression of NF-kappaB signaling by KEAP1 regulation of IKKbeta activity through autophagic degradation and inhibition of phosphorylation. Cellular signalling 22, 1645-1654 (2010).
39. W. Fan et al., Keap1 facilitates p62-mediated ubiquitin aggregate clearance via autophagy. Autophagy 6, 614-621 (2010).
40. A. Orthwein et al., A mechanism for the suppression of homologous recombination in G1 cells.

Nature 528, 422-426 (2015).
41. R. H. Wijdeven et al., Genome-Wide Identification and Characterization of Novel Factors Conferring Resistance to Topoisomerase II Poisons in Cancer. Cancer Res 75, 4176-4187 (2015).
42. A. Ito et al., The subcellular localization and activity of cortactin is regulated by acetylation and interaction with Keap1. Science signaling 8, ra120 (2015).
43. M. Abou El Hassan, T. Yu, L. Song, R. Bremner, Polycomb Repressive Complex 2 Confers BRG1 Dependency on the CIITA Locus. Journal of immunology (Baltimore, Md. : 1950) 194, 5007-5013 (2015).
44. A. C. Morris, W. E. Spangler, J. M. Boss, Methylation of class II trans-activator promoter IV: a novel mechanism of MHC class II gene control. Journal of immunology (Baltimore, Md. : 1950) 164, 4143-4149 (2000).
45. S. K. Verma et al., Identification of Potent, Selective, Cell-Active Inhibitors of the Histone Lysine Methyltransferase EZH2. ACS medicinal chemistry letters 3, 1091-1096 (2012).
46. S. K. Knutson et al., Durable tumor regression in genetically altered malignant rhabdoid tumors by inhibition of methyltransferase EZH2. Proceedings of the National Academy of Sciences of the United States of America 110, 7922-7927 (2013).
47. N. Khan et al., Determination of the class and isoform selectivity of small-molecule histone deacetylase inhibitors. The Biochemical journal 409, 581-589 (2008).
48. R. H. Wilting et al., Overlapping functions of Hdac1 and Hdac2 in cell cycle regulation and haematopoiesis. The EMBO journal 29, 2586-2597 (2010).
49. B. E. Hast et al., Proteomic analysis of ubiquitin ligase KEAP1 reveals associated proteins that inhibit NRF2 ubiquitination. Cancer research 73, 2199-2210 (2013).
50. A. Jain et al., p62/SQSTM1 is a target gene for transcription factor NRF2 and creates a positive feedback loop by inducing antioxidant response element-driven gene transcription. The Journal of biological chemistry 285, 22576-22591 (2010).
51. B. E. Hast et al., Cancer-derived mutations in KEAP1 impair NRF2 degradation but not ubiquitination. Cancer research 74, 808-817 (2014).
52. A. J. Ruthenburg et al., Recognition of a mononucleosomal histone modification pattern by BPTF via multivalent interactions. Cell 145, 692-706 (2011).
53. J. Wysocka et al., A PHD finger of NURF couples histone H3 lysine 4 trimethylation with chromatin remodelling. Nature 442, 86-90 (2006).
54. S. Pankiv et al., p62/SQSTM1 binds directly to Atg8/LC3 to facilitate degradation of ubiquitinated protein aggregates by autophagy. The Journal of biological chemistry 282, 24131-24145 (2007).
55. M. L. Jongsma et al., An ER-Associated Pathway Defines Endosomal Architecture for Controlled Cargo Transport. Cell 166, 152-166 (2016).
56. A. Duran et al., The signaling adaptor p62 is an important NF-kappaB mediator in tumorigenesis. Cancer cell 13, 343-354 (2008).
57. M. Komatsu et al., The selective autophagy substrate p62 activates the stress responsive transcription factor Nrf2 through inactivation of Keap1. Nature cell biology 12, 213-223 (2010).
58. G. D. Strachan et al., Fetal Alz-50 clone 1 interacts with the human orthologue of the Kelch-like Ech-associated protein. Biochemistry 43, 12113-12122 (2004).
59. A. S. Andrew et al., Drinking-water arsenic exposure modulates gene expression in human lymphocytes from a U.S. population. Environmental health perspectives 116, 524-531 (2008).
60. E. E. Sikorski, L. A. Burns, K. L. McCoy, M. Stern, A. E. Munson, Suppression of splenic accessory cell function in mice exposed to gallium arsenide. Toxicology and applied pharmacology 110, 143-156 (1991).
61. D. Liu et al., Arsenic Trioxide Reduces Global Histone H4 Acetylation at Lysine 16 through Direct Binding to Histone Acetyltransferase hMOF in Human Cells. PloS one 10, e0141014 (2015).
62. K. Takaya et al., Validation of the multiple sensor mechanism of the Keap1-Nrf2 system. Free radical biology & medicine 53, 817-827 (2012).
63. C. E. Rockwell, M. Zhang, P. E. Fields, C. D. Klaassen, Th2 skewing by activation of Nrf2 in CD4(+) T cells. Journal of immunology (Baltimore, Md. : 1950) 188, 1630-1637 (2012).
64. U. Schulze-Topphoff et al., Dimethyl fumarate treatment induces adaptive and innate immune modulation independent of Nrf2. Proceedings of the National Academy of Sciences of the United States of America 113, 4777-4782 (2016).
65. U. Mrowietz, E. Christophers, P. Altmeyer, Treatment of severe psoriasis with fumaric acid esters: scientific background and guidelines for therapeutic use. The German Fumaric Acid Ester Con-

sensus Conference. The British journal of dermatology 141, 424-429 (1999).
66. R. J. Fox et al., Placebo-controlled phase 3 study of oral BG-12 or glatiramer in multiple sclerosis. The New England journal of medicine 367, 1087-1097 (2012).
67. R. Gold et al., Placebo-controlled phase 3 study of oral BG-12 for relapsing multiple sclerosis. The New England journal of medicine 367, 1098-1107 (2012).
68. I. Kryczek et al., Induction of IL-17+ T cell trafficking and development by IFN-gamma: mechanism and pathological relevance in psoriasis. Journal of immunology (Baltimore, Md. : 1950) 181, 4733-4741 (2008).
69. J. Karczewski, A. Dobrowolska, A. Rychlewska-Hanczewska, Z. Adamski, New insights into the role of T cells in pathogenesis of psoriasis and psoriatic arthritis. Autoimmunity, 1-16 (2016).
70. X. Fan et al., Double Roles of Macrophages in Human Neuroimmune Diseases and Their Animal Models. Mediators of inflammation 2016, 8489251 (2016).
71. L. A. Boven et al., Myelin-laden macrophages are anti-inflammatory, consistent with foam cells in multiple sclerosis. Brain : a journal of neurology 129, 517-526 (2006).
72. T. J. Stoof et al., The antipsoriatic drug dimethylfumarate strongly suppresses chemokine production in human keratinocytes and peripheral blood mononuclear cells. The British journal of dermatology 144, 1114-1120 (2001).
73. Z. Al-Jaderi, A. A. Maghazachi, Utilization of Dimethyl Fumarate and Related Molecules for Treatment of Multiple Sclerosis, Cancer, and Other Diseases. Frontiers in immunology 7, 278 (2016).
74. D. Dubey et al., Dimethyl fumarate in relapsing-remitting multiple sclerosis: rationale, mechanisms of action, pharmacokinetics, efficacy and safety. Expert review of neurotherapeutics 15, 339-346 (2015).
75. K. Ghoreschi et al., Fumarates improve psoriasis and multiple sclerosis by inducing type II dendritic cells. The Journal of experimental medicine 208, 2291-2303 (2011).
76. K. Zhu, U. Mrowietz, Inhibition of dendritic cell differentiation by fumaric acid esters. The Journal of investigative dermatology 116, 203-208 (2001).
77. H. Peng et al., Dimethyl fumarate inhibits dendritic cell maturation via nuclear factor kappaB (NF-kappaB) and extracellular signal-regulated kinase 1 and 2 (ERK1/2) and mitogen stress-activated kinase 1 (MSK1) signaling. The Journal of biological chemistry 287, 28017-28026 (2012).
78. M. M. Blewett et al., Chemical proteomic map of dimethyl fumarate-sensitive cysteines in primary human T cells. Science signaling 9, rs10 (2016).
79. H. M. Ockenfels, T. Schultewolter, G. Ockenfels, R. Funk, M. Goos, The antipsoriatic agent dimethylfumarate immunomodulates T-cell cytokine secretion and inhibits cytokines of the psoriatic cytokine network. The British journal of dermatology 139, 390-395 (1998).
80. R. de Jong et al., Selective stimulation of T helper 2 cytokine responses by the anti-psoriasis agent monomethylfumarate. European journal of immunology 26, 2067-2074 (1996).
81. A. J. Gill, D. L. Kolson, Dimethyl fumarate modulation of immune and antioxidant responses: application to HIV therapy. Critical reviews in immunology 33, 307-359 (2013).
82. L. Zheng et al., Fumarate induces redox-dependent senescence by modifying glutathione metabolism. Nature communications 6, 6001 (2015).
83. S. V. Jadhav et al., Arsenic and fluoride contaminated groundwaters: A review of current technologies for contaminants removal. Journal of environmental management 162, 306-325 (2015).
84. N. Kavian et al., Arsenic trioxide prevents murine sclerodermatous graft-versus-host disease. Journal of immunology (Baltimore, Md. : 1950) 188, 5142-5149 (2012).
85. S. Yan et al., Arsenic trioxide attenuated the rejection of major histocompatibility complex fully-mismatched cardiac allografts in mice. Transplantation proceedings 41, 1855-1858 (2009).
86. A. P. Arrigo, Acetylation and methylation patterns of core histones are modified after heat or arsenite treatment of Drosophila tissue culture cells. Nucleic acids research 11, 1389-1404 (1983).
87. A. Arita et al., The effect of exposure to carcinogenic metals on histone tail modifications and gene expression in human subjects. Journal of trace elements in medicine and biology : organ of the Society for Minerals and Trace Elements (GMS) 26, 174-178 (2012).
88. W. J. Jo et al., Acetylated H4K16 by MYST1 protects UROtsa cells from arsenic toxicity and is decreased following chronic arsenic exposure. Toxicology and applied pharmacology 241, 294-302 (2009).
89. J. Yan et al., SQSTM1/p62 interacts with HDAC6 and regulates deacetylase activity. PloS one 8, e76016 (2013).
90. H. Zhong, R. E. Voll, S. Ghosh, Phosphorylation of NF-kappa B p65 by PKA stimulates tran-

scriptional activity by promoting a novel bivalent interaction with the coactivator CBP/p300. Molecular cell 1, 661-671 (1998).
91. G. P. Delcuve, D. H. Khan, J. R. Davie, Roles of histone deacetylases in epigenetic regulation: emerging paradigms from studies with inhibitors. Clinical epigenetics 4, 5 (2012).
92. G. David, M. A. Neptune, R. A. DePinho, SUMO-1 modification of histone deacetylase 1 (HDAC1) modulates its biological activities. The Journal of biological chemistry 277, 23658-23663 (2002).
93. J. Fullgrabe et al., The histone H4 lysine 16 acetyltransferase hMOF regulates the outcome of autophagy. Nature 500, 468-471 (2013).
94. A. Singh et al., Dysfunctional KEAP1-NRF2 interaction in non-small-cell lung cancer. PLoS medicine 3, e420 (2006).
95. M. Uhlen et al., Proteomics. Tissue-based map of the human proteome. Science (New York, N.Y.) 347, 1260419 (2015).
96. N. Rocha et al., Cholesterol sensor ORP1L contacts the ER protein VAP to control Rab7-RILP-p150 Glued and late endosome positioning. The Journal of cell biology 185, 1209-1225 (2009).
97. P. Paul et al., A Genome-wide multidimensional RNAi screen reveals pathways controlling MHC class II antigen presentation. Cell 145, 268-283 (2011).

Chapter 8:
Old drugs, novel ways out: drug resistance towards cytotoxic chemotherapeutics

Ruud H Wijdeven[1,4], Baoxu Pang[2,4], Yehuda Assaraf[3], and Jacques Neefjes[1]

[1] Division of Cell Biology, The Netherlands Cancer Institute, Plesmanlaan 121, 1066CX Amsterdam, the Netherlands, and Department of Chemical Immunology, LUMC, Leiden;
[2] Department of Genetics, School of Medicine, Stanford University, Stanford, California 94305, USA;
[3] The Fred Wyszkowski Cancer Research Laboratory, Department of Biology, Technion-Israel Institute of Technology, Haifa, Israel.
[4] These authors contributed equally to this work.

Drug Resistance Updates 28, 65-81

Abstract

Efficacy of chemotherapy in the treatment of malignancies is often hampered by drug resistance arising in the tumor. Understanding the molecular basis of resistance and translating this knowledge into personalized treatment decisions can enhance therapeutic and even curative outcome. Over the years, multiple drug resistance mechanisms have been identified that enable tumors to cope with the damage instigated by a specific drug or group of drugs. Here we provide an overview of the molecular pathways leading to resistance against conventional anti-cancer drugs, with emphasis on the utility of these pathways for rational selection of treatments for individual cancer patients. We further complement the review by discussing the pitfalls and difficulties in translating these findings into novel treatment strategies.

Introduction

Conventional chemotherapy is a major arm of anti-cancer therapy, but its effectiveness is often hampered by intrinsic, as well as acquired drug resistance (1-3). Understanding the resistance mechanisms for the different chemotherapeutic agents is crucial to develop better treatment strategies, ideally leading to a personalized drug regimen for better treatment responses, as well as preventing treatment with ineffective drugs (4, 5). Over the years ample evidence has delineated a multitude of drug resistance mechanisms, both general multi-drug resistance factors and factors specific for one (class of) drugs. Most of these mechanisms were initially discovered in tumor cell lines, and some have subsequently been validated in a clinical setting. Yet, few, if any, factors are actually used in the clinic as prognostic markers to select the appropriate individual cancer patient's treatment regimen for conventional chemotherapy.

On the other hand, personalized medicine is used successfully for targeted drugs. The evolution of genomic, proteomic and screening tools has yielded extensive knowledge about the molecular basis driving growth of individual tumors. Based on this information, drugs have been developed that specifically target a protein or pathway that is activated in the tumor. These are often activated kinases, like EGFR in lung cancer, BRAF in melanoma and FLT3 in AML patients (6, 7). Alternatively, targeted drugs instigate cytotoxic activity specifically in the context of a tumor-specific mutation, a concept known as synthetic lethality. This is exemplified by the usage of PARP-inhibitors for BRCA1/BRCA2 mutant tumors (8). These targeted drugs often present limited side effects compared to conventional chemotherapeutics and are effective during the initial responses. Unfortunately however, genomic instability and consequent tumor heterogeneity often allows cells to acquire drug resistance, by mutations in the drug target or activation of alternative signaling pathways, ultimately leading to ineffective treatment and poor outcome (9, 10).

Though conventional chemotherapeutic drugs also include antitumor agents with a molecularly defined target (like the antifolates) (3), most drugs target essential cellular systems that cannot be bypassed by the tumor. This does not imply that conventional chemotherapeutic drugs are spared from drug resistance, but merely that drug resistance is often multifactorial. Given the strong untoward side effects associated with most chemotherapeutics, drug resistance not only limits the therapeutic efficacy but also exposes patients to unnecessary toxicity in healthy tissues.

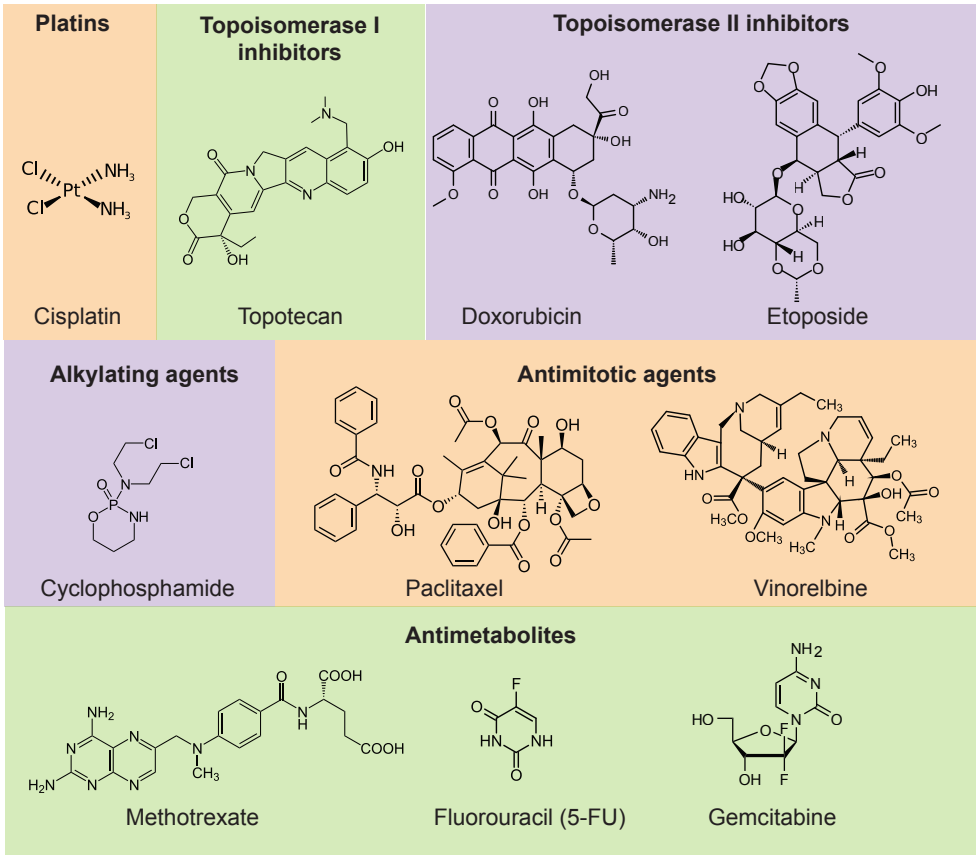


Figure 1: Chemical structures of members of the different classes of chemotherapeutics. *Six different chemotherapy classes are distinguished, some of which are divided into several subclasses. For every subclass, the structure of the most commonly used analogue is shown.*

Resistance mechanisms towards the different chemotherapeutic classes (Figure 1) have been extensively studied, both in tumor cell lines and in mouse models. Major mechanisms include enhanced drug efflux by multidrug transporters of the ABC superfamily, chemical modifications to convert drugs into non-effective metabolites, down-regulation of the major drug target, or bypassing the inhibited pathway (Figure 2). Only a few of these mechanisms have been shown to be operational outside the laboratory setting (i.e. in patients) and the translation of this fundamental knowledge into clinical practice has not been very successful. However, the recent sequencing of cancer genomes, as well as the discovery of novel molecular mechanisms of drug resistance, might spur the identification and validation of clinically relevant resistance mechanisms, yielding a better framework for implementing personalized treatment regimens.

In this review, we summarize the current challenges for personalized cancer medicine and provide an overview of the resistance modalities employed by tumors towards the different classes of anti-cancer drugs, with emphasis on novel, as well as clinically validated mechanisms.

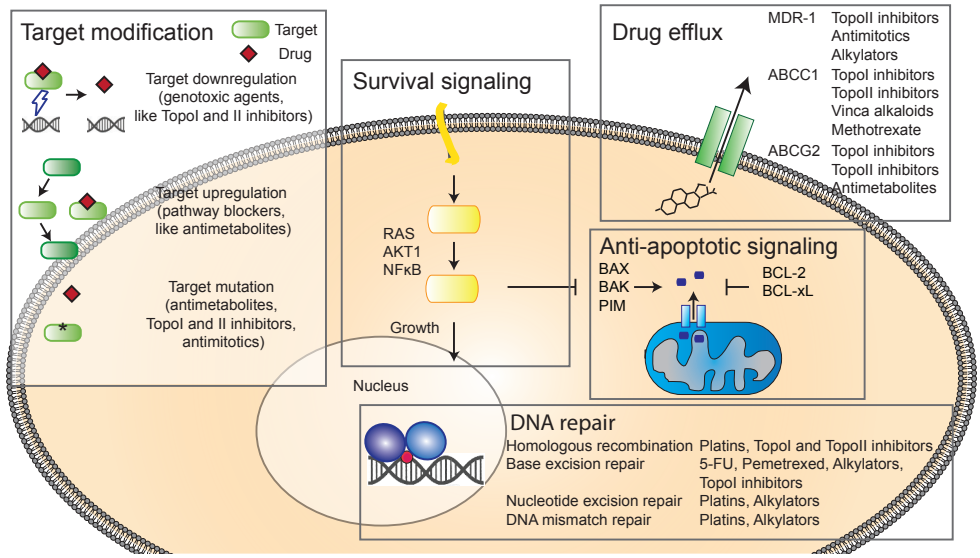


Figure 2: Common cell-intrinsic resistance mechanisms to chemotherapeutics. *Cancer cells can become generally resistant to chemotherapeutics by inhibiting the apoptotic pathway or constitutive activation of growth signaling pathways, which also inhibit apoptosis. Alternatively, the expression of drug transporters is upregulated, leading to resistance to a subset of drugs (as indicated). Cells also activate DNA damage repair pathways to cope with genotoxic stress induced by several chemotherapeutics. To avoid effective target inhibition, cells can mutate the drug target, upregulate its expression (in case of pathways blockers, as to prevent full inhibition of the total enzyme pool), or downregulate its expression (for genotoxic agents, to prevent harmful targeting by the drug).*

Challenges for predicting patient chemosensitivity

Applying personalized cancer treatment with conventional chemotherapeutics requires an accurate prediction of tumor sensitivity towards the different approved antitumor drugs. Given the varying responses observed in the clinic, molecular determinants that mediate chemoresistance should be at hand in order to allow selection of the appropriate individual drugs. Identifying and implementing these resistance factors have thus far been hampered by several issues, ranging from tumor heterogeneity to the difficulty of translating drug resistance mechanisms into reliable diagnostics and therapeutics. Overcoming or bypassing these impediments will provide a major headway towards personalized selection of the most efficacious drug(s) for optimal treatment as well as the lowest side effects.

The general types of chemoresistance

Generally speaking, drug resistance can be intrinsic (i.e. primary or inherent) or acquired during and/or following treatment. Intrinsic drug resistance arises when the tumor inherently contains traits that enable it to cope with the damage inflicted by the drug; for example, increased anti-apoptotic signaling or mutations in the DNA-damage response pathway. These characteristics are often instrumental in the establishment of the tumor and are intimately associated with its general survival. Since the therapeutic window of anti-cancer drugs is usually narrow, a relatively small resistance effect may render drugs therapeutically ineffective. Yet, decipher-

ing the molecular basis of such drug resistance mechanisms warrants tailored drug selection based on the characteristics of the tumor. This is more difficult in the case of acquired chemoresistance, where tumors acquire drug resistance during treatment, often by rewiring signaling pathways or epigenetic alterations that change the transcriptional landscape. Alternatively, resistance arises from the outgrowth of a preexisting subpopulation of tumor cells that already harbored mutations or altered expression of resistance genes, which is inherent to the heterogeneous nature of the tumor (11). These infrequent mutations can sometimes be detected using deep sequencing (10), while complex gene signatures may be able to predict acquired resistance (10, 12).
From a molecular perspective, drug resistance can be based on expression (quantitative alterations) and/or based on mutations (qualitative alterations). Mutation-based mechanisms of chemoresistance are often more stable, especially when these are cancer driver mutations essential for the growth of the tumor, or when they are somatic. Cells can also become drug resistant by up- or downregulating expression of relevant genes or pathways, expanding the inherent variation within the tumor and fueling resistance development (13). Given the heterogeneity of gene expression, selection on the basis of mutations seems most feasible as they are more stable and relatively homogeneous.

Multi-drug treatments

Whilst modeling of resistance towards a single drug seems feasible, most cancer patients are actually treated with drug combinations. In fact, combinatorial drug treatments constitute the treatment of choice in cancer therapy and yield better responses (14, 15). The concept of multi-drug treatments is that the tumor is simultaneously attacked from different angles for more effective eradication of the tumor and –in addition- preventing the occurrence of drug resistance phenomena. However, the contribution of each individual drug to the combined treatment effect is often unclear, which hampers linking drug resistance mechanisms observed in the clinic to a well-defined drug. Furthermore, in vivo validation of mechanisms identified in the lab is harder, since clinical effects can arise from drug-drug interactions in such a multi-drug chemotherapeutic cocktail. It is therefore often necessary to extrapolate the interactions between drugs and their individual resistance mechanisms based on data from mouse models or tumor cell lines to pin-point the mechanisms underlying resistance to drug-cocktails in cancer patients (16). This argues for more laboratory studies combining several anti-cancer drugs to model resistance to drug combinations that better reflect the genuine clinical treatment.

Tissue specific resistance

The efficacy of different chemotherapeutics varies markedly per tumor type. Whilst these differences can be partly attributed to different pharmacokinetics and pharmacodynamics (such as drug uptake by the tissue and tumor metabolism, reviewed in (17)), the genetic make-up of the tissue of origin affects many of the tumor's properties, among which is its drug sensitivity. As an extreme example of this, patients with hepatocellular carcinomas generally do not benefit from any type of chemotherapy, due to the high expression of multidrug efflux transporters, oxidative stress proteins

and metabolic enzymes, which is physiologically intrinsic to this tissue, the liver (18). Other tumors display more specific drug resistance or sensitivity profiles, for example testicular cancers are extremely sensitive to cisplatin, in part due to their wild-type p53 status (19).

While these are simple concepts, they cannot be employed by default as clinical oncologists have often observed excellent responses to such 'ineffective' drugs in a certain subset of patients. Hence, the inevitable question is; what are the molecular traits that define these subsets of patients or their tumors? Sometimes the underlying molecular basis can be well defined. For example, the EGFR inhibitor Cetuximab has only a small overall survival benefit for lung cancer patients, but it is effective on patients with lung tumors overexpressing EGFR (20). The effect on this small subgroup of patients is masked by the overall lung cancer population and would not have been noticed without phenotyping the individual patient. Retrospective studies with recently identified biomarkers on tumor tissues from responder versus non-responder patients could be useful in identifying subgroups of patients that might benefit from well-defined chemotherapeutics. One example is the use of platinum compounds in breast cancer therapy. Whereas cisplatin is hardly used in the clinic for the treatment of breast cancer due to a lack of activity, recent data have demonstrated that this may be different for breast tumors with mutations in BRCA1 or high levels of p63 (21, 22). This subgroup of breast cancer patients would thus favorably respond to a drug that is not generally used for this type of tumors. Similarly, it was recently shown in the laboratory setting that colon cancers harboring a BRAF mutant phenotype are very sensitive to vinorelbine, whereas overall, colon cancers are known to be resistant to this anti-microtubule agent (23). These examples illustrate that individual cancer patient profiling may facilitate stratification of patient subgroups that may respond to a well-defined anti-cancer drug, which has been omitted for therapy for the entire group of patients in that tumor type. Considering not only tissue types but also individual tumors may be a better and broader approach, yielding alternative treatment options for patients on the basis of traditional chemotherapy.

Clinical detection methods and validation of potential biomarkers

Most biomarkers identified in the lab for predicting chemotherapy response fail to be validated in the clinical setting. There are various reasons for this disparity. Firstly, tumor cell cultures markedly differ from the clinical in vivo setting, which includes the tumor microenvironment, drug bioavailability, pharmacokinetics and pharmacodynamics. While drug sensitivity screens are usually performed upon 48-72 hrs of continuous drug exposure on tissue cultured tumor cells, the pharmacokinetics of drugs in patients differ considerably (many compounds have half-lives of 4-8 hours). Secondly, it is difficult to establish and confirm a biomarker as being predictive of response to a given cytotoxic drug. This requires a randomized trial with patients treated with the single drug, as well as a control population that is untreated or treated with a different drug. Thirdly, potential biomarkers are often instrumental to the survival of the tumor, blurring the analysis. This is exemplified by βIII-tubulin, a subunit of the microtubules, which was initially discovered as a predictor for response to paclitaxel in NSCLC and ovarian cancer. Later findings indicated that βIII-tubulin expression actually acts as a prognostic factor independent of treatment, by promot-

ing cell survival in general (reviewed in (24)). These data indicate that when using a non-randomized trial, it is important to analyze the response to chemotherapy, rather than survival after treatment, to investigate the effect of a potential predictive biomarker for treatment outcome.
When it can be established that a well-defined genetic alteration allows the prediction of treatment responses to a defined drug, these can be used in a diagnostic setting as part of the treatment protocol for the patient. These should be robust methods of the detection with ideally a binary outcome (i.e. YES or NO predicted response), since decreased sensitivity is difficult to comprehend. Qualitative differences in a tumor, such as mutations, deletions and SNPs are mostly determined at the DNA level with little variation and allow for binary outcomes. Quantitative differences can be detected with immunohistochemistry, or at the RNA level using deep-sequencing, which requires a cut-off for expression to allow binary decisions. Given the complexity of anticancer drug resistance, it is likely that multiple resistance markers need to be combined in order to form a bona fide signature, hence arguing in favor of high-throughput measurements. The advantage of these drug resistance biomarker combinations is that the excess of obtained data could be correlated with the clinical responses of cancer patients to identify novel biomarkers predicting response. Understanding the relevant mechanisms may then de-convolute these data sets to define a condensed set of biomarkers for more easy prediction of treatment responses towards conventional anti-cancer drugs.

General drug resistance mechanisms

Influx and efflux drug transporters

The simplest way for a cancer cell to become resistant is by restricting intracellular drug accumulation. This can be achieved by either inhibiting import or by accelerating drug export. How drugs enter cells is not always clear. The general idea is that hydrophobic anticancer drugs mostly enter cells by passive diffusion across the membrane, but various transporters have been identified that can transport drugs into cells. Cisplatin can be imported by the VRAC transporter whose physiological function is to regulate anion transport (25), the anti-folates methotrexate and pemetrexed use specific influx transporters including the reduced folate carrier (RFC/SLC19A1) as well as the proton-coupled folate transporter (PCFT; SLC46A1) (26-28), and the DNA base analogue gemcitabine uses nucleoside transporters for cell entry (29). How anthracyclines and other DNA damaging drugs enter cells is not entirely clear at this point, though studies have shown a role for flip-flop based diffusion of anthracyclines as a mode of entry into cells (30, 31). Of note, anti-cancer drugs may compete with endogenous substrates to use these influx transporters, and such competition may also affect cell growth when essential cellular building blocks are not efficiently taken up by cells. This could be a secondary mechanism of action for some anti-cancer drugs.
Mechanisms of ATP-driven drug export have been extensively studied. Many drugs can be extruded from cells by members of the ATP-binding cassette (ABC) transporter superfamily (see Figure 2). These efficient drug efflux pumps display promiscuous substrate specificity and are hence termed multidrug resistance (MDR) proteins. Upregulation of ABCB1 (also named P-gp or MDR1), the best studied member of this

ABC superfamily, markedly decreases the intracellular accumulation of a multitude of drugs, including taxanes, anthracyclines epipodophylotoxins, Vinca alkaloids and actinomycin D, as well as lipophilic antifolates (1, 32, 33), leading to multidrug resistance (MDR). Other extensively studied members of the ABC transporter superfamily include ABCC1 (MRP1) and ABCG2 (BCRP), which have partially overlapping drug substrate specificities (reviewed in (34)). Transporters are highly expressed in the liver, the blood-brain barrier, the intestine and several endothelial tissues and are believed to be one of the reasons why hepatocellular carcinomas respond poorly to chemotherapy and why chemotherapy of brain tumors is often inefficient (35). Also, cancer cells can upregulate the expression of these ATP-driven drug exporters in response to drug exposure. Due to the collection of anti-cancer drugs that are sensitive to MDR1 expression, several transport inhibitors have been developed that specifically target MDR1 and other ABC transporter family members. While strongly linked to resistance in vitro and in mouse models, the clinical correlation between MDR1 expression and drug resistance is relatively poor, as is the clinical benefit from the use of MDR1 transport inhibitors (34, 36). This could be due to the redundancy of the different transporters, or because the drug dose during treatment is so high that ABC transporter activity contributes only marginally to intracellular drug accumulation.
While it is likely that ABC transporters and especially MDR1 contribute to MDR, expression of these drug pump proteins cannot be directly correlated to the clinical effect of drug resistance. Probably, the combination of impaired drug uptake and accelerated drug export will generate a more convincing clinical drug resistance case, but these data are yet unavailable.

Alterations in the anti-apoptotic pathway

The most common mechanism for cancer cells to undergo cell death in response to chemotherapy is via apoptosis. This programmed cell death (PCD) response is induced by an array of stimuli that eventually leads to activation of caspases that execute the PCD program (37). Many chemotherapeutic drugs instigate DNA damage that is sensed by p53, which subsequently provokes the BCL-2 family of pro-apoptotic and anti-apoptotic proteins. Induction of apoptosis results from an alteration in the balance towards pro-apoptotic factors, leading to mitochondrial membrane permeabilization and release of cytochrome c, hereby activating caspases that execute apoptosis (38). Due to their tumor promoting nature, genetic mutations or alterations that block apoptosis are frequently observed in various cancers (39), suggesting that these tumors are intrinsically more resistant to anti-cancer drugs. Indeed, cells overexpressing the anti-apoptotic BCL-2 protein are resistant to various chemotherapeutics (40). Especially in hematopoietic malignancies, which are exquisitely sensitive to apoptosis due to their immunological origin, a strong correlation between apoptotic capacity and response to chemotherapy has been observed (41). This has sparked strategies for patient selection on the basis of apoptotic protein expression, as well as the development of inhibitors for BCL-2 members, to be used as monotherapy or to increase the efficacy of chemotherapy (reviewed in (42)). Unfortunately, thus far, none of these inhibitors is clinically used due to severe side effects, but the development of more specific inhibitors might avoid this undesired toxicity (43). In solid

tumor types, some apoptotic factors correlate with response to chemotherapy as well. For example, in triple-negative breast cancer (TNBC), low expression of BCL-2 is associated with a better response to chemotherapy (44, 45). However, overall, the effects are less pronounced than in hematopoietic tumors. This could be explained by other BCL members that are functional in these tumors or because solid tumors have a different balance of apoptotic factors (46).
Cell death can also proceed via other pathways, like necroptosis, or via immunogenic cell death, or cells can become senescent, thereby not contributing to tumor growth (47, 48). The contribution of immunogenic cell death to treatment is of interest as chemotherapy responses are coupled to immune responses against tumors. As a result, the primed immune system can recognize tumor mutations and clear the tumor by the activity of the adaptive immune system (see Figure 3). For example, doxorubicin can trigger CD73 and A2A adenosine receptor signaling to activate the immune system (49), thereby stimulating a systemic response against the tumor, at least in mouse models. This type of cell death is not induced by all chemotherapeutics and the molecular basis is still being studied in more detail. Yet, the contribution of the immune system to tumor eradication following chemotherapy could be a great example for achieving two effects in a single drug maneuver.

Cell growth signaling pathways

In general, cancer is linked to systematic activation of growth signaling pathways and de-regulation of cell-cycle checkpoints (7, 39). These characteristics also enable tumor cells to counteract the cytotoxic effects inflicted by chemotherapeutics, by providing pro-survival signals and decreasing sensitivity to DNA damage. Combining classical chemotherapy with drugs that inhibit signaling pathways which promote tumor cell growth could alleviate the negative impact of sustained cell-signaling. Indeed, this concept is applied to a wide spectrum of tumors harboring activated growth receptors. For example, HER2-positive breast cancers and EGFR-mutated colon cancers are treated with a combination of receptor antagonists and conventional chemotherapeutics (50, 51). Clinical benefit is observed for many of these therapies combining novel drugs targeting signaling pathways with conventional chemotherapeutics. If drug resistance to the targeted therapy arises via signaling bypass, combinations of drugs that also target the signaling pathways bypass may prevent drug resistance, as illustrated for the addition of TGF-βR inhibitors to the EGFR inhibitor regimen (52).
Due to the robust nature of drug resistance provoked by these growth signals, activation of most signaling pathways acts as a general negative prognostic factor for response to chemotherapy. However, this picture is more complex, as signaling can also be required for optimal chemotherapy efficacy. This is perhaps best illustrated by NFκB, a master transcription factor for pro-survival genes and pro-inflammatory cytokines, that is activated in a variety of tumors and is actively linked to chemoresistance by inhibiting apoptosis (53). Although most patients with tumors containing active NFκB poorly respond to chemotherapy, recent studies demonstrated that under conditions where apoptosis is already inhibited, NFκB promotes senescence and is actually a positive prognostic factor for the response to the alkylating agent cyclophosphamide (54). Furthermore, NFκB is involved in activation of the immune

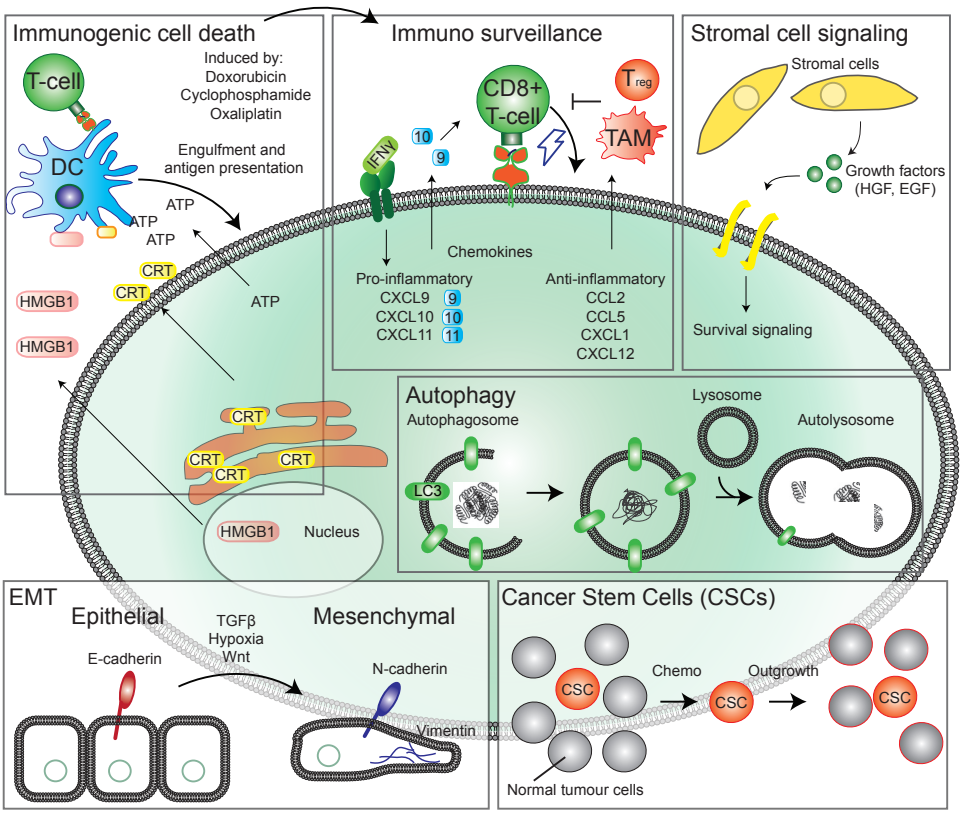


Figure 3: Overview of common cell-extrinsic or systemic mechanisms of drug resistance. *The tumor microenvironment can regulate resistance to chemotherapeutics via several mechanisms. Chemotherapeutics can induce immunogenic cell death, where dying cells secrete ATP and HMGB1, and present ER-resident protein calreticulin (CRT) at their cell surface. These signals are recognized by dendritic cells, which subsequently endocytose fragments of the dying cell and present their antigens by MHC-I molecules to CD8+ T-cells. This activates the T-cells, which can kill other tumor cells presenting the same antigens (immuno-surveillance). These T-cells can be recruited by IFNγ-induced chemokine expression and inhibited by tumor-associated macrophages (TAMs) or regulatory T-cells (Tregs), which can in turn be recruited by anti-inflammatory chemokine expression by the tumor. Alternatively, the tumor-microenvironment promotes drug resistance by secretion of growth factors that in turn activate survival signals in the tumor. Upregulation of autophagy by intrinsic or extrinsic factors also promotes survival of tumor cells, by sequestering damaged proteins and organelles. Drug sensitivity also depends on the differentiation status of the cell. Cells that have undergone epithelial-to-mesenchymal transition (EMT) or cancer stem cells (CSCs), are generally more resistant to chemotherapeutics. Some of these slow-cycling tumor cells can grow out to reform the tumor.*

system upon cell death (55), arguing that drugs that use an immune-system component following activation of the immunogenic cell death pathway are more effective in the presence of active NFκB. The balance of direct killing by chemotherapy versus indirect mechanisms utilizing the immune system is poorly understood, but can be important in the case of so-called immunogenic tumors like melanoma, lung and bladder cancer (56). A poor response to chemotherapy may then be compensated by an accelerated anti-tumor immune response that suffices to achieve the desired clinical effect, namely systemic eradication of the tumor.

Molecular resistance mechanisms to anticancer drugs

Platinum-containing drugs

One of the benchmark treatments for many malignancies are platinum-containing drugs, the most commonly used being cis-diaminedichloroplatinum(II) (CDDP or cisplatin, for structure see Figure 1). This important class of antitumor drugs, which also includes the analogs carboplatin and oxaliplatin, relies on a platinum at the core of the structure which, upon activation in the cytosol (via Cl- substitution for OH-, reviewed in (57)), reacts with several cellular structures, most notably guanine nucleobases, generating inter- and intra-strand DNA cross-links. These cross-links are believed to be the primary mode of cytotoxicity, leading to a block in cell growth, senescence and apoptosis (58). Tumor cells are more susceptible to cisplatin or its variants because they grow faster and can harbor mutations in the DNA repair machinery, rendering them less efficient in removing cross-links and thus inducing cell death.

Platinumdrug resistance

Although platinum drugs are effective in cancer therapy, resistance to these drugs is commonly observed (59-62). Most described resistance factors are related to DNA damage response (DDR; Table 1), supporting the notion that this is the main mode of action of cisplatin. However, several factors have been identified that act at other steps in the cisplatin action cycle and also contribute to drug resistance, as discussed below.

Mechanisms of DNA repair

Cisplatin induced inter- or intra-strand DNA crosslinks are mainly repaired by Nucleotide Excision Repair (NER), which is orchestrated by a multi-subunit complex of about 20 proteins, including Excision Repair Cross-complementation group 1 (ERCC1). Loss of NER increases the sensitivity of cells to cisplatin, but given the complex nature of this pathway, it is difficult to determine the limiting factor that effectively governs NER activity. In several tissues, ERCC1 is the limiting factor and its reduced expression is correlated with increased progression free survival (PFS) and overall survival (OS) after cisplatin treatment; however, a direct role of ERCC1 in the clinical response to cisplatin has not been demonstrated (reviewed in (63)). Inactivating or destabilizing mutations in any of the NER subunits also leads to increased sensitivity, as shown for mutations in ERCC2 in bladder cancer (64), XPG in NSCLC (65), ERCC1 in several tumor types (66, 67) and mutations in several NER proteins in a subset of epithelial ovarian cancers (68). Given the complexity of the NER pathway, other studies have measured DNA repair activity in peripheral blood cells as a surrogate for total NER activity and correlated that with the response of NSCLC to cisplatin (69). Collectively, these studies suggest an association between NER and the cellular sensitivity to cisplatin and its variants, but have not yielded a singular biomarker for selecting non-responding or responding patients.

Alternatively, DNA breaks are repaired by the Mismatch Repair machinery (MMR), which is also implicated in cisplatin resistance, albeit to a lesser extent. In vitro studies showed that cells deficient in MMR proteins, such as MSH2, are more resistant to cisplatin and carboplatin (but surprisingly not to oxaliplatin), likely because MMR members block efficient error-free repair of inter-strand crosslinks (70, 71). This was

Table 1: Summary of resistance mechanisms towards the different chemotherapeutic classes.

Drug class / gene	Mechanism	Mutation / expression	Effect	Occurrence	Impact	Prognostic factor[1]	Linked to response[2]	Predictive factor[3]
Platinum compounds								
ERCC1/2	Nucleotide Excision Repair	low expression / mutation	sensitizing	frequent	medium	yes	yes	yes, in NSCLC (Kamal et al., 2010)
BRCA1/2	Homologous Recombination	inactivating mutations	sensitizing	frequent	high	yes	yes	
MSH2	DNA mismatch repair	low expression	sensitizing	na	low	yes		yes, in NSCLC (Kamal et al., 2010)
LRRC8d	Imports cisplatin and carboplatin	low expression	resistance	na	low	yes		
Microtubule drugs								
Stathmin	Destabilizes microtubules	upregulation / activation	resistance	na	medium	yes	yes	
Syk	Destabilizes microtubules	upregulation	resistance	upregulated by treatment	medium		yes	
TEKT4	Functional part of microtubules	SNP	resistance	na	medium /low	yes		
CLIP-170	Stabilizes microtubules	low expression	resistance	na	low		yes	
Tau	Competititve binding with taxol	high expression	resistance	na	medium	yes	yes	
Methotrexate								
RCF	importer of MTX	low expression / mutation	resistance	na	high	yes	yes	
DHFR	Functional target	upregulation	resistance	na	high	yes	yes	
FPGS	polyglutamylates MTX for intracellular retention	downregulation / SNPs	resistance	na	low	yes		
Pemetrexed								
TS	Functional target	upregulation	resistance	na	high	yes	yes	yes, in mesothelioma (Righi et al., 2010)
FPGS	polyglutamylates PMX for intracellular retention	downregulation / SNPs	resistance	na	medium /low	yes		
dUTPase	Decreases dUTP pool to alleviate toxicity	upregulation	resistance	na	medium /low			
UDG	Removes misincorporated dUTP	low expression	sensitivity	na	medium /low			
Fluorouracil								
TS	Functional target	upregulation	resistance (most tumours, see text)	na	high	yes	yes	
dUTPase	Decreases dUTP pool to alleviate toxicity	upregulation	resistance	na	medium /low	yes		
DPD	Inactivation of 5-FU by enzymatic conversion	upregulation	resistance	na	low	yes		

Gemcitabine								
hENT1	Importer for gemcitabine	downregulation	resistance	na	high/ medium	yes	yes	yes, in pancreatic cancer (Greenhalf et al., 2014)
RRM1/2	Involved in formation of cytidine	upregulation	resistance	na	medium	yes		
dCK	Converts gemcitabine into active form	downregulation	resistance	na	medium	yes		
Topoisomerase I inhibitors								
Topoisomerase I	Functional target	low expression	resistance	na	medium	yes	yes	
Topoisomerase II inhibitors								
Topoisomerase II	Functional target	amplified	sensitizing	co-amplified with HER2 in breast tumours	low	yes	yes, in some cases	
SWI/SNF complex	Loading and activity of TopoII	Inactivating mutations	resistance	frequently deleted in many tumours	medium		yes	
BRCA1/2	Essential for Homologous Recombination	inactivating mutations	sensitizing	frequently mutated in multiple tumours	high	yes	yes	
Alkylating agents								
CYP2B6	enzymatic activation in the liver	SNP	Less drug exposure	frequent	medium	yes	yes	yes, in leukemia (Johnson et al., 2013)
MGMT	DNA de-alkylation	upregulation	resistance	na	low	yes		
XRCC1	Base excision repair	SNP	resistance	frequent	medium /low	yes		

Abbreviations: na. not applicable because the cohort was analyzed by division into high/low expression. [1] Factors linked to disease-free survival or progression free-survival after treatment with the respective drug. [2] Factors linked to the response towards the drug. [3] Factors for which randomized trials have demonstrated an effect specifically in the patient group treated with the indicated drug. References
W. Greenhalf, P. Ghaneh et al. Pancreatic cancer hENT1 expression and survival from gemcitabine in patients from the ESPAC-3 trial, Journal of the National Cancer Institute 106 (2014), p. djt347.
*G.G. Johnson, K. Lin et al. CYP2B6*6 is an independent determinant of inferior response to fludarabine plus cyclophosphamide in chronic lymphocytic leukemia, Blood 122 (2013), pp. 4253-4258.*
N.S. Kamal, J.C. Soria et al. MutS homologue 2 and the long-term benefit of adjuvant chemotherapy in lung cancer, Clinical cancer research : an official journal of the American Association for Cancer Research 16 (2010), pp. 1206-1215.
L. Righi, M.G. Papotti et al. Thymidylate synthase but not excision repair cross-complementation group 1 tumor expression predicts outcome in patients with malignant pleural mesothelioma treated with pemetrexed-based chemotherapy, Journal of clinical oncology : official journal of the American Society of Clinical Oncology 28 (2010), pp. 1534-1539.

further corroborated in a large NSCLC cohort study demonstrating a correlation between low MSH2 levels and overall survival after cisplatin-based therapy (72). Why oxaliplatin deviated from its platinum family members is unclear, as this drug inflicts similar DNA inter- and intra-strand cross-links.

The third machinery to repair DNA crosslinks is Homologous Recombination (HR), which repairs double-strand breaks (DSBs) arising from inter-strand cross-links. Tumors deficient in HR are highly sensitive to platinum compounds and two HR genes, BRCA1 and BRCA2, are frequently inactivated in breast, ovarian and pancreatic

tumors, either somatic or during the course of treatment. These tumors are very sensitive to cisplatin but often restore HR via a secondary mutation in BRCA1/2 which re-activates the gene (9, 73). Recently, the DNA/RNA helicase SLFN11 was identified as a negative regulator of HR (74) and its loss is associated with cisplatin resistance, as well as topoisomerase (75) and PARP inhibitors (76). Together, these data indicate that patients with defective HR respond favorably to cisplatin, as well as to other drugs that rely on DSB repair. A defective HR is often observed in tumors and may be a useful biomarker for treatment stratification (77).

Alternative mechanisms of drug resistance

Platinum-based drugs must first enter tumor cells and accumulate in sufficient concentrations to target their macromolecular substrate (DNA). Reduced intracellular accumulation has been observed in several cisplatin-resistant cell lines and yielded several uptake and export receptors. Although a substantial part of cisplatin uptake appears to be via passive membrane diffusion (Ivy and Kaplan, 2013), uptake is also facilitated by the volume regulated anion channel (VRAC) subunits LRRC8a and LRRC8d (Planells-Cases et al., 2015), and their loss induces resistance to both cisplatin and carboplatin. Unlike many other anti-cancer drugs, export of cisplatin or its variants from cells is not mediated by P-gp, but probably by MRP2/ABCC2 (Borst et al., 2000), since MRP2 overexpression induces resistance to cisplatin. Other drug resistance determinants that reduce the amount of active platinum-based drugs that form DNA adducts are p22phox, which prevents translocation of cisplatin to the nucleus (Hung et al., 2015), and enzymes that produce nucleophilic species such as GSH, which convert hydroxylated cisplatin into an inactive glutathione-modified molecule (Galluzzi et al., 2012).

Other mechanisms contributing to cisplatin resistance that have recently been uncovered include downregulation of apoptotic factor FHIT (78), which is frequently mutated in tumors (79), upregulation of cell cycle regulator Dyrk1B (80), as well as activation of several signaling pathways, including p38MAPK and AKT1 (reviewed in (81)); though, due to their general nature, these factors are likely involved in resistance to other types of chemotherapeutics as well. While other pathways upstream or downstream of the DDR are also involved in cisplatin sensitivity, their relative contribution seems minor.

Topoisomerase I inhibitors

While platinum drugs directly target DNA, other chemotherapeutics inflict DNA damage by targeting enzymes that unwind DNA. These enzymes are topoisomerase I and topoisomerase II and inhibitors of both enzymes are major drug classes in cancer therapeutics. In normal physiology, topoisomerases are important to resolve topological problems that cells encounter during DNA replication, DNA repair, transcription and chromosomal segregation (Berger et al., 1996; Nitiss, 2009a). Topoisomerase I (Topo I) resolves DNA supercoiling by introducing single-strand breaks, allowing uncoiling followed by re-ligation of the introduced break (Stewart et al., 1998). Several drugs have been developed that target Topo I, with camptothecin and its analogues topotecan and irinotecan being best known in clinical practice (Hsiang et al., 1985; Pommier, 2013). These drugs bind and trap the cleavable complex of Topo I before re-ligation occurs, thereby leading to single-strand DNA breaks. At

lower doses, toxicity of Topo I inhibitors are replication dependent (Holm et al., 1989; Horwitz and Horwitz, 1973), and DNA double-strand breaks can be induced when replication forks collide with the drug-stabilized Topo I complex (Hsiang et al., 1989). In addition, DNA damage is generated during transcription, as Topo I is involved in transcription elongation, when DNA is in an uncoiled, open configuration (Wang, 2002). Since Topo I and Topo II are involved in similar cellular pathways during DNA replication and transcription, drugs targeting these different topoisomerases induce similar patterns of DNA damage at defined regions in the genome (Pang et al., 2015). Given the partial redundancy between both topoisomerases, sequential treatment with Topo I and Topo II inhibitors is currently tested as a strategy to prevent resistance by upregulation of the other topoisomerase (82).

Resistance to topoisomerase I inhibitors

One of the major mechanisms of resistance to Topo I drugs is drug efflux, predominantly via the multidrug efflux transporter ABCG2 (Schellens et al., 2000; Tiwari et al., 2013). Topo I is the only known target of camptothecin drugs, and most resistance mechanisms are centered on Topo I-dependent DNA break formation and repair. Multiple studies have shown that reduced expression of Topo I renders tumor cells resistant to treatment (Burgess et al., 2008; Horisberger et al., 2009; Ikeguchi et al., 2011). This suggests that determining Topo I expression levels could be a biomarker for predicting patients' drug response. In addition, Topo I mutations could confer resistance upon tumor cells to camptothecin (Pommier et al., 1999), though clinical correlations for this are still lacking. Modulators of Topo I activity also control sensitivity to camptothecins, as demonstrated for CK2. This kinase phosphorylates and activates Topo I and its loss desensitizes cells to camptothecin (Bandyopadhyay and Gjerset, 2011; Bandyopadhyay et al., 2012).

Alternatively, resistance can arise from alterations in the DDR pathway, leading to increased DNA repair or failure to induce apoptosis. The main pathway for cells to repair Topo I inhibitor-dependent single-stranded DNA damage is the DNA base repair pathway, involving PARP1, XRCC1, TDP1, among others (83). Indeed, overexpression of XRCC1 promotes resistance to camptothecin (84), whereas TDP1 depletion sensitizes cells (85). Furthermore, PARP1 inhibition was found to synergize with inhibition of Topo I (86). Repair of DNA DSBs induced by camptothecins is orchestrated by HR (87), as DSBs occur in S-phase during replication, and cells deficient in HR are more sensitive to Topo I inhibitors.

All mechanisms described herein await clinical validation, which is complicated by the fact that Topo I inhibitors are usually part of a multidrug regimen that also involves Topo II inhibitors or platinum drugs, which also rely on induction of DNA damage.

Topoisomerase II inhibitors

Like its counterpart, topoisomerase II inhibitors are an important class of chemotherapeutic agents. By introducing a DNA double-strand break, topoisomerase II unwinds the DNA to allow one DNA strand to pass another, followed by re-ligation of the broken strand. Topo II poisons block Topo II in its active form, when the transient DNA double-strand break is formed but before DNA ligation, yielding toxic DNA double-strand breaks. Since proliferating cells like cancer cells frequently have high levels of topoisomerase IIα (the most prevalent of the two isoforms) to adapt to more

active DNA replication and transcription (88, 89), cancer cells are supposedly more susceptible to inhibition by Topo II inhibitors than normal cells.
The best known class of Topo II inhibitors is the anthracycline family. Originally discovered as an antibiotic produced by Streptomyces bacteria, a striking anti-tumor activity was noticed for daunorubicin (Daun), which transformed its use into an anti-cancer drug. Subsequent mutagenesis of the daunorubicin-producing bacteria resulted in a superior analogue with minor chemical differences, named adriamycin (after the Adriatic Sea, only a few kilometers from where the producing strain was originally isolated) but later re-named doxorubicin (Doxo). Doxo is the most effective and broadly used member of the anthracycline family and it is used as a first line chemotherapeutic for a broad spectrum of cancers (90-93). Other structurally unrelated drugs have also been developed that target Topo II, among which Etoposide (Etop), a derivate of podophyllotoxin, is most frequently used in cancer chemotherapy. Interestingly, while Doxo and Etop share the same molecular target and induce DNA double-strand breaks in an almost identical manner, Doxo is more effective and has a broader anti-tumor spectrum (93). In fact, Doxo is used as monotherapy for some tumors (for instance breast cancer), whilst Etop is usually used in combination therapy. The difference between these drugs could be the consequence of a secondary effect of the anthracyclines; eviction of histones from the DNA (94, 95). Histone eviction by anthracyclines attenuates DNA repair by removal of histone H2AX, which is critical in the initiation of the DDR, thereby leading to prolonged DNA damage and enhanced p53 activation (96). Furthermore, histone eviction erases epigenetic marks based on histone modifications and alters the transcriptional landscape. Such effects disturb the normal cellular physiology and can also contribute to the cytotoxicity of this class of cytotoxic drugs. Different anthracycline drugs display selectivity for different histone modifications or chromatin structure, as Doxo and Daun prefer active chromatin regions marked by H3K4me3 and H3K36me3, whilst Acla (aclarubicin, an anthracycline that evicts histones but does not generate DNA breaks) also targets repressive chromatin regions decorated with H3K27me3 (96). Intercalation of Doxo into the DNA is sufficient to induce histone eviction and does not require active machinery, therefore identified resistance mechanisms against anthracyclines and etoposide are centered mostly around Topo II-mediated DNA break formation and repair (97).

Resistance to topoisomerase II poisons

The treatment of cancer patients with anthracyclines is limited by the cardiotoxic side effects that accumulate with increasing doses. This implies that many patients do not receive further treatment due to cardiotoxicity, whereas they still would have responded to the drug. Yet, patients can become resistant to Topo II poisons. The best studied resistance mechanism for both Doxo and Etop is drug efflux by the ABC transporter P-gp. Whereas in mice P-gp is certainly important in imparting Doxo resistance, its role in human cancer patients is less clear. Transport inhibitors of P-gp have not shown any clinical benefit for cancer patients treated with Doxo (34), suggesting that other mechanisms of resistance may be more prominent. Being a weak base that undergoes protonation in the highly acidic lumen of lysosomes, anthracyclines can also be sequestered in lysosomes (98-101), which effectively decreases nuclear drug exposure and efficacy. Lysosomal alkalinization achieved by treatment

with bafolimycin A1, which blocks vesicular ATPase, prevents this drug accumulation in lysosomes, restoring drug sensitivity (100).
Although Doxo is a Topo II inhibitor, the role of this enzyme in Doxo resistance is not unequivocal. Many reports have shown that in tissue cultured tumor cells or mouse models, decreased Topo II levels lead to Doxo resistance (102). Furthermore, clinical studies showed that HER2 amplified breast tumors with co-amplification of the neighboring Topo II gene are more sensitive to treatment with anthracyclines (103). However, in other tumor types, this correlation was not confirmed (104), suggesting that merely in the case of Topo II gene amplification there is a difference in sensitivity. In some cases, even tumor cells without detectable Topo IIα expression responded to Doxo (94). A potential explanation for this apparent discrepancy is the redundancy between Topo IIα and Topo IIβ, or alternatively additional regulators of Topo II activity are important determinants of Doxo sensitivity. The latter is supported by a recent genome-wide analysis of factors contributing to Doxo-resistance. This study identified the SWI/SNF complex, a chromatin remodeling complex that loads Topo II onto DNA and which is frequently mutated in cancer, as a factor mediating resistance to Doxo and Etop (97). Clinically, tumors with deletion or downregulation of this complex displayed an inferior response to Doxo-containing treatments, supporting the notion that factors controlling Topo II activity can influence sensitivity to Doxo. By using short incubation times with Doxo to recapitulate the clinical situation (mimicking the pharmacokinetics in patients), this screen also identified Keap1 and C9orf82/CAAP1 as factors involved in resistance to Topo II poisons. These respectively act by modulating Topo II poisoning and accelerating DNA repair. Other factors recently shown to be involved in resistance are regulators of homologous recombination (as for platinum-drugs and Topo I inhibitors), cell survival signaling, such as a pathway activating AKT1 that involves E2F7, Sphk1 and RacGAP1 (105, 106), DNA repair regulator FOXM1 (107) and inhibitor of apoptosis p57kip2 (108). Thus, resistance is analogous to other drug classes and centers around the control of DNA damage and subsequent repair.
Drug resistance to Topo II inhibitors could also be potentially averted by the use of different anthracycline analogues. For example, Acla does not induce DNA breaks and is not susceptible to at least some of the mechanisms contributing to Doxo resistance, including mutations in the SWI/SNF complex (97). This is confirmed in AML patients, where identical responses to an Acla-containing regimen were observed in patients refractory to Doxo/Daun-based chemotherapy versus chemo-naive patients, suggesting resistance to Doxo/Daun does not induce resistance to Acla (109). Furthermore, a fraction of diffuse large B-cell lymphomas harbors mutations in EZH2, which increases its H3K27me3 levels and renders the tumor cells more susceptible to Acla, which evicts those marked histones (96). It is compelling that in some instances deletion of the SWI/SNF complex increases H3K27me3 levels (110), suggesting that cells might actually become more sensitive to Acla. Elucidating the contribution of histone eviction to the overall anti-cancer effects of Doxo might thus yield novel treatment options to overcome resistance to anthracyclines.

Alkylating agents

Alkylating agents such as cyclophosphamide and ifosfamide are used mainly in com-

bination treatments for several malignancies. Synthesized as pro-drugs, they are bio-activated by the liver into their active nitrogen mustard moiety, which interacts with the DNA guanine base. The alkylated DNA can subsequently form intra-strand and inter-strand cross-links, leading to a DDR and subsequent cell death in a manner similar to platinum-based drugs (111).

Resistance to alkylating agents

Clinically, resistance to alkylating agents is poorly understood and few factors are correlated to response, possibly because cyclophosphamide is often administered in conjunction with other DNA damaging agents. The molecular determinants known to contribute to resistance center around its enzymatic activation and DNA repair following DNA alkylation. Enzymatic activation in the liver is orchestrated by the Cytochrome p450 family, and SNPs within this family, as well as liver expression levels of CYP2B6 have been linked to response (112, 113). On the other hand, CYP2B6 is also linked to the adverse effects observed from alkylating agents. Since higher p450 activity increases the conversion of the prodrug into the active form, CYP2B6 expression is better used as a biomarker for the dose that should be given to the patient, since higher p450 activity increases the total body exposure to the drug and hence untoward toxicity.

Upon hydroxylation, alkylating drugs diffuse into cells presumably via a flip-flop mechanism and can be inactivated by the action of aldehyde dehydrogenases, most notably ALDH1. Indeed, high ALDH1 levels correlate with a poor response to cyclophosphamide in breast cancer (114). However, ALDH1 is a marker for cancer stem cells and associated with the response to several chemotherapeutics, suggesting that ALDH1 is not a specific marker for response to these drugs (reviewed in (115)). Alkylating agents can also be modified by glutathione, but it is unclear what the clinical relevance of this pathway is (113). In addition, P-gp (ABCB1) or MRP2 (ABCC2) can be involved in clearing the drug from cells (113, 116).

Upon DNA alkylation, several repair mechanisms are involved in the restoration of DNA integrity. Direct de-alkylation of DNA is mediated by the enzyme MGMT, thus ablating the effect of alkylation and preventing cytotoxicity. Clinically, a correlation between MGMT expression and treatment outcome was found in some tumor types, which could not be confirmed in other tumors (117, 118). Cells can also repair DNA by removal of the alkylated guanine base, via the BER, NER or MMR pathways. Polymorphisms in XRCC1, involved in the BER pathway, are linked to survival after cyclophosphamide-containing treatment in several tumors (119, 120). Thus far, the NER and MMR pathways have not been associated with resistance to alkylating anti-cancer drugs. In summary, alkylating agents modify DNA and alterations in DNA repair appear to contribute to resistance to these drugs. MGMT and XRCC1 are the most promising markers, but convincing clinical validation is still lacking.

Antimetabolites

Another class of anti-cancer drugs, the antimetabolites, inhibits the formation of purine and pyrimidine nucleotides, effectively blocking DNA replication of rapidly proliferating cells. These drugs mimic endogenous reduced folates metabolites and act by either inhibiting enzymes essential in the biosynthesis of nucleotides, or by mimicking nucleotides to get incorporated into DNA or RNA, hereby frustrating repli-

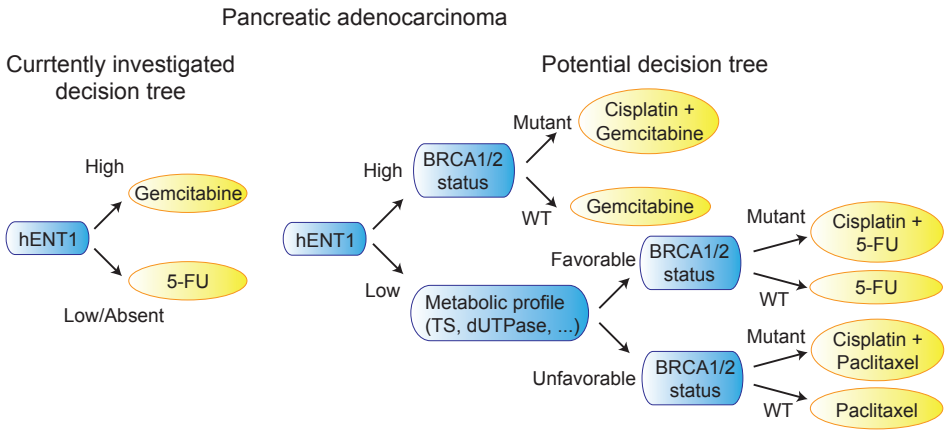


Figure 4: Potential stratification strategy for treatment decisions with conventional anti-cancer drugs. *A predictive factor for sensitivity to Gemcitabine in pancreatic cancer is the expression level of transporter hENT1. Tumors with low expression of hENT1 respond better to 5-FU treatment, while tumors with high expression respond favorably to Gemcitabine. BRCA1/2 mutations in pancreatic tumors and breast cancer can also be determined as they render tumors more susceptible to cisplatin treatment. The expression of Thymidylate Synthase, dUTPase or other factors potentially involved in resistance to 5-FU can be determined to select patients that will likely respond to 5-FU. Most mechanisms require validation in prospective studies.*

cation and inducing cell death (3). The first class is represented by the antifolate pioneer drug methotrexate (MTX), together with pemetrexed (PMX) and more recently pralatrexate, which inhibit the key enzymes in folate metabolism dihydrofolate reductase (DHFR) and thymidylate synthase (TS), both of which are important for purine and thymidine biosynthesis (26). Of the fluoropyrimidine nucleotide analogues, 5-fluorouracil (5-FU, and its pro-drug capecitabine) as well as gemcitabine are most commonly used. 5-FU is a thymidine analogue that blocks TS and gets incorporated into DNA, whereas gemcitabine is a cytidine analogue for which its incorporation into DNA is the main mode of antitumor activity.

Drug resistance mechanisms

Resistance to antimetabolites is frequently observed; the best documented resistance mechanism involves increased expression or mutation of the drug target. For 5-FU and PMX this means upregulation of TS, for which a prognostic role has been established in many different tumors. In the case of MTX, overexpression or mutations in its target DHFR affect drug sensitivity (reviewed in (3, 26)). However, in some settings and tissues high expression of TS can actually be beneficial for response to 5-FU, probably because cells with a higher expression of TS are metabolically more active and thus more vulnerable to inhibition of DNA building block synthesis (121).

Similar to other drugs, cancer cells can reduce import or increase export of the antimetabolites. 5-FU likely diffuses passively over the membrane, while MTX, PMX and pralatrexate are actively imported into cells, with MTX and pralatrexate predominantly transported by the reduced folate carrier (RFC) and PMX transported by both RFC and the proton-coupled folate transporter (PCFT), the latter one with higher affinity. RFC expression or polymorphisms are correlated to response to MTX in several tumor types (122-126), while for PMX a correlation between response

and mutation/expression of either RFC1 or PCFT has been less clear, probably due to the redundancy between the two transporters (3). Drug export can be mediated by several multidrug efflux transporters, including ABCC1-5, 11 and ABCG2, but no clinical relation has been established between any of these transporters and treatment outcome (26). Upon cellular entry, MTX, PMX and pralatrexate undergo polyglutamylation by folylpoly-gamma-glutamyl synthetase (FPGS), resulting in enhanced retention of these antifolate polyglutamates as they are no longer substrates for efflux transporters (127). As such, decreased FPGS expression, inactivating FPGS mutations as well as upregulation of γ-glutamyl hydrolase (GGH), which removes the polyglutamate tails, reduces sensitivity of cells to these drugs (128, 129). Clinically, high levels of polyglutamate-MTX are indeed correlated with enhanced drug responses (130, 131). Similar correlations with polymorphisms and increased expression of FPGS are also established (132, 133). For GGH, an effect on intracellular drug levels is observed but a clinical correlation to treatment outcome has only been established for a single polymorphism (134). This could be because GGH also modifies endogenous folates and its overexpression induces their export, reducing the production of DNA bases (3). Other factors influencing the response to antifolates are the levels of their natural reduced folate cofactor competitors. Increased reduced folate levels has been shown to induce resistance to MTX and PMX in vitro and in mouse models (135-138), however, a clinical correlation has not been established yet.

Mechanisms specific to TS inhibitors (5-FU and PMX) are related to dUTP metabolism, as blockade of TS leads to depletion of dTTP and accumulation of dUMP, which can be further phosphorylated to dUTP, shifting the nucleotide pool from dTTP to dUTP. This leads to the misincorporation of dUTP into DNA, which is subsequently repaired by the BER pathway. Loss of uracil–DNA glycosylase (UDG), responsible for the removal of dUTP incorporated into DNA, sensitizes cells in vitro to PMX, and to some extent to 5-FU (139, 140). High levels of dUTPase protect cells from 5-FU and PMX exposure by decreasing the concentration of dUTP, and this has been associated with poor treatment outcome in colorectal cancer (141-144).

5-FU resistance is also associated with decreased expression of genes involved in its conversion to the active metabolite FdUMP, namely thymidine kinase (TK), uridinemonophosphate kinase (UMPK) and orotate phosphorylase transferase (OPRT) (145), as well as overexpression of dihydropyrimidine dehydrogenase (DPD), which converts 5-FU into an inactive metabolite, and thymidine phosphorylase (TP), which opposes TK activity (26). The levels of TK, TP and DPD have been clinically correlated with treatment outcome, but results are conflicting and suggest a minor contribution for these enzymes in resistance against 5-FU (26, 146, 147).

Gemcitabine resistance relies on similar principles as the other antimetabolites. Cellular uptake of gemcitabine predominantly proceeds via the nucleoside transporters hENT1, hCNT1 and hCNT3 (148) of which low hENT1 has been correlated with poor overall survival of pancreatic patients after gemcitabine treatment (149-151). Similar results were obtained in other cancer types (152). No clinical correlation has been established for hCNT1, while a correlation between expression of hCNT3 and favorable responses in pancreatic cancer has been reported in one study (153). This suggests that hENT1 is likely the dominant influx transporter of gemcitabine.

Following uptake, the rate-limiting step for the conversion of gemcitabine into its active phosphorylated form is deoxycytidine kinase (dCK), whose expression has been linked to therapy response in several studies and tumor types (154). Before phosphorylation, gemcitabine can be converted by cytidine deaminase (CDA) into a metabolite that is secreted from cells, and high levels of CDA have been clinically linked to an unfavorable response. However, most CDA is produced in the liver and patients with low CDA levels generally also suffer from more side effects following gemcitabine treatment (155). Whether CDA can be used in individualized patient selection and/or whether the dose of gemcitabine should be adjusted to the patient's CDA levels remains unclear. Other enzymes involved in the conversion of gemcitabine are NMPK, NDPK and 5'-Nucleotidase, but no correlation between these enzymes and drug resistance has been documented in the clinic (29). Gemcitabin's active form dFdCTP competes with cytidine during incorporation into DNA. Cellular levels of cytidine are maintained by ribonucleotide reductase (RR). Upregulation of its two subunits RRM1 and RRM2 accelerates cytidine synthesis to compete with gemcitabine incorporation thus resulting in gemcitabine resistance, both under in vitro and in vivo conditions. Several studies have reported altered efficacy of gemcitabine in patients harboring SNPs or altered expression of RRM1, while other groups have failed to make these associations (156-158).

Out of all anticancer drug classes, the existence of predictive resistance markers has been most clearly demonstrated for the antimetabolites. A number of resistance factors either act at the level of intracellular accumulation or at the level of DNA base synthesis and incorporation. Currently, treatment of pancreatic patients on the basis of hENT1 expression is being evaluated in a clinical trial (159), rendering it the first stratification factor tested for conventional chemotherapy (Figure 4).

Anti-microtubule agents

This last class of conventional anti-cancer drugs targets another machinery essential for rapidly proliferating cells - the microtubules. Microtubules are critical for cytoskeletal structure, signaling and transport, as well as chromosome segregation during cell division. Dividing cells are very sensitive to cytoskeletal perturbations and hence multiple drugs have been developed that interfere with microtubule dynamics. These so-called spindle poisons bind β-tubulin and either stabilize microtubules (for example taxanes and epothilones), or destabilize microtubules (the Vinca alkaloids). Both drug classes act primarily by preventing proper spindle formation, thereby activating the spindle checkpoint, leading to a mitotic arrest. A prolonged arrest activates the apoptotic pathway or alternatively induces mitotic slippage, where cells exit the cell cycle without undergoing cell division (Kavallaris, 2010). Given their similar mechanism of action, many resistance mechanisms described are shared between both classes of spindle poisons (Dumontet and Jordan, 2010; van Vuuren et al., 2015).

Drug resistance mechanisms

Several mechanisms mediate resistance to tubulin-binding agents (TBAs), some of which are shared with other anti-cancer drug classes, like export via P-gp and upregulation of anti-apoptotic pathways, while others are more specific for the anti-microtubule agents, like mutations in β1-tubulin and overexpression of microtubule-associated proteins (MAPs).

β1-tubulin is a direct target for anti-microtubule drugs and multiple mutations have been identified that diminish drug sensitivity (Giannakakou et al., 1997; Hari et al., 2006; Yin et al., 2010), reviewed in (Kanakkanthara et al., 2013). Two types of mutations can be distinguished: mutations that alter drug binding, thus specific for a defined class of TBAs; and mutations that alter the general stability of microtubules. The latter destabilize microtubules to counteract the stabilization induced by taxanes (like paclitaxel), but sensitize cells to microtubule destabilizing drugs like the Vinca alkaloid vinblastine. These mutations are not germline mutations but acquired during treatment and thus difficult to use for patient stratification for treatment. Although resistance through β1-tubulin mutations is only tested in a tissue culture setting, several of these mutations are also found in tumors (Yin et al., 2010). However, the mutation frequency in β1-tubulin is low (<2%) (Gao et al., 2013), disfavoring the diagnostic value of such mutations.

An alternative escape route for cancer cells is to increase the expression of different β-tubulin isoforms, especially βIII-tubulin (Kavallaris, 2010). βIII-tubulin likely inhibits apoptosis via the PIM1-BCL2 mitochondrial pathway (160), contributing to a survival benefit for the tumor and a more general resistance to multiple types of chemotherapeutics (24, 161). Thus, βIII-tubulin acts as a general activator of anti-apoptotic pathways and not a specific factor that can predict responses to certain TBAs.

Apart from microtubules, microtubule associated proteins (MAPs) also influence microtubule dynamics and interfere with drug binding. For example, the Tau protein occupies the same binding site as taxanes (Kar et al., 2003), and de-sensitizes cells to paclitaxel (Rouzier et al., 2005). In vitro studies also demonstrated a role for mitotic centrosome associated kinase (MCAK) (Ganguly et al., 2011) and stathmin in sensitivity to paclitaxel (Alli et al., 2002), as well as FOXM1, a transcription factor regulating stathmin expression (Li et al., 2014a; Zhao et al., 2014). Clinically, the correlation between Tau and tumor sensitivity to paclitaxel has been confusing, with several studies validating an inverse correlation between response to paclitaxel and expression of Tau (Smoter et al., 2013; Werner et al., 2014), while others reported no significant impact of Tau (Bonneau et al., 2015). An inverse correlation between response to paclitaxel and (phosphorylated) stathmin expression has been demonstrated in several tumor types (Kuang et al., 2015; Werner et al., 2014), but it is unclear whether stathmin is a general prognostic factor or controls the actual response to paclitaxel under clinical conditions. Alternatively, cells can upregulate the expression of SYK kinase upon paclitaxel treatment to destabilize microtubules, likely by phosphorylating tubulin and several MAPS, which affects the effectivity of paclitaxel in recurrent ovarian carcinoma treatment (Yu et al., 2015). A different study has demonstrated that two germline variations in TEKT4 can destabilize microtubules and impair outcome (Jiang et al., 2014). Thus, several MAPs seem to be involved in regulating resistance to paclitaxel.

Translating microtubule deregulation to a cell death program is mediated by the spindle activation checkpoint (SAC), which in turn is activated by the chromosomal passenger complex (CPC) (Carmena et al., 2012). Downregulation of the SAC-members MAD2 and BubR1 (Furlong et al., 2012; Sudo et al., 2004), as well as overexpression of Aurora A, which overrides SAC activation (Anand et al., 2003), induces resistance to paclitaxel. Conversely, downregulation of CPC member Aurora B leads

to resistance, probably by defective targeting of MAD2 and BubR1 to the mitotic spindle (Ditchfield et al., 2003). In contrast to this, upregulation of survivin, also part of the CPC, leads to resistance to several TBAs. Survivin upregulation also leads to resistance to other chemotherapeutics such as doxorubicin and cisplatin, probably via its function as an anti-apoptotic factor (Zaffaroni et al., 2002). For several cancer types, such as breast cancer and NSCLC, high survivin levels are correlated with disease progression and poor response to chemotherapy (Huang et al., 2013; Li et al., 2014b). More mitotic factors have been recently linked to paclitaxel sensitivity, like PDCD4 (Xu et al., 2015), CASC1 and TRIM69 (Sinnott et al., 2014).
Since cells die by apoptosis in response to TBAs, deregulation of survival signaling pathways plays an important role in chemosensitivity. This has been demonstrated for the Keap1-Nrf2 oxidative stress signaling pathway (Leinonen et al., 2014), HER2 signaling (Knuefermann et al., 2003), Hippo signaling via TAZ (Lai et al., 2011), NFκb signaling (Kelly et al., 2006; Wee et al., 2015), and FAK1/YB-1 signaling (Kang et al., 2013). These pathways will not allow patient stratification, but inhibition of the mutated pathway enhances the efficacy of anti-microtubule agents, as demonstrated for the combination of HER2 inhibition (trastuzumab) and paclitaxel (Schramm et al., 2015).
Resistance to microtubule agents revolves around microtubule dynamics and translation of altered dynamics into a cell death program. Clinically, few factors have been unequivocally linked to clinical responses but the current evidence points towards the MAPs as the most likely prognostic factors for TBA resistance in patients.

Conclusions

Development of resistance is one of the major reasons for treatment failure of anti-cancer drugs. Over the years, a multitude of mechanisms have been identified that are employed by tumors to decrease their sensitivity to chemotherapy. Unfortunately, translation of these findings into personalized selection of patients for such drugs has proven difficult. Several reasons underlie this poor translation:

1. Most resistance mechanisms are initially identified in tissue culture systems and mouse models. Validation of these factors requires extensive prospective studies which take time and effort, delaying implementation. Large clinical datasets correlating response to gene expression can bridge the gap between the lab and clinic and used to filter out the most promising factors. Yet, a double blind prospective study remains essential for acceptance of prognostic markers for cancer therapy decisions.
2. Cancer treatment is often a multidrug treatment and resistance mechanisms to a combination therapeutic regimen are poorly understood.
3. Resistance mechanisms may not be present prior to treatment but acquired through selection under the pressure of chemotherapy. Only germline resistance mechanisms can be monitored for treatment decisions. Acquired resistance mechanisms may be avoided by searching for mechanisms of synthetic lethality and drugs (alone or in combination) that selectively act on the resistant tumor cells.
4. Tumors are heterogeneous and a small subpopulation of cells can harbor a mutation that renders them resistant. These cells will eventually become the recurrent tumor. Alternatively, cells that are intrinsically more resistant to chemotherapy,

such as cancer stem cells (162) and cells that underwent EMT (163, 164), grow out to re-form a tumor (Figure 3).

5. Tumor extrinsic factors such as the microenvironment (165) and even the microbiome (166, 167) can contribute to drug resistance, by producing growth factors or modulating the immune system. These factors are usually not included in studies focusing on drug resistance.

Despite these serious impediments, the first trial with personalized medicine for conventional chemotherapeutics is being set-up, likely followed by many others. The identification and validation of other resistance factors will yield leads that potentially influence the response to individual drugs, resulting in a multi-step decision process to select the optimal treatment of choice (see example in Figure 4). These biomarkers will hopefully aid the development of better and more optimized treatments for the individual cancer patient.

Acknowledgements

This work was supported by the Institute for Chemical Immunology, an NWO Gravitation project funded by the Ministry of Education, Culture and Science of the government of the Netherlands, a grant from the Dutch Cancer Society KWF, an NWO TOP grant and an ERC Advanced grant to J.N.

References

1. G. Szakacs, J. K. Paterson, J. A. Ludwig, C. Booth-Genthe, M. M. Gottesman, Targeting multidrug resistance in cancer. Nature reviews. Drug discovery 5, 219-234 (2006).
2. Y. G. Assaraf, Molecular basis of antifolate resistance. Cancer metastasis reviews 26, 153-181 (2007).
3. N. Gonen, Y. G. Assaraf, Antifolates in cancer therapy: structure, activity and mechanisms of drug resistance. Drug resistance updates : reviews and commentaries in antimicrobial and anticancer chemotherapy 15, 183-210 (2012).
4. Y. D. Livney, Y. G. Assaraf, Rationally designed nanovehicles to overcome cancer chemoresistance. Advanced drug delivery reviews 65, 1716-1730 (2013).
5. A. Shapira, Y. D. Livney, H. J. Broxterman, Y. G. Assaraf, Nanomedicine for targeted cancer therapy: towards the overcoming of drug resistance. Drug resistance updates : reviews and commentaries in antimicrobial and anticancer chemotherapy 14, 150-163 (2011).
6. P. P. Zarrinkar et al., AC220 is a uniquely potent and selective inhibitor of FLT3 for the treatment of acute myeloid leukemia (AML). Blood 114, 2984-2992 (2009).
7. C. Holohan, S. Van Schaeybroeck, D. B. Longley, P. G. Johnston, Cancer drug resistance: an evolving paradigm. Nature reviews. Cancer 13, 714-726 (2013).
8. H. Farmer et al., Targeting the DNA repair defect in BRCA mutant cells as a therapeutic strategy. Nature 434, 917-921 (2005).
9. S. L. Edwards et al., Resistance to therapy caused by intragenic deletion in BRCA2. Nature 451, 1111-1115 (2008).
10. C. C. Smith et al., Validation of ITD mutations in FLT3 as a therapeutic target in human acute myeloid leukaemia. Nature 485, 260-263 (2012).
11. S. V. Sharma et al., A chromatin-mediated reversible drug-tolerant state in cancer cell subpopulations. Cell 141, 69-80 (2010).
12. H. K. Kim et al., A gene expression signature of acquired chemoresistance to cisplatin and fluorouracil combination chemotherapy in gastric cancer patients. PloS one 6, e16694 (2011).
13. M. Hofree, J. P. Shen, H. Carter, A. Gross, T. Ideker, Network-based stratification of tumor mutations. Nature methods 10, 1108-1115 (2013).
14. R. F. Dear et al., Combination versus sequential single agent chemotherapy for metastatic breast cancer. The Cochrane database of systematic reviews 12, Cd008792 (2013).
15. C. Morth, A. Valachis, Single-agent versus combination chemotherapy as first-line treatment for patients with advanced non-small cell lung cancer and performance status 2: a literature-based me-

ta-analysis of randomized studies. Lung cancer (Amsterdam, Netherlands) 84, 209-214 (2014).
16. J. R. Pritchard, D. A. Lauffenburger, M. T. Hemann, Understanding resistance to combination chemotherapy. Drug resistance updates : reviews and commentaries in antimicrobial and anticancer chemotherapy 15, 249-257 (2012).
17. S. D. Undevia, G. Gomez-Abuin, M. J. Ratain, Pharmacokinetic variability of anticancer agents. Nature reviews. Cancer 5, 447-458 (2005).
18. H. Cao, H. Phan, L. X. Yang, Improved chemotherapy for hepatocellular carcinoma. Anticancer research 32, 1379-1386 (2012).
19. R. Koster, M. A. van Vugt, H. Timmer-Bosscha, J. A. Gietema, S. de Jong, Unravelling mechanisms of cisplatin sensitivity and resistance in testicular cancer. Expert reviews in molecular medicine 15, e12 (2013).
20. R. Pirker et al., EGFR expression as a predictor of survival for first-line chemotherapy plus cetuximab in patients with advanced non-small-cell lung cancer: analysis of data from the phase 3 FLEX study. The Lancet. Oncology 13, 33-42 (2012).
21. I. A. Mayer, V. G. Abramson, B. D. Lehmann, J. A. Pietenpol, New strategies for triple-negative breast cancer--deciphering the heterogeneity. Clinical cancer research : an official journal of the American Association for Cancer Research 20, 782-790 (2014).
22. C. O. Leong, N. Vidnovic, M. P. DeYoung, D. Sgroi, L. W. Ellisen, The p63/p73 network mediates chemosensitivity to cisplatin in a biologically defined subset of primary breast cancers. The Journal of clinical investigation 117, 1370-1380 (2007).
23. L. Vecchione et al., A Vulnerability of a Subset of Colon Cancers with Potential Clinical Utility. Cell 165, 317-330 (2016).
24. R. Karki et al., betaIII-Tubulin: biomarker of taxane resistance or drug target? Expert opinion on therapeutic targets 17, 461-472 (2013).
25. R. Planells-Cases et al., Subunit composition of VRAC channels determines substrate specificity and cellular resistance to Pt-based anti-cancer drugs. The EMBO journal 34, 2993-3008 (2015).
26. L. Taddia et al., Inside the biochemical pathways of thymidylate synthase perturbed by anticancer drugs: Novel strategies to overcome cancer chemoresistance. Drug resistance updates : reviews and commentaries in antimicrobial and anticancer chemotherapy 23, 20-54 (2015).
27. A. Qiu et al., Identification of an intestinal folate transporter and the molecular basis for hereditary folate malabsorption. Cell 127, 917-928 (2006).
28. L. Rothem et al., Resistance to multiple novel antifolates is mediated via defective drug transport resulting from clustered mutations in the reduced folate carrier gene in human leukaemia cell lines. The Biochemical journal 367, 741-750 (2002).
29. Y. Binenbaum, S. Na'ara, Z. Gil, Gemcitabine resistance in pancreatic ductal adenocarcinoma. Drug resistance updates : reviews and commentaries in antimicrobial and anticancer chemotherapy 23, 55-68 (2015).
30. R. Regev, G. D. Eytan, Flip-flop of doxorubicin across erythrocyte and lipid membranes. Biochemical pharmacology 54, 1151-1158 (1997).
31. R. Regev, D. Yeheskely-Hayon, H. Katzir, G. D. Eytan, Transport of anthracyclines and mitoxantrone across membranes by a flip-flop mechanism. Biochemical pharmacology 70, 161-169 (2005).
32. M. M. Gottesman, T. Fojo, S. E. Bates, Multidrug resistance in cancer: role of ATP-dependent transporters. Nature reviews. Cancer 2, 48-58 (2002).
33. Y. G. Assaraf, The role of multidrug resistance efflux transporters in antifolate resistance and folate homeostasis. Drug resistance updates : reviews and commentaries in antimicrobial and anticancer chemotherapy 9, 227-246 (2006).
34. R. J. Kathawala, P. Gupta, C. R. Ashby, Jr., Z. S. Chen, The modulation of ABC transporter-mediated multidrug resistance in cancer: a review of the past decade. Drug resistance updates : reviews and commentaries in antimicrobial and anticancer chemotherapy 18, 1-17 (2015).
35. R. Mazzanti, L. Gramantieri, L. Bolondi, Hepatocellular carcinoma: epidemiology and clinical aspects. Molecular aspects of medicine 29, 130-143 (2008).
36. R. Callaghan, F. Luk, M. Bebawy, Inhibition of the multidrug resistance P-glycoprotein: time for a change of strategy? Drug metabolism and disposition: the biological fate of chemicals 42, 623-631 (2014).
37. S. Elmore, Apoptosis: a review of programmed cell death. Toxicologic pathology 35, 495-516 (2007).
38. F. H. Igney, P. H. Krammer, Death and anti-death: tumour resistance to apoptosis. Nature re-

views. Cancer 2, 277-288 (2002).
39. D. Hanahan, R. A. Weinberg, Hallmarks of cancer: the next generation. Cell 144, 646-674 (2011).
40. T. Miyashita, J. C. Reed, bcl-2 gene transfer increases relative resistance of S49.1 and WEHI7.2 lymphoid cells to cell death and DNA fragmentation induced by glucocorticoids and multiple chemotherapeutic drugs. Cancer research 52, 5407-5411 (1992).
41. T. Ni Chonghaile et al., Pretreatment mitochondrial priming correlates with clinical response to cytotoxic chemotherapy. Science (New York, N.Y.) 334, 1129-1133 (2011).
42. P. E. Czabotar, G. Lessene, A. Strasser, J. M. Adams, Control of apoptosis by the BCL-2 protein family: implications for physiology and therapy. Nature reviews. Molecular cell biology 15, 49-63 (2014).
43. A. J. Souers et al., ABT-199, a potent and selective BCL-2 inhibitor, achieves antitumor activity while sparing platelets. Nature medicine 19, 202-208 (2013).
44. K. Bouchalova et al., Triple negative breast cancer - BCL2 in prognosis and prediction. Review. Current drug targets 15, 1166-1175 (2014).
45. D. Yang et al., Bcl-2 expression predicts sensitivity to chemotherapy in breast cancer: a systematic review and meta-analysis. Journal of experimental & clinical cancer research : CR 32, 105 (2013).
46. M. Vogler, Targeting BCL2-Proteins for the Treatment of Solid Tumours. Advances in medicine 2014, 943648 (2014).
47. M. Rebucci, C. Michiels, Molecular aspects of cancer cell resistance to chemotherapy. Biochemical pharmacology 85, 1219-1226 (2013).
48. G. Kroemer, L. Galluzzi, O. Kepp, L. Zitvogel, Immunogenic cell death in cancer therapy. Annual review of immunology 31, 51-72 (2013).
49. S. Loi et al., CD73 promotes anthracycline resistance and poor prognosis in triple negative breast cancer. Proceedings of the National Academy of Sciences of the United States of America 110, 11091-11096 (2013).
50. D. J. Slamon et al., Use of chemotherapy plus a monoclonal antibody against HER2 for metastatic breast cancer that overexpresses HER2. The New England journal of medicine 344, 783-792 (2001).
51. D. Cunningham et al., Cetuximab monotherapy and cetuximab plus irinotecan in irinotecan-refractory metastatic colorectal cancer. The New England journal of medicine 351, 337-345 (2004).
52. S. Huang et al., MED12 controls the response to multiple cancer drugs through regulation of TGF-beta receptor signaling. Cell 151, 937-950 (2012).
53. F. Li, G. Sethi, Targeting transcription factor NF-kappaB to overcome chemoresistance and radioresistance in cancer therapy. Biochimica et biophysica acta 1805, 167-180 (2010).
54. H. Jing et al., Opposing roles of NF-kappaB in anti-cancer treatment outcome unveiled by cross-species investigations. Genes & development 25, 2137-2146 (2011).
55. N. Yatim et al., RIPK1 and NF-kappaB signaling in dying cells determines cross-priming of CD8(+) T cells. Science (New York, N.Y.) 350, 328-334 (2015).
56. T. N. Schumacher, R. D. Schreiber, Neoantigens in cancer immunotherapy. Science (New York, N.Y.) 348, 69-74 (2015).
57. Z. H. Siddik, Cisplatin: mode of cytotoxic action and molecular basis of resistance. Oncogene 22, 7265-7279 (2003).
58. L. Galluzzi et al., Molecular mechanisms of cisplatin resistance. Oncogene 31, 1869-1883 (2012).
59. N. G. Alkema, G. B. Wisman, A. G. van der Zee, M. A. van Vugt, S. de Jong, Studying platinum sensitivity and resistance in high-grade serous ovarian cancer: Different models for different questions. Drug resistance updates : reviews and commentaries in antimicrobial and anticancer chemotherapy 24, 55-69 (2016).
60. J. A. Ferreira et al., Mechanisms of cisplatin resistance and targeting of cancer stem cells: Adding glycosylation to the equation. Drug resistance updates : reviews and commentaries in antimicrobial and anticancer chemotherapy 24, 34-54 (2016).
61. D. Mokady, D. Meiri, RhoGTPases - A novel link between cytoskeleton organization and cisplatin resistance. Drug resistance updates : reviews and commentaries in antimicrobial and anticancer chemotherapy 19, 22-32 (2015).
62. L. Gatti, G. Cassinelli, N. Zaffaroni, C. Lanzi, P. Perego, New mechanisms for old drugs: Insights into DNA-unrelated effects of platinum compounds and drug resistance determinants. Drug resistance updates : reviews and commentaries in antimicrobial and anticancer chemotherapy 20, 1-11 (2015).

63. N. A. Bowden, Nucleotide excision repair: why is it not used to predict response to platinum-based chemotherapy? Cancer letters 346, 163-171 (2014).
64. E. M. Van Allen et al., Somatic ERCC2 mutations correlate with cisplatin sensitivity in muscle-invasive urothelial carcinoma. Cancer discovery 4, 1140-1153 (2014).
65. D. Huang, Y. Zhou, Nucleotide excision repair gene polymorphisms and prognosis of non-small cell lung cancer patients receiving platinum-based chemotherapy: A meta-analysis based on 44 studies. Biomedical reports 2, 452-462 (2014).
66. Y. Wang et al., Genetic polymorphisms of ERCC1 and their effects on the efficacy of cisplatin-based chemotherapy in advanced esophageal carcinoma. Oncology reports 25, 1047-1052 (2011).
67. S. Z. Wei et al., Predictive value of ERCC1 and XPD polymorphism in patients with advanced non-small cell lung cancer receiving platinum-based chemotherapy: a systematic review and meta-analysis. Medical oncology (Northwood, London, England) 28, 315-321 (2011).
68. R. Ceccaldi et al., A unique subset of epithelial ovarian cancers with platinum sensitivity and PARP inhibitor resistance. Cancer research 75, 628-634 (2015).
69. L. E. Wang et al., DNA repair capacity in peripheral lymphocytes predicts survival of patients with non-small-cell lung cancer treated with first-line platinum-based chemotherapy. Journal of clinical oncology : official journal of the American Society of Clinical Oncology 29, 4121-4128 (2011).
70. D. Fink et al., The role of DNA mismatch repair in platinum drug resistance. Cancer research 56, 4881-4886 (1996).
71. A. Sawant, A. Kothandapani, A. Zhitkovich, R. W. Sobol, S. M. Patrick, Role of mismatch repair proteins in the processing of cisplatin interstrand cross-links. DNA repair 35, 126-136 (2015).
72. N. S. Kamal et al., MutS homologue 2 and the long-term benefit of adjuvant chemotherapy in lung cancer. Clinical cancer research : an official journal of the American Association for Cancer Research 16, 1206-1215 (2010).
73. W. Sakai et al., Secondary mutations as a mechanism of cisplatin resistance in BRCA2-mutated cancers. Nature 451, 1116-1120 (2008).
74. Y. Mu et al., SLFN11 inhibits checkpoint maintenance and homologous recombination repair. EMBO reports, (2015).
75. G. Zoppoli et al., Putative DNA/RNA helicase Schlafen-11 (SLFN11) sensitizes cancer cells to DNA-damaging agents. Proceedings of the National Academy of Sciences of the United States of America 109, 15030-15035 (2012).
76. S. W. Tang et al., SLFN11 Is a Transcriptional Target of EWS-FLI1 and a Determinant of Drug Response in Ewing Sarcoma. Clinical cancer research : an official journal of the American Association for Cancer Research 21, 4184-4193 (2015).
77. B. Norquist et al., Secondary somatic mutations restoring BRCA1/2 predict chemotherapy resistance in hereditary ovarian carcinomas. Journal of clinical oncology : official journal of the American Society of Clinical Oncology 29, 3008-3015 (2011).
78. D. W. Wu et al., FHIT loss confers cisplatin resistance in lung cancer via the AKT/NF-kappaB/Slug-mediated PUMA reduction. Oncogene 34, 2505-2515 (2015).
79. C. E. Waters, J. C. Saldivar, S. A. Hosseini, K. Huebner, The FHIT gene product: tumor suppressor and genome “caretaker”. Cellular and molecular life sciences : CMLS 71, 4577-4587 (2014).
80. J. Gao et al., Mirk/Dyrk1B, a novel therapeutic target, mediates cell survival in non-small cell lung cancer cells. Cancer biology & therapy 8, 1671-1679 (2009).
81. L. Galluzzi et al., Systems biology of cisplatin resistance: past, present and future. Cell death & disease 5, e1257 (2014).
82. N. A. Patankar, J. Pritchard, M. van Grinsven, M. Osooly, M. B. Bally, Topotecan and doxorubicin combination to treat recurrent ovarian cancer: the influence of drug exposure time and delivery systems to achieve optimum therapeutic activity. Clinical cancer research : an official journal of the American Association for Cancer Research 19, 865-877 (2013).
83. Y. Xu, C. Her, Inhibition of Topoisomerase (DNA) I (TOP1): DNA Damage Repair and Anticancer Therapy. Biomolecules 5, 1652-1670 (2015).
84. S. Y. Park, W. Lam, Y. C. Cheng, X-ray repair cross-complementing gene I protein plays an important role in camptothecin resistance. Cancer research 62, 459-465 (2002).
85. C. Meisenberg et al., Clinical and cellular roles for TDP1 and TOP1 in modulating colorectal cancer response to irinotecan. Molecular cancer therapeutics 14, 575-585 (2015).
86. C. A. Delaney et al., Potentiation of temozolomide and topotecan growth inhibition and cytotoxicity by novel poly(adenosine diphosphoribose) polymerase inhibitors in a panel of human tumor cell

lines. Clinical cancer research : an official journal of the American Association for Cancer Research 6, 2860-2867 (2000).
87. J. R. Chapman, M. R. Taylor, S. J. Boulton, Playing the end game: DNA double-strand break repair pathway choice. Molecular cell 47, 497-510 (2012).
88. J. S. Coon et al., Amplification and Overexpression of Topoisomerase IIα Predict Response to Anthracycline-based Therapy in Locally Advanced Breast Cancer. Clinical Cancer Research 8, 1061-1067 (2002).
89. T. A. Järvinen, J. Kononen, M. Pelto-Huikko, J. Isola, Expression of topoisomerase IIalpha is associated with rapid cell proliferation, aneuploidy, and c-erbB2 overexpression in breast cancer. The American journal of pathology 148, 2073-2082 (1996).
90. L. Gianni et al., Anthracycline Cardiotoxicity: From Bench to Bedside. Journal of Clinical Oncology 26, 3777-3784 (2008).
91. G. Minotti, P. Menna, E. Salvatorelli, G. Cairo, L. Gianni, Anthracyclines: Molecular Advances and Pharmacologic Developments in Antitumor Activity and Cardiotoxicity. Pharmacological Reviews 56, 185-229 (2004).
92. R. B. Weiss, The anthracyclines: will we ever find a better doxorubicin? Seminars in oncology 19, 670-686 (1992).
93. K. R. Hande, Clinical applications of anticancer drugs targeted to topoisomerase II. Biochimica et Biophysica Acta (BBA) - Gene Structure and Expression 1400, 173-184 (1998).
94. B. Pang et al., Drug-induced histone eviction from open chromatin contributes to the chemotherapeutic effects of doxorubicin. Nature communications 4, 1908 (2013).
95. F. Yang, C. J. Kemp, S. Henikoff, Doxorubicin enhances nucleosome turnover around promoters. Current biology : CB 23, 782-787 (2013).
96. B. Pang, J. de Jong, X. Qiao, L. F. Wessels, J. Neefjes, Chemical profiling of the genome with anti-cancer drugs defines target specificities. Nature chemical biology 11, 472-480 (2015).
97. R. H. Wijdeven et al., Genome-Wide Identification and Characterization of Novel Factors Conferring Resistance to Topoisomerase II Poisons in Cancer. Cancer Res 75, 4176-4187 (2015).
98. M. Herlevsen, G. Oxford, C. R. Owens, M. Conaway, D. Theodorescu, Depletion of major vault protein increases doxorubicin sensitivity and nuclear accumulation and disrupts its sequestration in lysosomes. Molecular cancer therapeutics 6, 1804-1813 (2007).
99. Y. Adar et al., Imidazoacridinone-dependent lysosomal photodestruction: a pharmacological Trojan horse approach to eradicate multidrug-resistant cancers. Cell death & disease 3, e293 (2012).
100. B. Zhitomirsky, Y. G. Assaraf, Lysosomal sequestration of hydrophobic weak base chemotherapeutics triggers lysosomal biogenesis and lysosome-dependent cancer multidrug resistance. Oncotarget 6, 1143-1156 (2015).
101. B. Zhitomirsky, Y. G. Assaraf, Lysosomes as mediators of drug resistance in cancer. Drug resistance updates : reviews and commentaries in antimicrobial and anticancer chemotherapy 24, 23-33 (2016).
102. D. J. Burgess et al., Topoisomerase levels determine chemotherapy response in vitro and in vivo. Proceedings of the National Academy of Sciences of the United States of America 105, 9053-9058 (2008).
103. Y. Miyoshi et al., Predictive factors for anthracycline-based chemotherapy for human breast cancer. Breast cancer (Tokyo, Japan) 17, 103-109 (2010).
104. J. L. Nitiss, Targeting DNA topoisomerase II in cancer chemotherapy. Nature reviews. Cancer 9, 338-350 (2009).
105. M. Hazar-Rethinam et al., A novel E2F/sphingosine kinase 1 axis regulates anthracycline response in squamous cell carcinoma. Clinical cancer research : an official journal of the American Association for Cancer Research 21, 417-427 (2015).
106. M. Hazar-Rethinam et al., RacGAP1 Is a Novel Downstream Effector of E2F7-Dependent Resistance to Doxorubicin and Is Prognostic for Overall Survival in Squamous Cell Carcinoma. Molecular cancer therapeutics 14, 1939-1950 (2015).
107. L. J. Monteiro et al., The Forkhead Box M1 protein regulates BRIP1 expression and DNA damage repair in epirubicin treatment. Oncogene 32, 4634-4645 (2013).
108. H. Jia et al., p57Kip2 is an unrecognized DNA damage response effector molecule that functions in tumor suppression and chemoresistance. Oncogene 34, 3568-3581 (2015).
109. G. Wei et al., A meta-analysis of CAG (cytarabine, aclarubicin, G-CSF) regimen for the treatment of 1029 patients with acute myeloid leukemia and myelodysplastic syndrome. Journal of hematology

& oncology 4, 46 (2011).
110. K. H. Kim, C. W. Roberts, Targeting EZH2 in cancer. Nature medicine 22, 128-134 (2016).
111. A. Emadi, R. J. Jones, R. A. Brodsky, Cyclophosphamide and cancer: golden anniversary. Nature reviews. Clinical oncology 6, 638-647 (2009).
112. G. G. Johnson et al., CYP2B6*6 is an independent determinant of inferior response to fludarabine plus cyclophosphamide in chronic lymphocytic leukemia. Blood 122, 4253-4258 (2013).
113. J. Zhang, Q. Tian, S. Y. Chan, W. Duan, S. Zhou, Insights into oxazaphosphorine resistance and possible approaches to its circumvention. Drug resistance updates : reviews and commentaries in antimicrobial and anticancer chemotherapy 8, 271-297 (2005).
114. N. E. Sladek, R. Kollander, L. Sreerama, D. T. Kiang, Cellular levels of aldehyde dehydrogenases (ALDH1A1 and ALDH3A1) as predictors of therapeutic responses to cyclophosphamide-based chemotherapy of breast cancer: a retrospective study. Rational individualization of oxazaphosphorine-based cancer chemotherapeutic regimens. Cancer chemotherapy and pharmacology 49, 309-321 (2002).
115. R. Januchowski, K. Wojtowicz, M. Zabel, The role of aldehyde dehydrogenase (ALDH) in cancer drug resistance. Biomedicine & pharmacotherapy = Biomedecine & pharmacotherapie 67, 669-680 (2013).
116. O. A. Patutina et al., The siRNA targeted to mdr1b and mdr1a mRNAs in vivo sensitizes murine lymphosarcoma to chemotherapy. BMC cancer 10, 204 (2010).
117. A. Cayre et al., O(6)-methylguanine-DNA methyl transferase gene expression and prognosis in breast carcinoma. International journal of oncology 21, 1125-1131 (2002).
118. T. Ohno et al., Loss of O6-methylguanine-DNA methyltransferase protein expression is a favorable prognostic marker in diffuse large B-cell lymphoma. International journal of hematology 83, 341-347 (2006).
119. M. Jaremko et al., Polymorphism of the DNA repair enzyme XRCC1 is associated with treatment prediction in anthracycline and cyclophosphamide/methotrexate/5-fluorouracil-based chemotherapy of patients with primary invasive breast cancer. Pharmacogenetics and genomics 17, 529-538 (2007).
120. K. Przybylowska-Sygut, M. Stanczyk, R. Kusinska, R. Kordek, I. Majsterek, Association of the Arg194Trp and the Arg399Gln polymorphisms of the XRCC1 gene with risk occurrence and the response to adjuvant therapy among Polish women with breast cancer. Clinical breast cancer 13, 61-68 (2013).
121. A. Formentini, D. Henne-Bruns, M. Kornmann, Thymidylate synthase expression and prognosis of patients with gastrointestinal cancers receiving adjuvant chemotherapy: a review. Langenbeck's archives of surgery / Deutsche Gesellschaft fur Chirurgie 389, 405-413 (2004).
122. S. Jabeen et al., Impact of genetic variants of RFC1, DHFR and MTHFR in osteosarcoma patients treated with high-dose methotrexate. The pharmacogenomics journal 15, 385-390 (2015).
123. W. Guo et al., Mechanisms of methotrexate resistance in osteosarcoma. Clinical cancer research : an official journal of the American Association for Cancer Research 5, 621-627 (1999).
124. R. Gorlick et al., Defective transport is a common mechanism of acquired methotrexate resistance in acute lymphocytic leukemia and is associated with decreased reduced folate carrier expression. Blood 89, 1013-1018 (1997).
125. S. Drori, G. Jansen, R. Mauritz, G. J. Peters, Y. G. Assaraf, Clustering of mutations in the first transmembrane domain of the human reduced folate carrier in GW1843U89-resistant leukemia cells with impaired antifolate transport and augmented folate uptake. The Journal of biological chemistry 275, 30855-30863 (2000).
126. G. Jansen et al., A structurally altered human reduced folate carrier with increased folic acid transport mediates a novel mechanism of antifolate resistance. The Journal of biological chemistry 273, 30189-30198 (1998).
127. S. Raz, M. Stark, Y. G. Assaraf, Folylpoly-γ-glutamate synthetase: A key determinant of folate homeostasis and antifolate resistance in cancer. Drug Resistance Updates, (2016).
128. S. Raz, M. Stark, Y. G. Assaraf, Binding of a Smad4/Ets-1 complex to a novel intragenic regulatory element in exon12 of FPGS underlies decreased gene expression and antifolate resistance in leukemia. Oncotarget 5, 9183-9198 (2014).
129. A. Wojtuszkiewicz et al., Folylpolyglutamate synthetase splicing alterations in acute lymphoblastic leukemia are provoked by methotrexate and other chemotherapeutics and mediate chemoresistance. International journal of cancer. Journal international du cancer 138, 1645-1656 (2016).
130. A. Wojtuszkiewicz et al., Methotrexate resistance in relation to treatment outcome in childhood acute lymphoblastic leukemia. Journal of hematology & oncology 8, 61 (2015).
131. V. M. Whitehead et al., Accumulation of methotrexate and methotrexate polyglutamates in

lymphoblasts at diagnosis of childhood acute lymphoblastic leukemia: a pilot prognostic factor analysis. Blood 76, 44-49 (1990).
132. S. G. Liu et al., FPGS rs1544105 polymorphism is associated with treatment outcome in pediatric B-cell precursor acute lymphoblastic leukemia. Cancer cell international 13, 107 (2013).
133. M. G. Rots et al., Role of folylpolyglutamate synthetase and folylpolyglutamate hydrolase in methotrexate accumulation and polyglutamylation in childhood leukemia. Blood 93, 1677-1683 (1999).
134. J. Organista-Nava et al., Polymorphisms of the gamma-glutamyl hydrolase gene and risk of relapse to acute lymphoblastic leukemia in Mexico. Leukemia research 34, 728-732 (2010).
135. C. L. van der Wilt et al., Modulation of both endogenous folates and thymidine enhance the therapeutic efficacy of thymidylate synthase inhibitors. Cancer research 61, 3675-3681 (2001).
136. S. Chattopadhyay et al., Commentary: a case for minimizing folate supplementation in clinical regimens with pemetrexed based on the marked sensitivity of the drug to folate availability. The oncologist 12, 808-815 (2007).
137. Y. G. Assaraf, I. D. Goldman, Loss of folic acid exporter function with markedly augmented folate accumulation in lipophilic antifolate-resistant mammalian cells. The Journal of biological chemistry 272, 17460-17466 (1997).
138. M. Stark et al., Antifolate resistance associated with loss of MRP1 expression and function in Chinese hamster ovary cells with markedly impaired export of folate and cholate. Molecular pharmacology 64, 220-227 (2003).
139. L. D. Weeks, P. Fu, S. L. Gerson, Uracil-DNA glycosylase expression determines human lung cancer cell sensitivity to pemetrexed. Molecular cancer therapeutics 12, 2248-2260 (2013).
140. A. D. Bulgar et al., Removal of uracil by uracil DNA glycosylase limits pemetrexed cytotoxicity: overriding the limit with methoxyamine to inhibit base excision repair. Cell death & disease 3, e252 (2012).
141. S. Nobili et al., Identification of potential pharmacogenomic markers of clinical efficacy of 5-fluorouracil in colorectal cancer. International journal of cancer. Journal international du cancer 128, 1935-1945 (2011).
142. A. Kawahara et al., Higher expression of deoxyuridine triphosphatase (dUTPase) may predict the metastasis potential of colorectal cancer. Journal of clinical pathology 62, 364-369 (2009).
143. P. M. Wilson, M. J. LaBonte, H. J. Lenz, P. C. Mack, R. D. Ladner, Inhibition of dUTPase induces synthetic lethality with thymidylate synthase-targeted therapies in non-small cell lung cancer. Molecular cancer therapeutics 11, 616-628 (2012).
144. S. E. Koehler, R. D. Ladner, Small interfering RNA-mediated suppression of dUTPase sensitizes cancer cell lines to thymidylate synthase inhibition. Molecular pharmacology 66, 620-626 (2004).
145. P. M. Wilson, P. V. Danenberg, P. G. Johnston, H. J. Lenz, R. D. Ladner, Standing the test of time: targeting thymidylate biosynthesis in cancer therapy. Nature reviews. Clinical oncology 11, 282-298 (2014).
146. D. Salonga et al., Colorectal tumors responding to 5-fluorouracil have low gene expression levels of dihydropyrimidine dehydrogenase, thymidylate synthase, and thymidine phosphorylase. Clinical cancer research : an official journal of the American Association for Cancer Research 6, 1322-1327 (2000).
147. W. Bai, Y. Wu, P. Zhang, Y. Xi, Correlations between expression levels of thymidylate synthase, thymidine phosphorylase and dihydropyrimidine dehydrogenase, and efficacy of 5-fluorouracil-based chemotherapy for advanced colorectal cancer. International journal of clinical and experimental pathology 8, 12333-12345 (2015).
148. J. R. Mackey et al., Functional nucleoside transporters are required for gemcitabine influx and manifestation of toxicity in cancer cell lines. Cancer research 58, 4349-4357 (1998).
149. J. Spratlin et al., The absence of human equilibrative nucleoside transporter 1 is associated with reduced survival in patients with gemcitabine-treated pancreas adenocarcinoma. Clinical cancer research : an official journal of the American Association for Cancer Research 10, 6956-6961 (2004).
150. W. Greenhalf et al., Pancreatic cancer hENT1 expression and survival from gemcitabine in patients from the ESPAC-3 trial. Journal of the National Cancer Institute 106, djt347 (2014).
151. S. Nordh, D. Ansari, R. Andersson, hENT1 expression is predictive of gemcitabine outcome in pancreatic cancer: a systematic review. World journal of gastroenterology 20, 8482-8490 (2014).
152. M. Pastor-Anglada, S. Perez-Torras, Nucleoside transporter proteins as biomarkers of drug responsiveness and drug targets. Frontiers in pharmacology 6, 13 (2015).
153. R. Marechal et al., Human equilibrative nucleoside transporter 1 and human concentrative nucleoside transporter 3 predict survival after adjuvant gemcitabine therapy in resected pancreatic adeno-

carcinoma. Clinical cancer research : an official journal of the American Association for Cancer Research 15, 2913-2919 (2009).
154. C. H. Wei et al., A meta-analysis of gemcitabine biomarkers in patients with pancreaticobiliary cancers. Pancreas 42, 1303-1310 (2013).
155. C. Serdjebi, G. Milano, J. Ciccolini, Role of cytidine deaminase in toxicity and efficacy of nucleosidic analogs. Expert opinion on drug metabolism & toxicology 11, 665-672 (2015).
156. E. Giovannetti et al., Transcription analysis of human equilibrative nucleoside transporter-1 predicts survival in pancreas cancer patients treated with gemcitabine. Cancer research 66, 3928-3935 (2006).
157. H. Fujita et al., Gene expression levels as predictive markers of outcome in pancreatic cancer after gemcitabine-based adjuvant chemotherapy. Neoplasia (New York, N.Y.) 12, 807-817 (2010).
158. R. Mlak et al., The relationship between RRM1 gene polymorphisms and effectiveness of gemcitabine-based first-line chemotherapy in advanced NSCLC patient. Clinical & translational oncology : official publication of the Federation of Spanish Oncology Societies and of the National Cancer Institute of Mexico, (2015).
159. S. N. U. H. ClinicalTrial, Adjuvant Gemcitabine Versus 5-FU/Leucovorin Based on hENT1 Immunostaining. ClinicalTrials.gov [Internet] NCT02486497, (2015).
160. M. De Donato et al., Class III beta-tubulin and the cytoskeletal gateway for drug resistance in ovarian cancer. Journal of cellular physiology 227, 1034-1041 (2012).
161. J. A. McCarroll, P. P. Gan, M. Liu, M. Kavallaris, betaIII-tubulin is a multifunctional protein involved in drug sensitivity and tumorigenesis in non-small cell lung cancer. Cancer research 70, 4995-5003 (2010).
162. S. J. Vidal, V. Rodriguez-Bravo, M. Galsky, C. Cordon-Cardo, J. Domingo-Domenech, Targeting cancer stem cells to suppress acquired chemotherapy resistance. Oncogene 33, 4451-4463 (2014).
163. X. Zheng et al., Epithelial-to-mesenchymal transition is dispensable for metastasis but induces chemoresistance in pancreatic cancer. Nature 527, 525-530 (2015).
164. K. R. Fischer et al., Epithelial-to-mesenchymal transition is not required for lung metastasis but contributes to chemoresistance. Nature 527, 472-476 (2015).
165. A. Albini, M. B. Sporn, The tumour microenvironment as a target for chemoprevention. Nature reviews. Cancer 7, 139-147 (2007).
166. N. Iida et al., Commensal bacteria control cancer response to therapy by modulating the tumor microenvironment. Science (New York, N.Y.) 342, 967-970 (2013).
167. S. Viaud et al., The intestinal microbiota modulates the anticancer immune effects of cyclophosphamide. Science (New York, N.Y.) 342, 971-976 (2013).

Chapter 9: Genome-wide identification and characterization of novel factors conferring resistance to topoisomerase II poisons in cancer

Ruud H Wijdeven[1,6], Baoxu Pang[1,6], Sabina van der Zanden[1], Xiaohang Qiao[1], Vincent Blomen[2], Marlous Hoogstraat[3,4], Esther H Lips[3,5], Lennert Janssen[1], Lodewyk Wessels[4], Thijn Brummelkamp[2] and Jacques Neefjes[1]

[1] Division of Cell Biology,
[2] Division of Biochemistry,
[3] Division of Molecular Pathology,
[4] Division of Molecular Carcinogenesis,
[5] Division of Pathology, The Netherlands Cancer Institute, Plesmanlaan 121, 1066CX Amsterdam, the Netherlands.
[6] These authors contributed equally to this work.

Cancer Research. 2015: 75(19) 4176-4187

Abstract

The Topoisomerase II poisons doxorubicin and etoposide constitute longstanding cornerstones of chemotherapy. Despite their extensive clinical use, many patients do not respond to these drugs. Using a genome-wide gene knockout approach, we identified Keap1, the SWI/SNF complex, and C9orf82 as independent factors capable of driving drug resistance through diverse molecular mechanisms, all converging on the DNA double-strand break (DSB) and repair pathway. Loss of Keap1 or the SWI/SNF complex inhibits generation of DSB by attenuating expression and activity of topoisomerase IIα, respectively, while deletion of C9orf82 augments subsequent DSB repair. Their corresponding genes, frequently mutated or deleted in human tumors, may impact drug sensitivity, as exemplified by triple-negative breast cancer patients with diminished SWI/SNF core member expression who exhibit reduced responsiveness to chemotherapy regimens containing doxorubicin. Collectively, our work identifies genes
that may predict the response of cancer patients to the broadly used topoisomerase II poisons and defines alternative pathways that could be therapeutically exploited in treatment-resistant patients.

Introduction

Topoisomerase II (Topo II) poisons, including those of the anthracycline and podophyllotoxin families, are among the major classes of chemotherapeutics used to treat a wide spectrum of tumors. These drugs trap Topo II onto the DNA and inhibit DNA re-ligation, hereby 'poisoning' the enzyme and generating DNA double-strand breaks (1). Despite their broad applicability, resistance constitutes a frequent clinical limitation (2). Given the serious side effects associated with their administration, development of a comprehensive panel of treatment predicting factors could provide a useful clinical tool for matching chemotherapy to individual patients (1).

Anthracyclines, with doxorubicin (Doxo) as their prominent example, constitute an especially effective class of anti-cancer drugs, as they intercalate into the DNA and evict histones from the chromatin, concomitant to inhibiting Topo II after the formation of a DNA double-strand break (3, 4). As a result, the DNA damage response is attenuated and the epigenome becomes deregulated at defined regions in the genome (3, 5). The cellular pathways contributing to Doxo resistance have been interrogated extensively, and the drug transporter ABCB1 (MDR1), capable of exporting Doxo from cells (2), has emerged as a major player in this context. Despite its role in drug removal at the blood-brain barrier, inhibition of ABCB1 failed to satisfactorily revert unresponsiveness to Doxo in the clinic (6). Other factors, acting either alone or in combination with proteins such as ABCB1, have been implicated in Doxo resistance through the downregulation of either Topo II or other DNA damage response (DDR) pathway constituents (7, 8). Thus far, none of the above factors have been shown to individually account for the observed variability in patients' responses to Doxo (1, 9). Taken together, the findings reported to date suggest the existence of other as of yet undefined molecular determinants instrumental in the conversion to a Doxo-resistant state.

Herein we report on a genome-wide screen for factors driving resistance to Doxo using a knockout approach in haploid cells (10). With the aim of approximating the

physiological situation of patient drug exposure—and by extension drug resistance—in the tissue culture environment, we iteratively subjected cells to Doxo for three brief periods as a means of selecting for relative drug resistance. Our screening methodology yielded two previously described contributors to drug resistance: the aforementioned transporter ABCB1 (2) and the stress response gene Keap1 (11). We also identified several novel factors: the gene product of C9orf82 that appears to function as an inhibitor of DNA damage repair and the chromatin remodeling SWI/SNF complex subunits SMARCB1 and SMARCE1. Depletion of either Keap1, C9orf82 or SMARCB1 was found to induce cellular resistance to Topo II poisons, without significantly affecting sensitivity to either Topo I inhibitors or aclarubicin (Acla), an analog of Doxo that does not induce DNA damage (3, 5). All genes identified in the resistance screen were found to regulate Topo II-induced DNA break formation or subsequent DNA repair. In the clinic, tumors frequently harbor mutations or deletions in Keap1, C9orf82 or components of the SWI/SNF complex (12-14). These may be relevant for patient stratification to Doxo-based therapies, as illustrated by the correlation between expression levels of Keap1 and the SWI/SNF complex subunits and the response of triple negative breast cancer patients to Doxo-based treatment. Our data provide a molecular basis for patient selection in the clinic with regards to the broadly used Topo II poisons in cancer therapy.

Results

Identification and validation of doxorubicin-resistance factors Keap1, C9orf82 and the SWI/SNF complex

To identify genetic determinants involved in resistance to Doxo, we performed a genome-wide insertional mutagenesis screen in haploid cells using a gene trap retrovirus (10). A genomic insertion of the virus into the sense direction of a gene disrupts its expression and often results in a complete knockout of the gene. HAP1 cells were infected with a gene trap retrovirus to generate a pool of randomly mutagenized cells and briefly passaged prior to drug exposure. To recapitulate the normal pharmacokinetics of Doxo in a tissue culture setting, we exposed these cells for 2 hours to 1μM Doxo, which is within the peak plasma dose of standard treatment of cancer patients (15). Cells were treated weekly for three weeks, after which surviving cells were grown out and insertions were mapped and aligned to the human genome (Fig. 1A). Disruptions of six genes were significantly enriched ($p<0.00005$) in the surviving population compared to the untreated control (Fig. 1B and Table S1) Among these were two previously reported factors, ABCB1 (6) and Keap1 (16), as well as novel factors, including the SWI/SNF subunits, SMARCB1 and SMARCE1, the C9orf82 gene, and the translation initiation factor Eif4a1. Canonical Doxo-target Topo IIα appeared just below the threshold, with an adjusted p-value of 0.01. ABCB1 contained mostly anti-sense mutations following selection, which could enhance its expression (unpublished observation). All other enriched genes contained at least five independent insertions in the sense direction, leading to their inactivation. Identification of Keap1 provided validation of the screening methodology, as it has already been associated with resistance to several anti-cancer drugs, including Doxo (11, 12, 17). To validate the screen hits, we generated HAP1 cells stably expressing either control shRNA or two independent shRNAs targeting Keap1, which reduced Keap1 expres-

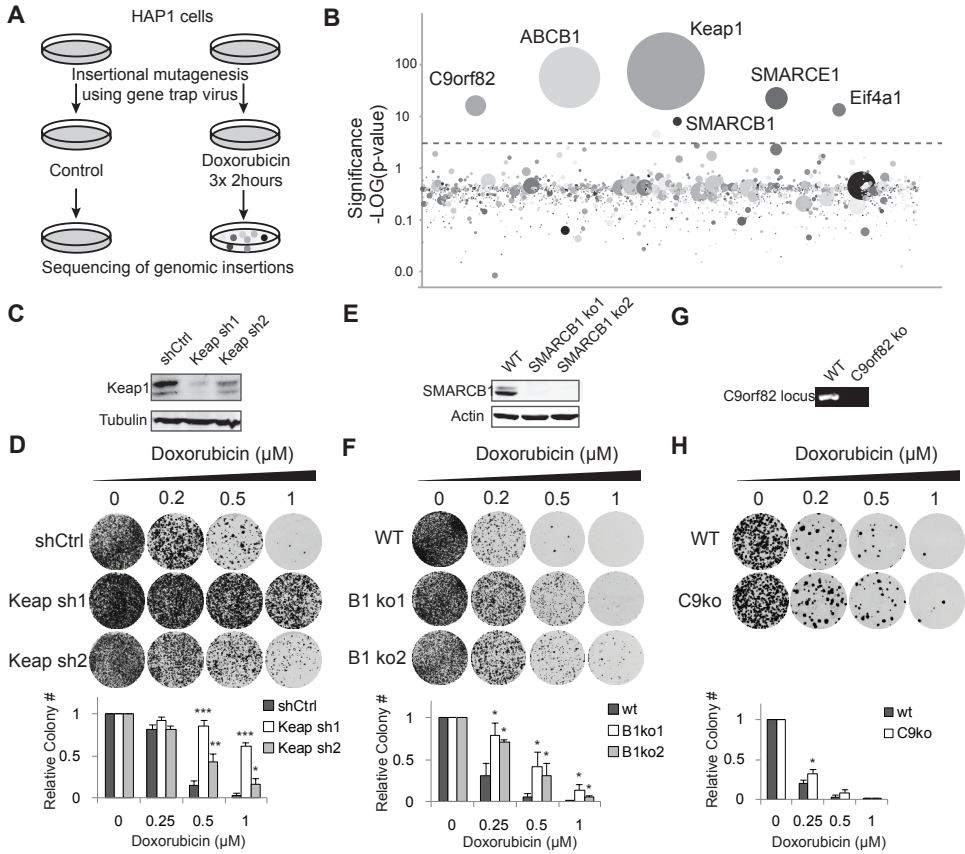


Figure 1: Genome-wide mutagenesis screen identifies Keap1, the SWI/SNF complex and C9orf82 as regulators of doxorubicin resistance*. (A) Schematic set-up of the haploid genetics screen to identify genes involved in Doxo resistance. (B) Screening results. The y axis indicates the significance of enrichment of gene-trap insertions in Doxo-treated compared to non-treated control cells. The circles represent genes and their size corresponds to the number of independent insertions mapped in the gene. For more hits, see Table S1. (C) Keap1 silencing was determined by Western blotting analysis. (D) Long-term colony formation assay with HAP1 cells transduced with shRNAs targeting Keap1 or a control shRNA. Cells were treated with the indicated concentration Doxo for 2h and left to grow out. After 9 days, cells were fixed, stained and imaged. Quantification of colony numbers per plate and condition from three independent experiments (+SD) are shown below the images. (E) Western blotting showing depletion of SmarcB1 by two independent CRISPR-targeting sequences. (F) Long term colony formation assays for wild-type and SMARCB1-depleted cells. Results from three independent experiments (+SD) were quantified and are shown below the images. (G) Genomic PCR showing the knockout of C9orf82. (H) Long-term colony formation assay for wild-type and C9orf82-depleted cells. Results from three independent experiments (+SD) were quantified and are shown below the images. Statistical significance was calculated compared to control (* p < 0.05, ** p < 0.01, *** p < 0.001).*

sion by 50-80% (Fig. 1C and Fig. S1A). These knockdown cell lines were subsequently exposed to Doxo for two hours, followed by drug wash out and outgrowth. As expected, Keap1 depletion conferred Doxo resistance as illustrated in both colony formation and viability assays (Fig. 1D and Fig. S1B).

We then proceeded to validate the novel screen hits. Two independent CRISPR/

Cas9 constructs targeting the SMARCB1 gene (Fig. 1E) rendered the cells more resistant to Doxo, both in colony formation and viability assays (Fig. 1F and Fig. S1C). Independent identification of two members of the SWI/SNF chromatin-remodeling complex (18), SMARCB1 and SMARCE1, suggested that deregulation of the complex as a whole may drive resistance to Doxo. Although we could not validate a role for SMARCE1 in resistance to Doxo, shRNA-mediated depletion of the SWI/SNF core members SMARCA4 and ARID1A, alongside SMARCB1, induced resistance to Doxo (Fig. S1D and S1E), supporting the notion that loss of the SWI/SNF complex functionality confers resistance to Doxo.
While we did not further pursue the translational elongation complex subunit Eif4a1, we tested the contribution of the open reading frame 82 on chromosome 9 (C9orf82) to Doxo sensitivity. A small but significant growth advantage was observed in response to Doxo treatment in C9orf82 knockout cells using a colony formation assay (Fig. 1G and H). Collectively, our genome-wide screen identified multiple novel factors capable of incurring resistance to Doxo in a cell culture setting.

Cross-resistance to other DNA-damaging drugs

Doxo is known to act on cells by a combination of Topo II poisoning, eviction of histones from the chromatin and the generation of reactive oxygen species (ROS) (3, 4, 19). To establish which of these mechanisms are affected by Keap1, the SWI/SNF complex and C9orf82, we treated the respective knockdown or knockout cell lines with either the different Topo II poisons daunorubicin (Daun; an anthracycline with a structure and activity similar to Doxo) or etoposide (Etop; a Topo II poison structurally unrelated to Doxo and incapable of evicting histones), or with aclarubicin (Acla; an anthracycline family member that evicts histones, induces ROS and inhibits Topo II but does not induce DNA damage (20)). Silencing Keap1 or eliminating SMARCB1 or C9orf82 rendered cells more resistant to both Etop and Daun, but not Acla (Fig. 2A-2C) as indicated by viability as well as colony formation assays. Given the properties of the three drugs, these observations provide hints as to the molecular mechanisms underlying Doxo resistance via these genes – through the DNA damage arm. Interestingly, C9orf82 depletion rendered cells more resistant to Etop than to Doxo or Daun, suggesting that fast DNA repair may be critical for this gene's mode of action, as Doxo and Daun attenuate DNA repair by eviction of H2AX (5).
Importantly, depletion of none of our hits induced measurable resistance to the topoisomerase I poison topotecan (TPT) that induces single-strand DNA breaks (Fig 2C and 2D), suggesting that Keap1, the SWI/SNF complex and C9orf82 are involved in the Topo II-dependent DDR pathway.

Keap1 controls the expression of Topo IIα independently of Nrf2

Of the three validated resistance factors from the screen, Keap1 has been previously linked to chemoresistance (11, 16, 21). Keap1 functions as an E3 ligase adaptor and is known to mediate the degradation of Nrf2, a transcription factor for oxidative stress response genes (22). Upregulation of Nrf2 desensitizes cells to several anti-cancer drugs, including alkylating and anti-mitotic agents, which suggests that downregulation of Keap1 may induce drug resistance by stabilizing Nrf2 (12, 16, 17). To test this, we used CRISPR/Cas9 technology to generate Nrf2 knockout cells (Fig.

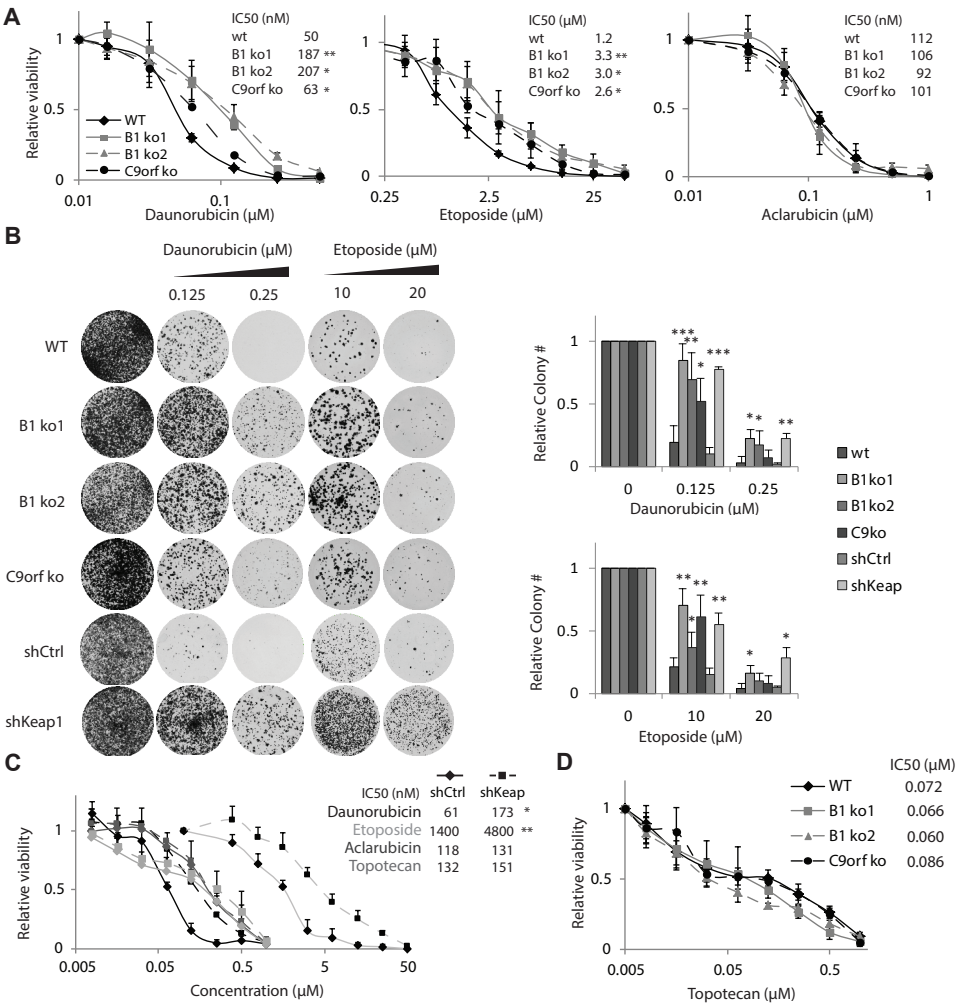


Figure 2: Keap1, SWI/SNF and C9orf82 control to sensitivity to TopoII but not the TopoI inhibitor or Acla. *(A) HAP1 cells depleted for SMARCB1 or C9orf82 were treated for 2h with Daun, Etop or Acla and cell viability was analyzed 72h later by a cell titer blue (CTB) assay. (B) Long term colony formation assay with HAP1 cells depleted for SMARCB1, C9orf82 or Keap1 that were treated for 2h with the indicated drug at different concentrations. (C) HAP1 cells stably expressing shCtrl or shKeap1 were treated for 2h with Daun, Etop, Acla or topotecan and cell viability was analyzed 72h later by a CTB assay. (D) HAP1 cells depleted for SMARCB1 or C9orf82 were treated for 2h with TPT and cell viability was analyzed 72h later by a CTB assay. All experiments shown are representatives of at least three independent experiments. Statistical significance was calculated as compared to control cells (* $p < 0.05$, ** $p < 0.01$, *** $p < 0.001$).*

3A), functionally validated by a drastic reduction of expression of Nrf2 target gene NQO1 (Fig. S2A). Unexpectedly, silencing of Keap1 in the Nrf2 null background still endowed cells more resistance to Doxo and Etop (Fig. 3A), implying the existence of an Nrf2-independent mechanism for Keap1 in modulating cellular responsiveness to Topo II dependent DNA-damage inducers.

Double-strand DNA break analysis indicated that loss of Keap1 significantly de-

creases the amount of such breaks induced by either Etop or Doxo treatment (Fig. 3B). These results were corroborated by the observed reduction in the DNA damage response as measured by γ-H2AX following exposure to Etop (Doxo evicts H2AX from the DNA and was therefore not used to measure the DDR after drug exposure) (Fig. 3C). Keap1 silencing did not affect uptake of Doxo (monitored by intrinsic fluorescence of the drug by flow cytometry, Fig. 3D), suggesting that Keap1 may control either the levels or activity of the drug target, Topo IIα. Cells depleted of Keap1 had lower Topo IIα expression levels relative to the control (Fig. 3E), which was independent of Nrf2 activity (Fig. 3F). A link between Topo IIα expression levels and resistance against Topo II poisons has been previously suggested (7, 23, 24).

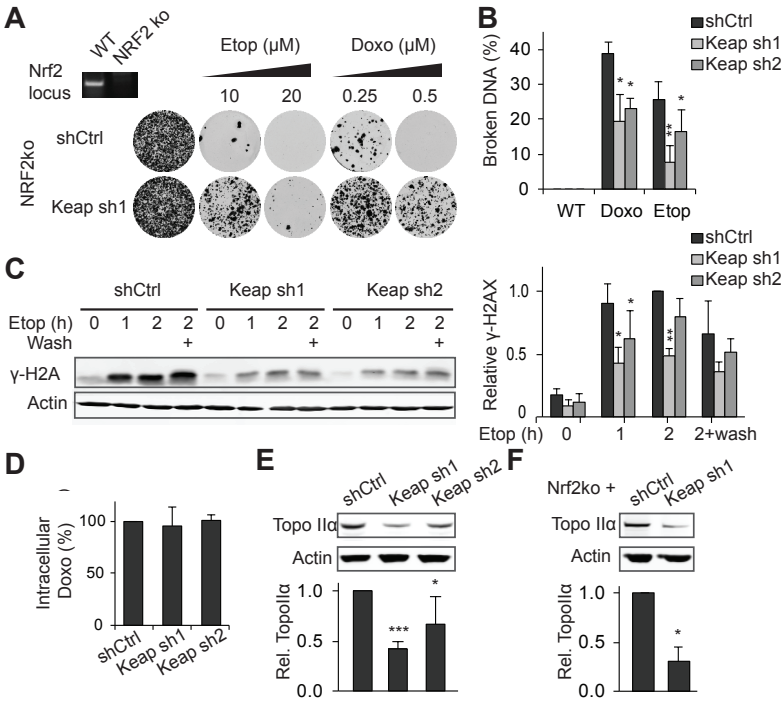


Figure 3: Keap1 controls Topo IIα expression independently of Nrf2. *(A) Long-term colony growth assay for HAP1 cells depleted for Nrf2 and further stably transduced with shKeap1 or shCtrl. Cells were treated for 2h with Doxo or Etop at the indicated concentrations and left to grow out for 9 days. Insert: the DNA gel shows loss of the genomic Nrf2 locus in the knockout cells. (B) Analysis of the amount of Etop- or Doxo-induced DNA breaks using constant field gel electrophoresis. HAP1 cells were treated for 2h with 1μM Etop or Doxo, lysed and analyzed. Shown is the quantification of the broken DNA relative to input. (C) Hap1 cells were treated with 5μM Etop for the indicated time points, or the drug was washed out after 2h and cells were left to recover for another 2h (lanes '+'), lysed and analyzed by SDS-PAGE and Western blotting. Right: quantification of the γ-H2AX signal normalized to actin. The signal of wild-type cells treated for 2h was set at 1. (D) Cells were treated with 2μM Doxo for 1h and Doxo levels were analyzed using flow cytometry. Control shRNA was set at 1. (E) Western blotting analysis for expression of Topo IIα in HAP1 cells silenced for Keap1. For quantification, the signal is normalized to actin and the shCtrl was set at 1. (F) Western blotting analysis for expression of Topo IIα in HAP1 Nrf2ko cells stably depleted or not for Keap1. All results are mean +/-SD of biological triplicates, except for (E), which are biological quadruplicates. Statistical significance was calculated compared to control (* p < 0.05, ** p < 0.01, *** p < 0.001).*

These observations indicate that Keap1 can control resistance to Topo II poisons by two distinct mechanisms—regulating Nrf2 expression to control a series of stress-response genes and by mediating the expression of the canonical target Topo IIα.

C9orf82 regulates repair of DNA damage induced by TopoII poisons

By contrast to the previously studied role of Keap1 in drug resistance, the role of C9orf82 in this context has not been addressed, with its only function thus far assigned being negative regulation of apoptosis (25). We began by addressing the effect of this gene on Topo II induced DSB formation and repair as pertaining to Topo II function. Monitoring the DNA DSBs and the resulting DNA damage response following exposure to either Doxo or Etop revealed no difference in the initial levels of DNA damage incurred between the control and C9orf82 knockout cells (Fig. 4A and 4B). Strikingly, the resolution of the DNA damage response signal following Etop treatment (as visualized by γ-H2AX) was significantly accelerated in C9orf82 knockout cells (Fig. 4B). Similar results were obtained with another independently generated C9orf82 knockout clone (Fig. S3A-C). Conversely, ectopic expression of GFP-tagged C9orf82 in MelJuSo melanoma cells (a cell line with fast DNA re-

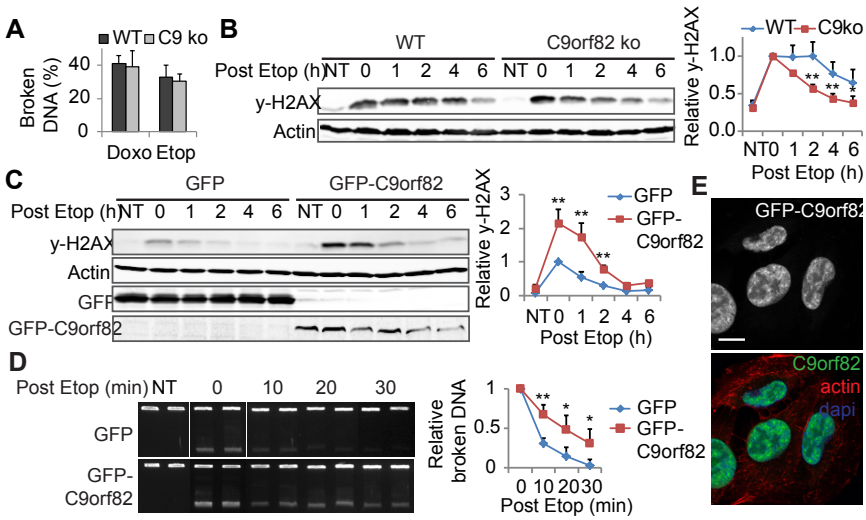


Figure 4: C9orf82 regulates DNA double-strand break repair. *(A) Analysis of the amount of Etop- or Doxo-induced DNA breaks using constant field gel electrophoresis. HAP1 cells were treated for 2h with 1μM Etop or Doxo, lysed and analyzed. Shown is the quantification of broken DNA relative to input. (B) Western blotting analysis for γ-H2AX. Cells were treated with 1μM Etop for 1h, washed and lysed at the indicated time points. Right panel: quantification of the signals detected on the WB. Signals were normalized to actin and t=0 was set at 1. (C) GFP or GFP-C9orf82 over-expressing MelJuSo cells were exposed to 5μM Etop and analyzed for γ-H2AX as in (B). (D) MelJuSo cells stably over-expressing GFP or GFP-C9orf82 were treated with 1μM Etop for 2h. Drugs were removed before further culture. Cells were lysed at the indicated time points post drug removal. DNA break repair was analyzed using constant field gel electrophoresis. Lower band represents the broken DNA and the top band the intact DNA. Separate panels are different cut-outs from the same gel. For quantification, t=0 of the GFP or GFP-C9orf82 cells was set at 1. (E) Cellular localization of C9orf82 by confocal imaging of MelJuSo cells stably expressing GFP-C9orf82 and stained for DAPI (blue) and actin (red). Scale bar: 10μm. All experiments shown are mean+SD of three independent experiments. Statistical significance compared to control (* $p < 0.05$, ** $p < 0.01$). NT = non-treated.*

pair kinetics) led to a stronger and more persistent γ-H2AX DNA damage response upon Etop treatment (Fig. 4C). Since DNA repair already takes place during the first hour of Etop treatment, these data indicate that C9orf82 influences the kinetics of γ-H2AX resolution and hereby the DNA damage response. To assess whether C9orf82 regulates DSB repair itself, we determined the DSB repair kinetics in cells overexpressing either GFP or GFP-C9orf82 (Fig. 4D), with the latter resulting in decreased Etop-induced DNA DSB repair. This suggests that C9orf82 decreases the rate of DNA repair.
Although C9orf82 localizes primarily in the nucleus (Fig. 4E), it is unlikely to directly inhibit DNA repair, since it is not recruited to Etop-induced γ-H2AX foci (Fig. S3D). On this basis, C9orf82 appears to attenuate DNA double-strand break repair induced by Topo II poisons, for its loss serves to accelerate DNA damage repair, thereby promoting resistance to DNA double-strand break inducers such as Doxo and Etop. The exact molecular mechanism of DNA repair modulation by this novel protein is at present unclear.

The SWI/SNF complex controls chromatin loading of Topo II to confer drug resistance

In addition to the resistance factors described above, we also identified two subunits of the SWI/SNF complex involved in the resistance to Topo II poisons. The SWI/SNF complex is known to modulate transcription through chromatin remodeling (18). Additionally, it has recently been shown to mediate decatenation of chromatids during mitosis by loading Topo IIα onto the DNA (26). The latter suggests a possible means by which the SWI/SNF complex may affect the susceptibility of cells to Topo II poisons, by reducing the chromatin loading and activity of Topo IIα. To address this, HAP1 cells either proficient in or depleted of the SWI/SNF subunit SMARCB1 were exposed to Etop or Doxo, and the resulting DNA double-strand breaks were quantified. The SMARCB1-depleted cells exhibited significantly lower levels of such DNA breaks (Fig. 5A), as well as reduced DNA damage response signaling, as visualized by γ-H2AX analysis (Fig. 5B and 5C). These changes were not a result of drug uptake deficiency (Fig. 5D) or altered expression levels of Topo IIα (Fig. 5E). Given that SMARCB1 interacts with Topo IIα (Fig. 5F) (26), the expected reduction in loading of Topo IIα onto the DNA in cells compromised for SMARCB1 presents a likely explanation for the diminished efficacy of Topo II poisons in these cells. To confirm this, we assessed the association of Topo IIα to the chromatin using a chromatin binding assay as described in (26). Treatment of cells with Etop yielded more Topo IIα loaded onto chromatin (Fig 4G), indicating this assay can be used to assess Topo IIα activity and arrest. In line with our hypothesis, SMARCB1 depletion resulted in a decreased amount of Topo IIα loaded onto chromatin after Etop exposure (Fig 4G), indicating that loss of SMARCB1 reduces the level of Topo IIα that is poisoned on the chromatin. These results suggest that the SWI/SNF complex modulates resistance to TopoII poisons by controlling the loading of Topo IIα onto the DNA.

Expression of SWI/SNF subunits in epithelioid sarcoma and triple negative breast cancers correlate to doxorubicin response

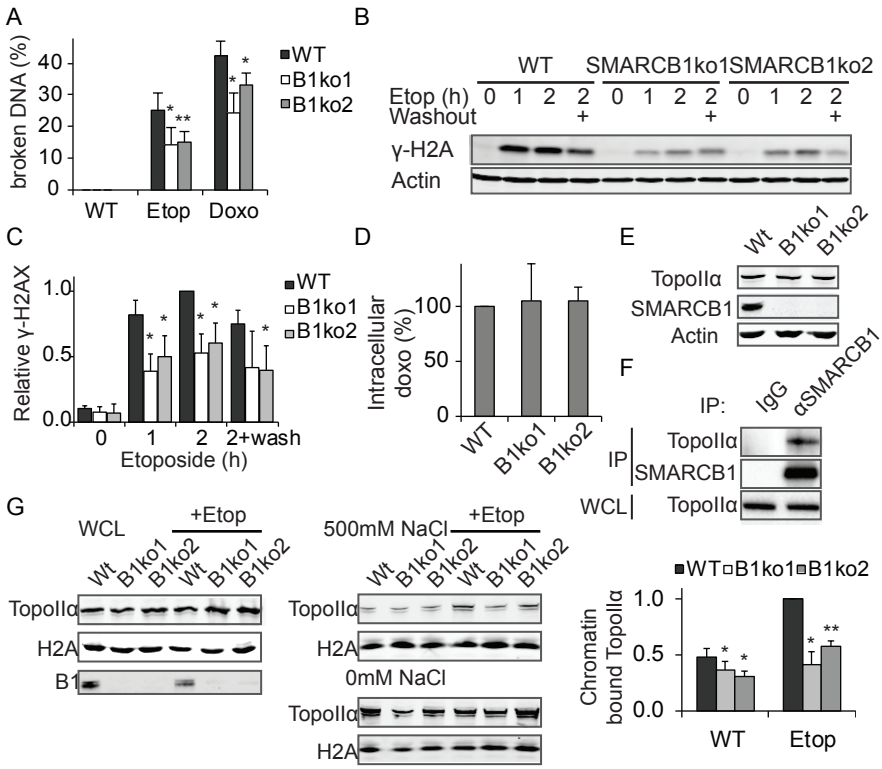


Figure 5: The SWI/SNF complex regulates Topo IIα chromatin loading and activity. *(A) The amount of Etop- or Doxo-induced DNA breaks was quantified by constant field gel electrophoresis. HAP1 WT and SMARCB1 knockout cells were treated for 2h with 1μM Etop or Doxo. Shown is the quantification of the relative amount of broken DNA. (B) Western blot analysis for γ-H2AX after exposing cells to 5μM Etop for the indicated time points, or first treated for 2h and lysed 2h (lanes '+') after Etop removal. Actin is probed as a loading control. (C) Quantification of (B). The γ-H2AX signal is normalized to the actin signal and t=2 hours for WT is set at 1. (D) Quantification of Doxo uptake levels by flow cytometry. The different cells were incubated for 1h with 2μM Doxo before analysis. (E) Western blot analysis of Topo IIα expression levels in HAP1 cells either or not depleted for SMARCB1, as indicated. Actin is shown as loading control. (F) Co-immunoprecipitation (IP) of SMARCB1 and Topo IIin HAP1 cells followed by SDS-PAGE and Western blotting. IgG IP is used as control. WCL: Topo II in total lysates are shown as loading control. (G) Chromatin association assay for TopoIIα. Chromatin pellets of indicated HAP1 cells untreated or treated with 1μM Etop for 15min were lysed directly (WCL), or treated with the indicated salt concentration (0mM or 500mM) before lysis. For quantification, the 500mM NaCl Topo IIα signal was corrected for loading (H2A) and WCL input signal. WT Etop 15 min was set at 1. All experiments shown are mean+SD of independent triplicates. Statistical significance was calculated compared to control (* p < 0.05, ** p < 0.01).*

Although mutations in the SWI/SNF members are frequently observed in human tumors (14), their relationship to clinical outcome is lacking. Epithelioid sarcomas are known to harbor deletions of the SMARCB1 gene in 60-90% of the cases (27, 28) and are commonly treated with Doxo-containing regimens. Re-analysis of a previously reported dataset (28) revealed that patients with a deletion for SMARCB1 experienced more relapses after treatment (Fig. 6A), suggesting a relationship between SMARCB1 expression and treatment outcome. To further assess whether SWI/SNF status correlates directly with patient responses to treatment with Topo II poisons,

we used an expression dataset of 116 human triple-negative breast cancer (TNBC) patients treated at our cancer center with a regimen of Doxo and cyclophosphamide. We compared the expression of the SWI/SNF complex subunits SMARCB1, SMARCA4, SMARCE1 and ARID1a with the clinical response to this treatment. Our analysis showed that patients with a pathological complete response had a significantly higher expression of SMARCB1 and SMARCA4 (Fig 6B), but not ARID1a or SMARCE1 (Fig S4A). Furthermore, by analyzing the other genes identified from the screen, we found a significant correlation between response and expression for Keap1, but not C9orf82 (Fig S4A). These data suggest that in triple-negative breast cancer patients, low expression of SMARCB1 and SMARCA4 is associated with poor response to a Doxo-containing regimen.
To validate that SMARCB1 and SMARCA4 causally regulate sensitivity to Doxo in TNBC settings, we silenced both genes in two TNBC cell lines, HCC1937 and SKBR7 (Keap1 silencing was toxic for these cells and could not be tested). Silencing of both genes rendered cells more resistant to Doxo (Fig 6C) and led to a reduced induction of DNA damage signaling (Fig 6D).
Taken together, loss or reduced expression of SMARCB1 and SMARCA4 negatively impacts Doxo-induced DNA double-strand break formation and leads to drug resistance in triple negative breast cancer cell lines and patients.

Discussion

Annually, nearly 1 million cancer patients are treated with Topo II poisons such as Doxo, Daun or Etop. Yet, resistance to these drugs persists as a major complication in cancer treatment. Because the molecular basis for this resistance is not fully understood, many patients receive ineffective treatments accompanied by adverse side effects in the absence of the corresponding clinical benefit (1). To facilitate treatment outcome predictions for Doxo relative to other available alternative drugs, improved insights into the mechanisms of drug resistance are necessary. Using a genome-wide screening approach, we identified and characterized several novel factors involved in resistance to Topo II poisons. In addition to the previously described factors, including the drug transporter ABCB1 and adaptor Keap1, we identified C9orf82 and the SWI/SNF complex as novel regulators of Doxo resistance. Keap1, C9orf82 and SWI/SNF can all be placed in the pathway involving Topo II-induced DNA double-strand break formation and the subsequent DDR (Fig 7). Consequently, depletion of these genes does not confer resistance to either the Topo I inhibitor TPT, or Acla, an anthracycline that does not induce DNA double-strand breaks (3).
Keap1 has already been studied in the context of chemosensitivity to several classes of anti-cancer drugs, including alkylating agents, anti-mitotic agents and Topo II poisons (11, 17, 21). Inhibition of its cognate substrate Nrf2 sensitizes cells to a number of these drugs, suggesting that Keap1 influences sensitivity by virtue of Nrf2 destabilization (11, 17). However, Keap1 controls several other signaling pathways (29-31), and could thus affect drug resistance in other ways. We interrogated these two options by depleting Nrf2 and found that asides from regulating Nrf2, Keap1 induces resistance to Topo II poisons by controlling the expression levels of Topo IIα . Clinically, we show that the expression of Keap1 is correlated to the response

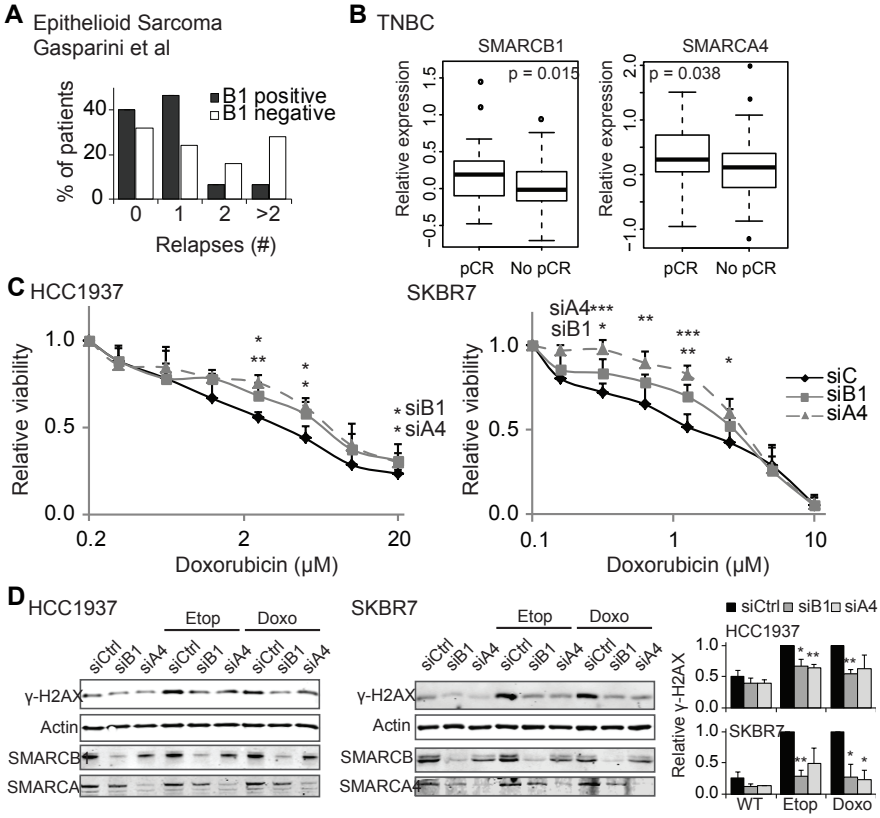


Figure 6: SMARCB1 and SMARCA4 expression correlates to responses to Doxo in triple negative breast cancer cells and patients. *(A) Re-analysis of the number of relapses in 25 SMARCB1 negative and 15 SMARCB1 positive epithelioid sarcoma patients, as described in (28). (B) Box plot representing the expression of SMARCB1 and SMARCA4 in 113 triple-negative breast cancer patients with a pathological complete response (pCR, 46 patients) or not (no pCR, 67 patients) following a Doxo containing regimen. Statistical significance was calculated using a Student's T-test. (C) HCC1937 or SKBR7 cells were transfected with control siRNAs or siRNAs targeting SMARCB1 or SMARCA4. 72h after transfection, cells were treated with the indicated doses of Doxo for 2h and cell viability was analyzed 72h after drug exposure. (D) HCC1937 or SKBR7 cells were transfected with siRNAs as in (C) and treated 72h later with 5μM Etop or Doxo for 1h, lysed and analyzed with SDS-PAGE and western blotting analysis. Quantifications in C-D are mean+SD of independent triplicate experiments. Statistical significance was calculated compared to control (* p < 0.05, ** p < 0.01, *** p < 0.001).*

of triple negative breast cancer patients to Doxo and cyclophosphamide. Keap1 inactivating mutations and deletions are frequently observed in human tumors (32, 33). For example, 12-15% of lung tumors have inactivated Keap1 (32) and since these tumors are frequently treated with combinations of Etop and cisplatin, it may be beneficial to determine patients' Keap1 mutational status to assess the proper treatment protocol.

We also defined C9orf82 as a novel factor involved in resistance to Topo II poisons, most notably Etop. A previous study has identified C9orf82 as a negative regulator of caspase-mediated apoptosis (25), which is not in line with our observations that C9orf82 depletion desensitizes cells to Etop. Our data indicate that C9orf82 is a nu-

clear protein that controls the rate of DNA double-strand break repair after exposure to Topo II poisons. Doxo itself slows down DNA repair, which might explain why the resistance is most prominent following Etop exposure. Given that most Etop-induced DNA double-strand breaks are repaired by non-homologous end-joining (NHEJ) (34), C9orf82 may impinge on this arm of the DNA repair pathway, but how is currently unclear. C9orf82 is found mutated in 7-11% of glioblastoma tumors (13, 35), which makes it a potential prognostic factor in the treatment of such patients with Etop. However, further studies integrating clinical response data with mutational analyses are required to substantiate this possibility.

Besides this relatively unknown protein, we characterized the role of the SWI/SNF complex in the resistance to TopoII poisons. The SWI/SNF complex is mutated in around 20% of human tumors (14) and has been linked to tumor suppression (26). SWI/SNF complex subunits like SMARCB1 control the loading of Topo IIα onto the DNA and hereby determine the extent of DNA damage induced following exposure to Topo II poisons. SMARCB1 depleted cells therefore have less DNA breaks when exposed to Topo II poisons and thus a growth advantage. As many of the tumors that harbor mutations in the SWI/SNF complex are treated with Topo II poisons, drug-resistance could arise even when Topo IIα is expressed.

Several lines of evidence support this notion in patients. For example, SMARCB1 is mutated in 90-100% of the rhabdoid tumors (36, 37), a very aggressive childhood tumor that is unresponsive to Doxo (38). Also, epithelioid sarcoma patients harboring deletions for SMARCB1 have a higher chance of relapse following treatment protocols that usually includes Topo II poisons (28). Furthermore, we explored a

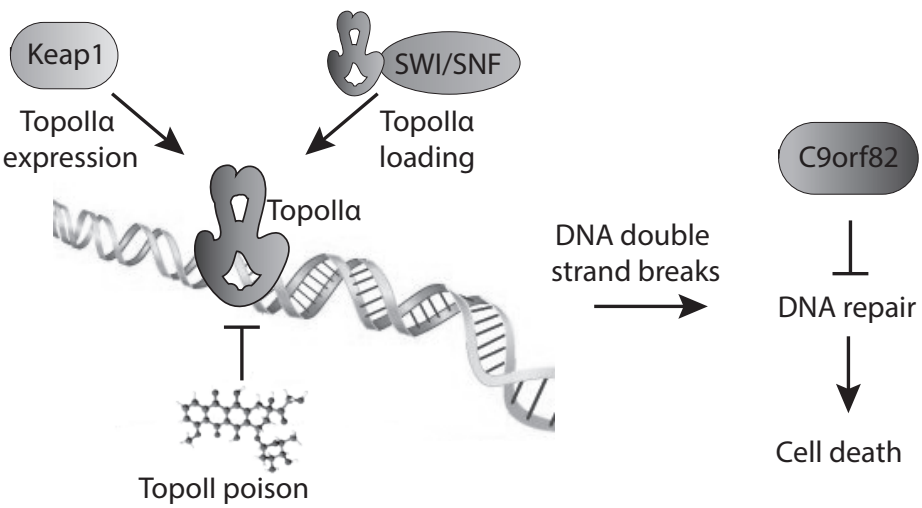


Figure 7: Model of SWI/SNF, Keap1 and C9orf82 regulating different phases of Topo II poison-induced DNA break formation and DDR*. Topo II poisons like Doxo induce DNA double-strand breaks by trapping Topo II on the DNA. If not sufficiently repaired, this leads to cell death. Keap1 controls the expression of Topo IIα, while SWI/SNF regulates the loading and hereby activity of Topo IIα. Loss of these genes therefore attenuates DNA double-strand break formation by Topo II poisons. In the next phase of the DNA breaks and repair cycle, C9orf82 controls DNA repair. Loss of C9orf82 accelerates DNA repair, reducing cell death induced by Topo II poisons.*

data set of triple negative breast cancer patients where both gene expression and treatment responses were documented. A correlation between treatment response and expression of SWI/SNF subunits SMARCB1 and SMARCA4 was observed within patients treated with Doxo and cyclophosphamide. No correlation was observed for SMARCE1 and ARID1a, which could be because SMARCE1 is not a part of the core complex essential for activity and ARID1a has redundancy with ARID1b (18), or because the expression of these factors is not the limiting factor for the complex to function. Given the resistance to Doxo observed in our cell culture experiments, these data suggest that patients with low or depleted SWI/SNF expression should not be treated with Doxo, but rather with Acla or TPT, which are drugs that work through a different mechanism and that do not show any cross-resistance in our experiments.

In conclusion, we identified and characterized three factors controlling sensitivity to the frequently used anti-cancer drugs Doxo and Etop. Keap1, C9orf82 and the SWI/SNF chromatin remodeling complex all act by affecting DNA double-strand break formation or repair following exposure to these drugs. Mutations in these genes are frequently observed in human tumors and expected to yield tumors that are resistant to these drugs, as we show for triple negative breast cancer patients. Profiling patients for mutations in these genes can further stratify treatment options as non-responding patients can be selected for other treatments rather than given ineffective treatment containing Topo II poisons.

Materials and methods

Cell culture and constructs

HAP1 and MelJuSo cells were grown in IMDM supplemented with 8% FCS. SKBR7 and HCC1937 cells were grown in RPMI with 8% FCS. HAP1 cells were generated as described in (39), sequence verified during the screen and kept under low passage afterwards. MelJuSo cells were initially described in (40) and sequence verified in 2013 (3), since then identity was confirmed by staining for marker MHCII. HCC1937 cells were obtained from ATCC (www.ATCC.org), where they were validated using STR profiling, and kept under low passage after receipt. SKBR7 cells were a kind gift from Klaas de Lint (Netherlands Cancer Institute, division of Molecular Carcinogenesis) and analyzed using STR profiling in 2015. Keap1 knockdown cells were generated by transduction with lentiviral vectors containing an shRNA sequence targeting Keap1. Keap1 sh1 targeted the 5'-GCGAATGATCACAGCAATGAA-3' sequence of Keap1 and Keap1 sh2 the 5'-CGGGAGTACATCTACATGCAT-3' sequence. Cells were maintained under puromycin (2.5 µg/ml) selection to generate stable knockdown cells. For GFP-C9orf82, the sequence of full length C9orf82 was cloned from an Image clone (#4648932) into the mGFP-C1 vector (Clontech) using the primers 5'-CCCAAAGCTTCCATGACGGGGAAAAAGTCCTC-3' and 5'-CCCAGGTACCCTAGGCTGGCTTTTTTATATC-3'. MelJuSo cells were transfected using effectene (Qiagen) and cells expressing GFP or GFP-C9orf82 were maintained under continuous selection with G418 (200 µg/ml).

Haploid genetic screen

The haploid genetics screen was performed as described (10). In brief, gene trap

virus was produced by transfecting the gene-trap plasmid together with packaging plasmids in HEK 293T cells. Virus was harvested, concentrated, and used to infect 1 x 108 HAP1 cells. After brief passaging to allow for protein turnover, mutagenized cells were exposed to the doxorubicin regimen described below. Drug resistant cells were expanded, genomic DNA was isolated and subsequently retroviral insertion sites were amplified by inverse PCR and mapped by parallel sequencing (Illumina HiSeq2000) of the genomic inserts. The enrichment of insertions in the drug-treated group was calculated by comparing the number of insertions between the doxorubicin-treated group and an unselected population (39) using a one-sided Fisher's exact test. These values were corrected for false discovery rate using the Benjamini and Hochberg method (10).

Generation of null alleles using CRISPR-Cas9

CRISPR targeting sequences were designed based on the tool from crispr.mit.edu (41). Oligo's were cloned into the pX330 backbone (42) and transfected using effectene (Qiagen) together with a vector containing a guide RNA to the zebrafish TIA gene (5'-ggtatgtcgggaacctctcc-3') and a blasticidin resistance gene with a 2A sequence that is flanked by two TIA target sites. Cells positive for both vectors excise the blasticidin resistance gene from the vector and will sporadically incorporate it into the targeted genomic locus by non-homologous end-joining (43). Successful integration of the cassette into the targeted gene disrupts the allele and renders cells resistant to blasticidin. The targeting sequences were: SMARCB1: KO1, 5'-TGGCGCTGAGCAAGACCTTC-3' and KO2, 5'-TGGCGCTGAGCAAGACCTTC-3', C9orf82: KO1, 5'-CAACGCGGGTACGATGTCCG-3' and KO2, 5'-TGACGGGGAAAAAGTCCTCC-3', and Nrf2: 5'-TGGAGGCAAGATATAGATCT-3'. Cells were selected on blasticidin (10µg/ml) for two days and knockout clones were validated by sequencing the genomic DNA. The following primers were used to detect deletion at the genomic level: SMARCB1 fw: 5'-CATTTCGCCTTCCGGCTTCGG-3', SMARCB1 rv: 5'-CTCGGAGCCGATCATGTAGAACTC-3', C9orf82 fw: 5'-GGAAGTGACGCATAACCTGCGAC-3', C9orf82 rv: 5'-CTGCAAGGAGCCCGAGACG-3', Nrf2 fw: 5'-GACATGGATTTGATTGACATACTTTGGAGGC-3', Nrf2 rv: 5'-CTGACTGGATGTGCTGGGCTGG-3' .

Reagents and siRNA transfections

Doxorubicin, etoposide and topotecan were obtained from Pharmachemie and daunorubicin was obtained from Sanofi-Aventis. Aclarubicin was obtained from Santa Cruz. Antibodies used for IP, Western blot and microscopy: mouse anti-Keap1, mouse anti-tubulin, mouse anti-actin (all from Sigma), rabbit anti-Topoisomerase II, rabbit anti-SMARCB1, rabbit anti-SmarcA4, rabbit anti-SMARCE1, rabbit anti-ARID1a (all from Bethyl laboratories), mouse anti-γH2AX, rabbit anti-H2A (Millipore). For siRNA mediated depletion of SMARCA4 and SMARCB1, cells were reverse transfected with DharmaFECT transfection reagent #1 and 50 nM siRNA (Human siGenome SMARTpool, Dharmacon) according to the manufacturing protocol. Briefly, siRNAs and DharmaFECT were mixed and incubated for 20 minutes, after which cells were added and left to adhere. Three days later, cells were treated and lysed for SDS-PAGE and Western blotting analysis or left to grow out for three more days for the cell viability assay.

Long-term proliferation assays

Cells were seeded into 12-well plates (5000 cells per well). The next day, drugs were added at concentrations indicated and cultured for two hours. Subsequently, drugs were removed and cells were left to grow for 7-9 days, fixed using 3.7% formaldehyde and stained using 0.1% Crystal violet solution (Sigma). Quantification of colonies was done by Image J.

Short-term growth inhibition assays

Cells were seeded into 96-well plates (2,000 cells per well) and exposed the next day to the indicated drugs (for siRNA knockdowns, cells were seeded three days before treatment). Drugs were removed two hours later and cultured for an additional 72 hours. Cell viability was measured using the Cell Titer Blue viability assay (Promega). Relative survival was normalized to the untreated control and corrected for background signal.

Co-immunoprecipitation and Western blotting

For co-immunoprecipitation experiments of nuclear proteins, cells were trypsinized, counted and lysed (25mM HEPES pH 7.6, 5mM MgCl2, 25mM KCl, 0.05mM EDTA, 10% glycerol and 0.1% NP-40 supplemented with complete EDTA-free Protease Inhibitor Cocktail (Roche)). Nuclei were isolated by spinning at 1,300 g and subsequently sonicated for 30 minutes in lysis buffer (50 mM Tris-HCl, pH 8.0, 150 mM NaCl, 0.1% NP-40 supplemented with Protease Inhibitor Cocktail (Roche)). Chromatin was removed by centrifugation (5 min at 12,000 g) and the supernatant was pre-cleared with protein G dynabeads (Life Technologies). Lysate was incubated overnight with 3µg antibody and 20µl protein G Dynabeads. Beads were washed extensively and re-suspended in SDS-sample buffer (2% SDS, 10% glycerol, 5% β-mercaptoethanol, 60mM Tris-HCl pH 6.8 and 0.01% bromophenol blue) before analysis by SDS-PAGE.

For whole cell lysate analyses, cells were lysed directly in SDS sample buffer (2% SDS, 10% glycerol, 5% β-mercaptoethanol, 60mM Tris-HCl pH 6.8 and 0.01% bromophenol blue). Samples were analyzed by SDS-PAGE and Western blotting. Blocking of the filter and antibody incubations were done in PBS supplemented with 0.1 (v/v)% Tween and 5% (w/v) bovine milk powder.

Constant-field gel electrophoresis

DNA double-strand breaks were quantified by constant-field gel electrophoresis as described (44). In short, HAP1 cells were treated with Doxo or Etop for two hours. Drugs were removed and cells were lysed and processed immediately to isolate the DNA. Samples were separated on a 0.8% agarose gel to separate faster migrating broken DNA from intact DNA and fragments of over >1 MB. Images were analyzed by ImageJ.

Flow cytometry

Cells were treated with Doxo (2µM) for one hour and trypsinized and fixed with 3.7% formaldehyde. Fluorescence of Doxo was measured directly using a FACSCalibur flow cytometer (BD Bioscience) and further analyzed by FlowJo software.

cDNA synthesis and qPCR

RNA isolation, cDNA synthesis and quantitative RT-PCR were performed as described previously (45). The primers for detection of Keap1, NQO1 and GAPDH expression were: Keap1 fw: 5'-CTGGAGGATCATACCAAGCAGG-3', Keap1 rv: 5'-GAA-

CATGGCCTTGAAGACAGG-3', NQO1 fw: 5'-GGGCAAGTCCATCCCAACTG-3', NQO1 rv: 5'-GCAAGTCAGGGAAGCCTGGA-3', GAPDH fw: 5'-TGTTGCCATCAATGACCCCTT-3', GAPDH rv: 5'-CTCCACGACGTACTCAGCG-3'.

Confocal microscopy

MelJuSo cells were seeded on coverslips and treated as indicated in the respective experiments. Cells were fixed in 3.7% formaldehyde for 10 min and permeabilized by 0.1% Triton X-100. Staining was performed with the antibodies mentioned above or with phalloidin (Invitrogen) to stain F-actin and DAPI (Invitrogen) to stain DNA. Images were acquired using a Leica TCS SP5 confocal microscope.

Chromatin association assay

HAP1 cells were seeded and treated with Etop for 15 min before lysis when indicated. Cells were lysed in lysis buffer (25 mM HEPES pH7.6, 5mM MgCl2, 25mM KCl, 0.05mM EDTA, 10% glycerol, 0.1% NP-40) and nuclei were spun down and resuspended at a concentration of 60 million/ml in buffer (20mM Tris-HCl pH 7.6, 3mM EDTA). 25ul samples were adjusted to the indicated NaCl concentrations to a total volume of 50ul. After mixing and incubation on ice for 20 min, chromatin was spun down and re-suspended in sample buffer. After sonication, samples were analyzed by SDS-PAGE and Western blotting.

Gene expression analysis of the neoadjuvant breast cancer cohort

Gene expression data was obtained from 113 pre-treatment biopsies of triple negative breast cancer patients treated at the Antoni van Leeuwenhoek hospital (associated to the NKI) and scheduled to receive neoadjuvant chemotherapy. All patients had a breast carcinoma with either a primary tumor size of at least 3 cm, or the presence of axillary lymph node metastases. A treatment regimen was assigned to each patient, consisting of six courses of dose-dense doxorubicin/cyclophosphamide (ddAC). If the therapy response was considered unfavorable by MRI evaluation after three courses, ddAC was changed to capecitabine/docetaxel (XD). Response to therapy was defined as pathological complete response (pCR) or no pathological complete response at the time of surgery.

63 Samples were labeled and hybridized to Illumina 6v3 arrays (Illumina, La Jolla, CA). Data were log2 transformed and between-array normalized using simple scaling. When a single gene was represented by multiple probes, the probe with the highest variance was chosen. The data is made available through the GEO database, accession GSE34138 (http://www.ncbi.nlm.nih.gov/geo/query/acc.cgi?acc=GSE34138) (46). 50 samples were profiled using RNAseq. Strand-specific sequencing libraries were generated using the TruSeq Stranded mRNA sample preparation guide (Illumina Part # 15031047 Rev. E) according to the manufacturer's instructions. Deep Sequencing was done with a HiSeq2000 machine (Illumina Inc). The reads are mapped against the human reference (hg19) using Tophat (version 2.0.6) (47). Tophat was supplied with a known set of genemodels using a GTF file (Ensembl version 66). HTSeq-count (48) was used to define gene expressions. This tool generates a list of the total number of uniquely mapped reads for each gene that was provided in the GTF. These data were normalized based on the relative library size using the DESeq2 R package (49) and subsequently log transformed.

Statistical methods

All experiments were performed at least three times in an independent manner. All

data are presented as means ± SD. The results were analyzed by using a paired two-tailed Student's T-test (unpaired for the data in Figure 6B). Significance was calculated using Excel and defined as $p < 0.05$.

Acknowledgments

We thank the NKI Genomics Core Facility for help with the sequencing data and the NKI Flow Cytometry Facility and the NKI Digital Microscopy Facility for support. We thank Piet Borst and Ilana Berlin for critically reading the manuscript and Jelle Wesseling and members of the Neefjes lab for fruitful discussions. This work was supported by the Institute for Chemical Immunology, an NWO Gravitation project funded by the Ministry of Education, Culture and Science of the government of the Netherlands. This work was further supported by grants from the Netherlands Organization of Scientific Research NWO and an ERC Advanced Grant. R.W., B.P., S.vd.Z., X.Q. and JN designed and performed the experiments. V.B. and T.B. analyzed the screening data. M.H., E.L. and L.W. performed the expression analyses on the clinical samples. L.J. made constructs. R.W., B.P. and J.N. wrote the manuscript with input from all authors.

References

1. Y. Pommier, Drugging topoisomerases: lessons and challenges. ACS chemical biology 8, 82-95 (2013).
2. P. Borst, Cancer drug pan-resistance: pumps, cancer stem cells, quiescence, epithelial to mesenchymal transition, blocked cell death pathways, persisters or what? Open biology 2, 120066 (2012).
3. B. Pang et al., Drug-induced histone eviction from open chromatin contributes to the chemotherapeutic effects of doxorubicin. Nat Commun 4, 1908 (2013).
4. F. Yang, ChristopherÂ J. Kemp, S. Henikoff, Doxorubicin Enhances Nucleosome Turnover around Promoters. Current Biology 23, 782-787 (2013).
5. B. Pang, J. de Jong, X. Qiao, L. F. Wessels, J. Neefjes, Chemical profiling of the genome with anti-cancer drugs defines target specificities. Nature chemical biology, (2015).
6. R. Callaghan, F. Luk, M. Bebawy, Inhibition of the multidrug resistance P-glycoprotein: time for a change of strategy? Drug metabolism and disposition: the biological fate of chemicals 42, 623-631 (2014).
7. D. J. Burgess et al., Topoisomerase levels determine chemotherapy response in vitro and in vivo. Proceedings of the National Academy of Sciences of the United States of America 105, 9053-9058 (2008).
8. P. Bouwman, J. Jonkers, The effects of deregulated DNA damage signalling on cancer chemotherapy response and resistance. Nature reviews. Cancer 12, 587-598 (2012).
9. G. Zoppoli et al., Putative DNA/RNA helicase Schlafen-11 (SLFN11) sensitizes cancer cells to DNA-damaging agents. Proceedings of the National Academy of Sciences of the United States of America 109, 15030-15035 (2012).
10. J. E. Carette et al., Global gene disruption in human cells to assign genes to phenotypes by deep sequencing. Nature biotechnology 29, 542-546 (2011).
11. T. Shibata et al., Genetic alteration of Keap1 confers constitutive Nrf2 activation and resistance to chemotherapy in gallbladder cancer. Gastroenterology 135, 1358-1368, 1368.e1351-1354 (2008).
12. A. Singh et al., Dysfunctional KEAP1-NRF2 interaction in non-small-cell lung cancer. PLoS medicine 3, e420 (2006).
13. C. G. A. R. Network, Comprehensive genomic characterization defines human glioblastoma genes and core pathways. Nature 455, 1061-1068 (2008).
14. C. Kadoch et al., Proteomic and bioinformatic analysis of mammalian SWI/SNF complexes identifies extensive roles in human malignancy. Nature genetics 45, 592-601 (2013).
15. R. S. Benjamin, C. E. Riggs, Jr., N. R. Bachur, Plasma pharmacokinetics of adriamycin and its metabolites in humans with normal hepatic and renal function. Cancer research 37, 1416-1420 (1977).

16. T. Ohta et al., Loss of Keap1 function activates Nrf2 and provides advantages for lung cancer cell growth. Cancer research 68, 1303-1309 (2008).
17. X. J. Wang et al., Nrf2 enhances resistance of cancer cells to chemotherapeutic drugs, the dark side of Nrf2. Carcinogenesis 29, 1235-1243 (2008).
18. A. F. Hohmann, C. R. Vakoc, A rationale to target the SWI/SNF complex for cancer therapy. Trends in genetics : TIG 30, 356-363 (2014).
19. W. P. Tsang, S. P. Chau, S. K. Kong, K. P. Fung, T. T. Kwok, Reactive oxygen species mediate doxorubicin induced p53-independent apoptosis. Life sciences 73, 2047-2058 (2003).
20. A. Rogalska, A. Koceva-Chyla, Z. Jozwiak, Aclarubicin-induced ROS generation and collapse of mitochondrial membrane potential in human cancer cell lines. Chemico-biological interactions 176, 58-70 (2008).
21. P. A. Konstantinopoulos et al., Keap1 mutations and Nrf2 pathway activation in epithelial ovarian cancer. Cancer research 71, 5081-5089 (2011).
22. M. B. Sporn, K. T. Liby, NRF2 and cancer: the good, the bad and the importance of context. Nature reviews. Cancer 12, 564-571 (2012).
23. Y. Miyoshi et al., Predictive factors for anthracycline-based chemotherapy for human breast cancer. Breast cancer (Tokyo, Japan) 17, 103-109 (2010).
24. B. K. Sinha, N. Haim, L. Dusre, D. Kerrigan, Y. Pommier, DNA strand breaks produced by etoposide (VP-16,213) in sensitive and resistant human breast tumor cells: implications for the mechanism of action. Cancer research 48, 5096-5100 (1988).
25. Y. Zhang et al., Identification of a conserved anti-apoptotic protein that modulates the mitochondrial apoptosis pathway. PloS one 6, e25284 (2011).
26. E. C. Dykhuizen et al., BAF complexes facilitate decatenation of DNA by topoisomerase IIalpha. Nature 497, 624-627 (2013).
27. J. L. Hornick, P. Dal Cin, C. D. Fletcher, Loss of INI1 expression is characteristic of both conventional and proximal-type epithelioid sarcoma. The American journal of surgical pathology 33, 542-550 (2009).
28. P. Gasparini et al., Prognostic determinants in epithelioid sarcoma. European journal of cancer (Oxford, England : 1990) 47, 287-295 (2011).
29. D. F. Lee et al., KEAP1 E3 ligase-mediated downregulation of NF-kappaB signaling by targeting IKKbeta. Molecular cell 36, 131-140 (2009).
30. W. Fan et al., Keap1 facilitates p62-mediated ubiquitin aggregate clearance via autophagy. Autophagy 6, 614-621 (2010).
31. L. Zhan et al., Regulatory role of KEAP1 and NRF2 in PPARgamma expression and chemoresistance in human non-small-cell lung carcinoma cells. Free radical biology & medicine 53, 758-768 (2012).
32. M. S. Lawrence et al., Discovery and saturation analysis of cancer genes across 21 tumour types. Nature 505, 495-501 (2014).
33. R. Barbano et al., Aberrant Keap1 methylation in breast cancer and association with clinicopathological features. Epigenetics : official journal of the DNA Methylation Society 8, 105-112 (2013).
34. V. Quennet, A. Beucher, O. Barton, S. Takeda, M. Lobrich, CtIP and MRN promote non-homologous end-joining of etoposide-induced DNA double-strand breaks in G1. Nucleic acids research 39, 2144-2152 (2011).
35. C. W. Brennan et al., The somatic genomic landscape of glioblastoma. Cell 155, 462-477 (2013).
36. I. Versteege et al., Truncating mutations of hSNF5/INI1 in aggressive paediatric cancer. Nature 394, 203-206 (1998).
37. A. S. Margol, A. R. Judkins, Pathology and diagnosis of SMARCB1-deficient tumors. Cancer genetics, (2014).
38. G. E. Tomlinson et al., Rhabdoid tumor of the kidney in the National Wilms' Tumor Study: age at diagnosis as a prognostic factor. Journal of clinical oncology : official journal of the American Society of Clinical Oncology 23, 7641-7645 (2005).
39. J. E. Carette et al., Ebola virus entry requires the cholesterol transporter Niemann-Pick C1. Nature 477, 340-343 (2011).
40. J. P. Johnson, M. Demmer-Dieckmann, T. Meo, M. R. Hadam, G. Riethmuller, Surface antigens of human melanoma cells defined by monoclonal antibodies. I. Biochemical characterization of two antigens found on cell lines and fresh tumors of diverse tissue origin. European journal of immunology 11,

825-831 (1981).
41. P. D. Hsu et al., DNA targeting specificity of RNA-guided Cas9 nucleases. Nature biotechnology 31, 827-832 (2013).
42. H. Wang et al., One-step generation of mice carrying mutations in multiple genes by CRISPR/Cas-mediated genome engineering. Cell 153, 910-918 (2013).
43. T. O. Auer, K. Duroure, A. De Cian, J. P. Concordet, F. Del Bene, Highly efficient CRISPR/Cas9-mediated knock-in in zebrafish by homology-independent DNA repair. Genome research 24, 142-153 (2014).
44. S. Neijenhuis et al., Mechanism of cell killing after ionizing radiation by a dominant negative DNA polymerase beta. DNA repair 8, 336-346 (2009).
45. P. Paul et al., A Genome-wide multidimensional RNAi screen reveals pathways controlling MHC class II antigen presentation. Cell 145, 268-283 (2011).
46. J. J. de Ronde et al., SERPINA6, BEX1, AGTR1, SLC26A3, and LAPTM4B are markers of resistance to neoadjuvant chemotherapy in HER2-negative breast cancer. Breast cancer research and treatment 137, 213-223 (2013).
47. C. Trapnell, L. Pachter, S. L. Salzberg, TopHat: discovering splice junctions with RNA-Seq. Bioinformatics (Oxford, England) 25, 1105-1111 (2009).
48. S. Anders, P. T. Pyl, W. Huber, HTSeq-a Python framework to work with high-throughput sequencing data. Bioinformatics (Oxford, England), (2014).
49. M. I. Love, W. Huber, S. Anders, Moderated estimation of fold change and dispersion for RNA-Seq data with DESeq2. (2014).

Supplementary Figures

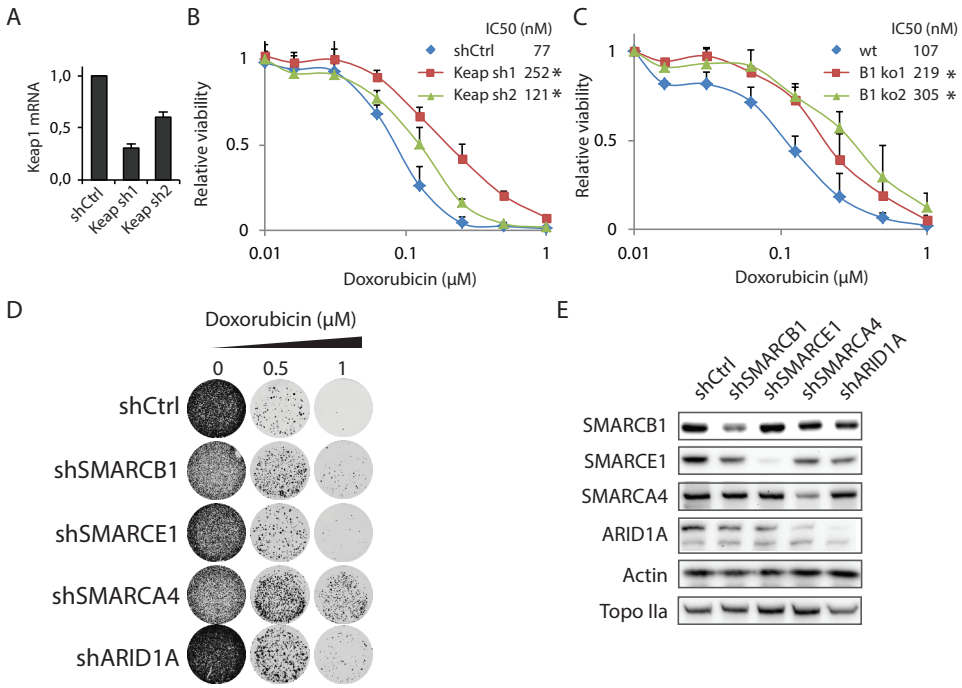


Figure S1: Keap1, SMARCB1, SMARCA4 and ARID1A regulate resistance to doxorubicin. *(A) Silencing of Keap1 by shRNAs was measured by qPCR. Keap1 mRNA signal was normalized to GAPDH and shCtrl was set at 1. Shown is the mean + SD of biological triplicates. (B) Short term growth assay of Keap1-silenced cells incubated with Doxo for 2h at the indicated concentration. Cell viability was analyzed 72 hours after drug removal and extensive washing. Data shown are mean +SD of biological triplicate experiments. (C) Short-term growth assay as in (B) for wild-type and SmarcB1-depleted cells. Data shown are mean +SD of biological triplicate experiments. (D) HAP1 cells stably expressing shCtrl or shRNAs targeting SMARCB1, SMARCA4 or ARID1a were treated with Doxo for 2h at the indicated concentrations. Doxo was removed and cells were left to grow out. 9 days later, cells were fixed, stained and imaged. (E) Western blot analysis showing silencing of the respective SWI/SNF complex subunits. Actin is shown as the loading control.*

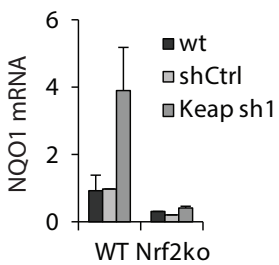


Figure S2: Keap1 controls expression of NQO1 through Nrf2*. mRNA expression analysis of Nrf2 target gene NQO1 using qPCR in cells either or not expressing Nrf2. Expression of NQO1 was calculated relative to GAPDH and data were normalized to WT shCtrl. Results are mean +SD of biological triplicate experiments.*

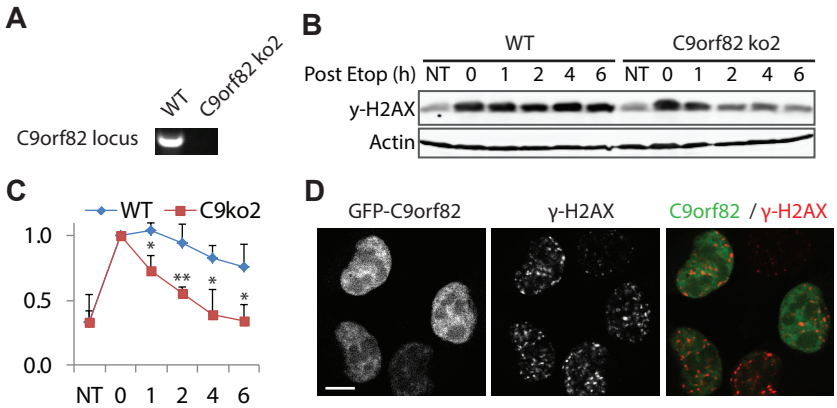


Figure S3: C9orf82 regulates DNA double strand break repair. *(A) DNA gel showing loss of C9orf82 by targeting its locus with a second CRISPR guide RNA. (B) Cells with C9orf82 inactivated were treated with 1μM Etop for 1hr, washed and lysed at the indicated time points post drug removal. Lysates were analyzed by SDS-PAGE and Western blotting analysis for γ-H2AX (upper panel) and actin as the loading control (lower panel). (C) quantification of the γ-H2AX signals from (B), normalized to actin. t=0 was set at 1. Quantification was done from three independent experiments. For all time-points, shown are mean+SD. (D) MelJuSo cells expressing GFP-C9orf82 were treated for 1 hr with 1μM Etop. Cells were fixed and stained for γ-H2AX before analyses by confocal laser scanning microscope. Bar: 10μm. NT are non-treated cells.*

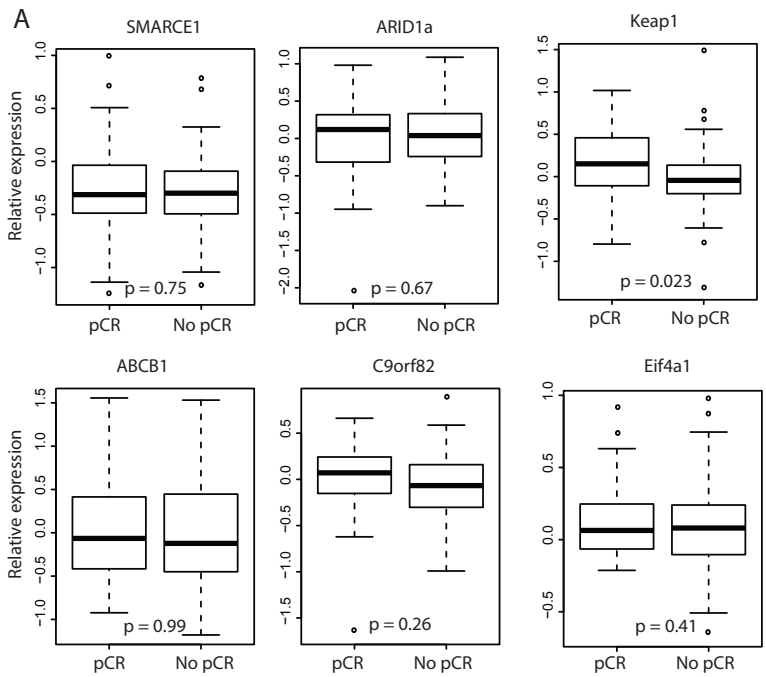


Figure S4: Expression of some SWI/SNF complex subunits correlates to clinical outcome. *Box plot of normalized expression of the indicated genes in 113 triple-negative breast cancer patients that showed pathological complete response (pCR, 46 patients) or not (no pCR, 67 patients) to the treatment with a Doxo containing regimen. p-values were calculated using a Student's T-test.*

Chapter 10:
Summary & Perspectives

Summary & Discussion

Understanding the fundamental organization of the cell, and to extent the collections of cells known as organisms, has marvelled scientists ever since Antoni van Leeuwenhoek. The last decades have seen a significant increase in the available tools and yielded an unprecedented view on the complexity of individual cells. Especially cell biological tools like microscopy have shifted biomedical science from a biochemical approach following a bulk of molecules to a more visual approach, allowing the analyses of biochemical processes in cellular time and space. Much is still to be discovered, but it becomes increasingly clear that different cellular processes are intimately linked, blurring the traditional boundaries between research fields. To get insight into the regulation of a process, roughly two approaches can be followed. The first is to focus on a cellular (or chemical) pathway or process and to delve into its details, using this as a means to discover novel proteins that fill a defined pathway. This approach was explored in Chapter 9, where a role for several novel proteins in sensitivity to Doxorubicin is described. Alternatively, one defined protein can be used as the centrepiece to investigate a complex biological process, as illustrated in Chapter 2. By focussing on the protein ORP1L we could demonstrate a role for late endosomes in regulating the rate of autophagosome maturation. Ideally, science combines both approaches, as shown in Chapter 3 and 5, where unstudied proteins were investigated to gain insight into endosome biology. In this Summary and Discussion chapter, the main conclusions from this dissertation will be summarized and put into perspective.

Regulation of and by the lysosome: positioning and function

Since its discovery by Christian de Duve (1, 2), the image of a lysosome (and its less acidic late endosomal counterpart) has slowly turned from an acidic bag full of proteolytic enzymes into a key regulator of a multitude of processes such as antigen presentation, autophagy and signal transduction (3). Execution of these functions requires the recruitment of a plethora of adaptor proteins, most notably to GTPases, leading to this diversity in function. A similar diversity is observed in the flavours in which lysosomes some. While classically detected with microscopy through staining for LAMP-1 or CD63, electron microscopy images expose a diverse range of endosome architectures associated with these markers, ranging from multi-vesicular bodies (MVBs) and multilamellar bodies to the traditional small, dense lysosome. There are also lysosome-related organelles specified by defined markers (such as tyrosines and melanosomes), whereas others are simply a merger between lysosomes and other compartments (eg. autolysosomes and amphisomes). However, a structure-function relationship is still poorly understood and will require coupling of structural data as obtained by EM to functional data from microscopy, for example by using a combination of correlative light electron microscopy (CLEM), biochemistry and cell biology.

Besides the structural differences, one of the functionally differentiating factors on LE/Lys are the GTPases, present in a somewhat mutually exclusive manner (4). Rab7 has emerged as the key GTPase on the LE/Ly, facilitating maturation of the originally Rab5 marked early endosome. Other LE/Ly are primarily marked by Arl8, Rab2a or Rab9 (5-7), although it is unclear whether these are temporary carriers

for bringing cargo to a different compartment or alternative branches (eg. maturation stages) of lysosomes. Given its predominant role in incoming traffic, Rab7 and its effectors impose important regulatory functions on the endolysosomal system as a whole, as well as on individual endosomes. Chapter 2 describes that by recruiting the cholesterol-binding and transporting protein ORP1L, Rab7 can toggle (or can be toggled if you will) decisions regarding incoming traffic of autophagosomes. Though at the cellular level this could be detrimental, since it leaves the cells with cargo destined for degradation, at the lysosomal level this can ensure fusion with individual lytic compartments capable of destructing the content of the enclosed cytosolic material. Our prediction is that subsets of Rab7-marked lysosomes that act as founding organelles for a series of lysosome-related organelles including melanosomes (8), lytic granules (9), and platelet-dense granules (10) could use this system to prevent their merger with other compartments, in order to maintain their integrity. Given the requirement for Rab7 and HOPS in the fusion of both early endosomes and autophagosomes with the LE/Ly, the ORP1L system probably does not ascertain specificity regarding incoming traffic. Spreading of cargo over different lysosomes by virtue of ORP1L could also aide in the distribution of nutrients and corresponding growth signals. For example, sufficiency of amino acids (predominantly arginine and leucine) in the lysosome leads to the activation of mTOR (11-13), which consequently inhibits TFEB-mediated transcription of LE/Ly and autophagy genes. On the other hand, ‘starving’ lysosomes signal amino acid deprivation to activate TFEB, leading to the opposite signal (14, 15). At the cellular level it would thus be advantageous to distribute nutrients evenly to cancel out both signals, which can be facilitated by ORP1L.
Interestingly, ORP1L has the ability to bind cholesterol. By placing Rab7 function under control of ORP1L, cholesterol as detected by the ORD domain of the latter orchestrates the timing and position of transport and fusion decisions. Cholesterol microdomains could hereby act as local transport and fusion hubs, where recruitment of dynein occurs, as well as HOPS and subsequently the SNARE proteins. This is corroborated by the notion that SNARE proteins on LE/Lys preferentially localize to cholesterol-enriched subdomains (16, 17), a phenotype similar for Rab7, ORP1L and dynein (18, 19). The latter suggests that by binding cholesterol, ORP1L might actually function to recruit Rab7 into these domains to facilitate transport and fusion. However, depletion of ORP1L does not impair minus-end transport or fusion, arguing against this. Our studies have indicated a crucial role for the ORD domain of ORP1L in the ability of Rab7 to recruit HOPS to organize late endosomal fusion. However, we did not observe impaired HOPS recruitment or fusion of autophagosomes with LE/Lys under low cholesterol conditions. Possibly cholesterol depletion was not complete, or alternatively, the function of the ORD domain extends beyond cholesterol and it interacts with other lipids or proteins, which can modulate its conformation and hereby the fusogenic capacity of its associated vesicle. Recently, a direct connection has been described between endosomal cholesterol levels and mTOR signalling (20), where it was shown that cholesterol drives activation of mTOR. Low endosomal cholesterol inactivates mTOR, leading to upregulation of autophagy. It will be interesting to investigate whether ORP1L and mTOR function on the same subsets of LE/Lys, and whether they are functionally connected.

RNF26: location, location, location

When cells are stained for endosomal markers, the bulk of all endosomal compartments, as well as the Golgi-network localize to a region close to the microtubule-organizing centre (MTOC), a phenomenon described in a wide range of cell types, including immune cells and neuronal cells (21-23). This is represented in nearly every cartoon about endocytosis, where more mature endosome stages are always depicted on the bottom, deeper into the cell. However, it has been elusive how this organization comes about and what the function of this compartment clustering is. Our data in Chapter 3 imply that all endosomal carriers are clustered at the MTOC by ubiquitin-dependent recruitment to ER-localized E3-ligase RNF26. Depletion of this enzyme lead to a scattering of all endosomal compartments, but not the Golgi. Furthermore, endosome fusion and maturation was perturbed upon RNF26 loss, indicating that the clustering of endosomes at the MTOC promotes cargo degradation and fusion. Mechanistically, RNF26 recruits different endosomal adaptor proteins via a p62-dependent ubiquitination step, hereby docking the vesicle to the ER and inducing its retention at the perinuclear region. De-ubiquitination organized by USP15 would release the vesicle and enable fast, microtubule-based transport, allowing the vesicle to travel to its desired location. Intriguingly, RNF26 was not found throughout the ER, but rather localized specifically to the perinuclear ER, though not completely overlapping with the here present ER-sheets (24). This localization depended on its RING-domain, implying other factors are involved in constricting the enzyme to the defined position. RNF26 thus facilitates a novel inter-organelle contact-site, between RNF26 and endosomal adaptor proteins. It will be interesting to investigate a potential interplay of RNF26 with endosomal transport decisions toggled by ORP1L/VAP-A (25) and Protrudin/Rab7 ER-LE contact sites (26). Together, our data from Chapter 3 suggest that organization of the endosomal system into a perinuclear cloud by RNF26 facilitates cargo exchange and serves to optimize efficient functioning of the endosomal system.

OTUD1: a novel regulator of endosome biology

The endocytic pathway is regulated by a collection of factors, which can roughly be divided into three interconnected groups. The first are the factors on the endosome itself, the hardware like the Rab7-RILP-ORP1L system, serving its own interest and safeguarding the integrity of the LE/Ly compartment. The second group is the cargo, which signals its preferred destination towards the endosome, hereby influencing the endocytic events. A third group, probably most sensitive to external (both intracellularly or extracellularly derived) stimuli, are the proteins that control the quality and quantity of the hardware, either at the cellular or endosomal level. These are the modifiers of post-translational modifications. A novel factor in the latter category described in chapter 4 of this thesis is OTUD1, a de-ubiquitinating enzyme (DUB) of the OTU-family. Loss of OTUD1 inflicted a scattering of the early and late endocytic compartment, as well as a decreased capacity of cells to degrade ligand-bound EGFR, implying a broad dysfunctioning of the early-late endocytic pathway. Given its cytosolic and actin-bound nature, OTUD1 most likely acts as an indirect regulator of endosome maturation. Whereas the phenotype of OTUD1 loss is evident, two fundamental questions are required for understanding

the function of OTUD1. First, what is the substrate of this DUB, which has been shown to specifically cleave lysine-63 linked poly-ubiquitin chains (27), and what is the function of ubiquitination on this substrate? Given the importance for K63-chains in endosomal signaling (28), it seems reasonable to assume that OTUD1 de-ubiquitinates an endosomal adaptor or cargo protein, likely terminating their functionality. Ubiquitin-proteomics in combination with site-directed mutagenesis of the substrate will be required for studying this part of the OTUD1 cascade. Second, how is the activation or targeting of OTUD1 towards the substrate organized. This aspect is often underrepresented in studies focussing on DUBs. Especially for DUBs counteracting proteasomal substrate degradation this is often the most interesting part, since it provides information as to why the DUB has functionally evolved to reverse an complex energy consuming process. Simply counteracting an E3-ligase is inefficient, so DUBs are usually regulated by alternative pathways to introduce crosstalk between different signalling routes. Our studies described in this chapter show that the actin cross-linking Filamin proteins and oxidative stress sensor Keap1 bind OTUD1 at different sites. Both proteins were not substrates for OTUD1, arguing that they could serve as recruitment or regulatory factors for OTUD1, thus linking the actin cytoskeleton to regulation of endocytosis. This would be in agreement with the known role of Filamin A in the regulation of EGFR degradation and lysosome positioning (29, 30). It will be interesting to investigate the function of OTUD1 from this perspective, whereby OTUD1 possibly act as a spatial regulator of endosome maturation.

USP54 connects endosomes to cellular contact sites

Crosstalk between cellular compartments is essential for major re-organization programs such as cell migration and polarity instalment (31-33). Such communication can be of physical manner, such as transport of cargo, or of immaterial manner, like signal transduction pathways leading to activation of proteins at a different compartment. In Chapter 5 we identify another DUB acting on the endosomal system. We show that the DUB USP54 localizes to different compartments and travels between at least some of them, potentially serving as a messenger for crosstalk between compartments. USP54 is among the largest DUBs (187 kDa (34)) and proposed to be an inactive DUB. We show that besides the USP-domain it contains multiple additional domains that control localization to specific compartments in the cell. Mass spec analysis of the interactors of these different domains yielded proteins marking roughly four cellular compartments; tight/adherens junctions, cilia, endosomes and actin. USP54 traffics from endosomes to cell-cell junctions and is critical for the integrity of tight and adherens junctions, by controlling the recruitment of its interactor ZO-1, an integral junction member, to these sites of intercellular contact. On endosomes, USP54 was found to co-localize and interact with a select few members of the HOPS complex (VPS11, VPS18 and VPS39), but these endosomes were not positive for any marker known to co-localize with these VPS-proteins. Other HOPS members did not co-localize with USP54, arguing for a novel role for these VPS-proteins in the transport of USP54-positive carriers, possibly towards cell-cell contacts. Actin localization of USP54 is probably accounted for by myosin binding, as three myosin motors were found to interact with the

actin-localizing domain. Given the intimate coupling of both endosome recycling and tight junction assembly to actin polymerization (35, 36), USP54 could recruit these motors to perform critical functions such as endosome fusion with the plasma membrane, or could be recruited by these motors to catalyse de-ubiquitination of a potential substrate. Besides impaired membrane localization of ZO-1, USP54 depletion yielded cells with a more peripheral and stable microtubule network. A similar change in microtubule structure is observed in polarized cells, which are characterized by their presence of strong tight and adherens junctions (31, 37). In summary, we believe that by influencing cell-cell contact assembly, USP54 is in control of the establishment of cell polarity, which will be the focus of future research on this DUB.

USP54 has been described as an inactive DUB, based on a missing histidine near the catalytic site (38). However, we find that USP54 is capable of catalysing de-ubiquitination, albeit at a low rate. This catalytic action is required for its function, since overexpression of a catalytically incompetent USP54 mimics its depletion in terms of microtubule reorganization, suggesting DUB activity is essential for its function. In order to understand its full mechanism of action, it will thus be essential to identify the substrates of USP54.

The common denominator of many of the USP54-interactors is a function in plasma membrane trafficking of glucose receptor GLUT4 in adipocytes. This process is executed by endosomes labeling positive for the GTPase Rab4, which also controls recycling of many tight and adherens junction proteins (39, 40). It will be interesting to investigate whether the USP54-positive endosomes are indeed co-labeling with Rab4 and whether USP54 influences Rab4-mediated recycling of GLUT4. Interestingly, USP54 deficient mice are characterized by an increase in adipocyte mass (41), a phenotype similar to mice harbouring increased GLUT4 at the plasma membrane (42, 43). Thus, whereas the exact mechanism of action of USP54 is still unknown, our data support a model in which USP54 controls cell polarity by functioning at the interface of endosome recycling and tight junction formation.

Keap1: a versitile regulator of sorts

Cells are exposed to different forms of stresses, each activating one or more pathways that enable the cell to cope, for example autophagy to counteract nutrient stress. Another stressor is the increased presence of oxygen radicals, which cause damage by reacting with proteins, DNA and lipids (44). To quench these radicals, cells express enzymes catalyzing reducing reactions such as NQO-1 and GST, under the control of transcription factor NRF2. The latter is kept inactive and targeted for degradation by Keap1, which contains exposed cysteines prone to oxidation and hereby functions as an oxidative stress sensor. Besides targeting NRF2, Keap1 functions in multiple pathways such as the DNA damage response, autophagosome degradation, and TGFβ- and NFκB signalling (45-48). In Chapter 7 we report another function for Keap1, namely to control the level of histone acetylation in the cell. Decreased histone acetylation was correlated with impaired expression of MHCII induced by the cytokine IFNγ, arguing that the absence of Keap1 reduced MHCII antigen presentation. Interestingly, in Chapter 9 we describe a novel role for Keap1 in the expression of Topoisomerase IIα, without having established the

molecular mechanism. Given the regulation of Topoisomerase IIα expression by histone acetylation (49), it is tempting to speculate that this hampered expression created by loss of Keap1 is a result of an altered epigenetic landscape. Indeed, HDAC inhibitors have been shown to increase Topoisomerase IIα expression in several tumours (50-52), potentially counteracting the negative effect instigated by loss of Keap1.
Keap1 interacts with and regulates a large number of proteins, mostly via binding to their putative ETGE motif. Given the global de-regulation of Keap1 function by oxidative stress, it might be most interesting to analyse the common denominators of the pathways regulated by Keap1. This is most notably the stress response. Loss of Keap1 induces expression of oxidative stress response genes, NFκB signaling, inhibits PGAM5/Bcl-xL mediated apoptosis, and impairs epithelial-mesenchymal transition (EMT), all programs leading to or activated by stress control. In this context, decreased histone acetylation could help to negate expression of factors unrelated to stress control, providing resources for the processes of primary interest to the cell. Under homeostatic conditions, Keap1 thus acts as an inhibitor of the oxidative stress response, ensuring that cells can utilize their energy for things other than stress control.

Novel factors controlling resistance to doxorubicin

Chemotherapy is one of the cornerstones of cancer treatment, but its effectivity is often hampered by drug resistance in the tumour. This is also the case for treatment with topoisomerase II (TopoII) poisons such as doxorubicin, which is among the most frequently used anti-cancer drugs. To identify novel factors that control resistance to doxorubicin, we performed a genome-wide haploid genetics screen (Chapter 7). Using short incubations with doxorubicin to mimic the clinical condition, loss of Keap1, the SWI/SNF complex and CAAP1 rendered cells more resistant to this anthracycline. Keap1 and SWI/SNF controlled the extent to which TopoII poisons generate DNA damage, whereas CAAP1 influenced the resolution of the DNA damage response, as measured by DNA damage marker γ-H2AX. Given the known role for SWI/SNF in the loading of TopoII onto the DNA (53), we concluded that loss of the SWI/SNF complex decreased TopoII activity and hereby DNA double strand break formation. Several tumours harbour mutations in SWI/SNF complex members (54), suggesting a potential for treatment selection. This is supported by the finding that rhabdoid tumours, which are characterized by a nearly full penetrance SMARCB1 deletion (55, 56), respond poorly to doxorubicin (57). Also, epithelioid sarcoma patients harbouring deletions for SMARCB1 have a higher chance of relapse following treatment protocols that usually includes Topo II poisons (58). Furthermore, a dataset of triple negative breast cancer patients treated with a doxorubicin containing regimen showed a correlation between treatment response and expression of SWI/SNF subunits SMARCB1 and SMARCA4. Whereas often viewed as a single complex, mutations in SWI/SNF subunits occur at very distinct rates in different tumour types. For example, while rhabdoid tumours have a nearly full deletion of SMARCB1, small cell carcinoma of the ovary is characterized by deletion of the SMARCA4 subunit (59), and endometrial tumours have deletions in ARID1A and ARID5B (60). Thus, the SWI/SNF complex members

execute different functions and it will be interesting to determine the contribution of the individual members to the processes it has been linked to.
In summary, this thesis describes novel functions for several proteins and pathways controlling or feeding MHC class II presentation, as well as responses to an anti-cancer drugs. Along the way, we identified three nearly unstudied proteins, the E3-ligase RNF26 and the DUBs OTUD1 and USP54, that control the endosomal pathway in a distinct fashion.

References

1. F. Appelmans, R. Wattiaux, C. De Duve, Tissue fractionation studies. 5. The association of acid phosphatase with a special class of cytoplasmic granules in rat liver. The Biochemical journal 59, 438-445 (1955).
2. D. D. Sabatini, M. Adesnik, Christian de Duve: Explorer of the cell who discovered new organelles by using a centrifuge. Proceedings of the National Academy of Sciences of the United States of America 110, 13234-13235 (2013).
3. A. Ballabio, The awesome lysosome. EMBO molecular medicine 8, 73-76 (2016).
4. H. Stenmark, Rab GTPases as coordinators of vesicle traffic. Nature reviews. Molecular cell biology 10, 513-525 (2009).
5. R. D. Bagshaw, J. W. Callahan, D. J. Mahuran, The Arf-family protein, Arl8b, is involved in the spatial distribution of lysosomes. Biochemical and biophysical research communications 344, 1186-1191 (2006).
6. H. Kajiho et al., RAB2A controls MT1-MMP endocytic and E-cadherin polarized Golgi trafficking to promote invasive breast cancer programs. EMBO reports 17, 1061-1080 (2016).
7. M. A. Riederer, T. Soldati, A. D. Shapiro, J. Lin, S. R. Pfeffer, Lysosome biogenesis requires Rab9 function and receptor recycling from endosomes to the trans-Golgi network. The Journal of cell biology 125, 573-582 (1994).
8. P. F. Gomez et al., Identification of rab7 as a melanosome-associated protein involved in the intracellular transport of tyrosinase-related protein 1. The Journal of investigative dermatology 117, 81-90 (2001).
9. T. Daniele et al., A role for Rab7 in the movement of secretory granules in cytotoxic T lymphocytes. Traffic (Copenhagen, Denmark) 12, 902-911 (2011).
10. A. L. Ambrosio, J. A. Boyle, S. M. Di Pietro, Mechanism of platelet dense granule biogenesis: study of cargo transport and function of Rab32 and Rab38 in a model system. Blood 120, 4072-4081 (2012).
11. M. Rebsamen et al., SLC38A9 is a component of the lysosomal amino acid sensing machinery that controls mTORC1. Nature 519, 477-481 (2015).
12. R. L. Wolfson et al., Sestrin2 is a leucine sensor for the mTORC1 pathway. Science (New York, N.Y.) 351, 43-48 (2016).
13. S. Wang et al., Metabolism. Lysosomal amino acid transporter SLC38A9 signals arginine sufficiency to mTORC1. Science (New York, N.Y.) 347, 188-194 (2015).
14. D. L. Medina et al., Lysosomal calcium signalling regulates autophagy through calcineurin and TFEB. Nature cell biology 17, 288-299 (2015).
15. C. Settembre, A. Fraldi, D. L. Medina, A. Ballabio, Signals from the lysosome: a control centre for cellular clearance and energy metabolism. Nature reviews. Molecular cell biology 14, 283-296 (2013).
16. T. Lang et al., SNAREs are concentrated in cholesterol-dependent clusters that define docking and fusion sites for exocytosis. The EMBO journal 20, 2202-2213 (2001).
17. G. van den Bogaart, T. Lang, R. Jahn, Microdomains of SNARE proteins in the plasma membrane. Current topics in membranes 72, 193-230 (2013).
18. G. Goyette et al., Proteomic characterization of phagosomal membrane microdomains during phagolysosome biogenesis and evolution. Molecular & cellular proteomics : MCP 11, 1365-1377 (2012).
19. A. Rai et al., Dynein Clusters into Lipid Microdomains on Phagosomes to Drive Rapid Transport toward Lysosomes. Cell 164, 722-734 (2016).
20. B. M. Castellano et al., Lysosomal cholesterol activates mTORC1 via an SLC38A9-Niemann-Pick C1 signaling complex. Science (New York, N.Y.) 355, 1306-1311 (2017).

21. A. Alloatti et al., Toll-like Receptor 4 Engagement on Dendritic Cells Restrains Phago-Lysosome Fusion and Promotes Cross-Presentation of Antigens. Immunity 43, 1087-1100 (2015).
22. P. Steiner et al., Modulation of receptor cycling by neuron-enriched endosomal protein of 21 kD. The Journal of cell biology 157, 1197-1209 (2002).
23. J. Huotari, A. Helenius, Endosome maturation. The EMBO journal 30, 3481-3500 (2011).
24. Y. Shibata, G. K. Voeltz, T. A. Rapoport, Rough sheets and smooth tubules. Cell 126, 435-439 (2006).
25. N. Rocha et al., Cholesterol sensor ORP1L contacts the ER protein VAP to control Rab7-RILP-p150 Glued and late endosome positioning. The Journal of cell biology 185, 1209-1225 (2009).
26. C. Raiborg et al., Repeated ER-endosome contacts promote endosome translocation and neurite outgrowth. Nature 520, 234-238 (2015).
27. T. E. Mevissen et al., OTU deubiquitinases reveal mechanisms of linkage specificity and enable ubiquitin chain restriction analysis. Cell 154, 169-184 (2013).
28. Z. Erpapazoglou, O. Walker, R. Haguenauer-Tsapis, Versatile roles of k63-linked ubiquitin chains in trafficking. Cells 3, 1027-1088 (2014).
29. J. L. Fiori et al., Filamin A modulates kinase activation and intracellular trafficking of epidermal growth factor receptors in human melanoma cells. Endocrinology 150, 2551-2560 (2009).
30. G. Liu et al., Cytoskeletal protein ABP-280 directs the intracellular trafficking of furin and modulates proprotein processing in the endocytic pathway. The Journal of cell biology 139, 1719-1733 (1997).
31. D. M. Bryant, K. E. Mostov, From cells to organs: building polarized tissue. Nature reviews. Molecular cell biology 9, 887-901 (2008).
32. P. T. Caswell, S. Vadrevu, J. C. Norman, Integrins: masters and slaves of endocytic transport. Nature reviews. Molecular cell biology 10, 843-853 (2009).
33. M. C. Jones, P. T. Caswell, J. C. Norman, Endocytic recycling pathways: emerging regulators of cell migration. Current opinion in cell biology 18, 549-557 (2006).
34. D. Komander, M. J. Clague, S. Urbe, Breaking the chains: structure and function of the deubiquitinases. Nature reviews. Molecular cell biology 10, 550-563 (2009).
35. A. Bose et al., Unconventional myosin Myo1c promotes membrane fusion in a regulated exocytic pathway. Molecular and cellular biology 24, 5447-5458 (2004).
36. C. Zihni, C. Mills, K. Matter, M. S. Balda, Tight junctions: from simple barriers to multifunctional molecular gates. Nature reviews. Molecular cell biology 17, 564-580 (2016).
37. E. Rodriguez-Boulan, I. G. Macara, Organization and execution of the epithelial polarity programme. Nature reviews. Molecular cell biology 15, 225-242 (2014).
38. V. Quesada et al., Cloning and enzymatic analysis of 22 novel human ubiquitin-specific proteases. Biochemical and biophysical research communications 314, 54-62 (2004).
39. M. Matsuda, A. Kubo, M. Furuse, S. Tsukita, A peculiar internalization of claudins, tight junction-specific adhesion molecules, during the intercellular movement of epithelial cells. Journal of cell science 117, 1247-1257 (2004).
40. A. I. Ivanov, A. Nusrat, C. A. Parkos, Endocytosis of epithelial apical junctional proteins by a clathrin-mediated pathway into a unique storage compartment. Molecular biology of the cell 15, 176-188 (2004).
41. J. M. Fraile, D. Campos-Iglesias, F. Rodriguez, Y. Espanol, J. M. Freije, The deubiquitinase USP54 is overexpressed in colorectal cancer stem cells and promotes intestinal tumorigenesis. Oncotarget 7, 74427-74434 (2016).
42. M. A. Herman et al., A novel ChREBP isoform in adipose tissue regulates systemic glucose metabolism. Nature 484, 333-338 (2012).
43. P. R. Shepherd et al., Adipose cell hyperplasia and enhanced glucose disposal in transgenic mice overexpressing GLUT4 selectively in adipose tissue. The Journal of biological chemistry 268, 22243-22246 (1993).
44. R. E. Pacifici, K. J. Davies, Protein, lipid and DNA repair systems in oxidative stress: the free-radical theory of aging revisited. Gerontology 37, 166-180 (1991).
45. A. Orthwein et al., A mechanism for the suppression of homologous recombination in G1 cells. Nature 528, 422-426 (2015).
46. W. Fan et al., Keap1 facilitates p62-mediated ubiquitin aggregate clearance via autophagy. Autophagy 6, 614-621 (2010).
47. I. G. Ryoo, H. Ha, M. K. Kwak, Inhibitory role of the KEAP1-NRF2 pathway in TGFbeta1-stim-

ulated renal epithelial transition to fibroblastic cells: a modulatory effect on SMAD signaling. PloS one 9, e93265 (2014).
48. D. F. Lee et al., KEAP1 E3 ligase-mediated downregulation of NF-kappaB signaling by targeting IKKbeta. Molecular cell 36, 131-140 (2009).
49. K. Yu et al., Decreased topoisomerase IIalpha expression and altered histone and regulatory factors of topoisomerase IIalpha promoter in patients with chronic benzene poisoning. Toxicology letters 203, 111-117 (2011).
50. M. G. Catalano et al., Valproic acid, a histone deacetylase inhibitor, enhances sensitivity to doxorubicin in anaplastic thyroid cancer cells. The Journal of endocrinology 191, 465-472 (2006).
51. C. M. Das et al., Valproic acid induces p21 and topoisomerase-II (alpha/beta) expression and synergistically enhances etoposide cytotoxicity in human glioblastoma cell lines. Journal of neuro-oncology 85, 159-170 (2007).
52. E. U. Kurz et al., The histone deacetylase inhibitor sodium butyrate induces DNA topoisomerase II alpha expression and confers hypersensitivity to etoposide in human leukemic cell lines. Molecular cancer therapeutics 1, 121-131 (2001).
53. E. C. Dykhuizen et al., BAF complexes facilitate decatenation of DNA by topoisomerase IIalpha. Nature 497, 624-627 (2013).
54. C. Kadoch et al., Proteomic and bioinformatic analysis of mammalian SWI/SNF complexes identifies extensive roles in human malignancy. Nature genetics 45, 592-601 (2013).
55. I. Versteege et al., Truncating mutations of hSNF5/INI1 in aggressive paediatric cancer. Nature 394, 203-206 (1998).
56. A. S. Margol, A. R. Judkins, Pathology and diagnosis of SMARCB1-deficient tumors. Cancer genetics 207, 358-364 (2014).
57. G. E. Tomlinson et al., Rhabdoid tumor of the kidney in the National Wilms' Tumor Study: age at diagnosis as a prognostic factor. Journal of clinical oncology : official journal of the American Society of Clinical Oncology 23, 7641-7645 (2005).
58. P. Gasparini et al., Prognostic determinants in epithelioid sarcoma. European journal of cancer (Oxford, England : 1990) 47, 287-295 (2011).
59. P. Jelinic et al., Recurrent SMARCA4 mutations in small cell carcinoma of the ovary. Nature genetics 46, 424-426 (2014).
60. C. Kandoth et al., Integrated genomic characterization of endometrial carcinoma. Nature 497, 67-73 (2013).

Nederlandse Samenvatting

Het lichaam is opgebouwd uit ongeveer 22.000 verschillende eiwitten, elk met een andere functie, zoals hemoglobine voor het transport van zuurstof, tubuline eiwitten die het skelet van de cel vormen en lichtreceptoren waarmee we kunnen zien. Van ongeveer een kwart hebben we nog geen idee wat ze doen, en van de rest vaak maar een van de vele functies, welke we vaak niet begrijpen in de context van de andere eiwitten in de cel. Het uitzoeken van nieuwe functies voor (onbekende) eiwitten kan belangrijke inzichten geven in hoe processen gereguleerd worden, omdat een nieuw eiwit vaak een functie blijkt te hebben die vooraf moeilijk te voorspellen is. Deze manier van onderzoek heeft bijvoorbeeld geleid tot de ontdekking van het systeem waarmee eiwitten in de cel afgebroken worden (ubiquitin-proteasoom systeem), alsmede hoe cellen communiceren met hun omgeving (het endosomale systeem). De vele nieuwe technieken die de laatste jaren ontwikkeld zijn dragen enorm bij aan deze vorm van onderzoek, waarbij het genereren van empirische data voorafgaat aan het rationeel overdenken van het systeem.
Dit proefschrift bevat bevindingen van onderzoek uit drie verschillende gebieden in de biologie van cellen, te weten het endosomale systeem, antigeen presentatie en chemoresistentie tegen een kanker medicijn. Voor de meeste onderzoeken hebben we getracht nieuwe eiwitten te vinden die deze processen reguleren, met als doel het proces beter te begrijpen en aanknopingspunten te vinden voor nieuwe medicijnen of het optimaliseren van bestaande therapieën.

Nieuwe regulatoren van het endosomale systeem

In **hoofdstuk 2** beschrijven we nieuwe regulatoren van een proces genaamd autofagie, ofwel 'zichzelf opeten'. Wanneer cellen een tekort aan nutriënten hebben, kunnen ze via autofagie een deel van hun eigen eiwitten afbreken om hier nieuwe voedingsstoffen uit te halen. Verder wordt dit proces gebruikt om grote eiwitcomplexen en aggregaten af te breken, maar ook bacteriën en virussen. Gebrekkige autofagie kan leiden tot neurodegeneratieve ziektes, terwijl in veel tumoren autofagie juist overgeactiveerd wordt. Moleculair gezien wordt het gewenste substraat, zoals een aggregaat, eerst omgeven door een membraan, waarna deze gesloten wordt en als autofagosoom fuseert met late endosomen en lysosomen, hun zuurdere variant. Late endosomen en lysosomen zijn de afbraakplekken in een cel en na deze fusie wordt het autofagiesubstraat afgebroken. Deze afbraak wordt gefaciliteerd door de lage pH en de aanwezige proteases, en zorgt ervoor dat de individuele bouwstoffen vrijkomen en opnieuw gebruikt kunnen worden. Autofagie is dus een soort recycling van oud materiaal en voorkomt dat dit ophoopt in de cel, met alle schadelijke gevolgen van dien. Hoe het transport van de autofagosomen naar lysosomen werkt, en vervolgens hoe de fusie van beide organellen tot stand komt, is nog onduidelijk. Ons werk laat zien dat een eiwit genaamd ORP1L zich op late endosomen en lysosomen bevindt en de fusie met autofagosomen kan blokkeren. Wij denken dat lysosomen op deze manier inkomend materiaal kunnen blokkeren, bijvoorbeeld omdat ze al materiaal hebben om af te breken, of omdat ze een speciale functie hebben, zoals melanosomen die pigment bij zich dragen. Verder laten we zien hoe late autofa-

gosomen (nadat ze gefuseerd zijn met late endosomen) getransporteerd worden in de cel, en hoe dit transport ook gereguleerd wordt door ORP1L. Interessant genoeg blijkt dat een ander organel betrokken is bij het blokkeren van dit transport, namelijk het endoplasmatisch reticulum (ER), een cellulaire structuur dat voornamelijk betrokken is bij de synthese van nieuwe eiwitten. Op het moment dat het ER contact maakt met de autofagosomen stopt het transport en blijven ze hangen op dezelfde plek in de cel. Wij denken dat dit het uitwisselen van voedingsstoffen mogelijk maakt maar de exacte functie is nog onbekend.
Buiten het afbreken van autofagosomen (inwendig materiaal), zorgen late endosomen en lysosomen ook voor de afbraak van voedingsstoffen die opgenomen worden van buitenaf, alsook voor de afbraak van signaalreceptoren. Dit gaat via de zogenaamde endocytische route, waarbij kleine blaasjes gevormd worden vanaf de buitenkant van de cel, die hiermee de voedingsstoffen opnemen. Deze blaasjes, of endosomen, fuseren vervolgens via verschillende tussenstappen met de late endosomen en lysosomen om hun inhoud af te breken. Problemen in de endocytische route kunnen leiden tot kanker, doordat groeireceptoren niet afgebroken worden en cellen blijven groeien, maar ook tot neurodegeneratieve ziektes doordat eiwitaggregaten niet goed verwijderd worden. Wanneer men kijkt naar endosomen in de cel, bevindt het overgrote deel van de verschillende endosoomtypes zich op een specifieke plek in de cel, naast de nucleus op de plek waar de microtubuli (het skelet van de cel) bij elkaar komen. Waarom en hoe de cel zo georganiseerd is, is lang onduidelijk geweest. In **hoofdstuk 3** hebben wij een nieuw eiwit gevonden, RNF26, wat de organisatie van de endosomen in deze perinucleaire regio verzorgd. RNF26 bevindt zich niet zelf op de endosomen, maar op een specifiek deel van het ER, en bindt adaptoreiwitten op verschillende endosoomtypes om ze op deze manier bij elkaar te houden. Het bij elkaar houden van deze endosoomtypes faciliteert fusie en uitwisseling, en stroomlijnt hiermee de snelle afbraak van extracellulair materiaal. Het rekruteren van de adaptoreiwitten, en hiermee de endosomen, gebeurt door middel van een klein eiwit genaamd ubiquitine, dat een soort brug vormt tussen RNF26 en de endosomen. RNF26 is een enzym dat dit eiwit op andere eiwitten kan plakken, waardoor deze -via de ubiquitine brug- adaptors van de verschillende endosomen kunnen binden. Dit maakt dat het proces dynamisch is. Wanneer het endosoom naar een andere plek in de cel gebracht moet worden dan gebeurt dit simpelweg door middel van het verwijderen van de ubiquitine brug.
In **hoofdstuk 4 en 5** hebben we getracht nieuwe functies te vinden voor de eiwitten die de ubiquitine verwijderen, de zogenaamde de-ubiquitinerende enzymen (DUBs). Van verschillende eiwitten uit deze klasse enzymen is nog niets bekend over wat ze doen, en om te kijken of deze eiwitten een rol spelen in de endocytische route hebben we ze een voor een weggehaald uit de cel en gekeken naar het effect op endosomen. Hiermee hebben we een nieuwe functie gevonden voor het eiwit OTUD1 in de afbraak van groeireceptoren en de positionering van endosomen. Verder hebben we gevonden dat USP54 -in tegenstelling tot voorspellingen- wel katalytische activiteit vertoond en dat dit eiwit specifiek lokaliseert naar endosomen en plekken waar cellen contact met elkaar maken, in zogenaamde tight junctions. Deze junctions zijn onder andere belangrijk in de darmen, waar ze onderdeel zijn van de barrière tussen de inhoud van de darm en het lichaam, en in de nieren, waar ze helpen bij het

filteren van het bloed. In cellen zien we dat USP54 belangrijk is voor het vormen van deze junctions en het is interessant om te kijken of dit ook in organismen zo is. Hoe USP54 dit exact doet zijn we nog aan het bestuderen.

Factoren die de expressie van MHCII beïnvloeden

Tijdens een infectie moet het immuunsysteem geactiveerd worden om de indringers (virussen, bacteriën etc.) te bestrijden. Activatie van het adaptieve deel van het immuunsysteem zorgt voor een reactie specifiek tegen een virus of bacterie en verloopt via zogenaamde major-histocompatibility complex (MHC) moleculen, die ook voor transplantatie afstoting verantwoordelijk zijn. Deze eiwitten presenteren kleine stukjes eiwit (peptiden) op de oppervlakte van de cel en de T-cellen scannen deze MHC-peptide complexen om te kijken of er verdachte (lichaamsvreemde) peptiden op zitten, wat duidt op een infectie of kanker. MHCI moleculen presenteren voornamelijk peptiden vanuit de binnenkant van de cel, terwijl MHCII eiwitten die opgenomen zijn uit de omgeving aan zich bindt, al kunnen MHCII moleculen ook eiwitten binden die via het eerder genoemde autofagie-proces in het lysosoom terecht zijn gekomen. De expressie van MHCII komt voornamelijk voor in gespecialiseerde afweercellen, maar stimulatie met cytokines (signaalstoffen) zoals Interferon-gamma (IFNγ) kan ook zorgen voor MHCII expressie op andere celtypes. Dit laatste is interessant omdat deze MHCII expressie bijdraagt aan transplantatie afstoting en autoimmuniteit. Verder kunnen tumoren (die gemuteerde eiwitten hebben en dus andere peptiden bezitten) herkend kunnen worden als lichaamsvreemd door de T-cellen, waarna de T-cellen de tumor aanvallen. Dit is de basis voor immunotherapie. Hoewel veel onderzoek gedaan wordt naar MHCI, is voor een goede afweerreaktie zowel MHCI als MHCII herkenning noodzakelijk. Het vinden van nieuwe eiwitten of stoffen die IFNγ-gemedieerde MHCII expressie reguleren zou dus nieuwe aanknopingspunten op kunnen leveren voor het voorspellen of beïnvloeden van de afweerrespons. In **hoofdstuk 7** beschrijven we twee eiwitten die betrokken zijn bij IFNγ-gemedieerde MHCII expressie in niet-immuun cellen, te weten Keap1 en p62. Om MHCII te produceren moet het DNA opgemaakt worden en dit gebeurt door verschillende modificaties, waaronder acetylatie van de histonen. Zowel Keap1 als p62 reguleren de transcriptie (productie) van MHCII via de acetylatie van histonen en het blokkeren van deacetylases zorgt ervoor dat Keap1 en p62 niet meer nodig zijn. Verder hebben we gevonden dat arsenicum, wat in veel landen in het drinkwater voorkomt, ook zorgt voor verminderde histon acetylatie en hiermee IFNγ-gemedieerde MHCII expressie. Interessant genoeg is al bekend dat arsenicum kan helpen om transplantatie afstoting tegen te gaan, wat dus potentieel verloopt via deze route. Ook is er een medicijn dat onder andere aangrijpt op Keap1, dimethyl fumaraat, dat IFNγ-gemedieerde MHCII expressie blokkeert. Dit gaat echter onafhankelijk van Keap1, via een mechanisme dat we nog niet helemaal begrijpen. Dit medicijn wordt gebruikt voor het behandelen van de auto-immuunziektes multiple sclerosis en psoriasis, en dit hoofdstuk laat een deel van het mechanisme zien dat dit zou kunnen verklaren.

Resistentie tegen chemotherapeuticum doxorubicine

Een van de belangrijkste redenen waarom niet alle patiënten reageren op chemo-

therapie is omdat de tumor ongevoelig wordt voor de chemo. In **hoofdstuk 8 en 9** beschrijven we enkele factoren die verantwoordelijk kunnen zijn voor verminderde gevoeligheid voor de chemotherapeutische medicijnen etoposide en doxorubicine. Deze medicijnen grijpen aan op het eiwit topoisomerase II, welke breuken maakt in het DNA om te voorkomen dat het DNA in de knoop komt te zitten, en zorgen hiermee voor DNA schade in de cel, wat leidt tot celdood. Vooral doxorubicine is een veelgebruikt medicijn en is heel effectief, maar heeft ook sterke bijwerkingen. Door middel van een mutagenese-screen waarbij een virus zich in een gen inbouwt en deze hiermee uitschakelt hebben we nieuwe eiwitten gevonden die betrokken zijn bij resistentie tegen topoisomerase II inhibitors. Een van deze factoren is het SWI/SNF chromatine remodeling complex. Van dit complex is bekend dat het betrokken is bij het binden van topoisomerase II aan het DNA. Het missen van een van de onderdelen van SWI/SNF leidt tot verminderde gevoeligheid van de tumor voor doxorubicine. Dit complex is gemuteerd in verschillende tumoren en van sommige van deze tumoren was al bekend dat ze heel ongevoelig waren voor doxorubicine. Verder zien we dat borsttumoren met een lage expressie van een van de subunits van SWI/SNF slechter reageren op doxorubicine. Het is dus interessant om verder te onderzoeken of patiënten met mutaties in dit complex met een andere chemotherapy behandeld moeten worden, en dat SWI/SNF dus als een selectiemarker kan werken voor het kiezen van de juiste behandeling.

Curriculum Vitae

Ruud Wijdeven is geboren op 14 februari 1985 in Langenboom, gemeente Mill en St. Hubert. Na basisschool 't Stekske heeft hij in 2003 zijn VWO-diploma behaald aan het Udens College. Vervolgens is hij naar Wageningen verhuisd om aldaar aan de Wageningen Universiteit Biotechnologie te gaan studeren. Zijn Bachelor werd succesvol afgerond in 2007, waarna hij de specialisatie Medische Biotechnologie is gaan volgen, welke in 2009 afgerond werd. Gedurende zijn Master heeft hij drie afstudeervakken gevolgd, de eerste bij de vakgroep Cell Biology en Immunology onder leiding van Lidy van Kemenade waarbij de functie en expressie van nieuwe antibody-isotypes in karpers centraal stond. De tweede stage is gedaan bij de vakgroep Biochemistry onder leiding van Sacco de Vries en Jose Aker met als focus de endocytose van plantenreceptoren BRI1 en SERK1. Tenslotte heeft hij stage gelopen op de Universiteit van California San Francisco in het lab van Abul Abbas, onder supervisie van Hans Dooms, met als thema de rol van IL-2 en IL-2 antilichamen in de initiatie van de CD4+ T-cell response. In 2009 is hij zijn promotieonderzoek gestart in de groep van Jacques Neefjes op het Nederlands Kanker Instituut. In 2016 is hij met de groep van Jacques verhuisd naar het LUMC. Na zijn promotie blijft Ruud aan als vaste postdoc in de groep van Jacques Neefjes.

List of publications

S. Ryo*, **R.H. Wijdeven***, A. Tyagi, T. Hermsen, T. Kono, I. Karunasagar, J.H. Rombout, M. Sakai, B.M. Verburg-van Kemenade and R. Savan
Common carp have two subclasses of bonyfish specific antibody IgZ showing differential expression in response to infection.
Developmental Comparative Immunology 34 (2010), pp. 1183-1190.

A. de Jong, R. Merkx, I. Berlin, B. Rodenko, **R.H. Wijdeven**, D. El Atmioui, Z. Yalcin, C.N. Robson, J.J. Neefjes and H. Ovaa
Ubiquitin-based probes prepared by total synthesis to profile the activity of deubiquitinating enzymes.
Chembiochem 13 (2012)

R.H. Wijdeven*, J.M. Bakker*, P. Paul and J. Neefjes
Exploring genome-wide datasets of MHC class II antigen presentation.
Molecular Immunology 55 (2013), pp. 172-174

R.H. Wijdeven, J. Neefjes and H. Ovaa
How chemistry supports cell biology: the chemical toolbox at your service.
Trends Cell Biology 24 (2014)

R.H. Wijdeven*, B. Pang*, S.Y. van der Zanden, X. Qiao, V. Blomen, M. Hoogstraat, E.H. Lips, L. Janssen, L. Wessels, T.R. Brummelkamp and J. Neefjes
Genome-Wide Identification and Characterization of Novel Factors Conferring Resistance to Topoisomerase II Poisons in Cancer.
Cancer Research 75 (2015)

R. van der Kant*, C.T. Jonker*, **R.H. Wijdeven**, J. Bakker, L. Janssen, J. Klumperman and J. Neefjes
Characterization of the Mammalian CORVET and HOPS Complexes and Their Modular Restructuring for Endosome Specificity.
Journal Biological Chemistry 290 (2015)

R.H. Wijdeven, M.L. Jongsma, J. Neefjes and I. Berlin
ER contact sites direct late endosome transport.
Bioessays 37 (2015)

S.C. Stolze*, N. Liu*, **R.H. Wijdeven**, A.W. Tuin, A.M. van den Nieuwendijk, B.I. Florea, M. van der Stelt, G.A. van der Marel, J.J. Neefjes and H.S. Overkleeft
Photo-crosslinking of clinically relevant kinases using H89-derived photo-affinity probes.
Molecular Biosystems 12 (2016)

R.H. Wijdeven, H. Janssen, L. Nahidiazar, L. Janssen, K. Jalink, I. Berlin and J. Neefjes
Cholesterol and ORP1L-mediated ER contact sites control autophagosome transport and fusion with the endocytic pathway.
Nature Communications 7 (2016)

M.L. Jongsma*, I. Berlin*, **R.H. Wijdeven**, L. Janssen, G.M. Janssen, M.A. Garstka, H. Janssen, M. Mensink, P.A. van Veelen, R.M. Spaapen and J. Neefjes
An ER-Associated Pathway Defines Endosomal Architecture for Controlled Cargo Transport.
Cell 166 (2016)

R.H. Wijdeven*, B. Pang* and J. Neefjes
Old drugs, novel ways out: Drug resistance toward cytotoxic chemotherapeutics.
Drug Resist Updates 28:65-81 (2016)

A.J.C. Dohmen, X. Qiao, A. Duursma, **R.H. Wijdeven**, C. Lieftink, F. Hageman, B. Morris, P. Halonen, C. Vens, M.W.M. van den Brekel, H. Ovaa, J. Neefjes and C.L. Zuur
Identification of a novel ATM inhibitor with cancer cell specific radiosensitization activity.
Oncotarget (2017)

* Authors contributed equally to this paper

Acknowledgements

I would like to thank all my colleagues and collaborators that helped me during my PhD and especially Jacques, my supervisor.